

**Parameter and Performance: Integrated Computational Performance Assessment of
Structural and Daylighting Efficiency in Perforated Concrete Shell Structures**

by

Niloufar Emami

A dissertation submitted in partial fulfillment
of the requirements for the degree of
Doctor of Philosophy
(Architecture)
in The University of Michigan
2018

Doctoral Committee:

Professor of Practice Harry Giles, Co-Chair
Professor Peter von Bülow, Co-Chair
Professor Karl Daubmann, Lawrence Technological University
Professor Panos Papalambros
Professor Christoph Reinhart, Massachusetts Institute of Technology

Niloufar Emami

nemami@umich.edu

ORCID iD: 0000-0001-6402-603X

© Niloufar Emami 2018

This dissertation is dedicated to my parents,

Ali and Flora

for their endless love and support

ACKNOWLEDGEMENTS

I would like to take this opportunity to express my gratitude to everyone who directly and indirectly supported and contributed to my dissertation. First and foremost, I would like to thank Professor Harry Giles, my academic adviser and co-chair, for his time, support, patience, and tremendous counsel, for sharing his knowledge of the field with me, for supporting my academic explorations, and for advising me on the pillars of research. I would like to thank my co-advisor and co-chair, Professor Peter von Bülow, for his time and constant guidance on my research and also on the different facets of an academic career to help me grow. I would like to express my gratitude to my committee members, Professor Karl Daubmann for his mentorship and constructive advice; to Professor Panos Papalambros for his critical encouragement on my research; and to Professor Christoph Reinhart for his insight and feedback on my research.

I would also like to thank Associate Professor Claire Zimmerman for her endless support throughout my studies; Professor Jean Wineman for her mentorship; Professor Linda Groat for her kindness; and Professor Moji Navvab for his technical and professional advice. I would also like to acknowledge Associate Professors John McMorrough, and Kathy Velikov, as well as Assistant Professors Sandra Maninger, Jonathan Rule, Ana Morcillo Pallares, Sean Vance, and Ana Paula Pimentel Walker for their mentorship, constructive feedback, and support. This paragraph would not be complete without thanking Dean Jonathan Massey for his tremendous support from the first day that he started leading Taubman College of Architecture and Urban Planning.

I would like to take this opportunity to thank individuals who were a tremendous help to me. I cannot thank Lisa Hauser enough; during my time at TCAUP, from the first day that I entered the building, she has always been more than the Assistant Director of Admissions and Recruiting. I would like to thank Rebecca Price, the extremely helpful librarian and kind individual who helped me beyond my expectations. I would like to thank Brady West from CSCAR (Consulting for Statistics, Computing & Analytical Research) for helping me with statistical analysis of my data. I would also like to thank Simone Sessolo from the Sweetland Center for helping me edit my dissertation chapters through Writing Workshops, as well as Sarah E. Knudsen who helped with

proofreading and reading the whole dissertation chapters. I would also like to thank Gerry D'Anza for providing me the license for the Rhino Membrane plugin, as well as Alstan Jakubiec for providing me the license for the DIVA plugin. I would also like to thank John Prescott from the International Center for facilitating many administration procedures for me. Finally, I would like to thank my colleagues and friends in the Building Technology group, as well as the doctoral students at TCAUP for their friendship and support.

I would like to express my heartfelt gratitude to my parents: Ali Emami who instilled in me academic passion and then supported me throughout my whole life, and Flora Abtahi, from whom I learned how to live every minute of my life with passion and enthusiasm. I should mention my siblings, Yasaman and Ferial, with whom my heart is connected although we are miles apart.

Last but not least, the biggest thanks to my spouse, Saeid Mofrad. He has been supportive from the day that we decided to relocate for my studies, and then throughout every step of it. His love, support, partnership, encouragement, friendship, consultation, and patience throughout this route has always been with me.

CONTENTS

DEDICATION.....	ii
ACKNOWLEDGMENT.....	iii
LIST OF FIGURES	ix
LIST OF TABLES.....	xix
LIST OF APPENDICES.....	xxii
ABBREVIATIONS.....	xxiii
ABSTRACT.....	xxiv
Chapter 1: Introduction.....	1
1.1 Background of the study	1
1.2 Statement of the problem.....	2
1.3 Research objectives.....	3
1.4 Organization of the dissertation	5
1.5 References.....	7
Chapter 2: Background.....	9
2.1 Introduction.....	9
2.2 Brief introduction to BIM and others.....	13
2.3 Parametric design, its implementation in architecture, and its limitations.....	16
2.3.1 Generative design.....	16
2.3.2 Parametric design.....	18
2.3.3 How does parametric modeling help us to understand design problems?	20
2.3.4 Considerations in modeling and implementation.....	21
2.3.5 Limitations	24
2.4 Performance	28
2.5 Large span roofs as a use case	30
2.6 Importance of structure and daylight as two objectives in shell design.....	34
2.7 Discussion summary	34
2.8 References.....	35

Chapter 3: Shell structures as large-span roof systems.....	38
3.1 Introduction.....	38
3.2 Perforated concrete shell structures	44
3.2.1 Eduardo Torroja	45
3.2.2 Pier Luigi Nervi	46
3.2.3 Felix Candela	49
3.2.4 Heinz Isler	50
3.2.5 Frei Otto	52
3.2.6 Recent precedents	53
3.2.7 Perforated concrete shell structures timeline	55
3.3 Topology, shape and sizing.....	55
3.3.1 Topology	57
3.3.2 Shape.....	61
3.3.3 Sizing	64
3.3.4 Summarizing topology, shape, and sizing in shells	64
3.4 Relevant metrics for performative shells	65
3.5 Discussion summary	68
3.6 References.....	68
Chapter 4: Daylighting in large-span roof systems	72
4.1 Introduction.....	72
4.2 Levels of daylight control	75
4.2.1 First level of daylight control: global geometry.....	76
4.2.2 Second level of daylight control: glazing.....	84
4.2.3 Third level of daylight control: interior elements	87
4.2.4 Summarizing various levels of daylight control in buildings	90
4.3 Daylighting performance and metrics to measure it	92
4.3.1 Performance criteria: illuminance, distribution, glare, and directionality of light	93
4.3.2 Static and dynamic metrics for measuring illuminance	95
4.3.3 Static and dynamic metrics for measuring glare	102
4.3.4 Summarizing static and dynamic metrics for measuring illuminance and glare.....	104
4.4 Discussion and summary in the context of large span roof systems	106
4.5 References.....	107
Chapter 5: Parameters.....	111
5.1 Introduction.....	111
5.2 Overlapping parameters in structure and daylighting disciplines	119

5.2.1	Perforation Ratio, Granularity, and Bias.....	122
5.2.2	Surface Curvature	126
5.3	Constructing a design space for shells	127
5.4	Discussion	129
5.5	References.....	132
Chapter 6:	Methodology	135
6.1	Introduction.....	135
6.2	ParaGen framework	144
6.3	Research methodology	146
6.4	Discussion	149
6.5	References.....	149
Chapter 7:	Analysis and application through case studies.....	151
7.1	Introduction.....	151
7.2	Parameter and performance	153
7.2.1	Variable 01 to 05: controlling the boundary curves of the roof geometry	158
7.2.2	Variable 06: zone combination index	159
7.2.3	Variable 07: perforation pattern	162
7.2.4	Variable 08: thickness.....	162
7.2.5	Exploring the size of the search space based on the variables	162
7.2.6	Parameter	164
7.2.7	Performance	165
7.3	Statistical analysis.....	167
7.3.1	Performance: weight	168
7.3.2	Performance: maximum deflection	169
7.3.3	Performance: von Mises stress.....	170
7.3.4	Performance: total structural costs	172
7.3.5	Performance: spatial Daylight Autonomy.....	174
7.3.6	Performance: light oversupply	175
7.3.7	Performance: total operational energy	176
7.3.8	Performance: total energy costs	179
7.3.9	Tradeoff between performance	179
7.4	Case study 01: High Life Textile Factory	181
7.4.1	The original design of the High Life Textile Factory	183
7.4.2	Adjusted High Life Textile Factory for daylighting simulation	188
7.4.3	Adjusted High Life Textile Factory for structural simulation.....	189

7.4.4	Mapping the abstract High Life Textile Factory onto the new solution space.....	194
7.5	Case study 02: COOP Warehouse, a bubble shell with multiple openings.....	195
7.5.1	The Original Design of the COOP Warehouse	197
7.5.2	COOP Warehouse adjusted for daylighting simulation	198
7.5.3	COOP Warehouse adjusted for structural simulation	199
7.5.4	Mapping the COOP Warehouse onto the shells generated using ParaGen.....	201
7.6	Discussion	201
7.6.1	Summarizing statistical results.....	202
7.6.2	Opportunities and limitations.....	205
7.7	References.....	207
Chapter 8:	Conclusion and future work.....	208
8.1	Problem statement.....	208
8.2	Contributions, and future work related to interdisciplinary design.....	209
8.2.1	Contributions.....	210
8.2.2	Future work.....	210
8.3	Results, contributions, and limitations related to the field of shell structures.....	210
8.3.1	Results.....	211
8.3.2	Contributions.....	214
8.3.3	Limitations	214
8.3.4	Future work.....	215
8.4	Results and contribution to solution space exploration.....	215
8.4.1	Contributions.....	216
8.4.2	Limitations	216
8.4.3	Future work.....	217
8.5	Impact	217
Appendices	218

LIST OF FIGURES

Figure 1.1. The outline of this dissertation	7
Figure 2.1. RIBA Plan of Work (RIBA, 2013).....	13
Figure 2.2. Design phases as an iterative loop	13
Figure 2.3. Level of influence on project costs (Paulson Jr., 1976).....	14
Figure 2.4. Shifting effort in the effort curve introduced by MacLeamy (Charmaine, 2011)	15
Figure 2.5. Davis introduces an alternative to Paulson and MacLeamy’s curve (Davis, 2013)	15
Figure 2.6. Various layers of properties related to six generative systems, (El-Khalidi, 2007).....	17
Figure 2.7. Associative and rule-based generative systems (a); Hierarchical and replacement systems (b), after (El-Khalidi, 2007).....	18
Figure 2.8. Hudson’s integrated workflow model and the role of parametric designer Hudson (2010).....	22
Figure 2.9. Use of parametric modeling in architectural projects in the period 1990 to 2008 (Hudson, 2010)	23
Figure 2.10. Various functions of a building envelope categorized by Fitch (1973).....	31
Figure 2.11. Different functions that a façade serves (Knaack et al., 2007)	32
Figure 2.12. Survey of structural systems (Engel, 1967) integrated with top-lighting strategies	33
Figure 3.1. In-plane stresses (a); and plate bending (b) (Williams, 2014).....	40
Figure 3.2. Comparison between a colander and a sieve (Williams, 2014).....	42
Figure 3.3. Church by Eladio Diesta (López et al., 2016) (a); Masonry shell by Rafael Guastavino (Ochsendorf & Block, 2014) (b)	42
Figure 3.4. The Pantheon in Rome (a); and the Chapel Lomas de Cuernavaca (b)	43
Figure 3.5. Centre Pompidou in Metz, 2010 (a); Haesley Nine Bridges golf clubhouse (b)	43
Figure 3.6. Steel gridshell of the New Milan Trade Fair in Italy (a); National Maritime Museum (b)	44
Figure 3.7. Inextensional deformation in the region of a hole in a sphere (Williams, 2014).....	45
Figure 3.8. Thin shell with triangulated openings in the Fronton Recoletos (Torroja, 1958).....	46
Figure 3.9. Construction and reinforcement of a thin shell with triangulated openings, part of the Fronton Recoletos (Torroja, 1958)	46
Figure 3.10. Thin slab samples reinforced with different layers of wire meshes (Greco, 1995)	47
Figure 3.11. Precast elements prior to the placement of the in-situ concrete (a); Festival Hall dome (b) (Nervi, 1965).....	48
Figure 3.12. Concrete plate with an oculus in the Papal Audience Hall.....	48
Figure 3.13. Nervi’s structural model for the Centre national des industries et technique (Nervi, 1965) ..	49

Figure 3.14. Perforated umbrella roof of the Textile Factory designed by Felix Candela (Garlock & Billington, 2008).....	50
Figure 3.15. Insignia of the Great Southwest Corporation, Texas (Mendoza, 2015)	50
Figure 3.16. Assembly of bubble shells (a); typical standard bubble shells (b) (Chilton, 2000).....	51
Figure 3.17. Concretion of the COOP storage and distribution center (a) (Chilton, 2000); completed shell (b) (Ramm, 2011).....	52
Figure 3.18. Kilcher free form shell (a); Sicli Factory in Geneva (b) (Chilton, 2000)	52
Figure 3.19. Soap film form finding (a); compression model (b); train station model (c) (Frei Otto, 2005)	53
Figure 3.20. Shell with a wiremesh (a) (Eisenbach, Vasudevan, Grohmann, Bollinger, & Hauser, 2014); a shell manufactured with CNC milled formwork (b) (Dombernowsky & Søndergaard, 2012).....	54
Figure 3.21. Teshima Art Museum, Japan (a); Rolex Learning Center, by SANAA (b); Mall at Chiasso (c)	54
Figure 3.22. Concrete shell in Confluence Park, San Antonio, Texas	55
Figure 3.23. Timeline of perforated concrete shell structures	55
Figure 3.24. Trinity of topology, shape, and sizing in structural design, and its correspondence with design stages	56
Figure 3.25. A sewing needle topologically changes into another shape with the same genus value (J. Liang et al., 2013)	57
Figure 3.26. Simple (a), two-fold (b), and three-fold (c) connected domains	57
Figure 3.27. Topological mapping of one domain into the other one (Eschenauer & Olhoff, 2001)	58
Figure 3.28. Classical geometric definition of a shape (a); versus the topological approach using graphs (b & c), after (Tedeschi, 2014).....	58
Figure 3.29. Topology in continuous and discrete structural systems	59
Figure 3.30. Cubical design space with varying support conditions (a); topology optimization (b) (Imgard Lochner-Aldinger & Schumacher, 2014).....	60
Figure 3.31. Topology spectrum from a continuous to a gridshell	61
Figure 3.32. Shape in continuous and discrete structural systems	62
Figure 3.33. A topology explored by Ito and later optimized by Sasaki for a continuous structure (Mustsuro Sasaki, 2007)	63
Figure 3.34. British Museum Courtyard (a); Renderings of the great court (b) (Burry & Burry, 2010)	64
Figure 3.35. Sizing in continuous (left) and discrete (right) systems	64
Figure 3.36. Topology, shape and sizing optimization in shells and gridshells.....	65
Figure 4.1. Various levels of daylight control	76
Figure 4.2. Daylight control through global geometry	77
Figure 4.3. MyZeil shopping mall, showing the alternating panels of glass and steel in the roof (Knippers & Helbig, 2009)	78
Figure 4.4. The diagram illustrates how a valley with various curvatures can be shadowed differently....	78

Figure 4.5. The surface shadows the valley differently under various sun angles.....	78
Figure 4.6. Daylight control through local geometry.....	79
Figure 4.7. Toplighting typologies, showing transformations from one typology to the other	80
Figure 4.8. Forum at the Eckenberg Academy (Gerfen, 2013).....	81
Figure 4.9. perspective view of the Graz museum (a) plan view (b), close-up view of a nozzle (c) (Chaszar, 2006)	82
Figure 4.10. Exterior blinds installed on the skylights of the Kimbel Museum extension (Piano, n.d.)	83
Figure 4.11. Vele on the roof of the museum designed by Renzo Piano	83
Figure 4.12. Daylight control through glazing.....	84
Figure 4.13. Fritting patterns on the glazings of the Cathedral of Christ the Light, California (photo by author).....	85
Figure 4.14. Interior of the main enclosure in the New Elephant House (a); detail of the frit pattern (b) (Foster, n.d.).....	86
Figure 4.15. 15%, 30%, 45%, 60% frit patterns (Woodbury, 2010).....	86
Figure 4.16. Kimbel Art Museum Expansion, showing translucent glazing in the roof (Piano, n.d.)	86
Figure 4.17. Alternating fritted and transparent panels at the New Elephant House, alternating opaque (a); transparent panels at the MyZeil Shopping Mall (b)	87
Figure 4.18. Daylight control through the use of interior elements	87
Figure 4.19. Interior blinds and the oculus ceiling of the Cathedral of Christ the Light (a); layers of the envelope from top to bottom include roof skylight, oculus ceiling, fritted glass, and wood louvers (b) (Sarkisian et al., 2011)	88
Figure 4.20. Kimbell Art Gallery designed by Louis Kahn.....	89
Figure 4.21. Dome-shaped coffers fabricated by Georgia-Pacific Gypsum LLC.....	89
Figure 4.22. The courtyard of the German Historical Museum in Berlin.....	90
Figure 4.23. Summary of various levels of daylight control with examples	90
Figure 4.24. Summary of various levels of daylight control in building envelopes	91
Figure 4.25. daylight factor of 2% when the outdoor global illuminance is 10000 lux (Ruck, 2000).....	96
Figure 4.26. Human subjects' rating of the DGP.....	104
Figure 5.1. Form has a priority (a); performance dictates form (b); integrating form and performance (c)	112
Figure 5.2. Integrating performance from multiple disciplines	114
Figure 5.3. interoperability at the tool level among disciplines	115
Figure 5.4. Placing the structural and daylighting categorization side by side.....	119
Figure 5.5. Placing the structural and daylighting design stages side by side	120
Figure 5.6. <i>Number of openings</i> as the first parameter that is common in two disciplines.....	120
Figure 5.7. <i>Size of the openings</i> as the second parameter that is common in two disciplines	121
Figure 5.8. <i>Surface curvature</i> as the third parameter that is common in two disciplines	121

Figure 5.9. Dividing a square into four equal sections to quantify bias.....	124
Figure 5.10. Dividing a square into four equal sections to quantify Bias	125
Figure 5.11. Dividing a square into nine equal sections to quantify bias	125
Figure 5.12. Dividing a square into nine equal sections to quantify bias	126
Figure 5.13. As the divisions become finer, the accuracy of quantifying bias increases but the process becomes more complex.....	126
Figure 5.14. A tangent plane can be passed through the points on the surface to draw principal curvatures	127
Figure 5.15. Synclastic, single curvature, and anticlastic forms with a positive, zero, and negative Gaussian curvature, created after (Blaauwendraad & Hoefakker, 2014).....	127
Figure 5.16. Change in the shape of a shell from a dome to a vault and then to a saddle	128
Figure 5.17. Potential change in perforation ratio, granularity, and bias in the spectrum of continuous to grid shells	128
Figure 5.18. Shell design space, spanning continuous to grid shells with varying shapes	129
Figure 5.19. Roadmap for designers for identifying the interdisciplinary design parameters	130
Figure 6.1. Multi-objective optimization (MOO), and Multi-disciplinary optimization (MDO), after (Yang, Sun, Turrin, Buelow, & Paul, 2015)	136
Figure 6.2. Describing non-dominant solutions falling in the Pareto set.....	138
Figure 6.3. Search space versus solution space.....	139
Figure 6.4. ParaGen framework, after von Buelow (2011).....	145
Figure 6.5. The commercial software systems used in the ParaGen framework for this study	146
Figure 6.6. Research methodology workflow	148
Figure 7.1. Computational design, performance assessment and validation framework	153
Figure 7.2. Conceptual design space for shells, reiterated from Chapter 5.....	154
Figure 7.3 . The actual search space created by the parametric model	155
Figure 7.4. Matches for zone combination index of 5, 305, 347, and 511 which result in symmetric opening patterns	156
Figure 7.5. The variables that control the parametric geometry generation in Grasshopper	157
Figure 7.6. Variable 01 is elevation of edge corners which affect the global geometry	158
Figure 7.7. Variable 02 is the rise of edge curve in width (a); Variable 03 is the rise of edge curve in length (b).....	158
Figure 7.8. Variable 04 is the tilt of edge curves in width	159
Figure 7.9. Variable 05 is the tilt of edge curve in length.....	159
Figure 7.10. Triangular pattern (a); isolating the triangular divisions at the edges for future structural analysis (b).....	160
Figure 7.11. Offsetting the triangular grid inward (a); and then filleting the corners to avoid high local stresses (b).....	160

Figure 7.12. The python algorithm implementation clusters triangulated divisions into nine zones.....	161
Figure 7.13. Possible perforation patterns mapped onto the pattern.....	162
Figure 7.14. Screenshot of the interactive webpage connected to the online SQL database as part of the ParaGen framework	166
Figure 7.15. Different alternatives can be explored qualitatively and quantitatively with regard to their multiple performance criteria.....	166
Figure 7.16. Surface plots for DV-1 (weight) plotted on the z-axis; perforation ratio and thickness are plotted on the x- and y-axes, respectively	168
Figure 7.17. Surface plots for DV-2 (maximum deflection) plotted on the z-axis, with perforation ratio and thickness plotted on the x- and y-axes, respectively	169
Figure 7.18. Although deflection is reduced by increasing perforation ratio in saddles, since the statistical analysis is not controlling for curvature, the results cannot be generalized.....	170
Figure 7.19. Surface plots for DV-3 (von Mises stress at Q3) plotted on the z-axis, with perforation ratio and thickness plotted on the x- and y-axes, respectively	171
Figure 7.20. Von Mises stress is reduced as the shells become more perforated	172
Figure 7.21. Surface plots for DV-4 (material and formwork costs) plotted on the z-axis, with perforation ratio and thickness are plotted on x- and y-axes, respectively	173
Figure 7.22. Surface plots for DV-5 (spatial daylight autonomy) plotted on the z-axis, while perforation ratio and thickness are plotted on x- and y-axes, respectively	174
Figure 7.23. Perforation ratio versus spatial daylight autonomy (sDA)	175
Figure 7.24. Surface plots for DV-6 (Light oversupply) plotted on the z-axis, where perforation ratio and thickness are plotted on x and y-axis	175
Figure 7.25. Perforation ratio versus light oversupply (DA _v)	176
Figure 7.26. Surface plots for DV-7 (Total operational energy) plotted on the z-axis, with perforation ratio and thickness plotted on x- and y-axes, respectively	177
Figure 7.27. By creating more holes, heating energy decreases (a); by making the shells thicker, heating energy decreases (b).....	178
Figure 7.28. By creating more holes, cooling loads increase (a); thickness does not seem to affect cooling loads (b)	178
Figure 7.29. Lighting energy reaches a plateau when the perforation ratio is more than 20% (a); thickness does not seem to affect lighting loads (b)	178
Figure 7.30. Surface plots for DV-8 (total energy costs) plotted on the z-axis, with perforation ratio and thickness plotted on x- and y-axes, respectively	179
Figure 7.31. Identifying contrasting colors on the heat map.....	180
Figure 7.32. Tradeoff between two performance criteria: structural cost versus operating costs.....	180
Figure 7.33. The process of adjusting the case studies for mapping onto the solution space	182
Figure 7.34. High Life Textile Factory with perforations (Garlock & Billington, 2008).....	184
Figure 7.35. Straight-edge hyper with an area identified in white (a) an umbrella shell compromised of four areas (b), after (Garlock & Billington, 2008).....	184

Figure 7.36. Plan and section drawings of Rio’s Warehouse with tilted umbrellas (Garlock & Billington, 2008).....	185
Figure 7.37. Force flow in the umbrella shell (a); reinforcement placement in the shell (b) (Garlock & Billington, 2008).....	186
Figure 7.38. The 45-degree rotation of perforations (a); factory in use (b) (Garlock & Billington, 2008)	186
Figure 7.39. Site plan (a); 3d view (b) of the High Life Textile Factory captured from Google Maps....	187
Figure 7.40. The plan view of High Life Textile Factory recreated in Rhino based on the measured dimensions (a); the magnified drawing of one umbrella unit with the assumed dimensions for the perforations (b).....	187
Figure 7.41. As-built High Life Textile Factory (a); eliminating North light (b); adjusting the size of each umbrella unit and arraying them in a 4 by 5 grid to cover a 50 by 60-m space (c)	188
Figure 7.42. Spatial daylight autonomy distribution and light oversupply of the High Life Textile Factory	189
Figure 7.43. (top row) 12.5 by 12-meter umbrellas are assembled to shape a larger square; (bottom row) four central sections at the intersection of the umbrellas are isolated and scaled up for structural analysis	190
Figure 7.44. Abstract morphology-A with a rise of 45 m (a); Abstract morphology-B with a rise of 15 m (b); Abstract morphology-C with a rise of 9 m (c)	191
Figure 7.45. C-15, the abstract model of Candela’s umbrella shell. Its structural performance will be mapped onto the ParaGen design space.....	194
Figure 7.46. The process of adjusting the case studies for structural and daylighting simulations	196
Figure 7.47. The COOP storage and distribution center by Heinz Isler (Ramm, 2011) (a); Google maps (b) (47° 20' 20.70" N, 7° 51' 50.78" E)	197
Figure 7.48. Isler’s sketch for COOP Warehouse, (Bösiger, 2011).....	197
Figure 7.49. Plan and section of COOP Warehouse (Chilton, 2011).....	198
Figure 7.50. Spatial daylight autonomy distribution and light oversupply of the COOP Warehouse	199
Figure 7.51. structural supports along the edge (a); maximum deflection (b); principle stress lines, blue representing compression and red representing tension (c)	199
Figure 7.52. Structural supports at the corners (a); maximum deflection (b); principle stress lines, blue representing compression and red representing tension (c)	200
Figure 7.53. An image that graphically shows the simulation results from two different disciplines such as structures (stress plots) and daylighting (spatial daylight autonomy plots)	202
Figure 7.54. Cases that have an acceptable perforation ratio are filtered for their structural performance	205
Figure 7.55. Morphology-A retrieved by scaling up the units (a) is seen in Church of Our Miraculous Lady (b)	205
Figure A.1. Ansys and Karamba corresponding support representing a simple support	224
Figure A.2. Ansys and Karamba corresponding support representing a fixed support.....	224

Figure A.3. Orthogonal cut of the shell (left), diagonal cut (right), and then reading the von Mises stress levels on top and bottom layer in Ansys	229
Figure A.4. step 01: principle stress of the desired layer are retrieved	229
Figure A.5. step 02: a python script calculates von Mises stress levels from the principal stress levels using $\sigma_{12} + \sigma_{22} - (\sigma_1 * \sigma_2)$	229
Figure A.6. step 03: The orthogonal and diagonal index numbers are identified based on the mesh numbers and then used as a list of indices to extract the related von Mises stress levels.	230
Figure A.7. von Mises stress on top and bottom layer of an orthogonally cut shell in Ansys	230
Figure A.8. von Mises stress on top and bottom layer of an orthogonally cut shell in Karamba	230
Figure A.9. von Mises stress on top and bottom layer of a diagonally cut shell in Ansys	231
Figure A.10. von Mises stress on top and bottom layer of a diagonally cut shell in Karamba	231
Figure B.1. Chamfering shell edges to avoid point supports	232
Figure B.2. Extracting edge lines to define supports	233
Figure B.3. Extracting edge vertices from edge lines to define supports.....	233
Figure B.4. Supports are restrained in x, y and z-direction for moving and rotation.....	233
Figure B.5. factoring load based on the solid area of the shells.....	234
Figure B.6. Loading the shell, gravity load to consider dead load, as well as an applied load for live load	234
Figure B.7. defining multiple thicknesses to feed the cross-section element	235
Figure B.8. Material properties to define concrete	236
Figure B.9. Assembling the shell element, supports, load, cross section and material for analysis	236
Figure B.10. Feeding the analysis results to model-view for post-processing.....	237
Figure B.11. Feeding the <i>model-view</i> to <i>shell-view</i> for graphical post-processing.....	237
Figure B.12. Feeding the <i>model-view</i> to <i>shell vector results</i> for numerical post-processing.....	238
Figure B.13. The python code developed for statistical analysis outputs the Q3 of von Mises stress levels	239
Figure B.14. <i>Assemble</i> module in Karamba outputs mass in kilograms, which is then converted to tones	242
Figure B.15. Calculating material cost using the mass output of Karamba's <i>Assemble</i> module	242
Figure C.1. DIVA setup	246
Figure C.2. Daylighting grid.....	247
Figure C.3. Grid settings	247
Figure C.4. Radiance settings	248
Figure C.5. Merging components for analysis.....	248
Figure C.6. Location settings	249
Figure C.7. Daylighting results.....	249

Figure C.8. Python script editor in grasshopper.....	250
Figure C.9. Exporting a daylighting schedule.....	251
Figure D.1. Creating new materials and adding them to the library	252
Figure D.2. Concrete with different thicknesses is created.....	253
Figure D.3. Using daylighting schedule in the energy runs	253
Figure D.4. Thermal zones.....	254
Figure D.5. Energy model visualization	255
Figure D.6. Adiabatic surfaces with Normals pointing inside	255
Figure D.7. Zone setting construction.....	256
Figure D.8. Zone load and conditioning settings	257
Figure D.9. Zone ventilation and hot water settings	258
Figure D.10. Window settings	258
Figure D.11. Energy plus component	259
Figure D.12. Energy plus output.....	260
Figure D.13. Model output from Energy Plus run	260
Figure D.14. Jules to KW.hr conversion.....	261
Figure E.1. Distribution of shell typologies in the whole population showing that it is skewed towards one typology upon using fitness functions	265
Figure E.2. Distribution of shell typologies in the trimmed population	265
Figure E.3. Final distribution of shell typologies subject to statistical analysis	266
Figure E.4. Flowchart of statistical analysis	267
Figure E.5. Distribution of Weight	269
Figure E.6. Scatter plots of Weight versus Perforation Ratio (a) and Weight versus Thickness (b)	269
Figure E.7. Saddles have the largest negative relationship with perforation ratio (a); saddles have the largest positive relationship with thickness (b).....	270
Figure E.8. Distribution of von Mises Stress levels.....	271
Figure E.9. Scatter plots of von Mises versus Perforation Ratio (a); and von Mises versus Thickness (b)	271
Figure E.10. Von Mises stress in case 389 (a) and 471 (b) which have unusually high values presented as outliers	272
Figure E.11. Saddles have the largest negative relationship with perforation ratio (a); domes have the strongest negative relationship with thickness (b)	273
Figure E.12. Distribution of structural costs	274
Figure E.13. Scatter plots of total structural costs versus perforation ratio (a); and total structural costs versus thickness (b).....	274
Figure E.14. Structural cost the cases that have unusually high Total structural costs.....	275

Figure E.15. Saddles have the largest negative relationship with perforation ratio (a); Saddles have the strongest positive relationship with thickness (b)	276
Figure E.16. Distribution of spatial daylight autonomy	277
Figure E.17. Scatter plots of sDA versus perforation ratio (a); and sDA versus thickness (b).....	277
Figure E.18. As perforation ratio increases, the log odds of having a higher sDA increases (a); as thickness increases, the log odds of having higher sDA does not change significantly (b).....	278
Figure E.19. Distribution of total operating cost in thousands	279
Figure E.20. Scatter plots of total operating costs versus perforation ratio (a); and total operating costs versus thickness (b).....	279
Figure E.21. As perforation ratio increases, the log odds of having an operational costs higher than \$45 in thousands increases (a); as thickness increases, the odds of having a higher operational costs slightly decreases (b).....	280
Figure E.22. Distribution of total operating cost in thousands	281
Figure E.23. Scatter plots of deflection versus perforation ratio (a); and deflection versus thickness (b)	281
Figure E.24. Front and left elevation of four arbitrary cases that have high deflection.....	282
Figure E.25. The cases with high deflections exist among shells with a range of thickness and perforation ratios.....	282
Figure E.26. As perforation ratio increases, the log odds of having deformation higher than 1-meter decreases (a); as thickness increases, the log odds of having deformation higher than 1-meter decreases (b).....	284
Figure E.27. As perforation ratio increases, the log odds of having deformation between 0.45 and 1 m decreases (a); as thickness increases, the log odds of having deformation between 0.45 and 1 m decreases (b).....	284
Figure E.28. As perforation ratio increases, the log odds of having deformation between 0.3 and 0.45-meter decreases (a); as thickness increases, the log odds of having deformation between 0.3 and 0.45-meter decreases (b)	284
Figure E.29. Distribution of total operating cost in thousands	285
Figure E.30. Scatter plots of light oversupply versus Perforation ratio (a), and light oversupply versus thickness (b).....	285
Figure E.31. As perforation ratio increases, the log odds of having light-oversupply higher than 0.5 increases (a); as thickness increases, the log odds of having light oversupply does not change significantly (b).....	287
Figure E.32. As perforation ratio increases, the log odds of having light-oversupply higher than 0.5 increases (a); as thickness increases, the log odds of having light oversupply does not change significantly (b).....	287
Figure E.33. As perforation ratio increases, the log odds of having light oversupply higher than 0.5 increases (a); as thickness increases, the log odds of having light-oversupply does not change significantly (b).....	287
Figure E.34. Distribution of total energy costs per volume	288
Figure E.35. Scatter plots of total operational energy versus perforation ratio (a); and total operational energy versus thickness (b).....	288

Figure E.36. As perforation ratio increases, the log odds of having total energy higher than 800 MWh/m ³ increase (a); as thickness increases, the log odds of having total energy higher than 800 MWh/m ³ decreases (b)	290
Figure E.37. As perforation ratio increases, the log odds of having total energy between 600 and 800 MWh/m ³ increase (a); as thickness increases, the log odds of having total energy between 600 and 800 MWh/m ³ decreases (b)	290
Figure E.38. Plotting dependent variables against two dependent variables for each roof geometry.....	292
Figure F.1. The surface of the shell is subdivided into 9 zones, where each zone can be used for subtracting holes	293
Figure F.2. False color rendering of sDA for a dome with low curvature when different zones are subtracted	294
Figure F.3. Comparing sDA between a dome with a low curvature and high curvature	294
Figure F.4. Maximum total deflection in shells starting from 5 cm to 30 cm thickness in 5 cm increments	296

LIST OF TABLES

Table 2.1. Design characteristics	12
Table 3.1. Key design parameters that are considered in the design of shell structures	67
Table 3.2. Some performance criteria that is measured in the design of shell structures	67
Table 3.3. The structural performance criteria that are considered in this research study	67
Table 4.1. Daylight Factor (DF).....	97
Table 4.2. Daylight autonomy (DA) and annual sunlight exposure (ASE)	99
Table 4.3. Continuous daylight autonomy (DA _{con}) and maximum daylight autonomy (DA _{max})	100
Table 4.4. Useful daylight illuminance (UDI)	101
Table 4.5. Daylight availability.....	102
Table 4.6. Metrics for measuring illuminance on a horizontal plane.....	105
Table 4.7. Metrics for measuring glare	106
Table 4.8. Metrics for daylighting performance assessment.....	107
Table 5.1. Inefficiency of Perforation Ratio (PR) in describing the size of the openings	123
Table 5.2. Granularity can be used alongside perforation ratio for a more comprehensive analysis.....	123
Table 5.3. importance of considering bias as well as perforation ratio and granularity	124
Table 7.1. Constants and variables in the parametric model.....	157
Table 7.2. Design parameters.....	165
Table 7.3. Performance criteria in two disciplines.....	165
Table 7.4. Heat map summarizing the correlation between parameters and performance	167
Table 7.5. comparing dimensions and thickness of the first umbrellas built by candela.....	188
Table 7.6. Comparing daylighting performance of the built shell with the adjusted variations	189
Table 7.7. Structural performance assessment of a 12 by 12-m assembly.....	190
Table 7.8. Dimensions of the scaled-up hypars	191
Table 7.9. Structural performance comparison of 5 cm shell with its scaled-up versions	192
Table 7.10. Selected hypar iterations with various rise/area ratios that have matching performance	193
Table 7.11. Hypars' performance mapped onto shells generated with ParaGen to find matching shells .	195
Table 7.12. Comparing dimensions and thickness of the first umbrellas built by Isler	198
Table 7.13. Daylighting performance of the adjusted COOP warehouse	199
Table 7.14. Performance values for the COOP warehouse with adjusted dimensions of 50 by 60 meter	200
Table 7.15. Hypars' performance mapped onto ParaGen's generated shells to find matching shells	201
Table A.1. Global geometrical properties	218

Table A.2. Loading	218
Table A.3. Material Properties defining <i>concrete</i>	218
Table A.4. Global geometrical dimensions.....	219
Table A.5. Global geometrical properties	219
Table A.6. Local geometrical properties.....	219
Table A.7. Comparing Ansys simulation results with numerical calculations	220
Table A.8. Comparing Ansys simulation results with numerical calculations and Karamba results.....	221
Table A.9. Comparing Ansys results with numerical calculation with fixed supports	222
Table A.10. Comparing Ansys with Karamba results with fixed edges	223
Table A.11. Comparing Ansys with Karamba results for a plate with one hole.....	225
Table A.12. Comparing Ansys with Karamba results for a plate with four holes	226
Table A.13. Comparing Ansys with Karamba results for a plate with nine holes	227
Table A.14. Comparing Ansys with Karamba results for a solid dome.....	228
Table B.1. Material properties	235
Table B.2. Material properties inserted in Karamba with related units	235
Table C.1. Surface properties in DIVA.....	246
Table C.2. Daylighting settings	247
Table C.3. <i>Radiance parameters</i>	248
Table D.1. material settings for the energy analysis	256
Table D.2. Electricity and natural gas costs.....	262
Table E.1. Process of deriving independent variables (control variables)	263
Table E.2. Summary of independent variables (IV) or control variables	264
Table E.3. Summary of Dependent Variables (DV) or response variables in structural discipline	264
Table E.4. Summary of dependent variables (DV) or response variables in daylighting discipline.....	264
Table E.5. distribution of shell typologies in the trimmed population.....	265
Table E.6. Final distribution of shell typologies in the trimmed population	266
Table E.7. Dependent variable (DV-1) - weight.....	270
Table E.8. Dependent Variable (DV-3) – von Mises Stress	273
Table E.9. Dependent variable (DV-4) – structural costs	276
Table E.10. Dependent Variable (DV-5) – Spatial Daylight Autonomy	278
Table E.11. Dependent Variable (DV-8) – total operating costs	280
Table E.12. Dependent Variable (DV-2) – deflections.....	283
Table E.13. Dependent Variable (DV-6) – light oversupply	286
Table E.14. Dependent variable (DV-7) – total energy	289
Table E.15. Heat map summarizing the correlation between parameters and performance	291

Table F.1. Comparing performance of four samples from the Solution space	295
Table F.2. Abstract Morphology A simulated with different thicknesses	296
Table F.3. Hypar shells with 45-meter rise, simulated using two thicknesses.....	297

LIST OF APPENDICES

Appendix A: Structural validation of Karamba with ANSYS and numerical calculations	218
Appendix B: Structural settings and analysis criteria in Karamba	232
Appendix C: Daylighting settings in DIVA	246
Appendix D: Energy settings in ARCHSIM.....	252
Appendix E: Statistical analysis	263
Appendix F: Case study validation and results	293

ABBREVIATIONS

AEC	Architecture, Engineering, and Construction
ASE	Annual Sunlight Exposure
BIM	Building Information Modeling
CAD	Computer Aided Design
CAM	Computer Aided Manufacturing
DA	Daylight Autonomy
DF	Daylight Factor
DGP	Daylight Glare Probability
DGR	Daylight Glare Rating
D.L.	Dead load
DOE	U.S. Department of Energy
FEM	Finite Element Method
GA	Genetic Algorithms
GC	Generative Component
IESNA	Illuminating Engineering Society of North America
LEED	Leadership in Energy & Environmental Design
L.L.	Live Load
MADM	Multi-Attribute Decision Making
MDA	Multidisciplinary Desig and Analysis
MDO	Multidisciplinary Design Optimization
MLA	Machine Learning Algorithms
NURBS	Non-Uniform Rational Bezier Spline
UDI	Useful Daylight Illuminance
USGBC	U.S. Green Building Council
RIBA	Royal British Institute of Architects
sDA	Spatial Daylight Autonomy
SHGC	Solar Heat Gain Coefficient

ABSTRACT

With the advancement of computational design tools paired with performance assessment technologies, taking an interdisciplinary design approach at the early stages of design is largely facilitated. The Master Builder whose role has been fragmented between multiple professionals of many disciplines is being recreated, this time by facilitating seamless collaboration among a plethora of minds and perspectives. In this mode of collaboration, studying disciplinary tradeoffs also becomes part of the design process. This calls for a new design approach with an understanding of other disciplines.

A building needs to stand up and needs to be illuminated, thus the structural and daylighting disciplines are associated with the purpose of architectural design. Despite the interaction between the two, there is little research showing the overlaps. Understanding this integration helps designers better understand how making a decision affects other stakeholders. This dissertation is at the intersection of computational design, structural performance, and daylighting performance assessment. Shells are the ideal typology for investigating this interrelation as their form is related with force flow, while adding holes to the shell's surface not only introduces daylight but also affects force flow thus structural performance. By employing a computational interdisciplinary design approach, and by choosing perforated concrete shell structures as the main structural typology, I ask:

How can the designer identify the design parameters that are shared between the discipline of architecture and an engineering discipline?

What are the design *parameters* that co-exist in the structural and daylighting design disciplines? How may these parameters be used by designers? How do the design *parameters* affect *performance* in structural and daylighting discipline? What is the tradeoff between performance in structural and daylighting design?

How can the results of a specific design case be useful for application to other design cases that do not necessarily have the same boundary conditions?

This research demonstrates how daylighting performance can be affected in the design of shell structures, a typology that is mainly driven by its structural design criteria in the literature. Also important is its demonstration of how a continuous shell can be perforated to the point at which becomes a grid shell; therefore, continuous and grid shells are two ends of a spectrum rather than two distinct structural typologies. A high-level significance of this dissertation is its marriage of the structural and daylighting disciplines and demonstration of how the two are closely related in shells by the perforation ratio. I find that perforation ratio is the most significant parameter that affects both disciplines and a number between 10% to 20% is the recommended limit for shell structures when translucent glazing is installed without any external or internal shading.

One of the most significant contributions of this research is its methodological approach, which uses a formalized framework for categorizing design parameters in the structural and daylighting disciplines and then identifying overlapping design parameters. This *design method*, presented as a roadmap is the fundamental new component arising from this research.

The final contribution of this dissertation explores how a generated solution space may become useful for other design projects which do not necessarily have the exact same boundary conditions. By abstracting the boundary conditions of new projects to match those in the solution space, the designer can examine possibilities and compare how making a decision in one field may affect performance in other fields.

Chapter 1 :

Introduction

“It is not the strongest or the most intelligent who will survive but those who can best manage change.”

-Charles Darwin

1.1 Background of the study

With the advancement of emergent computational design tools and technologies in architecture fields such as Computer Aided Design (CAD) and Building Information Modeling (BIM), design is taking new forms. Parametric design methods are widely used, and when paired with performance assessed through simulations, offer new avenues for design. Design thinking is particularly important in the early stages of the design process, where decisions will have a great impact on performance in multiple disciplines downstream. Therefore, taking an interdisciplinary performance-based approach in the early stages of the design process is widely encouraged and facilitated by new tools and technologies. The role of Master Builder, which has been fragmented between multiple professionals of many disciplines, is being recreated, this time by facilitating seamless collaboration among a plethora of minds and perspectives. In this mode of collaboration, studying disciplinary tradeoffs also becomes part of the design process. This calls for an understanding of other disciplines, different from the siloed design approach that was previously practiced.

From another point of view, computational approaches such as genetic algorithms (GA) and machine learning algorithms (MLA) offer new approaches to architectural design, aimed at creating design spaces filled with hundreds of alternative forms paired with data, ready to be explored. In this era, a data-driven design approach is becoming widespread.

The amalgam of the two paradigms in today’s design approach, fueled by the rapid development of computational tools by software companies such as Autodesk and McNeel, and reinvented design workflows in architectural design by firms such as Foster and Partners, SOM, and Shop Architects, has accelerated implementation of new design approaches. The new wave of

design has already reached architecture, albeit in a non-homogeneous way, and designers had better embrace it as it is the future of practice.

1.2 Statement of the problem

A building needs to stand up and needs to be illuminated; thus, the structural and daylighting disciplines are associated with the most fundamental purposes of architectural design. To create an effective building design, the designer needs to consider the interaction between disciplines, where making a decision in one field affects the other (Forest Flager & Haymaker, 2007). Previous researchers have mainly clustered climate-related issues such as heating, cooling, daylighting, and ventilation (Echenagucia, Capozzoli, Cascone, & Sassone, 2015; Galasiu & Veitch, 2006; Gerber & Lin, 2013; Lin, 2014; Palonen, Hamdy, & Hasan, 2013; Reinhart & Selkowitz, 2006), or structure-related issues such as structural topology, shape, sizing, and material design (F. Flager, Adya, Haymaker, & Fischer, 2014). However, consideration of multiple disciplines and their interaction is uncommon, which is key for an inclusive interdisciplinary design approach, which is not common. Moreover, there is currently no formalized method for integrating multiple disciplines to create an interdisciplinary design approach in architecture.

My research philosophy situates my work in opposition to the segregation of professions in the building industry. I believe that employing an interdisciplinary approach in design is an important part of the future of architecture. Therefore, taking a step toward better understanding the overlaps between disciplines, and formalizing the process of integration between disciplines accelerates progress in the field. My research hypothesis is that:

- The structural and daylighting disciplines can be integrated with each other through their common *design parameters*.
- The structural and daylighting *performance* should play an active role as a design driver, rather than considered and designed as independent components, since they could all influence each other.
- There needs to be integrated considerations in building design since one disciplines can affect the other, conducted interactively, resulting in certain trade offs in arriving at the final solution. It is the job of the designer to make the necessary value judgments on the trade offs which cannot always been objectified; rather is an evaluation that might include other factors such as costs, aesthetics, time, etc.

In examining an interdisciplinary design approach using computational design and simulation tools, while considering shell structures as a special case, specifically for spanning large-span roofs, I ask:

Research question a: How can the designer identify the design parameters that are shared between the discipline of architecture and an engineering discipline?

Research question b: What are the design *parameters* that co-exist in the structural and daylighting design disciplines? How may these parameters be used by designers? How do the design *parameters* affect *performance* in structural and daylighting discipline? What is the tradeoff between performance in structural and daylighting design?

Research question c: How can the results of a specific design case be useful for application to other design cases that do not necessarily have the same boundary conditions?

I believe this is an excellent time to examine the above-mentioned questions for three reasons: First, technological developments have come to a point where software companies such as Autodesk and Flux focus their efforts on developing computational tools and workflows that advance disciplinary and multidisciplinary collaborations. This is key in putting various disciplinary minds back together to recreate the fragmented Master Builder. Second, architects are increasingly using computational techniques in the process of design and thus have a deeper understanding of such tools and processes and an increased level of skill in using these platforms. Third, the profession is coming to value integrated interdisciplinary practices. As an example, the U.S. Green Building Council (USGBC) advocates for an integrated design approach through its Leadership in Energy & Environmental Design (LEED) certificate towards enhancing sustainability.

1.3 Research objectives

This research considers the application of parametric design methods at the early stages of design of high-performance buildings. Looking at high-performance building design using parametric modeling through an interdisciplinary design lens, it becomes clear that the design parameters that affect performance in multiple disciplines need to be embedded within the model. Implementing design parameters calls for an understanding of first, the ways in which parameters

affect performance; and second, a gradual increase in the level of detail in each discipline during the process of design. Structure and daylighting are the two main disciplines that are emphasized (among many possible choices) because of their key roles in realizing a building and making a space habitable. Thus, their interconnections will be examined in depth in the context of roof systems.

Shell structures for covering large-span roof systems are selected as the subject of study. The design of shells is closely integrated with their structural performance. In fact, form plays a significant role in the design of shells and determines whether a thin shell will be stable, safe, and sufficiently stiff. The foremost shell designers consider force flow when designing the form, to arrive at the best-performing alternative. On the other hand, shells provide various opportunities for introducing daylight to the space. Continuous shells can be perforated, and discrete shells can potentially introduce abundant light through the openings within the grids. The surface of shells can even be designed in a way that reduces direct radiation.

This research focuses on how creating perforations in the shell surface affects structural force flow and performance, as well as the amount of daylight that is brought into the space, to better understand the tradeoffs. Adding perforations to the continuous surface of a shell affects the force flow in the shell. In grid shells, however, force flow depends on the grid layout. On the other hand, daylighting performance is directly affected by adding perforations to a continuous shell, whereas changing the grid layout of a grid shell does not have a significant effect on its daylighting performance.

CAD modeling tools enable more designers to create free-form shells. Advanced manufacturing techniques such as using fabric formwork (West, 2017) have opened new doors in building shells with decreased formwork expenses. Therefore, shell structures are chosen as a model for studying the integration of disciplines at the early stages of design using computational design tools.

The main objectives of this research are:

Objective a-1: To formalize an interdisciplinary design approach regarding structural and daylighting disciplines. To this end, the design parameters that are relevant in both disciplines, as well those that are limited to affecting performance in only one discipline, are identified. Then, a design approach in which common design parameters are implemented in the model is proposed.

Objective a-2: To rationalize how the overlapping design parameters in engineering disciplines can be translated into architectural design parameters to be implemented in architectural models. This includes analyzing the design space that will be created, as well as the opportunities and restrictions offered by the resulting parametric model.

Objective b-1: To understand how the design parameters in shells affect performance across multiple disciplines.

Objective b-2: To study shells as an integrated design problem, by exploring how continuous and grid shells are related.

Objective c: To consider other perforated shell structures and try to map them on to the generated solution space. Investigate the effects of abstracting and changing the boundary conditions and determine how effective the resulting comparisons are.

This research has implications for interdisciplinary design approaches in the Architecture, Engineering, and Construction (AEC) industry. This dissertation demonstrates how the formalized methodological approach it puts forward can help differentiate the design parameters bound to one discipline from the design parameters that affect performance in multiple disciplines. It offers a roadmap for integrating structural and daylighting design with architecture at the early stages of design.

1.4 Organization of the dissertation

This chapter, Chapter 1, is the introduction, where the problem statement, research objective, and the organization of the dissertation are explained.

Chapter 2 discusses the key elements of the title of the dissertation. After discussing the importance of the early stages of design, the sense of *parameter* used in parametric design is discussed. Next, the paradigm of *performance* in performance-oriented design is introduced. Afterwards, building envelopes are discussed, and roof systems are introduced as a special case of building envelopes. This is followed by a discussion of the importance of structural and daylighting disciplines in the design of large-span roof systems.

Chapter 3 focuses on shell structures and first reviews the design history of perforated concrete shell structures. Afterwards, the topics of topology, shape, and sizing are discussed, and a categorization is reproduced in the context of continuous and grid shell structures. This

classification, and the detailed attributes, set the ground for linking each structural design phase to one or multiple design strategies from another discipline—in this case, daylighting design. Two key performance criteria will be measured: serviceability criteria, including maximum allowable deflection, and strength criteria, including allowable von Mises stress levels. The alternatives that meet these criteria are considered design proposals that can later be checked for other features, such as buckling behavior.

Chapter 4 focuses on daylighting through roof skylights and examines the different levels at which light hits a building enclosure and can be controlled. The outcome of this section is a classification of various levels of daylight control, which sets the ground for linking each daylighting design strategy to one or multiple design strategies from other disciplines, in this case, the discipline of structural design. The second section of the chapter introduces different metrics that are employed to measure the daylighting performance of space. The metrics for measuring illuminance on a horizontal plane as well as glare are studied. Measurement of daylighting availability and visual comfort is accomplished according to metrics in three overall performance categories, expressed as daylight availability, visual comfort, and thermal loads (Reinhart & Wienold, 2011); the lighting, heating, and cooling energy loads for a space are all relevant.

Chapter 5 starts with discussion of the notion of integrated design in architecture. The structural design classification diagram from Chapter 3, along with the daylighting classification diagram from Chapter 4 are carried over to this chapter to examine the overlaps of these two disciplines. This leads to isolation of the design parameters that simultaneously affect both disciplines, with the end of linking the two disciplines for an interdisciplinary design approach. After linking the design parameters, a hypothetical design space for shells is conceptualized. In addition, two design parameters, namely *granularity* and *bias*, are proposed.

Chapter 6 discusses a methodology for conducting research which is built on the foundation of the previous chapters. It first introduces the differentiation between optimization and optioneering. Next, the ParaGen computational framework is introduced, followed by the research methodology for implementing an integrated design approach using parametric and simulation tools for perforated concrete shell structures.

Chapter 7 first discusses the parametric model of the shell that is used for creating a database of shell structures associated with their structural and daylighting performance. It should be noted that the space that the roof is covering is set to be a hypothetical courtyard where the surrounding

walls are adiabatic and opaque, and the roof is the only possibility of admitting daylight into the space. The target required light level of 300 lux on the horizontal plane is set as the lighting level for the courtyard. Next, it discusses the results of the statistical analysis regarding the sensitivity of performance criteria to design parameters. Finally, different shell structures can potentially be mapped onto this design space. Two case studies of built perforated shell structures are computationally modeled and simulated to be mapped onto the ParaGen’s solution space.

Chapter 8 summarizes the study and results, discussing the future possible routes that can stem from this research study.

The organization of the dissertation is illustrated in Figure 1.1.

Chapter 02: Background	Parameter Performance Large-span roofs		
Chapter 03: Shell structures as large-span roof systems	Structural design by: Topology Shape Sizing	Chapter 04: Daylighting in large-span roof systems	Daylight control at: Geometry level Glazing level Interior level
Chapter 05: Parameters	Find common design parameters Propose Granularity and Bias design parameters Arrive at the shell conceptual design space axis		
Chapter 06: Methodology	Optioneering ParaGen computational framework		
Chapter 07: Case study and results	Result of statistical analysis Case study 01: High Life Textile Factory Case study 02: COOP Warehouse		
Chapter 08: Conclusions	Conclusions Future work		

Figure 1.1. The outline of this dissertation

1.5 References

Echenagucia, T. M., Capozzoli, A., Cascone, Y., & Sassone, M. (2015). The early design stage of a building envelope: Multi-objective search through heating, cooling and lighting energy performance analysis. *Applied Energy*, 154, 577–591. <https://doi.org/10.1016/j.apenergy.2015.04.090>

- Flager, F., Adya, A., Haymaker, J., & Fischer, M. (2014). A Bi-level method for shape and member sizing optimization of frame structures. *Computer and Structures*, 1–11. <https://doi.org/10.1016/j.compstruc.2013.10.004>
- Flager, F., & Haymaker, J. (2007). A comparison of multidisciplinary design, analysis and optimization processes in the building construction and aerospace industries. In *24th international conference on Information technology in construction* (pp. 625–630).
- Galasiu, A. D., & Veitch, J. a. (2006). Occupant preferences and satisfaction with the luminous environment and control systems in daylight offices: a literature review. *Energy and Buildings*, 38(7), 728–742. <https://doi.org/10.1016/j.enbuild.2006.03.001>
- Gerber, D. J., & Lin, S.-H. (2013). Geometric complexity and energy simulation. In *Open Systems: Proceedings of the 18th International Conference on Computer-Aided Architectural Design Research in Asia (CAARDIA)* (pp. 87–96). Hong Kong.
- Lin, S. E. (2014). *Designing-in Performance: Energy simulation feedback for early stage design decision making*. University of Southern California.
- Palonen, M., Hamdy, M., & Hasan, A. (2013). MOBO A New Software for Multi-Objective Building Performance Optimization. *13th Conference of International Building Performance Simulation Association*, 2567–2574.
- Reinhart, C., & Selkowitz, S. (2006). Daylighting—Light, form, and people. *Energy and Buildings*, 38(7), 715–717. <https://doi.org/10.1016/j.enbuild.2006.03.005>
- Reinhart, C., & Wienold, J. (2011). The daylighting dashboard - A simulation-based design analysis for daylight spaces. *Building and Environment*, 46(2), 386–396. <https://doi.org/10.1016/j.buildenv.2010.08.001>
- West, M. (2017). *The fabric formwork book : methods for building new architectural and structural forms in concrete*. London: Routledge, Taylor & Francis Group.

Chapter 2 :

Background

“When a problem is properly stated, in our epoch, it inevitably finds its solution.”

-Le Corbusier, *Towards a new architecture*, 1927, p. 102

2.1 Introduction

Researchers and designers have attempted to define the elements of design. points out that design is a journey characterized by ever-changing representations. He states that “design is not simply a leap into a premeditated solution but rather a messy journey necessitated by uncertainty and characterized by iteration” (Davis 2013, p. 3). He then emphasizes iteration, exploration, and reflection as the routes through which the problem becomes known. (Hudson, 2010, p. 133) focuses on problem definition, considering the process of problem description “as a series of knowledge acquisition steps”. He also emphasizes that “iteration” is an important strategy in design. These are only two recent examinations of the design process, built on a large body of literature. This section delves deep into inspecting three main characteristics of the design process revolving around its iterative nature, including:

- Design as a wicked problem with no definite formulation
- A satisfying solution can be proposed for a wicked problem
- The problem formulation can be changed in light of the solution

Many researchers have characterized design as an *ill-defined* or *wicked problem*. Ill-defined design problems are unlike typical engineering problems. (Rittel & Webber, 1973) in their paper *Dilemmas in a General Theory of Planning* characterize the problems that scientists and engineers focus upon as “tame” or “benign” problems with a clear mission, as opposed to planning problems as “ill-defined” or “wicked problems.” Every wicked problem is essentially unique, and there is no definitive formulation for it. Thus, wicked problems are formulated differently by different people based on their understanding of the problem. There is no stopping rule for a wicked problem, and the value of a solution is not true-or-false but rather good-or-bad. (Rittel & Webber,

1973). (Holzer, 2009, p. 27) points out that “dealing with uncertainty is one of the biggest challenges designers and consultants are faced with during the schematic and conceptual design stages.” This highlights *uncertainty* in design formulation, especially at the early phases of design in which the design space is not well bounded. Another researcher mentions that the certainty of an externally structured problem cannot be tracked in design; the designer needs to define, redefine and change the design problem in light of the solution that emerges to cope with an ill-defined problem (Cross, 2006). Not only does this illustrate the *iterative* nature of design, but also points out the ever-changing nature of problem formulation in the process.

When the notion of design as a wicked problem is accepted, problem formulation becomes a key factor. Different designers formulate the same problem differently, partly based on their varying levels of knowledge. Knowledge is the underlying driver of design. Pulsifer (2014) relates tacit and explicit knowledge to design activities. She illustrates the level of tacit and explicit reasoning applied during Ad Hoc,¹ core and non-core design activities (Pulsifer, 2014). However, since design problems vary case by case, there cannot be explicit knowledge about individual cases of design problems.

Kruger & Cross (2006) identify four design strategies utilized by designers, including problem-driven design, solution-driven design, information-driven design, and knowledge-driven design strategy. They define problem-driven design as a method in which the “designer focuses closely on the problem at hand and only uses information and knowledge that is strictly needed to solve the problem” (p. 534). On the other hand, they describe solution-driven design strategy as a method in which “the emphasis lies on generating solutions and little time is spent on defining the problem, which may be reframed to suite an emerging solution” (Kruger & Cross, 2006, p. 534). In other words, in a solution-driven strategy, more time is spent on solution generation and evaluation. Information-driven design refers to a situation where the designer focuses on gathering information from external sources. Finally, knowledge-driven strategy focuses on developing a solution based on using designer’s prior personal knowledge. Kruger & Cross (2006) express that “designers using a solution-driven strategy tend to have lower overall solution quality scores but higher creativity scores. Designers using a problem-driven design strategy tend to produce the best results in terms of the balance of both overall solution quality and creativity” (p. 527).

¹ Ad hoc is a Latin phrase meaning *for this*. It generally signifies a solution designed for a specific problem or task that is non-generalizable, and not intended to be adaptable to other purposes.

The use of parametric modeling tools is one of multiple ways of implementing iterative design. They offer a problem-driven design approach, as formulation of the parametric model is a problem-driven design activity. In fact, the implementation of the parameters in the model focuses on the problem and affects how it is defined. Once the parametric model is created, an array of possible design solutions can be generated and evaluated; thus, an opportunity for solution-based design approach is created.

More than two decades after Rittel and Webber referred to design as a wicked problem, researchers began to focus on solutions that can be proposed in response to these problems. A researcher refers to decision methods looking for a good solution for an ill-defined problem as “satisficing” (Simon, 1969). He reports, “since there did not seem to be any word in English for decision methods that look for good or satisfying solutions instead of optimal ones, some years ago I introduced the term satisfying to refer to such procedures” (p. 132).

Satisfaction derived from a design solution can be based on many factors, including but not limited to aesthetics, economics, environmental performance or choice of materials. Focusing on performance in its general meaning, it is important to note that it is particularly significant in architecture. The solution to an architectural design problem must fulfill a set of performance criteria which are implicitly or explicitly expressed. It also needs to be realized using building materials and structural systems. For instance, it is implicitly required that a building withstand external loads and provide safety for its residents. It might also be explicitly mentioned that a building needs to have a certain mass, a predefined façade material, meet an energy performance goal, or provide a defined level of daylight availability. Formulating design and then arriving at satisfying solutions is related to the defined goals for a project. In any case, the design process is iterative, and the design problem may be redefined in the light of initial solutions, leading to the emergence of better solutions.

Design exploration is an important part of the iterative design process, not only to arrive at satisfying solutions, but to facilitate creativity. Peter von Buelow counts three main characteristics for design activity, namely *purposeful*, *goal oriented* and *creative* (von Buelow, 2007). Nigel Cross (2006) points out that “the designer sets off to explore, to discover something new, rather than to return with yet another example of the already familiar” (Cross, 2006, p. 32). This points to *exploration* as an activity that aims toward incorporating *creativity* in design. Computational design tools and evolutionary search algorithms can support the search and exploration process.

I have identified the design practices that correspond with the aforementioned design characteristics. To address the wicked nature of architectural design problems, *parametric modeling* can be applied to loosely formulate the design problem facilitating iteration. To find satisfying solutions, *performance assessment* can be implemented to measure the performance of solutions quantitatively to test if they meet the criteria. This is also in line with the *goal-oriented* characteristic of design. Finally, exploration of the design space with the aid of computational methods can be used to shed light on possible solutions, leading to better understanding of the problem. This may lead to arrival at a satisfying solution, reformulation of the problem, or an informed decision. These components are summarized in Table 2.1.

Table 2.1. Design characteristics

	<i>Facilitate by</i>	<i>Allows</i>
<i>Design is a wicked problem</i>	Parametric modeling	Iteration
<i>Design solution can be satisfying</i>	Performance assessment	Goal orientation
<i>Design formulation can change in the light of solution by exploring the solution pool</i>	Computation and evolutionary algorithms	Exploration to understand the problem, redefine it, and make informed decisions

After the brief introduction of design problems in architecture, their key elements, and the associated challenges, the ground is set to introduce various design paradigms and methodologies that are proposed to address the challenges.

This chapter provides background on the early stages of design and its importance in designing high-performance buildings. It then touches on the key elements of the dissertation title, starting with *parameter* by providing a background on algorithmic and parametric design, along with the associated opportunities and limitations. It then touches on *performance*, introducing the concept of performance-oriented design. Afterward, it discusses building envelopes and large-span roof systems in architecture as the use-case to which the dissertation’s framework will be applied. Finally, it discusses the significance of structural and daylighting disciplines to be considered at the early stages of design. While the overall scope of the dissertation is defined in this chapter, Chapters 3 and 4 are built on its elements and dig deeper in discussing the structural and daylighting design principles, with a focus on shell structures used as roof systems. In Chapter 5, integrated design is highlighted, and the parameters and performance criteria of the two disciplines are meshed together. Chapter 6 discusses the methodology for conducting the study, while Chapter 7 discusses case study evaluations. Chapter 8 discusses the results and describes future work.

2.2 Brief introduction to BIM and others

Any design process has phases with increasing levels of detail. The Royal Institute of British Architects (RIBA) defines the key stages in the Architecture, Engineering and Construction (AEC) industry (Figure 2.1). The RIBA Plan of Work in 2013 includes eight stages, defined as Strategic Definition, Preparation and Brief, Concept Design, Developed Design, Technical Design, Construction, Handover and Close Out, and finally, the In Use stage (RIBA, 2013).



Figure 2.1. RIBA Plan of Work (RIBA, 2013)

Dominik Holzer refers to the 0 to 4 stages of RIBA’s classification, including feasibility studies, conceptual design, and design development as the *early design stages* (Holzer, 2009). Echenagucia (2013) points out that design goes from an *exploratory* phase to *development* phase and finally a *definition* phase. It should be noted that the design process is not linear as the RIBA diagram may suggest. Rather, it is iterative and circular, where the data from one stage is looped back into its previous stage while the design is being refined (Figure 2.2).

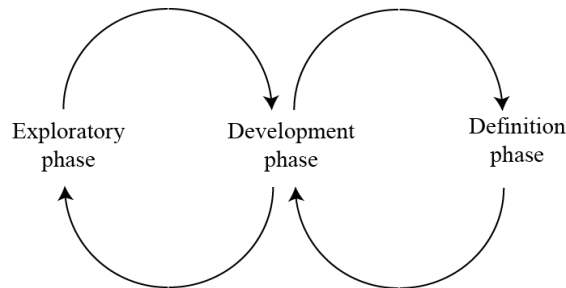


Figure 2.2. Design phases as an iterative loop

Boyd Paulson Jr. was probably the first to illustrate the relation between design stages and their “level of influence” in the context of engineering design, construction and operation costs (Paulson Jr., 1976). Looking at Figure 2.3 and by adopting the term “level of influence,” Paulson describes the upper portion of his plot illustrating two main curves: “The curve ascending to the right-hand ordinate tracks cumulative project expenditures and the curve descending from the left-hand ordinate shows the decreasing level of influence” (Paulson Jr., 1976, p. 588). He argues that in the early phases of a project, the relative expenditures are small compared to the amount spent on the

project as a whole; however, “decisions and commitments made during that period have orders of magnitude greater influence on what later expenditures will actually be” (Paulson Jr., 1976, p. 588).

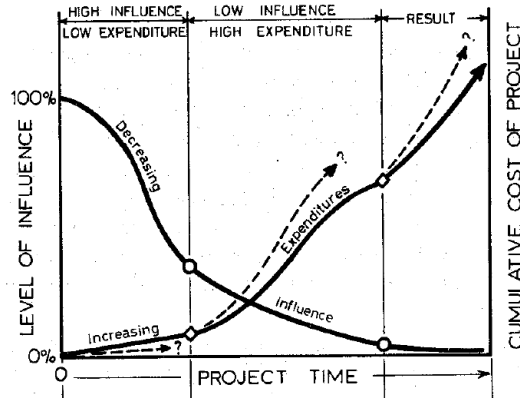


Figure 2.3. Level of influence on project costs (Paulson Jr., 1976)

Although this graph is widely cited in the literature, quantitative data in the literature confirms its accuracy. I consider it a graphic representation that demonstrates the importance of the early design stages. Looking at the graph presented in Figure 2.3, it can be seen that the potential for design improvement early on is huge, while in the later stages of design, changes are small and limited in scope, and associated with high costs. According to some authors, this implies that experienced designers tend to explore in breadth first and only later in depth (El-khaldi & Woodbury, 2015).

According to a researcher, “[Charles M.] Eastman has investigated building representations in a holistic manner from a computer scientist and a cognitive perspective since 1970” (Holzer, 2009, p. 18). Many of the findings arising from his research have influenced the *Building Smart* movement that promotes Building Information Modeling (BIM). BIM has been developed by Charles M. Eastman inspired by object-programming languages in computer science. “Eastman proposes an object-oriented framework linking geometrical data of building components to semantic information, relevant during construction, facility management and operation” (Holzer, 2009, p. 85). Following the BIM movement, MacLeamy introduces the “effort curve” in different stages of design (Figure 2.4). His two-dimensional graph maps design effort as a function of time, considering various phases of design. He advocates shifting the peak effort of the design phase to an earlier stage of the project, where decisions have the most impact and the lowest associated costs. He believes that BIM software makes this shift possible.

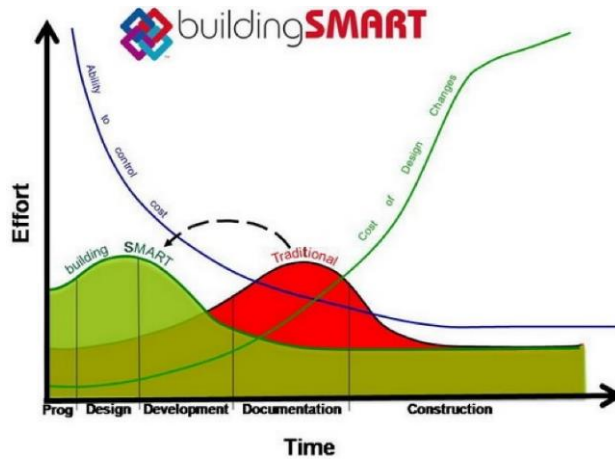


Figure 2.4. Shifting effort in the effort curve introduced by MacLeamy (Charmaine, 2011)

Pentilla (2007), however, offers a critical view on the possibility of applying BIM methodology in the early design phases, although its capabilities are unquestioned in terms of their usefulness in the advanced design stages. Pentilla feels that the BIM concept is a promising data exchange method which enables wide cross-platform interaction as well as life-long data management. Therefore, Pentilla sees BIM as a method to be used when interactive data exchange is required in later project phases. However, he scrutinizes whether object-oriented methodology assists architects in managing design formation during the early stages of design where the most important design ideas are created (Pentilla, 2007).

Davis (2013) proposes a rationale presented by a graph influenced by both Paulson’s influence curve and MacLeamy’s effort curve (Figure 2.5). He suggests that rather than shifting design effort relative to the cost of change (as MacLeamy suggests), it may be possible to shift the cost of change relative to design effort. He suggests that “parametric models can potentially lower the cost of design change, allowing designers to defer key decisions until later in the project, by which point they are likely to understand the decision’s design consequence better” (Davis, 2013, p. 208).

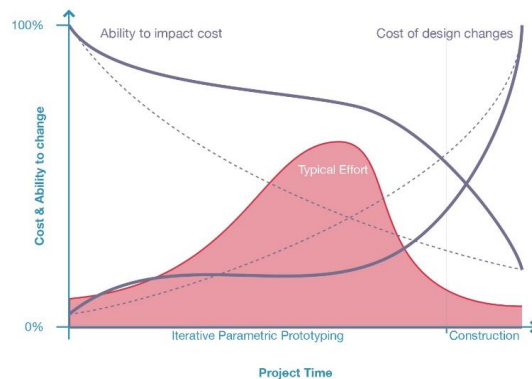


Figure 2.5. Davis introduces an alternative to Paulson and MacLeamy’s curve (Davis, 2013)

Reviewing this body of literature, it is clear that the design phase in architecture is crucial, as decisions made at that stage strongly influence the outcome downstream. In the early stages of design, the design space is much larger and thus, so is the amount of information considered. Investing time and energy in exploring different design scenarios in this phase leads to better-informed decisions, ultimately improving the outcome. In the final stages of design, the field of possible solutions is very small, and the cost of making changes at this stage is very high compared to the early design stage. Parametric design provides the opportunity to explore the entire design space in the early stages of design, while allowing the cost of changes to remain low even at later stages of the project while reducing the cost of change until later in the project.

The next section reviews algorithmic design as an overarching method in parametric design. It then focuses on parametric design and addresses some limitations associated with its implementation in architecture.

2.3 Parametric design, its implementation in architecture, and its limitations

Generative design system is an overarching term that embraces several design systems, one of which is parametric design. Generative systems allow regeneration instead of recreation, an important feature, since “creation requires constructing elements from the ground up every time a new result is needed” (El-Khalidi, 2007). Generative design is a process in which the output is generated by a set of rules. Hudson (2010) defines design as a task that involves defining a description of problem, then generating alternatives, and finally searching among alternatives to find a solution(s) that solves the initial problem. Generative design is discussed in depth, followed by a section discussing parametric design.

2.3.1 Generative design

El-Khalidi (2007) developed a provisional taxonomy of generative systems (Figure 2.6). In his taxonomy, algorithmic systems resemble the core of all generative systems and are the basic component on top of which other systems are built. He defines algorithms as “a set of instructions to achieve a certain goal” (El-Khalidi, 2007, p. 32). Algorithmic thinking can help designers define their goals better by breaking the design process into discrete tasks. His taxonomy shows various layers of properties related to six generative systems, namely *algorithms*, *parametric*, *l-systems*, *cellular Automata*, *fractals* and *shape grammars*.

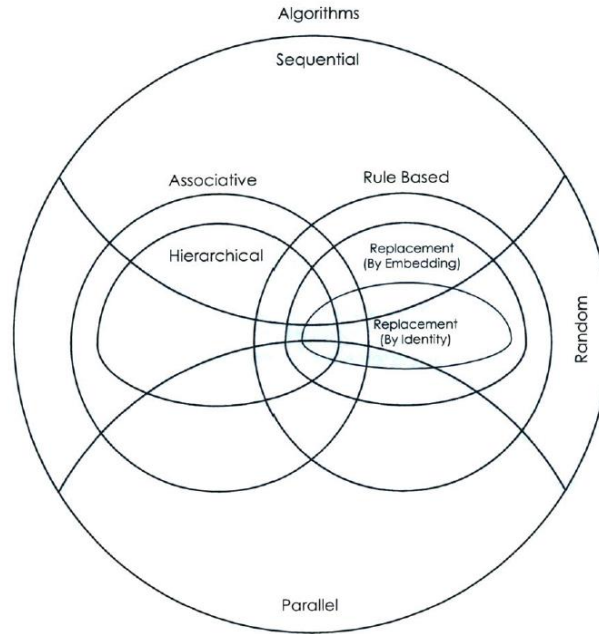


Figure 2.6. Various layers of properties related to six generative systems, (El-Khaldi, 2007)

To arrive at the taxonomy, El-Khaldi first categorizes the different modes of running any algorithmic systems, which may be in a parallel,² sequential,³ and/or a random fashion. This categorization can be excluded from the taxonomy, to focus more on different generative systems rather than how they run. Therefore, the running-modes for algorithms are excluded from the graphs that are adapted from El-Khaldi’s taxonomy.

El-Khaldi (2007) then adds a layer describing two broad algorithms, *associative* and *rule-based* (Figure 2.7a). Associative systems include associations and relationships such as linking parameters to one another, or an action to a series of actions.⁴ In rule-based systems, on the other hand, an “if...then” statement is expressed.⁵ A fine class of systems exists in the interaction of associative and rule-based systems, representing the systems in which parameters are related to one another, and there are some rules leading the design generation. He then categorizes hierarchical systems as a special case of an associative system (drawn within the associative

² Parallel refers to “simultaneous performance of operations,” a computing method where different sets of information are processed at the same time without affecting one another.

³ Sequential refers to “computing performed or used in sequence,” a computing method where a predecessor affects its successor (El-Khaldi, 2007, p. 28)

⁴ Regarding associativity, there are two types of associations: one-directional and bi-directional. “The first allows for data to flow from top to bottom only, what is known as a parent-child relationship. The second allows for data to flow both ways, where the change of one side will update the other.” (El-Khaldi, 2007, p. 45)

⁵ A rule is best described as a condition that should be matched before task is triggered, and rule-based systems include functions that only work if a defined condition is matched.

system boundary), and replacement systems⁶ within the boundary of rule-based systems (Figure 2.7b).

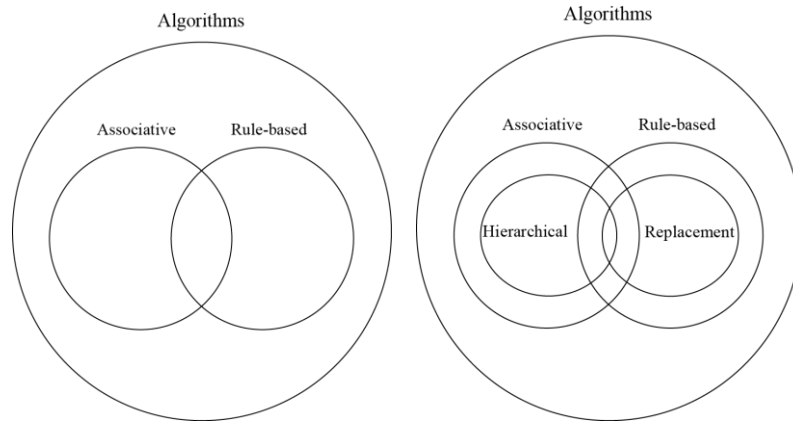


Figure 2.7. Associative and rule-based generative systems (a); Hierarchical and replacement systems (b), after (El-Khalidi, 2007)

Parametric design is situated in the context of algorithmic design, and the main two concepts that it is built around are *associativity* and *inheritance by hierarchy*. In El-Khalidi’s taxonomy, parametric design exists in the associative zone where elements and behaviors are driven by relationships. Parametric models are hierarchical, as he points out: “parametric systems are hierarchical-algorithmic systems controlled by one-directional associations” (El-Khalidi, 2007, p. 52). In hierarchical systems, a certain ranking exists in the organization of elements within the system. Inheritance also exists in hierarchical systems, which can be described using a parent and child analogy: a hierarchy allows for inheritance, as every child receives properties of its parents, and changes in parents ripple through the children. Hierarchic systems only allow for one-directional associations where *parents* drive *children* and not vice-versa. Studying parametric systems is the scope of this research, as described in the next section.

2.3.2 Parametric design

The notion of parametric design is that the designer establishes the relationships through which parts connect and edits these relationships by observing and selecting from among the results that

⁶ Replacement rules includes a left side (input), an operation (algorithm) and a right side (output) in order to define a condition to match, then a description of task, and finally the result, which replaces the element. l-systems, cellular automata, fractals and shape grammar are placed in the “replacement rule-based algorithm” zone, since they work by replacement rules.

are produced.⁷ Parametric models are dynamic, meaning that they can be constantly changed to answer *what if?* questions. However, they come at the cost of considering an additional phase in the broader design process, namely defining relationships, which is a *complex act of thinking*. This cost may have a benefit, though, extending the intellectual scope of design via requisite modes of thought and requiring the explicit representation of ideas (Woodbury, 2010).

There are some definitions for parameter and parametric design that vary according to the tasks involved in the process. Hudson (2010) defines a parameter as “any measurable factor that defines a system or determines its limits” (p. 21). He then defines parametric design as “a process where a description of a problem is created using variables. By changing the variables, a range of alternative solutions can be created, then based on some criteria a final solution selected” (Hudson 2010, p. 21). Parametric software offers users the opportunity to create relationships and associations between the variables that define the geometric objects. Therefore, parametric design is sometimes referred to as associative modeling. He defines parametric design tasks as being broken into two parts, namely “creating the model” and “exploring the design space” (Hudson 2010, p. 73). According to Hudson (2010), in the model creation phase, there are three main activities:

- a) developing problem description in an iterative process,
- b) initiating the design process by using an idea based on the problem description, and
- c) constructing the model by focusing on the relationships and control methods.

In exploring the design space phase, two activities are emphasized:

- a) finding values for parameters and generating alternatives,
- b) assessing the alternatives.

This is an iterative loop in which the designers return to the problem description and adjust it according to their findings, or they refine selected variables to generate the next alternative.

There are two main approaches in constructing the parametric model. According to Hudson (2010), Chaszer and Coenders describe two possible options for composing a parametric model, namely a top-down or bottom-up approach. In the former, “a global geometry is defined, which

⁷ The introductory explanation of CAD parametric design is usually made by comparing CAD to conventional design tools. In conventional design tools, an initial model is created by adding parts and relating them to each other. Erasing conventional work is easy by selecting and deleting, since they have no lasting relationship to other parts; thus it requires no more work to fix the representation. However, making changes to the model can be difficult as tools like these can limit exploration and effectively restrict design (Woodbury, 2014).

informs the positions of components” (p. 57). In the latter, the components or sub-assemblies are defined and interlink to form a global geometry.

Turrin (2014) folds various levels of parameterization among geometric modeling, cladding design, and structural design. The first group corresponds with the primary parameterization and to the general geometric properties of the building. The other two groups, cladding and the structure respectively, assume the geometric output of the primary parameterization as reference geometry, and contain parameters describing specific properties of their modules (Turrin 2014).

Apart from different strategies of implementing parametric modeling, different tools can enable and facilitate the application of parametric design approach. Software applications such as Grasshopper by McNeel, Generative Components (GC) by Bentley and DesignScript implemented in Dynamo by Autodesk are implementations of parametric computer-aided design (CAD) software. Software applications of this type “...use network graphs to aid in the creation and visualization of the associative links that govern the design” (Evins et al., 2012, p. 7).

2.3.3 How does parametric modeling help us to understand design problems?

The process of explicitly constructing relationships and control devices is a new design task necessitated by parametric design. Parametric design can help form a better understanding of the problem, since some form of problem-description is required to develop a parametric model.

Kilian (2006) explores ways and processes to understand the design problem, including to find the existing constraints and degrees of freedom in parametric modeling. Killian considers constraints a positive force that can be used as drivers for design ideas. He explains: “constraints are usually perceived as limitations in design exploration. With computational models and the ability to model even complex dependencies their role may be changing towards that of design drivers” (Kilian, 2006, p. 300). He notes that parameters should be identified first so that constraints and freedoms can be found next. The degrees of freedom are the number of values that can vary in the final set of relationships.

Hudson (2010) relates parametric modeling to the problem description and explains how application of parametric methods can be related to the completeness of the problem description. There are two main perspectives on when to apply parametric design. The first suggests that parametric design should begin as early as possible in the design process to support design development. The second proposes that the parametric model restricts the breadth of possible exploration, and so it should only be implemented once the initial concept is developed, after the

early design phases. The former perspective suggests that “problem descriptions could develop as part of the process of producing a parametric model” whereas the latter perspective argues for the “complete understanding of the problem before involving parametric design” (Hudson, 2010, p. 175). According to Hudson (2010, p. 64), Burry states that: “radical change in early design phase is crucial and no relational system can be flexible enough to incorporate this.”

If a task is already very well-defined, there is no need for exploration in breadth. In other words, constructing a parametric model after fully understanding the problem only enables exploring the problem in depth. Hudson explains this by saying: “the hierarchical model structures enable depth of exploration at the cost of breadth” (Hudson 2010, p. 75). However, there are some examples in practice where parametric modeling was implemented at the early stages of design while formulating the design problem. Hudson (2010) explains the design process of the Seating Bowl Modeler (SBM) stadium, which supported an integrated process of problem description and developing parametric models. This process was demonstrated at two levels, “first on the level of capturing the rules and knowledge relating to specific parts of the model,” and “second in the modular structure and functional hierarchy of the model” (Hudson 2010, p. 175).

It is difficult to imagine that the first parametric model that is built for a project can be used to explore the design in breadth. However, parametric models can be built and rebuilt at various scales and with multiple approaches at the early stages of design to help understand the design problem and better formulate them.

2.3.4 Considerations in modeling and implementation

According to a researcher, Mark Burry proposes that “parametric models should be developed to include factors of indeterminacy” (Hudson 2010, p. 62), in a manner similar to a parametric model that includes the ability to add vertices to a polygon. For this, it is necessary to consider scenarios in which vertices are removed. Burry believes that the computer is more capable of handling absence than super-presence; he also stresses the need to consider naming conventions in the design of shared parametric models. Burry also believes that where conventions are clearly established, the model can aid collaboration, whereas without convention the model will hinder it.

In a paper entitled, *Multi-Level Interactions in Parametric Design*, highlights that “the structure of design work using parametric systems remains poorly understood” (Aish & Woodbury, 2005, p.162). They note the difficulty of having one person act as the designer and parametric modeler concurrently, as he must “simultaneously attend to both the specific, concrete

design instance, and the graph structure that captures its conceptual and mathematical structure,” (Aish & Woodbury, 2005, p.162) all at the same time as he must attend to the *multi-faceted design task at hand*.

More than ten years have passed since their statement was published, and the question of how the structure of design work has changed since that time to accommodate parametric modeling naturally follows. Hudson (2010) points out that “a new role of parametric modeler, a person whose job is to develop a parametric model, has arisen in practice” (p. 106). The parametric modeler is either an in-house employee, or a person from a consulting company. He then describes different modes of applying parametric modeling in practice, and among all, the integral mode which incorporates the parametric modeler role into the design team, rather than acting as a consultant to the architectural design team. In this mode, the designer and the parametric modeler work side-by-side as a single team. A sample workflow for this mode of implementation in practice is presented by him in Figure 2.8. It should be noted that Hudson’s workflow suggests the manufacturer is disconnected from the architectural design process, which is widely debated. The integration of fabrication and construction with the design and analysis process is not discussed here, though, since it is out of the scope of this research.

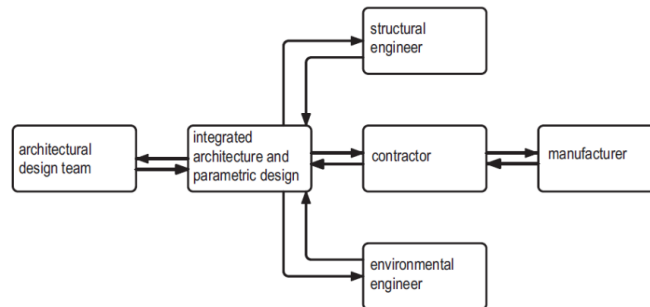


Figure 2.8. Hudson’s integrated workflow model and the role of parametric designer Hudson (2010)

Hudson (2010) also conducted a thorough study on the use of parametric modeling in architectural projects in the period 1990 to 2008 (Figure 2.9). Looking at that timeline, some companies, such as Computational Geometry Group (KPF), SOM, ONL, Buro Happold (BH) and Adams Kara Taylor (AKT), started to employ parametric modeling in practice from 2005 onward. In addition, companies such as Frank O Gehry and Partners (FG) and Foster and Partners (FP) who have started employing team parametric modelers, continue to use them.



Figure 2.9. Use of parametric modeling in architectural projects in the period 1990 to 2008 (Hudson, 2010)

2.3.5 Limitations

As parametric modeling is in widespread use and growing in popularity as a design tool, more people are starting to pay attention to the possible misconceptions and drawbacks of parametric modeling as a generative design tool, as a route to realizing its full potential. Regarding the limitations of parametric design, this study skips its stylistic inclinations, and instead focuses on the ways in which it may limit or affect creative design exploration in the design process. Daniel Davis (2013) studies shortcomings of parametric modeling in his Ph.D. dissertation, and bases his evaluation upon Rick Smith's critique on parametric modeling. He names the limitations:

1. Parametric models require a degree of front-loading
2. Anticipating flexibility can be difficult
3. Major changes break parametric models
4. Changes can be hard to see visually
5. Reusing and sharing models is problematic (Davis, 2013, p. 39).

Front loading at the early design phase of architectural design upon using parametric modeling is discussed in section 2.2. Other limitations of parametric modeling are included under three overarching titles, including "flexibility of parametric models," "sharing parametric models among disciplines," and "parametric modeling and design complexity," all discussed in the following subsections.

Flexibility of parametric models

Parametric design systems do not offer unlimited flexibility. A researcher discusses this by expressing: "The flexibility of a parametric modeling is a result of - and therefore limited to - the parameters that it internally describes" (Dino, 2012, p. 219). El-Khalid identified this limitation by stating that parametric models "generate results within a limited space for they are bound to relationships" (El-Khalidi, 2007, p. 52). In fact, the design space will be constrained as soon as the parameters are implemented. This is in contrast with the initial purpose of conceptual design phase, which is design exploration, and necessitates a certain level of agility to change the design or to reformulate the design problem. In parametric design, change can be accommodated only when it is within the current problem definition. Killian highlights that the parametric modeling approach offers a constrained explorative area based on dimensions or composition, and therefore falls short in generating conceptual variety (Kilian, 2006).

As parametric models fall short when exploring a large design space, some researchers have tried to build more than one model to explore a larger design space. More than one parametric model can be used for the same problem to test different design scenarios. In a study researchers created two parametric models and repeated the search processes to cover a large part of the solution space. One model included a single window that could cover at most the entire length and height of the façade, and one model included four windows distributed along the length of the façade that could cover at most one quarter of the length of the façade (Echenagucia, Capozzoli, Cascone, & Sassone, 2015). This approach has addressed the design problem by putting forward two different methods of creating the parametric model. As the difference between variations increases, the required number of models will be increased exponentially; thus, this approach may be a solution in certain limited cases but cannot be proposed as a general solution to the lack of flexibility of parametric models.

Some other researchers suggest that re-structuring parametric models should be anticipated at the time of implementation. A researcher points out that “changes to the structure of the model are essential in the development process of the model and during its use” (Hudson, 2010, p. 177), thus the re-structuring of models should be anticipated in all parametric design tasks.

There is research on ways to increase the flexibility of the parametric model. Harding et al. (2012) point out that usually only one typology can be explored per parametric model since “parametric design requires the user to construct a single directed acyclic graph (DAG) made up of parameters and components” (Harding, Joyce, Sheperd, & Williams, 2012, p. 68). They argue that the graph generation by itself is limited by top-down rules imposed by the designer and should be generated bottom-up. They suggest ways to improve the flexibility of parametric models to allow different building typologies to be explored. These methods suggest the graph representation to be easier to change. The strategies they propose to increase the flexibility of graph representation include *reusing commonly found design patterns*, *better structuring by using principles from modular programming*, and the *combination of user-created undirected graphs with a logical interpreter*. Finally, they suggest thinking not just numerically, but topologically in parametric design (Harding et al., 2012).

Similarly, some researchers have tried to improve the structure of the parametric schema to accommodate more flexibility. Davis (2013) refers to the studies of Woodbury et al. and relates parametric flexibility to the structure of the parametric schema, which can be improved through

appropriating software engineering principles from computer science. Davis also explains the differences in “dataflow programming” versus “logic programming.” The former is likely to be more flexible when propagating parameter changes through the model, whereas the latter is likely to be more flexible when converting explicit models to parametric models. Other work by Davis mentions that the current “limitation on parametric modeling is the designer’s ability to generate a flexible parametric model, particularly when faced with the complexity of pioneered projects (Davis, Burry, & Burry, 2011, p. 37).

In summary, different strategies are suggested to improve the flexibility of parametric model at the thinking level and the model structuring level:

- Thinking not just numerically, but topologically, in parametric design
- Thinking about if the parametric model is propagating parameter changes through the model, or is converting explicit models to parametric models
- Bottom–up structuring of the models instead of implementing top–down rules imposed by the designer
- Appropriating software engineering principles to improve the structure of the parametric model
- Anticipation of re-structuring of the parametric model when the resolution of the problem increases

Sharing parametric models among disciplines

Once a parametric model is created, sharing it with others can be problematic. A researcher points out that the “original programmer of the model becomes the owner of the model” (Davis, 2013, p. 45) and the original programmer is the only one who can work with the parametric model, especially when the program is too complex. One difficulty with sharing the model with other designers is to untangle it. Researchers suggest that architects and designers need to learn about some computer science fundamentals to make better parametric models. Davis (2011) points out that although structuring the code “provides a way of collaborating on a design that would be too complex otherwise,” still, “architects may have no option but to become real programmers and learn about abstraction, generality, and reuse” (Davis, 2011, p. 66).

The parametric model that is developed for a design will not only be shared with other designers but can also be shared with participants from other disciplines, namely engineers and

fabricators. When the parametric model is shared with other disciplines, assessing the design's performance and refining and resolving the design is the main goal. In this case, the parametric model can be seen as a means for collaboration among disciplines, where other design parties can have access to it for design development. But how do architects address performance in other disciplines while developing design using parametric models?

Hudson (2010) highlights that “in practice, basic assessment of design is undertaken by the parametric designer, but more sophisticated assessment is handled by specialists. Specialist assessment involves studies of building performance in terms of structure, environment and acoustics amongst others” (Hudson 2010, p. 110). The parametric designer, however, still needs to understand how parameters will affect performance to implement them in the model. These sets of parameters will interact with each other in a complex system that will be assessed later.

Shepherd, Hudson, & Hines (2011) describe the Aviva stadium as an example of a project which successfully employed this approach. In designing Aviva Stadium, a single parametric model was shared across the design disciplines. This model was used as both a design tool and a coordination platform. A framework was developed by which information could be exchanged between both parties (architects and structural engineers), but with the architects ultimately driving the overall form and cladding of the building, and the engineers driving the structural member sizing and positioning. This framework allowed rapid response to design changes and provided full coordination between teams.

In this process, first a single Generative Component (GC) script was produced to generate the set-out geometry. Next, the GC script referenced an external Excel spreadsheet containing the defining parameters. Then, architects and structural engineers separately developed a GC script file for cladding and member sizing. Both models were dependent on input from a single Excel document. By this process, the entire design of form, structure and cladding could ultimately be amended and redefined by altering the parameters defined in Excel, so the coordination between the disciplines relied on transfer of a single Excel document (Shepherd et al., 2011). The methods used in this project were developed in-house and did not exist in the commercial software. This framework is a successful example of sharing a parametric model to facilitate collaboration between disciplines.

Parametric modeling and design complexity

Dino (2012) argues that the increasing design complexity in architecture is mainly due to a new formal interest in free-form geometry and the underlying mathematical and geometrical concepts. Other external stimuli, such as increasing building performance requirements, new building functions, user requirements, urban settings, spatial configurations, integrated design processes, and the like, are also motivating factors. “The need to address a growing number of concerns and integrally deal with them introduces increased levels of complexity in architecture” (Dino, 2012, p. 219)

Assuming the designer already has the necessary skills to work with a set of tools (computational and parametric modeling in this case), he still needs to systematically formalize the design into a computational realm. This increases the complexity of the architect’s task, as he is not only modeling the artifact being designed, but conceptualizing a structure that guides variation. If the designer wants to consider performance in different disciplines, another layer of complexity is added to the process. As discussed in Section 2.3.4, a new role, parametric modeler, is introduced in the industry to reduce the design complexity associated with parametric modeling.

2.4 Performance

“Parametric design thinking and modeling enables relational, correlative, integral and explorative design process” (Gerber & Lin, 2013b, p. 937) . However, a parametric *form* which only represents the qualitative aspect of the design needs to be integrated with “performance,” as the quantitative aspect, to offer a holistic evaluation of an array of building topologies. A researcher argues that the divergence of design space facilitated by the parametric combinations can converge on the basis of performance criteria: “parametric manipulation of form is particularly valuable in performance-driven design processes, facilitating the rapid cycle of performance analysis and design synthesis as an integrated process” (Dino, 2012, p. 220). This statement points to design paradigms such as performance-aided design, performance-based design, or designing in performance. She even suggests parameterizing the design is suitable for downstream performance analysis, stating that “parameterization can be based on performance metrics to allow the solution space be meaningfully traversed while taking performance as a guiding tool” (Dino, 2012, p. 213). However, there are critical challenges that need to be addressed such as “multi-

disciplinary thinking, early performance integration, and mutual agreement on the driving performance parameters” (Dino, 2012, p. 213) if this route is taken.

Performance-based design is one of the performance-driven design paradigms which will be discussed more in depth. Performance-based design, in which building performance becomes a guiding design principle, emerged as a design paradigm due to emphasis on sustainability as a defining socio-economic issue as well as recent developments in technology and cultural theory (Koleravic, 2014). In performance-based design, the emphasis shifts from the *product* to the *process* of form generation based on performative strategies of design. Oxman & Oxman (2014) highlight the relationship between analysis and performance-based design by stating that performance-based design relates to a set of concepts engaging the analysis and understanding of how the environmental context may inform complex processes of design synthesis. Simulation is one of the influential concepts of performance-based design for analysis, which can also redefine *performative design* when integrated with generation (Oxman & Oxman, 2014). These strategies are grounded in intangibilities, such as cultural performance, at one end and in quantifiable performative aspects of building design, such as structure, environmental design or acoustics, at the other end. Koleravic highlights two main challenges associated with performance-based design, including first, how to determine the different performative aspects in a particular project, and second, how to reconcile conflicting performance goals in a creative and effective way (Koleravic, 2014).

Simulation is a powerful tool in performance-based design that analyzes the effect of various decisions on a building. But there are some drawbacks that make it hard to use simulation as a driver of fast design cycles. As Tsigkari et al. (2013, p. 155) point out, “first of all, many off-the-shelf simulation tools are limited by the amount of time they require to run a simulation. Secondly, the results are often difficult to interpret by the non-specialist in the particular domain analyzed.” To accommodate the need for quick results, they propose a trade-off between speed and accuracy when running simulations, assuming that the modeling and simulation of building physics phenomena already entails a certain amount of complexity and uncertainty, as it depends on noisy and often conflicting input data (Tsigkari et al., 2013). Others raise the same question. According to Holzer (2009), Moum raises the question of “how we can work with feedback from building performance analysis during early design. And is it possible to analyze design with a level of

precision high enough to yield correct trends, but not too precise to hinder creative design?”(Holzer, 2009, p. 54).

(Koleravic, 2014) describes one challenge of performance-based design is the difficulty of determining the different performative aspects in a particular project. On top of that, there exists another layer of difficulty when the designer implements performative aspects in the parametric model. The challenge is how the designer can assure that he has implemented all the crucial parameters in the parametric model that will ultimately yield an un-biased performance-based design. A group of researchers suggest collaboration at the early stages of design. According to Yao (2013), the concept of a systematic research framework encourages collaborative work among professions including architects, engineers, planners and assessors from different disciplines in the design stages, and specifically at the very early stages of design development.

Nevertheless, this approach has been limited by a lack of integration and understanding across various disciplines (Yao, 2013). According to Holzer (2009), Achton stresses “the importance for design partners to apply engineering knowledge in the early stages of design to enable consultants to engage more pro-actively in architectural design” (Holzer, 2009, p. 55). Collaboration at early stages of the design can lead to development of a more robust parametric model. Therefore, it is essential for the designer to implement some basic key features related to other disciplines in his parametric model so these key features can be further developed using feedback from other disciplines.

Koleravic (2014) mentions another challenge of performance-based design is difficulty in reconciling conflicting performance goals in a creative and effective way. This challenge becomes an issue when all performance values are retrieved. The question then is how to bring them all together to compare alternatives, weight various criteria and determine how to evaluate the trade-offs among these disciplines.

This study aims to address the aforementioned challenges as *how parametric modeling can be employed as a tool to enhance performance in multiple disciplines*, as well as *how it can be a design exploration tool for architects*.

2.5 Large span roofs as a use case

Parametric design paradigm and performance-oriented design are discussed in the previous sections. This section discusses building envelopes, an overarching term for large span roofs. Large span roofs are the use-case to which this dissertation’s framework will be applied.

A building's envelope forms the interface between interior and the environment of external world. According to (Moloney, 2011, p. 8) “*Envelope* is a generic term that describes the total enclosure of the building.” Another group defines building envelope as an interface that separates the indoor and outdoor environments of a building (Sadineni, Madala, & Boehm, 2011). There are a number of other terms in use to describe the zone between architectural exterior and interior. Moloney (2011) distinguishes envelope, wall, façade and skin in buildings, “*Wall* was traditionally used to describe a vertical load-bearing construction,” and “*façade* still retains association with wall,” which “defines a generally vertical plane of abstract composition, as observed externally” (Moloney, 2011, p. 8). *Skin* on the other hand, was initially coined to continue the distinguish between cladding and the structural bones of a wall, but has more recently been associated with conceiving the envelope as an intelligent environmental system (Moloney, 2011).

The last century witnessed a radical change in the nature of building envelopes (Lovell, 2010). Lovell highlights that “Building envelopes which were considered as part of the structure and as a single homogeneous plane perforated by opening, began to be conceived as a separate layer that was relieved from any structural responsibility” (2010, p. 8). Thus, there is a split in the definition of building envelope by researchers. Some researchers emphasize that the main function of a building envelope is to enclose space in such a way that its environmental characteristics can be regulated within acceptable limits (Rivard, Bfidard, Fazio, & Ha, 1995). Others define building envelopes as systems that fulfill both structural and environmental requirements. They define a building envelope as “a system enclosing and protecting the indoor environment from disturbing outdoor conditions” (Rivard, Bfidard, Fazio, & Ha, 1995, p. 391). James Fitch (1973) is perhaps the first to categorize various functions of an envelope (Figure 2.10).

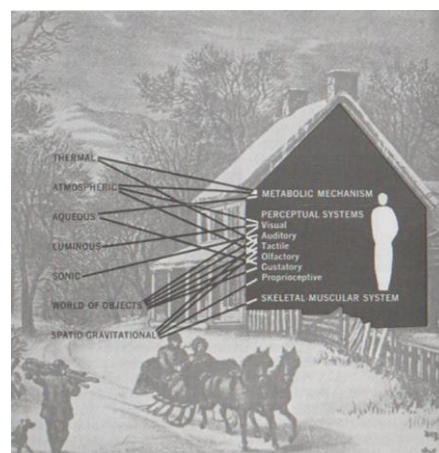


Figure 2.10. Various functions of a building envelope categorized by Fitch (1973)

Three decades later, (Knaack et al, 2007, p. 36) define the façade as a special case of building envelope, a system that “separates the usable interior space from the outside world” (Figure 2.11). They enumerate different functions that a façade serves, including identifying the architectural appearance of the building, providing a view to the inside and outside, absorbing push and pull forces from wind loads, bearing its self-weight as well as that of other building components, allowing sunlight to penetrate the building at the same time it provides protection from the sun, resisting the penetration of rain water, and handling humidity from within and without. The façade provides isolation against heat, cold and noise and can facilitate energy generation (Knaack, Klein, Bilow, & Auer, 2007).

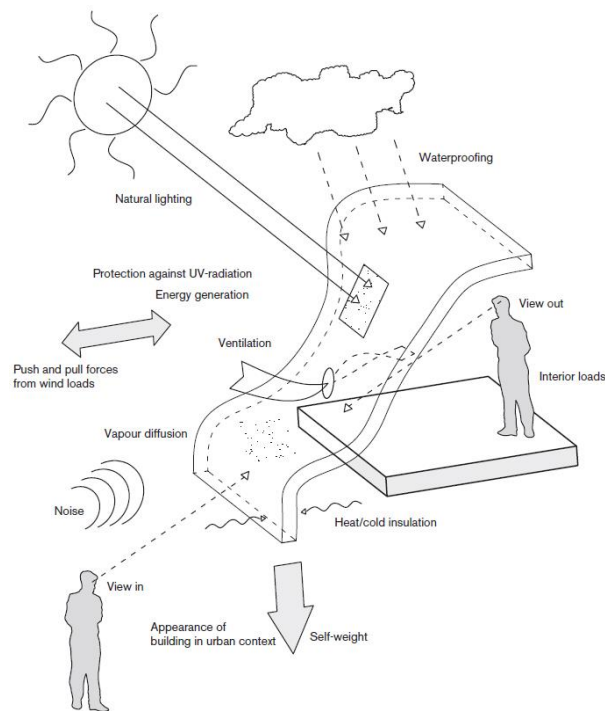


Figure 2.11. Different functions that a façade serves (Knaack et al., 2007)

Roof systems are a special case of building envelopes, as they can be a horizontal or curved entity covering the building. A researcher points out that “large roofs can also enclose areas that are isolated from the outdoors, commonly defined as indoor areas,” (Turrin, 2014, p. 137) and are thus considered a building envelope. This research focuses on large span roof systems as a special case of building envelopes. This study also recognizes building envelopes as systems that fulfill both structural and environmental responsibilities. Thus, energy savings and daylight control are not detached from the structural and material design of the envelope. Large span roof systems are considered as a special case of building envelopes in this work in particular.

A survey of structural systems considering the role of daylighting has been conducted, which shows how the two disciplines are interconnected (Figure 2.12). Among many structural typologies, shell structures are explained more in depth in the next section.

			Daylighting				
			Transparent		Translucent	Hybrid	
			Direct	Indirect	Direct	Translucent & transparent	
Structure	Linear elements: Post & Beam / Frame						
	Linear elements: Truss Structures						
	Plate		Surface plate				
			Grillage plate				
			Folded Plate				
	Barrel Vault		Cylindrical shell				
	Shell structures		Synclastic				
			Anticlastic				
			Synclastic				
			Anticlastic				
	Membrane Structure		Synclastic				
			Anticlastic				

Figure 2.12. Survey of structural systems (Engel, 1967) integrated with top-lighting strategies

2.6 Importance of structure and daylight as two objectives in shell design

This research draws connection between architectural, structural, and daylighting design in large span roof systems, and in particularly in shell structures. The association of structure and daylight may be questioned by the reader. I consider these two separate disciplines, as a building both needs to stand up and to be illuminated; thus, the disciplines of structural and daylighting design are directly associated with the purpose of architectural design. In the architectural design of a building envelope, a structure is designed to realize the building, while the existence of adequate daylight is crucial to create a healthy, pleasant and productive space for the occupants. Therefore, these two disciplines are directly associated with the purpose of architectural design and are an inevitable requirement in designing a functional space. The importance of geometry in affecting the structural and daylight performance of the building is exemplified. The hypothesis of this research is that geometry is the key element that integrates structural and daylighting disciplines.

Shell structures are selected as the subject of study for covering large span roof systems. The design of a shell is closely integrated with their structural performance. In fact, form plays a significant role in the design of shells and affects whether a thin shell will be stable, safe, and sufficiently stiff. Leading shell designers consider force flow when designing the form, to arrive at the alternative that offers the best performance.

Shells also provide various opportunities for introducing daylight to a space. Continuous shells can be perforated, and discrete shells can potentially introduce abundant light through the openings within the grids. The surface of the shell can be deformed to block the incident sun. With CAD modeling tools at hand, more designers create free-form shells. Advanced manufacturing techniques such as using fabric formworks have opened new doors in building shells at decreased expense. Therefore, shell structures are chosen as a special type of roof systems for studying the integration of disciplines at the early stages of design using computational design tools.

2.7 Discussion summary

This research considers the application of parametric design methods at the early stages of design for high-performance buildings. Looking at this through an interdisciplinary design lens, the design parameters that affect performance in multiple disciplines need to be embedded in the model. Implementing design parameters calls for an understanding of first, the ways in which

parameters affect performance; and second, increasing level of detail during design in each discipline. Structure and daylighting are the two main disciplines that are emphasized among many because of their respective key roles in realizing a building and making a space habitable. Thus, their interconnections will be examined in depth in the context of roof systems to demonstrate how common design parameters will affect performance in both disciplines.

This chapter provides an overview of the key elements of the title of the dissertation. It starts by introducing the importance of the early design stage, as the decisions made in this phase affect the design outcome downstream. It then discusses the concept of a *parameter* as it is used in parametric design, along with the attendant considerations and limitations. Next, it introduces the paradigm of *performance* in performance-oriented design. Afterward, building envelopes are discussed and roof systems introduced as a special case, followed by a discussion of the importance of the structural and daylighting disciplines in the design of large span roof systems.

The following chapters, Chapters 3 and 4, are built on the elements of this chapter and dig deeper in discussing structural and daylighting design principles, with a focus on shell structures as roof systems. In Chapter 5, integrated design is examined, and the parameters and performance criteria of the two disciplines meshed together. Chapter 6 discusses the methodology of this study, while Chapter 7 discusses the case studies. Chapter 8 lays out the conclusions of this work and highlights directions for future research.

2.8 References

- Aish, R., & Woodbury, R. (2005). Multi-Level Interaction in Parametric Design. *Smart Graphics*, 151–162. https://doi.org/10.1007/11536482_13
- Charmaine, A. (2011). *BIM , BAM , BOOM The life of a Building Information Model*. VIA University College.
- Cross, N. (2006). *Designerly ways of knowing*. Springer (Vol. 53). <https://doi.org/10.1017/CBO9781107415324.004>
- Davis, D. (2013). *Modelled on Software Engineering : Flexible Parametric Models in the Practice of Architecture*. Royal Melbourne Institute of Technology (RMIT).
- Davis, D., Burry, J., & Burry, M. (2011a). The flexibility of logic programming. In *Computer Aided Architectural Design Research in Asia (CAARDIA)* (pp. 29–38).
- Davis, D., Burry, J., & Burry, M. (2011b). Untangling Parametric Schemata : Enhancing Collaboration through Modular Programming. In *CAAD Futures 2011: Designing Together* (Vol. 09, pp. 55–68). <https://doi.org/10.1260/1478-0771.9.4.361>
- Dino, I. (2012). Creative Design Exploration By Parametric Generative Systems In Architecture. *Metu Journal of the Faculty of Architecture, 1*, 207–224. <https://doi.org/10.4305/METU.JFA.2012.1.12>
- Echenagucia, T. M. (2013). *Computational Search in Architectural Design*. Politecnico di Torino.
- Echenagucia, T. M., Capozzoli, A., Cascone, Y., & Sassone, M. (2015). The early design stage of a building envelope: Multi-objective search through heating, cooling and lighting energy performance analysis. *Applied Energy, 154*, 577–591. <https://doi.org/10.1016/j.apenergy.2015.04.090>

- El-Khaldi, M. (2007). *Mapping boundaries of generative systems for design synthesis*. Massachusetts Institute of Technology (MIT).
- El-khaldi, M., & Woodbury, R. (2015). Exploration with Alt . Text Interactive Design Exploration with Alt . Text. *International Journal of Architectural Computing*, 13(2).
- Engel, H. (1967). *Structure Systems*. Stuttgart, Deutsche Verlags-Anstalt.
- Evins, R., Joyce, S. C., Pointer, P., Sharma, S., Vaidyanathan, R., & Williams, C. (2012). Multi-objective design optimisation: getting more for less. *Proceedings of the Institution of Civil Engineering (ICE)*, 165(5), 5–10. <https://doi.org/10.1680/cien.11.00014>
- Gerber, D. J., & Lin, S.-H. E. (2013). Designing in complexity: Simulation, integration, and multidisciplinary design optimization for architecture. *Simulation*, 90(8), 936–959. <https://doi.org/10.1177/0037549713482027>
- Harding, J., Joyce, S., Sheperd, P., & Williams, C. (2012). Thinking topologically at early stages of design. In *Proceedings of the Advances in Architectural Geometry Conference* (pp. 67–76). Springer.
- Holzer, D. (2009). *Sense-making across collaborating disciplines in the early stages of architectural design*. School of Architecture and Design. Royal Melbourne Institute of Technology (RMIT).
- Hudson, R. (2010). *Strategies for parametric design in architecture*. University of Bath.
- Kilian, A. (2006). *Design Exploration through Bidirectional Modeling of Constraints*. Massachusetts Institute of Technology (MIT).
- Knaack, U., Klein, T., Bilow, M., & Auer, T. (2007). *Facades Principles of Construction*. *Journal of Chemical Information and Modeling* (Vol. 53). Birkhause Verlag AG. <https://doi.org/10.1017/CBO9781107415324.004>
- Knaack et al, U. (2007). *Facade Principles of Construction*. Birkhause Verlag AG.
- Koleravic, B. (2014). Computing the performance. In R. Oxman & R. Oxman (Eds.), *Theories of the digital in architecture* (pp. 103–111). Routledge.
- Kruger, C., & Cross, N. (2006). Solution driven versus problem driven design: strategies and outcomes. *Design Studies*, 27(5), 527–548. <https://doi.org/10.1016/j.destud.2006.01.001>
- Lovell, J. (2010). *Building Envelopes* (1st ed.). New York: Princeton Architectural press.
- Moloney, J. (2011). *Designing kinetics for architectural facades*. London. London: Routledge.
- Oxman, R., & Oxman, R. (2014). Performance/ Generation: from analysis to informed synthesis. In R. Oxman & R. Oxman (Eds.), *Theories of the digital in architecture* (pp. 97–102). Routledge.
- Paulson Jr., B. C. (1976). Designing to Reduce Construction Costs. *ASCE Journal of the Construction Division, Now Called, Journal of Construction Engineering and Management*, 102(4), 587–592. <https://doi.org/10.1080/19397030902947041>
- Pentilla, H. (2007). Early architectural design and BIM. In *Computer-Aided Architectural Design Futures (Caad Futures) 2007* (pp. 291–302). https://doi.org/10.1007/978-1-4020-6528-6_22
- Pulsifer, D. S. (2014). Knowledge Management. In *The architectural handbook of professional practice* (Fifteenth, pp. 308–322). Wiley.
- RIBA. (2013). RIBA Plan of Work 2013 Overview. (D. Sinclair, Ed.). London: Royal Institute of British Architects.
- Rittel, H. W. J., & Webber, M. M. (1973). Dilemmas in a General Theory of Planning, 4(December 1969), 155–169.
- Rivard, H., Bfidard, C., Fazio, P., & Ha, K. H. (1995). Functional Analysis of the Preliminary Building Envelope Design Process. *Building and Environment*, 30(3), 391–401.
- Sadineni, S. B., Madala, S., & Boehm, R. F. (2011). Passive building energy savings: A review of building envelope components. *Renewable and Sustainable Energy Reviews*, 15(8), 3617–3631. <https://doi.org/10.1016/j.rser.2011.07.014>
- Shepherd, P., Hudson, R., & Hines, D. (2011). Aviva Stadium: A parametric success. *International Journal of Architectural Computing*, 9(2), 167–186. <https://doi.org/10.1260/1478-0771.9.2.167>

- Simon, H. A. (1969). *The sciences of the artificial. Computers & Mathematics with Applications* (1st ed.). Massachusetts Institute of Technology. [https://doi.org/10.1016/S0898-1221\(97\)82941-0](https://doi.org/10.1016/S0898-1221(97)82941-0)
- Tsigkari, M., Chronis, A., Joyce, S. C., Davis, A., Feng, S., & Aish, F. (2013). Integrated design in the simulation process. *Symposium on Simulation for Architecture and Urban Design (SimAUD)* , 153–160.
- Turrin, M. (2014). *Performance Assessment Strategies: A computational framework for conceptual design of large roofs*. Architecture and the Built Environment.
- von Buelow, P. (2007). *Genetically engineered architecture: design exploration with evolutionary computation*. VDM Verlag.
- Woodbury, R. (2010). *Elements of Parametric Design*. Routledge.
- Woodbury, R. (2014). How designers use parameters. In R. Oxman & R. Oxman (Eds.), *Theories of the digital in architecture* (pp. 153–170). Routledge.
- Yao, R. (Ed.). (2013). *Design and Management of Sustainable Built Environments*. Springer.

Chapter 3 : Shell structures as large-span roof systems

“The shape of shells directly derives from their flow of forces and defines their load-bearing behavior and lightness. The more the form of a building or structure develops from its flow of forces, the more it is under the responsibility of the engineer.”

- Jörg Schlaich, On architects and engineers, 2014

3.1 Introduction

This research studies shell structures through a multidisciplinary design lens, examining structural efficiency and daylighting performance in the early stages of design. Shells have defining characteristics that differentiate them from other structural typologies that are used for covering large spans. First and foremost, their form and structural efficiency are inherently linked, as efficient shells are derived from the flow of their forces. Second, shells that cover architectural spaces without the opportunity of having sidelights are either perforated to bring daylight into the space, or a gridshell is used. The former approach, wherein the surface of the shell is perforated, makes local changes in the structure that affect the force flow, and thus the global structural performance of the shell. The latter approach, wherein a gridshell is used, provides the opportunity to place glazing between the discrete members, but might bring unwanted light and heat, which requires control. Therefore, the interrelation of form, structure and daylight is exemplary in shell structures, and they are selected as the main structural typology for this study.

This chapter first introduces shell structures, form finding methods for determining optimal shell form, shell typologies and the materials commonly used in the construction of shells. Afterwards, perforated concrete shells are examined, with a focus on the 1950 to 1970 era. Next, three main concepts in structural design, namely topology, shape, and sizing are reviewed. The concepts are then examined for two shell typologies. This categorization will be carried over to Chapter 5, along with a daylighting design categorization, to find the areas of overlap between the two disciplines and towards a multi-disciplinary design approach. Finally, this chapter reviews the

structural performance criteria that need to be met in the design of shell structures, information which is eventually used in the computational simulation and design space exploration described in Chapter 7.

Different terminologies are used for shell structures. Adriaenssens, Block, Veenendaal, & Williams (2014), in their book entitled *Shell structures for architecture*, define shell structures as “constructed systems described by three-dimensional curved surfaces, in which one dimension is significantly smaller compared to the other two. They are form-passive and resist external loads predominantly through membrane stresses” (Adriaenssens et al., 2014, p. 1). There are three key terms in the definition, namely *curved surfaces*, *membrane stresses*, and *form-passive*. These components are briefly reviewed in order to explain the load-carrying mechanism in shell structures, as well as to explain how they have led to the use of alternative names such as *surface structures*, *membrane structures*, or *form-passive membrane structures* for this structural typology.

Designers started to see the potentials offered by the plastic qualities of liquid concrete from the beginning of the 20th century. Pedreschi (2008) explains that the majority of designers started to use concrete as a tectonic compact, where its qualities go beyond being purely structural but tend towards becoming both shelter and skin. According to Pedreschi, Angerer was the person who proposed *surface structures* as a new classification of these structures to differentiate them from the historical classification of solid or skeleton and skin. This choice of name is tied to the geometrical properties of the shell, and the fact that one dimension is significantly smaller compared to the other two dimensions, like a surface.

From another point of view, when shells are well-formed, there will only be membrane forces: axial compression and axial tension forces with no bending forces present (Schlaich, 2014). In other words, the term membrane forces refer to in-plane forces and does not necessarily suggest a film or fabric for the structure (Adriaenssens et al., 2014). Membrane forces can be present as axial compressive stress in a masonry, concrete, or steel structure, or as axial tensile stress in a fabric structure. Williams (2014) describes the in-plane forces in a shell by explaining the in-plane and out-of-plane forces in a plate first. Looking at the in-plane stresses (Figure 3.1), the normal stress in the x and y-direction are presented by $\bar{\sigma}_x$ and $\bar{\sigma}_y$, respectively. The shear stress perpendicular to the x and y-direction are presented by τ_{xy} and τ_{yx} , respectively. In fact, the in-plane load-bearing behavior of shells is the feature that has led to occasional use of the term *membrane structures*.

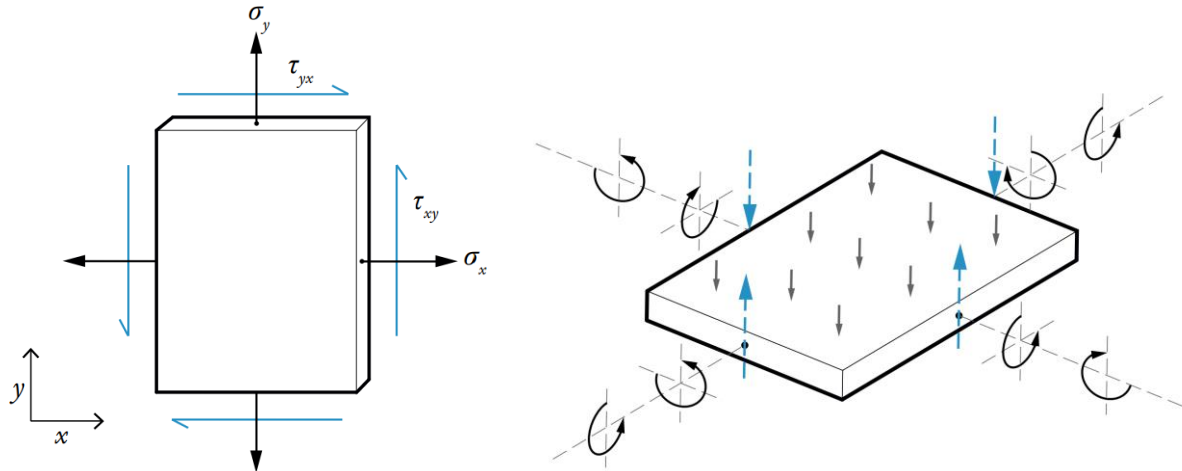


Figure 3.1. In-plane stresses (a); and plate bending (b) (Williams, 2014)

Other names in use for shell structures emphasize the rigid characteristic of these systems. Chris Williams describes a shell as a structure that “can be geometrically represented by surfaces”, where it is thin in the direction perpendicular to the surface, has the implication of something “relatively rigid”, and “work through a combination of membrane and bending action” (Williams, 2014, p. 31). Here, he emphasizes the rigidity of the shell structures, as well as the existence of bending action in shells. In general, membrane structures can either be “form-active” or “form-passive.” The shape of a form-active structure changes under loading conditions, unlike the shape of a form-passive system (Adriaenssens et al., 2014). As an instance, a cable is a form-active system without a flexural stiffness, where the shape of the cable under applied loads is a mirror of the axial tensile forces acting in it. Form-passive is another phrase that highlights the rigidity of these systems. However, a shell is a form-passive system; its shape cannot be self-adjusted to varying loading conditions. In addition, deformations due to the elasticity of material generate undesirable bending moments in shells (Ney & Adriaenssens, 2014). The closely related *form-passive membrane structure* is another term used for shell structures.

Throughout this dissertation, *shell structures* will be used consistently for systems that are made of rigid materials that primarily work in compression.

Once different terminologies used for shells have been discussed, different form finding methods are briefly reviewed. The shape of an efficient shell relates to its flow of forces. Therefore, form finding is required in the process of design (Adriaenssens et al., 2014). Ney and Adriaenssens note that “shape is the fundamental parameter to obtaining structural efficiency in a shell,” (Ney & Adriaenssens, 2014, p. 17) therefore, the first thing to generate is the form. The earliest example

of structural form finding, for an arch, was published by Robert Hooke (1635–1703) in his ten “Inventions,” which were written in the form of anagrams of Latin phrases. Hooke’s second invention was later published, and read “as hangs the flexible line, so but inverted will stand the rigid arch” (Ochsendorf & Block, 2014, p. 8). This principle is referred as “Hooke’s law of inversion,” and explains how a hanging chain in pure tension can be inverted to obtain the equivalent arch in pure compression (Ochsendorf & Block, 2014). The earliest known use of a physical model is observed in the design of St. Paul’s Cathedral in London. Christopher Wren (1632–1723) designed this structure in collaboration with Robert Hooke, and used form finding to help determine the form of a structure. One of his sketches shows the shape of a chain suspended over a cross section of a building (Addis, 2014).

Antoni Gaudi (1852–1926), Heinz Isler (1926–2009), and Frei Otto (1925–2015) are other designers who exploited physical, inverted hanging models loaded in gravity as form finding tools for designing shell structures (Ney & Adriaenssens, 2014). Antoni Gaudi used both two and three-dimensional hanging models made with strings and bags of sand to help find the form of his masonry buildings (Addis, 2014). Heinz Isler used a sheet of cloth rather than a chain or string to make hanging models. By soaking the cloth in a liquid plaster or resin to harden, or by making it wet and letting it freeze during winter nights, he not only generated the form of the shell, but the stiffening folds of the edges of the shell (Addis, 2014, p. 38). Frei Otto used innovative form finding methods to establish the form of membrane and cable-net structures wherein gravity loads play a minor role. He used soap bubbles, which have a constant surface tension; elastic sheets, whose surface tension depends on the strain; and nets, whose surface tension partly depend on the elastic extension of fibers and partly on shear deformation of the net (Addis, 2014, p. 39). He also used 3-d chain models to form find shells (Flächentragwerke, 1990).

Once a form is found using physical models, only the structural properties that are independent of scale can be scaled up linearly to predict full-size behavior, such as the equilibrium and the shape of a hanging chain, but not the strength and stiffness of the structure nor its buckling strength (Addis, 2014). In other words, characteristics that are dependent on the structural properties of a material cannot be scaled up linearly.

From a different point of view, a found form can be realized using a continuous surface, or with discrete elements following that surface (Adriaenssens et al., 2014). A researcher uses an analogy to differentiate the two. He notes that a colander is a curved surface structure which

contains holes, but these holes do not stop it from being a shell. A sieve, on the other hand, is a surface made from a large number of initially straight wires which are woven together into a flat sheet and then bent into a hemisphere, resembling a gridshell (Figure 3.2) (Williams, 2014).



Figure 3.2. Comparison between a colander and a sieve (Williams, 2014)

Whether continuous or discrete, shells can be realized with various materials such as masonry, concrete, steel, or wood. Garlock & Billington (2008, p. 76) note that “shell structures must be designed with proper shape, thickness, and material in order to properly distribute their own weight throughout the shell.”

Masonry shells in the form of arches, domes, and vaults have a long history in architecture. According to Ochsendorf & Block (2014), masonry shells work primarily in compression due to the inherent limitations of masonry materials such as brick and stone. The dominant loading is often due to self-weight of the structure, and the applied loadings, such as wind or snow, have a smaller effect. The supports must resist large reactive forces, or outward thrust, at the base of the structures, which is commonly accomplished by a tension ring (Ochsendorf & Block, 2014). Eladio Diesta (1917–2000) is an engineer who made brick-reinforced shells (López, Mele, & Block, 2016) (Figure 3.3a). There are examples of masonry shells that have numerous openings, such as in the dome of the Elephant House at the Bronx Zoo (1909). The resulting compressive forces flow around the openings in these cases.

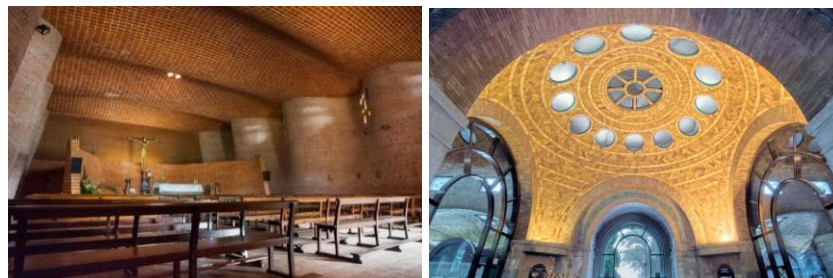


Figure 3.3. Church by Eladio Diesta (López et al., 2016) (a); Masonry shell by Rafael Guastavino (Ochsendorf & Block, 2014) (b)

Concrete is another material used for the construction of shells. The dome of the Pantheon in Rome is still the world's largest un-reinforced concrete dome; the height to the oculus and the diameter of the interior circle is 43.3 m (142 ft) (Goshima, Ohmori, Hagiwara, & Aoki, 2011). The Oculus is the main source of natural light. (Figure 3.4a). The Chapel Lomas de Cuernavaca by Felix Candela is a more recent example of a shell structure using reinforced concrete (Figure 3.4b).

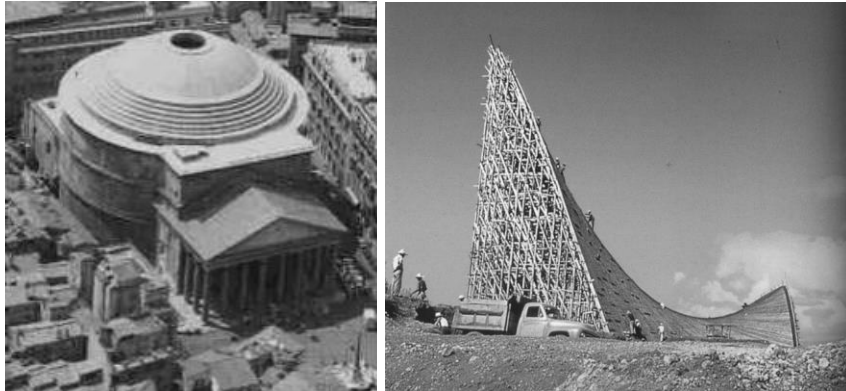


Figure 3.4. The Pantheon in Rome (a); and the Chapel Lomas de Cuernavaca (b)

Wood is another material employed in gridshells. Centre Pompidou in Metz and the Haesley Nine Bridges golf clubhouse are two examples of wooden gridshell structures (Figure 3.5). The former is designed as a large suspended surface, where parts of the system are in tension and other parts in compression. The latter case, however, is developed into a set of compressive arches because of the repetition of the supports (Ban, 2014).



Figure 3.5. Centre Pompidou in Metz, 2010 (a); Haesley Nine Bridges golf clubhouse (b)

Steel is another material used in gridshells. The roof of the New Milan Trade Fair in Italy is a steel gridshell with a triangulated pattern at the curved parts, and a square mesh at other parts, whereas the steel gridshell over the courtyard of the National Maritime Museum in Amsterdam is “based on rosettes with loxodromes, figures on historical sea charts, to mark out the courses of a ship” (Figure 3.6) (Ney & Adriaenssens, 2014, p. 18).



Figure 3.6. Steel gridshell of the New Milan Trade Fair in Italy (a); National Maritime Museum (b)

This research focuses on concrete shell structures, and the ways in which making perforations in the surface affects structural force flow and performance, as well as the amount of daylight that is brought into the space. Adding perforations to the continuous surface of a shell affects the force flow in the shell. In gridshells, however, force flow depends on the grid layout.

On the other hand, daylighting performance is directly affected by adding perforations to a continuous shell, whereas changing the grid layout of a gridshell does not have a significant effect on its daylighting performance. Perforations in a concrete shell can take any shape or size, and can be placed anywhere throughout the surface, in contrast to systems made out of modules, such as brick or stone shells. This provides the opportunity of mapping a layout with any pattern for perforating the shell; this layout can ultimately match the pattern of a hypothetical gridshell structure when all modules are perforated.

3.2 Perforated concrete shell structures

Putting a hole in a dome produces a structure that can undergo an inextensional deformation (Figure 3.7). Williams (2014, p. 25) notes that “if a shell is the wrong shape or it does not have enough boundary support, it may be a mechanism as far as the membrane theory is concerned, and be able to undergo inextensional deformation, that is, deformation in which the shell is bent without stretching.” However, if the holes are very small, the bending stiffness takes over and controls the deformation, just like a colander. Therefore, shells that undergo inextensional deformation rely on bending stiffness in order to carry the load. Bending stiffness prevents buckling as well. Thus, although shells work primarily by membrane action, they also possess the bending stiffness necessary to resist inextensional deformation and buckling (Williams, 2014).

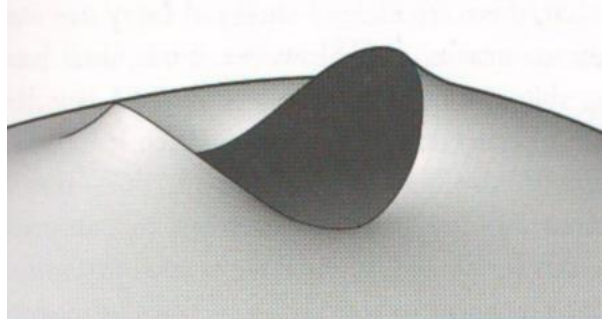


Figure 3.7. Inextensional deformation in the region of a hole in a sphere (Williams, 2014)

A great number of shells are designed with perforations; such shells are briefly reviewed in the following subsections. The works of master shell builders in 1950s, including Eduard Torroja (1899–1961), Pier Luigi Nervi (1891–1979), Felix Candela (1910–1997), Heinz Isler (1926–2009), and Frei Otto (1925–2015), are reviewed with a focus on the perforated concrete shell structures among their works. In addition, a number of contemporary perforated shells are reviewed. The goal of this review is to examine the history of perforated shell structures, and the future potential for constructing this structural typology.

3.2.1 Eduardo Torroja

Eduardo Torroja (1899–1961) is the brilliant Spanish engineer who designed many shells. One of his major creations is the thin shell for the roof of the Fronton Recoletos (1935), which was destroyed during the Spanish Civil War (Mungan & Abel, 2011). A thin concrete shell was designed to cover a 55 by 32.5-m surface designed for a ball game. The shell was defined by two circular arches of radii 12.2 m and 6.4 m which sprung from the outer supports and were joined orthogonally along a common line parallel to their axes. In the shell areas where skylights were needed, the shell was replaced by a triangulated structure designed for the insertion of glass panes (Figure 3.8) (Lozano-Galant & Payá-Zaforteza, 2011). According to them, the Fronton roof is an outstanding structure among barrel vault concrete shells for many reasons, one of which because “the continuous shell was replaced by a triangulated structure in highly stressed portions of the barrel vault to create skylights, constituting a major innovation” (Lozano-Galant & Payá-Zaforteza, 2011, p. 3).

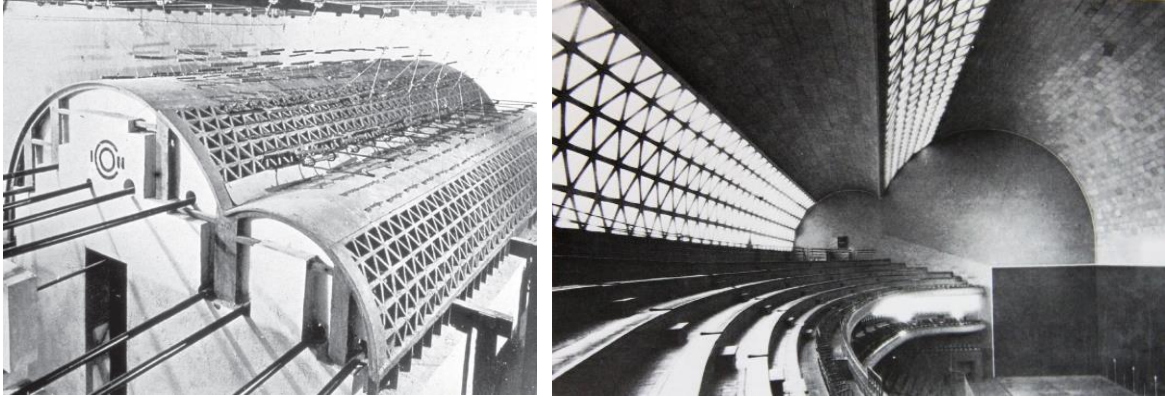


Figure 3.8. Thin shell with triangulated openings in the Fronton Recoletos (Torroja, 1958)

The thickness of the shell was 0.08 m (8 cm), except at the connection, where it was increased to 0.3 m (30 cm). The triangulated skylights were 55 m long, covering the whole length of the roof (Figure 3.9). The reinforced concrete elements of the triangulated structure of the skylights had a depth of 0.3 m, a width of 0.17 m and a length of 1.4 m. The roof structure was supported at its two extreme longitudinal edges (Lozano-Galant & Payá-Zaforteza, 2011).

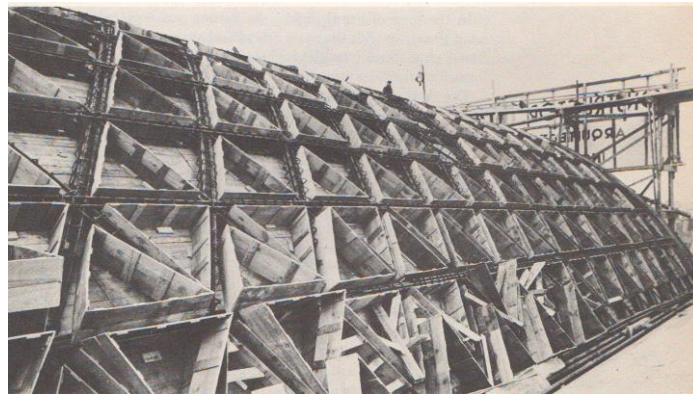


Figure 3.9. Construction and reinforcement of a thin shell with triangulated openings, part of the Fronton Recoletos (Torroja, 1958)

3.2.2 Pier Luigi Nervi

Pier Luigi Nervi (1891–1979), an Italian engineer, worked throughout his career with a structural type referred to as *vaulted architecture*, which consists of domes, vaults, and geodesic roofs (Solomita, 2015). Nervi worked with surfaces of revolution and translation, which guarantee maximum efficiency on the worksite, along with the repetition of smaller precast elements. He developed a vaulted roofing system featuring crossed ribbing, and first implemented it in the garage for agricultural machinery of the estate of Torre in Pietra in 1956 (Solomita, 2015). Solomita notes that Nervi observed the pattern of forces, as well as basing his structures on

“observation of the static behavior of objects in nature. Starting with the analysis of flower sepals, lanceolate leaves, eggshells, reeds, sea shells, insect shells, Nervi transfers the laws of nature into his structures” (Solomita, 2015, p. 45).

Nervi developed a material for the construction of his vaulted systems. He registered the *Ferrocement* patent, which was for a 3-centimeter concrete slab made of a certain number of small-diameter wire mesh nets (Figure 3.10) (Greco, 1994). He was inspired by solutions to naval construction problems and modified the relationship between concrete and steel by reducing the concrete’s role to that of a simple binder. This flexible and shapeable ferro-cement was then combined with fluid and malleable reinforced concrete to create a new material with higher potentials for curved, undulated and folded membranes (Greco, 1994). According to Chiorino, this thin layer of reinforced concrete with a thick mesh of small-diameter wires exhibited remarkable ductility and resistance to cracking (Chiorino, 2012). According to Nervi, this material presented all the mechanical behaviors of a homogeneous material (Nervi, 1956). Nervi designed flat ribbed slabs as well as curved roof surfaces using ferro-cement. Two built roof systems, among the many he designed, and one proposal for a roof system that allows daylight in through perforations, are briefly reviewed here.

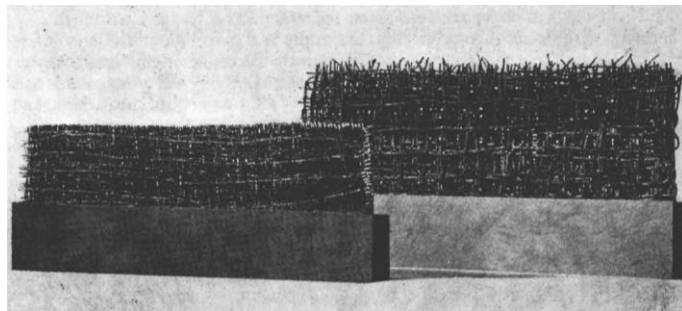


Figure 3.10. Thin slab samples reinforced with different layers of wire meshes (Greco, 1995)

Festival Hall, the elliptical dome built in 1952 in New Baths, Chianciano, Italy, is a 25.9 m by 32.3 m dome (85 by 106 foot) that was built with precast elements, and in which the disposition of the ribs is rather free (Figure 3.11) (Nervi, 1965). Nervi in *Aesthetics and Technology in Buildings* notes that “the first two rows of elements were left open to light the dome from the clerestory window placed around the perimeter” (Nervi, 1965, p. 134). He also compares this elliptical dome with domes of revolution “which present repeating patterns and require forms to be built only for a single sector” (Nervi, 1965, p. 81) to express that there were many different shapes that are required in the ellipsoidal roof. He then notes that “the elliptical shape of the

ballroom operated against prefabrication, and its economical advantage is doubtful” (Nervi, 1965, p. 81) although he concludes that there had been considerable savings in time and labor at the end.

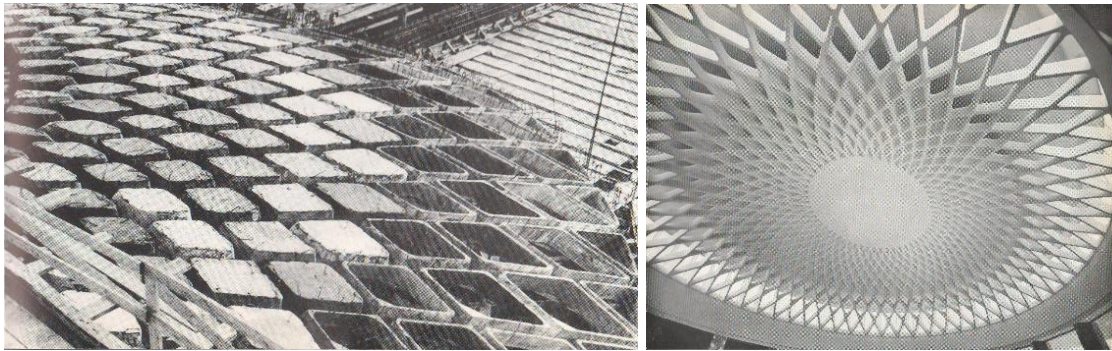


Figure 3.11. Precast elements prior to the placement of the in-situ concrete (a); Festival Hall dome (b) (Nervi, 1965)

The Papal Audience Hall in Vatican City is an example of a perforated concrete plate, designed and built in 1963–71 (Bergdoll & Pourtois, 2010). In the ribbed flat slab, the ribs follow the isostatic lines of the principal bending moments (Figure 3.12).

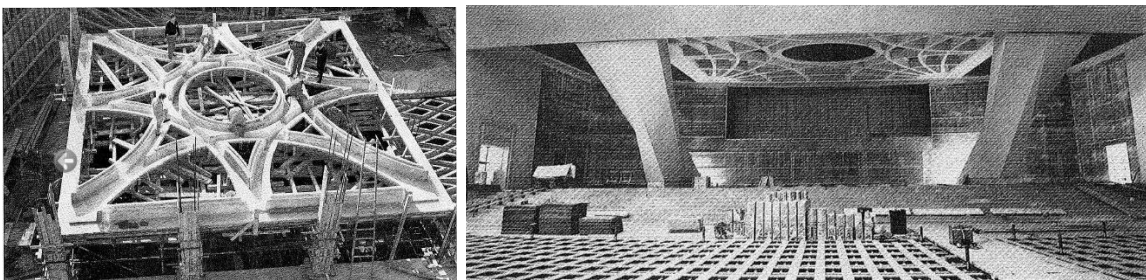


Figure 3.12. Concrete plate with an oculus in the Papal Audience Hall (“Paolo VI Audience Hall in Vatican City,” n.d.)

Another example is Nervi’s design for the “Centre national des industries et technique” in Paris in 1955. The structure consisted of three intersecting arches with diagrid vaulting between the ribs (Nervi & Joedicke, 1957). Although the geometry resembles a shell structure (Figure 3.13), its structural calculation is not based on the theory of shell construction, but on the principle of cross-vaulting. Nervi designed it with pre-stressed concrete and prefabricated elements of ferro-cement for the node points of the vaulting (Nervi, 1965).

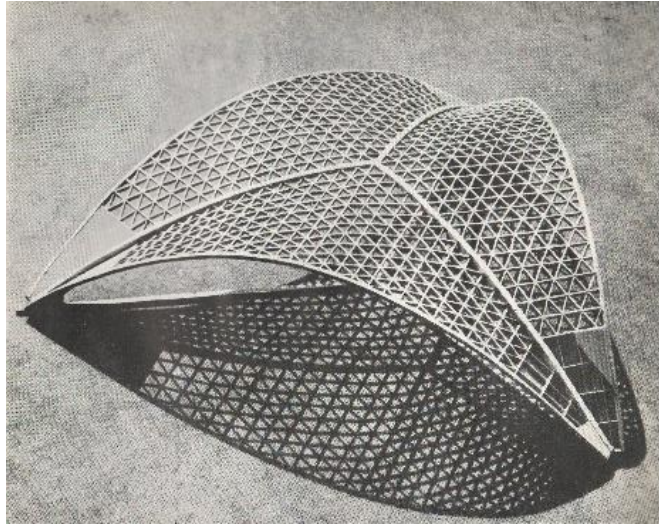


Figure 3.13. Nervi's structural model for the Centre national des industries et technique (Nervi, 1965)

3.2.3 Felix Candela

Felix Candela (1910–1997) is another Spanish-born master builder and structural engineer. He enrolled at the Central University of Madrid, where he had to take two demanding years of mathematics and physics before qualifying for enrolment in architecture or engineering. Eduardo Torroja had designed the mathematics curriculum for this program (Cassinello & Torroja, 2010). After he finished his studies in 1935, he became involved in the Spanish Civil War and was ultimately exiled to Mexico in 1939. The majority of his structures are built in Mexico.

Candela used hyperbolic paraboloids in the design of his shells and described them as the easiest and most practical to build (Garlock & Billington, 2008). The shape is also referred to as *hypar* and has the property of being defined by straight lines. The edges of the hypar can be straight or curved. He used a hypar with straight edges in many structures. According to Garlock & Billington (2008, p. 98) “Candela’s bread-and-butter structure was the umbrella, a hypar with straight edges all in the same plane.” In fact, he roofed 3,000,000 sq. foot in the new industrial zones of Mexico City with umbrellas, in the shapes of “square or rectangular, rhomboidal, polygonal” in “churches, warehouses, factories, hotels and restaurants, residences, in a bank and even in a casino” (Faber, 1963, p. 11).

An example of the perforated shell designed by Candela is the High Life Textile Factory (1954–55) in the Coyocan section of the Mexico City (Figure 3.14). The umbrella shells are sloped, presenting a saw-tooth profile. The shells are also perforated, and glass bricks are installed in the perforations. After the building was occupied, however, the glass bricks were covered with heavy

asphalt paper and tar, to reduce the excessive inside heat generated by ironing with steam, and by the hot Mexican sun. The use of glass brick in this manner was not repeated by Candela, although he used tilted umbrellas to allow light to enter the structure in other projects (Garlock & Billington, 2008).

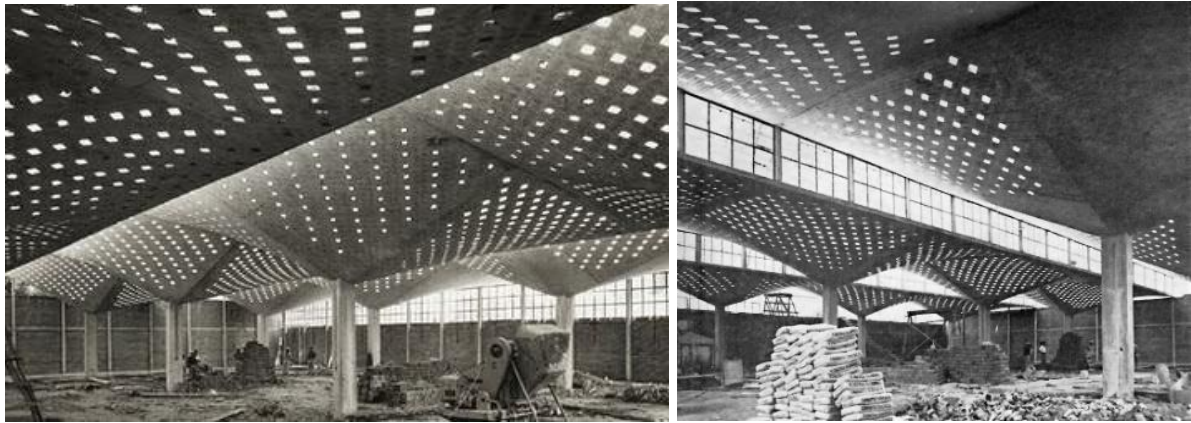


Figure 3.14. Perforated umbrella roof of the Textile Factory designed by Felix Candela (Garlock & Billington, 2008)

Later in 1958, Candela worked in collaboration with American engineer O’Neil Ford to erect a series of hyper structures for the Insignia of the Great Southwest Corporation in Fort Worth, Texas (Figure 3.15) (Mendoza, 2015). The perforations in these shells are fewer than in the High Life Textile Factory, and the purpose seems to be aesthetic, rather than the introduction of daylight.

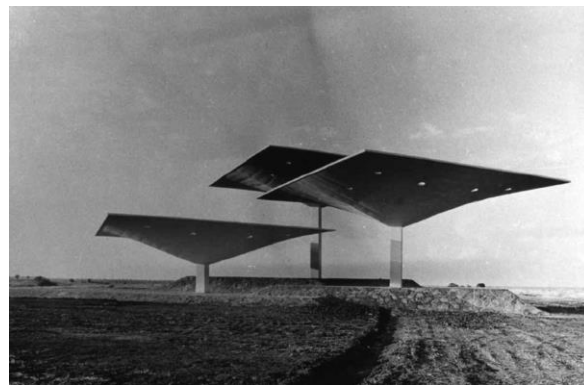


Figure 3.15. Insignia of the Great Southwest Corporation, Texas (Mendoza, 2015)

3.2.4 Heinz Isler

Heinz Isler (1926–2009) developed unique methods of designing shells primarily in Switzerland, south-west Germany, and France (Ramm, 2011). All previous shells constructed by other shell builders used forms that were based on simple geometries, such as cylinders, cones, spheres and hyperboloid surfaces. Isler’s shells were form found using physical models such as pneumatic forms and inverted membranes. He designed free-form shells “in the sense that they do

not have a regular geometry, however, they are essentially based on combinations of circular curves” (Chilton, 2000, p. 70).

Bubble shells are one of his best-known shells; he was inspired in their design by a plumped up pillow (Chilton, 2000). These were the standard shells that Isler designed for small industrial units, garages, warehouses and the like. He assembled multiple units to cover a large span with a limited number of internal supports. According to (Chilton, 2000, p. 51), “between 1955 and 1959, Isler built a total of 33 bubble shells ranging in size from 14 x 20 m up to a maximum size of 22 x 22 m.” The thicknesses of the edge beams are 1/25 of the span, and the apparent shell thickness around the skylight of the shell structures is in the region of 250 to 300 mm. This thickness includes the upstand around the skylight to prevent the entrance of rainwater, as well as the insulation and the permanent shuttering. Only 80 to 100 mm of this is the structural shell (Chilton, 2000).

The use of roof lights is a distinctive feature of bubble shells. (Chilton, 2000, p. 52) explains the standard number of the openings in relation to shell dimension and notes that “for the smaller shells, up to 25m x 25m, there is usually one central dome, but for bubble shells of 30m x 30m, four are generally used, one at the center of each quadrant” (Figure 3.16). These openings have the advantage of admitting light and had the potential of being opened to provide ventilation. This method also provided light with greater intensity compared to the light entering through the perimeter, into the center of the large clear span, reducing the need for artificial lighting (Chilton, 2000).

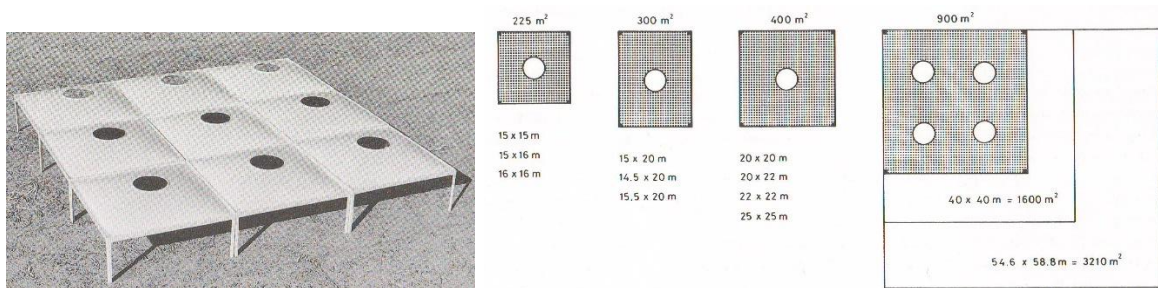


Figure 3.16. Assembly of bubble shells (a); typical standard bubble shells (b) (Chilton, 2000)

The largest of Isler’s early bubble shells is the 1960 COOP warehouse in Wangen bei Olten. The 54.6 m x 58.8 m shell has a rise of 9 m above the supports with an approximate thickness of 150 mm. The shell contains 17 circular openings, representing 4% of the total roof area where the 4.0 and 4.5 m diameter openings are organized so that the corner-to-corner arching of the shell is not interrupted (Chilton, 2000) (Figure 3.17).

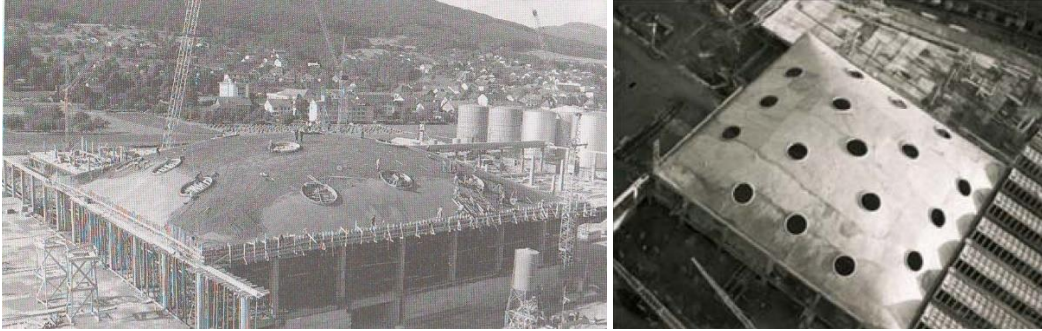


Figure 3.17. Concretion of the COOP storage and distribution center (a) (Chilton, 2000); completed shell (b) (Ramm, 2011)

Isler designed free-form shells as well. Wyss Garden Centre, built in 1962, is his first free-form shell, while the Kilcher Factory built in 1965 in Rechterswil, Solothurn, is his first free-form shell with an opening. The Kilcher Factory's 25.3 x 25.3 m shell has a thickness of 90 mm and a 5.0 m diameter skylight at the center (Figure 3.18a) (Chilton, 2000).

Isler also designed inverted membrane shells. The Sicli Factory in Geneva, built in 1969, is the most complex hanging free-form shells resting on seven supports with a general thickness of 100 mm. The larger portion of the shell has a roughly square plan, with a circular opening of 6.0 m in diameter in the middle, whereas the second portion is pierced by a series of small-diameter circular openings (Figure 3.18b) (Chilton, 2000).

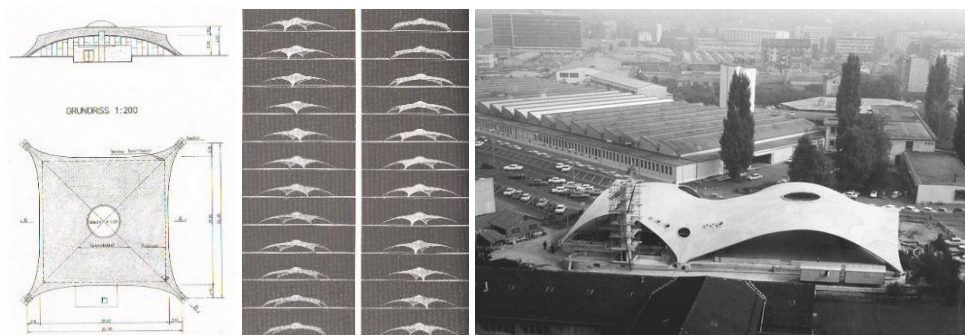


Figure 3.18. Kilcher free form shell (a); Sicli Factory in Geneva (b) (Chilton, 2000)

3.2.5 Frei Otto

Frei Otto (1925–2015) is the German architect and structural engineer who led the Institute for Lightweight Structures (IL) from 1964 to 1990. Minimal surface systems and minimal structures using soap bubble tests have been among his significant fields of study (Flächentragwerke, 1969). Although he mainly designed lightweight structures, including cable nets and gridshells, to realize

the forms that he found, he collaborated with Duesseldorf architects Ingenhoven, Overdiek und Partner, along with Buro Happold Engineers, to design a pressure-loaded shell for the main train station in Stuttgart in 1997 (Otto, 2005). The concept was influenced by a tear-shaped soap film, and they decided to use a pressure-loaded shell rather than a tensile-stressed membrane for design (Figure 3.19) (Frei Otto, 2005). The average thickness of the shell was designed to be 42 cm (Dickson, 1998).

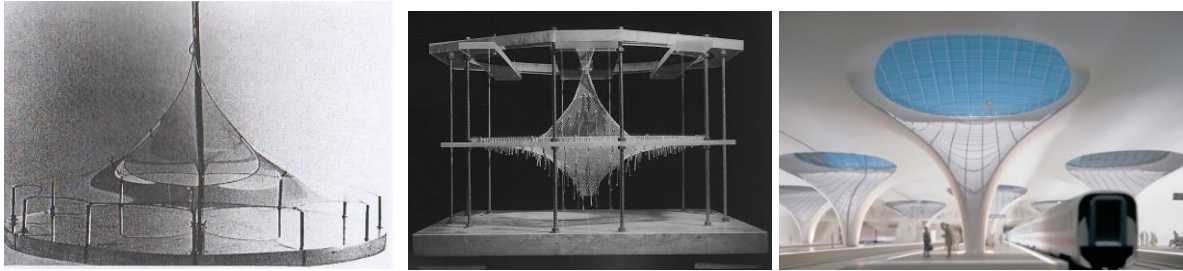


Figure 3.19. Soap film form finding (a); compression model (b); train station model (c) (Frei Otto, 2005)

3.2.6 Recent precedents

The previous section reflected on the works of shell design pioneers with an emphasis on the design of perforated shell structures. According to (Sasaki, 2014, p. 259), the “1950s and 1960s is referred as the era of Structural Expressionist- a period that generated new types of architectural spaces from structurally rational shells- and remembered as a peculiar age in the history of architecture.” However, during recent decades, and according to Jörg Schlaich, concrete shells lost more ground to cable nets, textile membranes, and steel grids (Schlaich, 2014). Sasaki lists the reasons for reduced construction of reinforced concrete structures nowadays as “scarcity of skilled workers, rising prices for formwork, cost and schedule challenges, the inefficiency of on-site fabrication, large deformations, deteriorations in the concrete, and a transition to steel gridshell to satisfy new demands” (Mutsuro Sasaki, 2014, p. 259).

Recently, and in the half-century following the decline of concrete shell construction, there is a renewed interest in these structures. The reason is threefold. Firstly, there is a rise of a new trend in architecture towards expressing free-form shapes with complex and organic characteristics, a contemporary shell design. Secondly, material developments have led to the availability of lightweight, thin reinforcement materials for concrete on one hand, and more efficient concrete mixes on the other hand. Thirdly, Computer Aided Manufacturing (CAM) methods have evolved as an aid in constructing these complex forms.

As an example, a group of researchers designed a micromesh which was stapled over the entire

cross section of a shell and built a prototype of their material system (Figure 3.20a) c. Another group of researchers used large-scale CNC milling to make the formwork for a concrete shell (Figure 3.20b) (Dombernowsky & Søndergaard, 2012).



Figure 3.20. Shell with a wiremesh (a) (Eisenbach, Vasudevan, Grohmann, Bollinger, & Hauser, 2014); a shell manufactured with CNC milled formwork (b) (Dombernowsky & Søndergaard, 2012)

There are other examples of modern shell structures. The shell built for the Teshima Art Museum in Japan is 25 cm thick and the arc of the dome is 4.5 m height, having one layer of reinforcement laid on top (Figure 3.21a). The Rolex Center, designed by SANAA, a porous rectangle perforated by fourteen rounded patios is another example (Mutsuro Sasaki, 2014) (Figure 3.21b). Finally, an ellipsoid-shaped concrete shell designed to cover a mall at Chiasso, Switzerland, 100 mm in thickness, is another contemporary example (Muttoni, Lurati, & Fernández Ruiz, 2013) (Figure 3.21c).



Figure 3.21. Teshima Art Museum, Japan (a); Rolex Learning Center, by SANAA (b); Mall at Chiasso (c)

The shell in the Confluence Park in San Antonio is the most recently constructed perforated shell at the time of writing (Figure 3.22). Its construction started in May 2016, and the opening ceremony was held in Spring 2018. Local architectural firm Lake/Flato was selected for the project and engaged Andrew Kudless, principal of Matsys design, to consult on the pavilion. The 30-foot-high canopy consists of concrete panels that capture and funnel rainwater into an underground storage tank. Fiberglass composite molds were built by Kreysler and Associates and shipped to Texas for on-site concrete construction. The structural engineering was done by aecollab.



Figure 3.22. Concrete shell in Confluence Park, San Antonio, Texas

3.2.7 Perforated concrete shell structures timeline

Looking at the history of shell construction and the work of the shell pioneer designers of the 1950s, triangulated and rhombic perforations are present in Torroja’s Fronton Recoletos roof and Nervi’s Festival Hall, respectively, as well as square and circular perforations in the hyperboloids designed by Candela, and Isler’s bubble shells, respectively. Free-form perforations are found in more contemporary projects, such as the Teshima Art Museum. Figure 3.23 illustrates the timeline of perforated shell design, starting from the Torroja’s example, through the 1950s–1970s, and ending with contemporary examples.

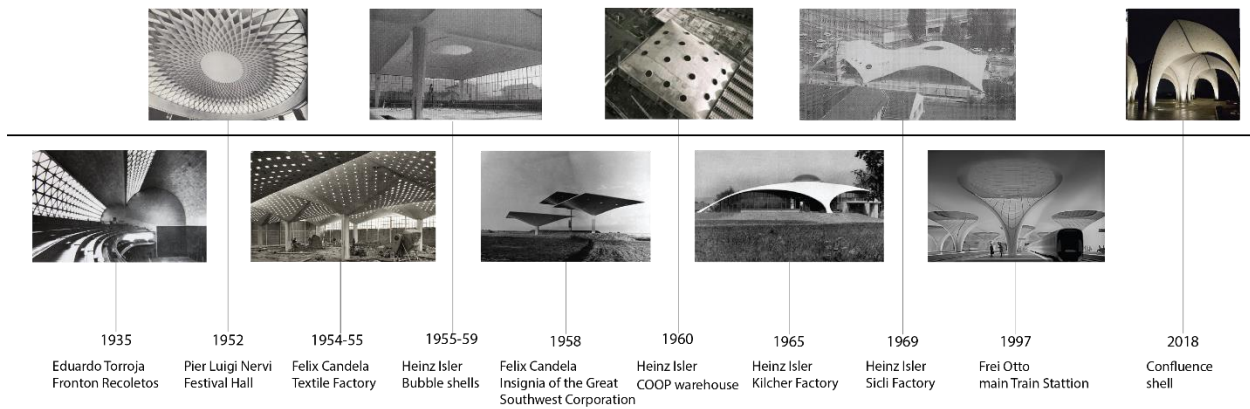


Figure 3.23. Timeline of perforated concrete shell structures

3.3 Topology, shape and sizing

This section aims to introduce the structural design principles, namely topology, shape, and sizing. Each concept is discussed first, and then explained in the context of shell structures. The outcome of this section is a categorization of the structural design principles for shells that will be carried over to Chapter 5.

Apart from material optimization, structural optimization addresses three major categories: topology (layout) optimization, looking for an optimal material layout of an engineering system; shape optimization, seeking an optimal contour or shape of a structural system whose topology is fixed; and sizing optimization, searching for optimal cross-sections or dimensions of elements of a structural system whose topology and shape is fixed (Kicinger, Arciszewski, & De Jong, 2005). They further note that the aforementioned three aspects of the structure correspond to major stages in the engineering design process, namely “conceptual design,” concerned with the functional requirements and architectural aesthetics, “embodiment or design development,” and “detail design,” respectively (Kicinger, Arciszewski, & De Jong, 2005, p. 1958) (Figure 3.24).

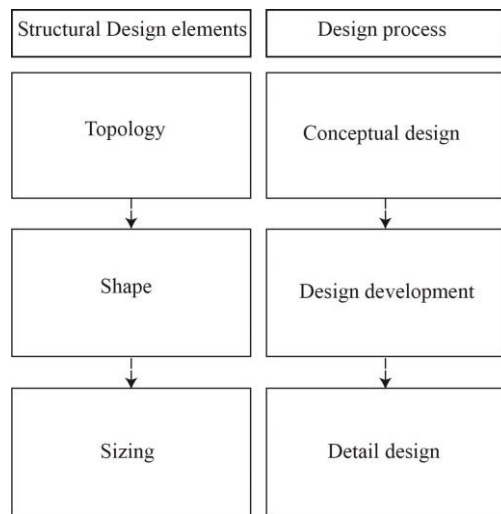


Figure 3.24. Trinity of topology, shape, and sizing in structural design, and its correspondence with design stages

There are different methods for topology, shape, and sizing optimization in structural design. According to a group of researchers there are single-level optimization methods in structure, meaning that a single optimization algorithm¹ is used to operate on the shape and sizing variable simultaneously. Considering deterministic methods, *stress-ratio* is one common method applicable to stress- and local buckling-constrained structures, which “seeks to proportion each member of the structure so that it is loaded to the maximum safe performance limit under the action of at least one of the applied load cases” (Flager, Adya, Haymaker, & Fischer, 2014, p. 2). A

¹ This includes deterministic and heuristic methods. “Linear programming,” “non-linear programming” and “branch and bound” methods are other deterministic methods. Heuristic methods including “genetic algorithms,” “simulated annealing” and “evolutionary strategies” are capable of handling both discrete and continuous variables simultaneously, thus can be applied to conceptual structural design problems involving topology as well as shape and sizing (Flager et al., 2014).

structural design problem can be further classified as continuous or discrete. This section reviews the concepts of topology, shape, and sizing in both continuous and gridshell structures.

3.3.1 Topology

Topology is a subfield of geometry that studies the continuous transformations of a graph or interface. “Etymologically, the word is derived from the Greek noun, *topos*, which means location, place, space, or domain. Mathematically speaking, topology is concerned with objects that are deformable in a so-called rubber-like manner” (Eschenauer & Olhoff, 2001, p. 335). In other words, and according to (J. Liang, Zhang, Xu, Li, & Huang, 2013), topological transformation refers to the continuous transformation of the interface, where the graphics can be arbitrarily bended, deformed, widened or narrowed as long as a surface is not cut open. In topology, any change that can continuously be undone is allowed. Therefore, a circle is the same as a triangle or a square, because one can just pull on parts of the circle to make corners, and then make those corners straight (Figure 3.25) (J. Liang et al., 2013).

Homeomorphous transformations is another term that refers to the continuous transformation of the interface. Tedeschi (2014) explains that homomorphism between two figures is controlled by a parameter called “genus.” The genus, or the *g*-value of a figure, is equivalent to the number of holes within the geometry. As an instance, a sphere and a cube both have a *g*-value of 0, while a torus has a *g*-value of 1.

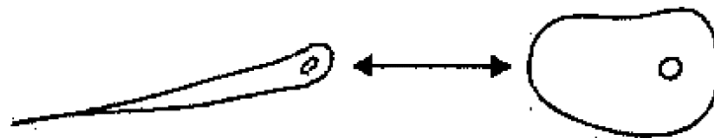


Figure 3.25. A sewing needle topologically changes into another shape with the same genus value (J. Liang et al., 2013)

From the mathematical point of view, researchers note that “a topology class is generally defined by the degree of connection of domains” (Eschenauer & Olhoff, 2001, p. 335). Figure 3.26 illustrates a simply connected domain as well as two- and three-fold connected domains.

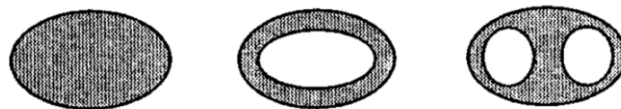


Figure 3.26. Simple (a), two-fold (b), and three-fold (c) connected domains

They further explain the concept of topological equivalence from the mathematical point of view by expressing that “two topological domains are termed topologically equivalent if there exists a topological mapping of one of the domains into the other” (Eschenauer & Olhoff, 2001, p. 335) (Figure 3.27).

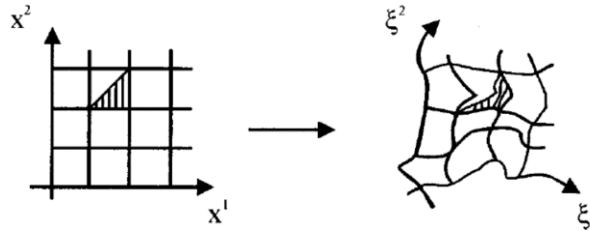


Figure 3.27. Topological mapping of one domain into the other one (Eschenauer & Olhoff, 2001)

Tedeschi (2014) also compares classical geometric definitions of a shape with the topological approach to a problem using graphs. The connection of domains is of interest in topology, whereas the exact dimensions and angles are the focus of geometric definitions (Figure 3.28).

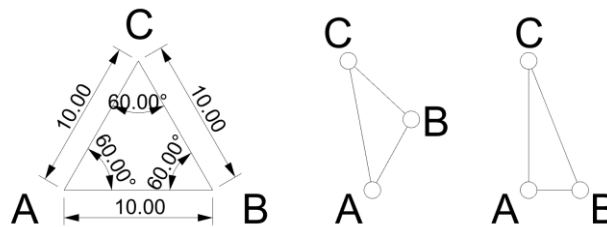


Figure 3.28. Classical geometric definition of a shape (a); versus the topological approach using graphs (b & c), after (Tedeschi, 2014)

In structural design and optimization, topology optimization is performed to obtain a first view of an optimal configuration for the structure considering the optimal load paths (Krog, Tucker, & Rollema, 2011). Topology optimization is rooted in the interest in improving the quality of products by finding the best possible topology in a very early stage of the design process. Topology optimization changes the neighborhood relations; the design object transforms into a different topology class. “The position and shape of the new domain is of no importance in topology optimization phase, although both positioning and shape influence the structural and mechanical behavior of a component ” (Eschenauer & Olhoff, 2001, p. 335). Therefore, the component is improved by both optimization of both topology and shape. The former is the focus of this section and the latter will be explained in the following section.

As noted, in continuous structures such as perforated shell structures, topology is defined by the number of holes in the structure, whereas in grid structures, topology depends upon the number and connectivity of the members, as illustrated in Figure 3.29.

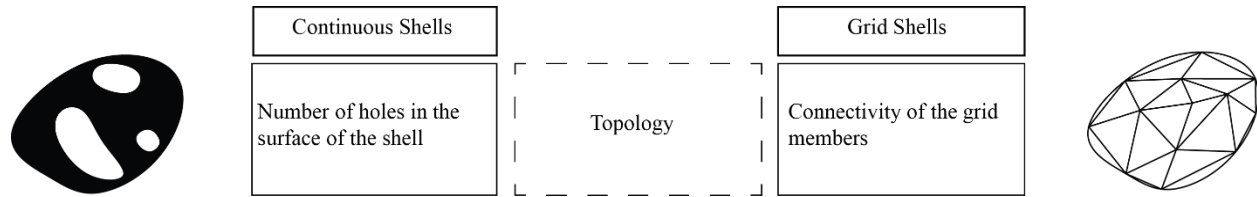


Figure 3.29. Topology in continuous and discrete structural systems

Topology optimization can be applied to the design of all structural systems including beams and bridges. A group of researchers used topology optimization to design three-dimensional concrete elements that are pre-fabricated and pre-stressed; they applied the methodology to concrete beams and slabs (Dombernowsky & Sondergaard, 2009). In another study, Grohmann et al. (2010) point to an evolutionary process that was employed to generate different generations for a pedestrian bridge in Reden, Germany, where the position of diagonals, and thus the topology of the lattice girder, was altered by the algorithm, while the upper and lower chord of the bridge were predefined by hyperbolic paraboloids (Grohmann & Tessmann, 2011). A researcher employed topology optimization as a concept design tool in architectural form finding of a bridge spanning 50 meter and a shelter (Frattari, Dagg, & Leoni, 2013), while another researcher compared natural structures to structural shapes designed by topology optimization (Irmgard Lochner-Aldinger, Karl, & Adriaenssens, 2015).

Topology optimization has been applied to the design of continuous shell structures in particular. It has been stated that significant reductions in the mass of the structure can be achieved through topology (and shape) optimization of the gridshells (Richardson, Adriaenssens, Coelho, & Bouillard, 2014). In one study, a researcher systematically varied the supporting conditions of a design space within a given volume while maintaining consistent loadings, objectives and constraints, in order to create comparable structural surface geometries (Irmgard Lochner-Aldinger, 2011). Once three-dimensional topology optimization was carried out to find an efficient shell surface shape (Figure 3.30a), that shape was used as an input for the second step to recognize the material distribution within a given curved surface by employing topology optimization (Figure 3.30b). Ultimately, the researchers retrieved a non-continuous, grid-shell-like surface structures which resemble the shape of diatoms. It should be noted that the structure resulting from

the optimization method is a design proposal, without consideration of stability problems such as buckling; therefore, it would need to be interpreted to generate a real structure.

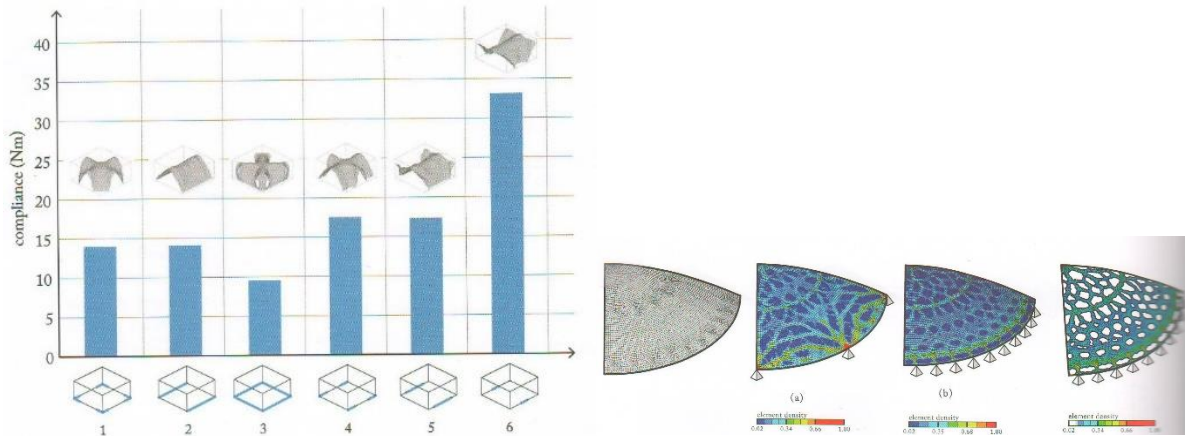


Figure 3.30. Cubical design space with varying support conditions (a); topology optimization (b) (Imgard Lochner-Aldinger & Schumacher, 2014)

There are many instances in which topology optimization is applied to the design of shell structures. In a research study, researchers use a GA to optimize a steel gridshell with voronoi patterns. The location of the shell supports is varied from four sides of the square base, to three, and then two, sides. In general, researchers note that the kinematic stability of a discrete structure, such as a gridshell, is linked to its topological variables. In another research study, an evenly distributed loading case consisting of an external static load and an approximation of the self-weight are considered as loading for a canopy. The objective of the optimization is to minimize the weight. Three constraints are considered in the optimization process, including the maximal stresses in the elements, the local buckling of the elements, and the total deflection of the structure obtained by an FE analysis. The researchers do not assess global buckling due to its computationally costly non-linear analysis, but suggest that once the optimal structure subject to these three constraints is found, the structure can be checked against nonlinear global buckling (Richardson et al., 2014). In another study, Winslow (2014, p. 170), breaks free-form engineering design problems into three stages, namely designing the surface form, the grid layout and the member sizing. He works with the assumption that the surface geometry is given, and the detailed member sizing will be carried out later, and thus focuses on the design of structural grid only, which is referred to as lattice or grid optimization. He notes that the general methodology is not limited to gridshells, and can be used for “ribbed reinforced concrete, ribbed steel shells, or fiber

reinforced polymers” (Winslow, 2014, p. 182). He points to the competing objectives that exist in a gridshell optimization problem, such as having equal member lengths, being efficient under load conditions, having a minimum weight, and so on. He emphasizes that the designer needs to explore the Pareto optimal set to understand the trade-offs between competing objectives (Winslow, 2014).

Taking a step back to consider the concept of topology in shells, it can be said that a continuous surface can be perforated to such an extent that it becomes a gridshell (Figure 3.31). The Fronton Recoletos roof designed by Torroja demonstrates a vault system where a perforated and a continuous shell, the two extremes, coexist within the same system. One of the hypotheses of this study is that depending on the material strength and position of the perforations, there is some point along the transition where the forces are mainly carried through discrete members; thus, a gridshell is a better typology to describe the structure.



Figure 3.31. Topology spectrum from a continuous to a gridshell

3.3.2 Shape

A shape is defined by the oriented boundary curves in two-dimensional structures, or by boundary surfaces in three-dimensional structures (Kicinger et al., 2005). Basic geometric objects such as a point, a line, a curve, and a plane are the building blocks that create simple geometric shapes. Many two-dimensional shapes can be defined by a set of points and lines, such as polygons,² or by bounding curves, such as a circle or an ellipse. Many three-dimensional geometric shapes can be defined by a set of points, lines and planar faces, such as polyhedrons,³ or be bounded by curved surfaces, such as a sphere or an ellipsoid. Many complex shapes, such as those seen in nature, cannot be described by descriptive geometry, and may be analyzed by differential geometry.

² Including triangles, squares, and pentagon

³ Including pyramids, cubes, and tetrahedrons

In structural design, shape optimization is performed to improve structural behavior of the systems. According to Veltkamp et al., “in common structural design of free-form structures, the shape is the foremost design parameter and the most effective to change the overall structural behaviour” (Veltkamp, Basso, & Lago, 2012, p. 248). Kicinger et al. (2005, p. 1959) note that “shape optimization maintains a fixed topology of structural designs but changes their shape or nodal locations.” Shape optimization can be applied to both continuous and discrete problems. When considering continuous design problems, “a shape is defined by the oriented boundary curves (of 2d structures) or boundary surfaces (of 3d structures) of the body...and the optimal form of these boundaries is computed” (Kicinger et al., 2005, p. 1939). Or, as stated by another researcher, the optimal shape of a continuum structure is obtained by changing the boundaries of the design domain (Q. Q. Liang, 2010). When considering discrete problems, the location of nodes can be changed to change the shape (Kicinger et al., 2005). Shape optimization in continuous and discrete systems is demonstrated in Figure 3.32.

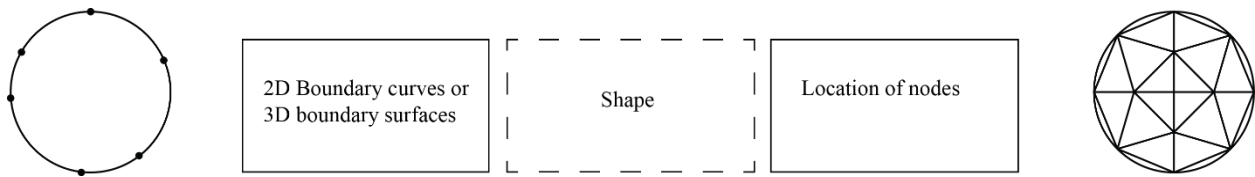


Figure 3.32. Shape in continuous and discrete structural systems

Shape optimization has been conducted for many shell structures. In a research study, the shape of a free form shell was modeled using a NURB (Non-uniform rational basis spline) surface inspired by the Kakamigahara Crematorium designed by Toyo Ito. The shell was then structurally optimized by means of a genetic algorithm (Pugnale & Sassone, 2007). In another research study, Richardson & Adriaenssens (2014) conducted shape optimization of a gridshell related to x- and y-coordinates of the nodes. The z-coordinates were constrained to a surface, interpolated through the original gridshell nodal positions (Richardson et al., 2014).

Another example of shape optimization is observed in the design of the greenhouse facility in Gringrin, Fukuoka. Toyo Ito imagined an initial shape for the main roof: a single continuous surface twisting twice to form three blocks. Sasaki used a shape design method (sensitivity analysis) to modify and optimize the initial shape. This generated the optimum structural shape with the least possible bending stress and a minimum of strain energy and deformation (Figure 3.33). Each block is made of reinforced concrete free-curved surface shell with 40 cm thickness,

spanning 50 meters by partially touching the ground (Mustsuro Sasaki, 2007). It should be noted that the sensitivity analysis did not modify the number of openings, and thus did not affect the topology of the surface, but instead slightly varied the shape of the surface to create a more efficient structure.

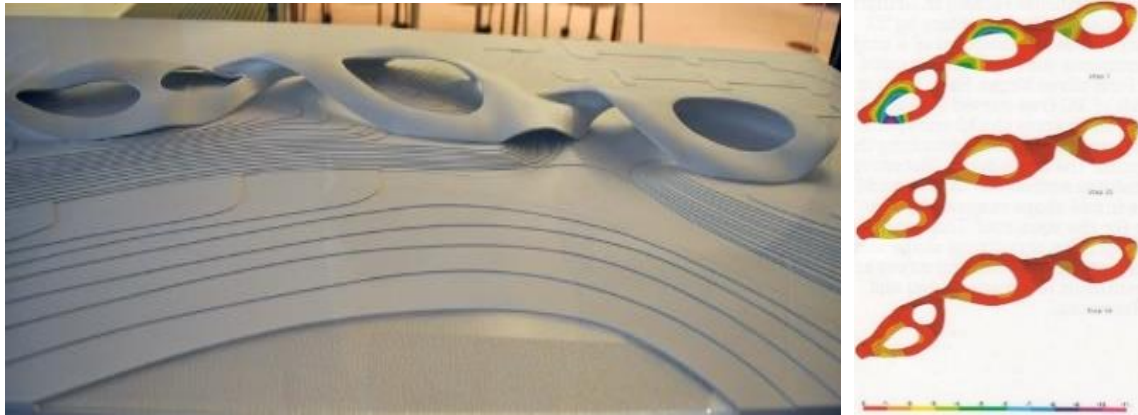


Figure 3.33. A topology explored by Ito and later optimized by Sasaki for a continuous structure (Mustsuro Sasaki, 2007)

In the design of the gridshell for the British Museum courtyard, the geometrical definition of the roof consisted of two parts: the shape of the surface and the pattern of steel members upon the surface (Burry & Burry, 2010). A researcher describes the process of generating the final geometry by pointing out that “the shape of the roof is defined by a surface on which the nodes of the steel grid lie” (Williams, 2001, p. 2). The *surface geometry* is defined by three main mathematical functions. The *structural grid*, on the other hand, is produced from a mathematical grid that is created by first dividing the outer rectangular and inner circular boundary lines equally, second, by joining them together, and third, dividing the formed radial lines into varying number of equal segments, and fourth, joining the dots. Finally, the grid is relaxed to remove the produced discontinuities, particularly in the diagonal directions. He also mentions that the limitation on glass size was the controlling factor in choosing the structural grid (Williams, 2001). In the design of the courtyard roof, the overall shape of the surface and the discretization of panels were changed together (Figure 3.34).



Figure 3.34. British Museum Courtyard (a); Renderings of the great court (b) (Burry & Burry, 2010)

3.3.3 Sizing

“Size optimization problems involve finding optimal cross-sections, or dimensions, of elements of a structural system whose topology and shape is fixed” (Kicinger et al., 2005, p. 1958). Sizing cross-sections in gridshells, or defining the thickness of the shell, and the size of the openings in perforated continuous shells, are examples of sizing (Figure 3.35).

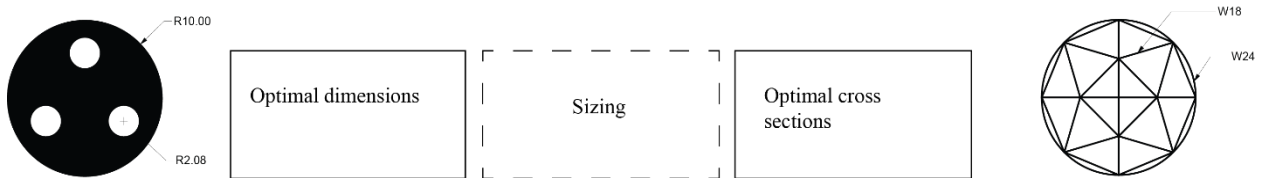


Figure 3.35. Sizing in continuous (left) and discrete (right) systems

It should be noted that the thickness of continuous shells can vary throughout the shell’s cross sections based on the varying loads on the surface. Thickness is not always constant, and it can be varied throughout the shell’s cross section.

3.3.4 Summarizing topology, shape, and sizing in shells

Structural optimization addresses three major categories, namely topology (layout), shape, and sizing to look for an optimal material layout, an optimal shape, and optimal cross-sections or dimensions of the elements, respectively. The performance of a component can be improved by optimization of both its topology and shape. Topology optimization changes the neighborhood relations, where the design object transforms into a different topology class. The position and shape of the new domain is of no importance in the topology optimization phase, although both

positioning and shape influence the structural and mechanical behavior of a component (H. A. Eschenauer & Olhoff, 2001, p. 335).

Looking at perforated concrete shells as an instance of continuous shells, topology is concerned with the number of openings, shape is concerned with the boundary curves of the underlying surface, and sizing is concerned with the thickness of the shell. Looking at gridshells, topology is concerned with the number and connectivity of the members, whereas shape is concerned with the location of structural joints, and finally, sizing is concerned with member cross-sections (Flager et al., 2014). These concepts are demonstrated in relation to continuous and gridshells in Figure 3.36.

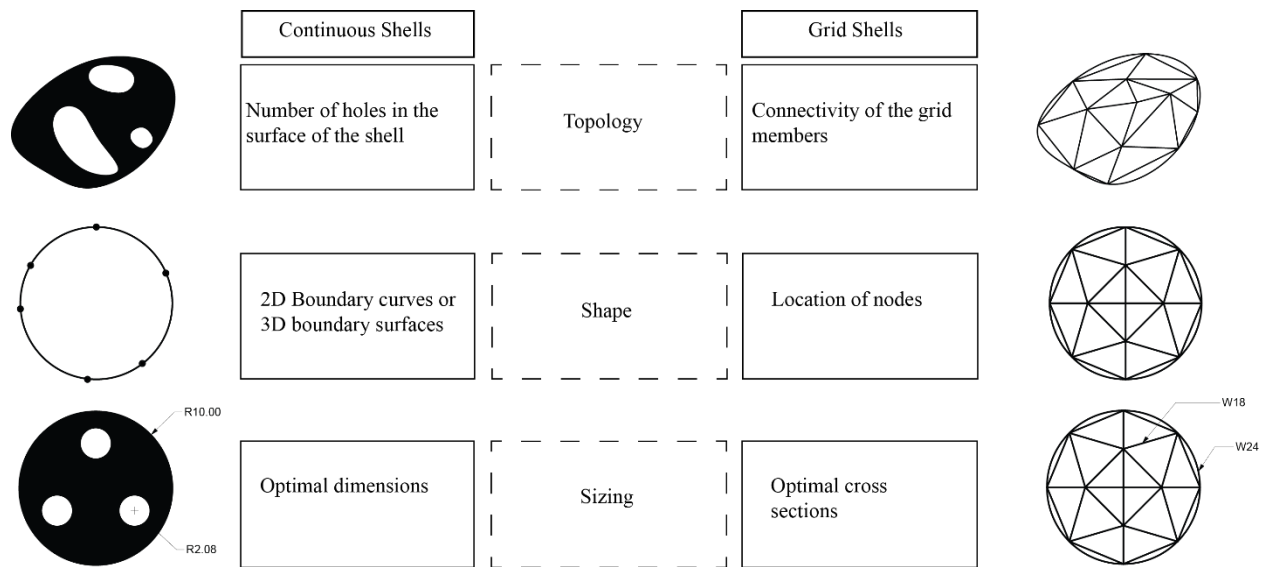


Figure 3.36. Topology, shape and sizing optimization in shells and gridshells

3.4 Relevant metrics for performative shells

The geometric properties of the shells, many of them expressed as ratios, affect the structural performance of the shells under loading. One important property is the span-to-rise ratio (L/d), which can vary widely; most shell structures occur in the range of $2 < L/d < 10$ (Ochsendorf & Block, 2014). As an example, a shell covering a 50-m span can typically have a rise of between 5 to 25 meters. Another property that affects a shell's structural behavior is curvature. As they note, when shells are loaded, the double curvature of a dome is structurally superior to the single curvature of a cone or a barrel vault in the event of asymmetrical live loading (Ochsendorf & Block, 2014).

From another point of view, there are dominant structural actions that appear in shells. As noted in the introduction, shells transfer loads through membrane forces (compression and tension)

and bending. According to (Williams, 2014), when a shell is in compression, it deflects, leading to buckling. Buckling is resisted by a combination of bending and in-plane action (Williams, 2014). Veltkamp et al. (2012) note that design criteria may be defined at various levels of abstraction for shell-like structures to facilitate optimal performance. These include criteria for strength and stability for ultimate limit state (ULS), and for the serviceability limit state (SLS). Focusing on the design stage in particular, they note: “for the design stage however, when the structural scheme is only decided in principle, but its precise dimensions are yet to be defined, the performance criteria may be too detailed for a meaningful assessment. Instead, from a design-perspective awareness, of the sensitivity of a scheme to variations of its design parameters, is of greater practical value: while a generally performing solution is presented in the stage of the concept design, the fine-tuning can be left to the detailed design stage. For such an approach, it is imperative to have knowledge of the variations that can still be made without impacting on the initial scheme” (Veltkamp et al., 2012, p. 248). They also note that the static design criteria can be defined as an allowable deformation relative to the height or span of the shell, whereas the dynamic design criteria⁴ is defined as a composition of the structure’s eigenmodes and frequencies, which is more elaborate.

In a study, Bertin (2013) utilized the static analysis and linear buckling analysis for gridshells. The former determines displacements, stresses, strains, and forces in structures caused by induced loading. The latter also referred to as eigenvalue or modal buckling predicts the “theoretical buckling strength of an ideal elastic structure” (Bertin, 2013, p. 36). Lochner-Aldinger did not consider buckling issues in her topology optimization studies, and noted that the structure resulting from the optimization method is a design proposal, without considering stability problems, such as buckling, and needs to be interpreted to generate a real structure (Irmgard Lochner-Aldinger, 2011). Richardson & Adriaenssens (2014) did not simulate global buckling in one of their studies, where they note that global buckling is not assessed due to its computationally costly non-linear analysis; however, they suggested that once the optimal structure is subjected to three constraints (the maximal stresses in the elements, the local buckling of the elements, and the total deflection of the structure), the structure can be checked for nonlinear global buckling (Richardson et al., 2014). The key design parameters that are employed in the design of shell structures are

⁴ Load from wind or seismic action

summarized in Table 3.1. Thereafter, some performance criteria that is measured by designers in the field is summarized in Table 3.2.

Table 3.1. Key design parameters that are considered in the design of shell structures

Design parameter	Recommendation
span-to-rise ratio (L/d)	$2 < L/d < 10$ *
curvature	A surface with double curvature is structurally superior to a surface with single curvature *
material	As discussed, a range of materials from masonry and concrete, to steel and wood can be used in the design of the shells**

*(Ochsendorf & Block, 2014)

**Section 3.1

Table 3.2. Some performance criteria that is measured in the design of shell structures

Performance criteria	Explanation/ recommendation
Stress-ratio	Applicable to stress- and local buckling-constrained structures, seeks to proportion each member of the structure so that it is loaded to the maximum safe performance limit*
Deflection-to-rise Deflection-to-span	Allowable deformation relative to the height or span of the shell**
Linear buckling (eigenvalue or modal buckling)	It predicts the “theoretical buckling strength of an ideal elastic structure***
Nonlinear global buckling	A researcher did not consider it in his analysis due to its computationally costly non-linear analysis ****

*(Flager et al., 2014)

** (Veltkamp et al., 2012)

*** (Bertin, 2013)

**** (Richardson et al., 2014)

In this multidisciplinary research study, where the overlay of structural and daylighting disciplines at the early stages of design is to be considered, two key performance criteria will be measured: the maximum allowable deflection for serviceability issues, and the allowable von Mises stress levels for strength criteria. Von Mises stress is measured at its third quartile to avoid considering high local stresses as opposed to general stress levels in the structure. This is explained in depth in Appendix B. In addition, weight will be measured which affects cost. The performance criteria are summarized in Table 3.3. The alternatives that meet these criteria are considered design proposals that can later be checked for buckling behavior.

Table 3.3. The structural performance criteria that are considered in this research study

Structural design criteria	Performance metric that is measured
Strength (Stress limits)	von Mises stress (at the third quartile)
Serviceability (deformations)	Maximum deflection
Stability (Buckling load)	Not considered in this research focusing on the early stages of design
Cost	Weight

3.5 Discussion summary

In the first section of this chapter, shell structures were introduced, with a focus on terminology, load carrying behavior, continuous versus grid typologies, and the different materials used to construct them. This introduction provides the fundamental knowledge needed to understand shell structures.

In the second section, the history of the design of perforated concrete shells was reviewed, focusing on the works of Eduardo Torroja, Pier Luigi Nervi, Felix Candela, Heinz Isler, and Frei Otto, built in the era from 1950 to 1970. This review showcases the different concrete shell typologies with different perforation patterns that are designed and built.

In the third section of the chapter, the topics of topology, shape and sizing are discussed, and a classic categorization of them is recreated in the context of continuous and gridshell structures. This classification, and the detailed attributes, create the basis for linking each structural design phase to one or multiple design strategies from another discipline, namely daylighting design. This classification will ultimately be carried over to Chapter 5, to examine the overlap between the structural and daylighting disciplines. Then, the design parameters that affect both disciplines will be isolated. This ultimately will guide the approach to link the two disciplines to define an interdisciplinary design approach.

In the fourth section of the chapter, structural criteria for evaluating the performance of shells in the early stages of design are discussed. The outcome of this phase of the study will be carried over to Chapter 6, where the methodology and simulation settings for performance assessment are explained.

3.6 References

- Addis, B. (2014). Physical modelling and form finding. In S. Adriaenssens, P. Block, D. Veenendaal, & C. Williams (Eds.), *Shell Structures for Architecture* (pp. 33–44). Routledge.
- Adriaenssens, S., Block, P., Veenendaal, D., & Williams, C. (Eds.). (2014). *Shell Structures for Architecture*. Routledge.
- Ban, S. (2014). Sharing the same spirit. In S. Adriaenssens, P. Block, D. Veenendaal, & C. Williams (Eds.), *Shell structures for architecture* (p. xii). Routledge.
- Bergdoll, B., & Pourtois, C. (2010). *Pier Luigi Nervi Architecture as Challenge*. (C. Chiorino & C. Olmo, Eds.).
- Bertin, T. B. (2013). *Evaluating the use of particle-spring systems in the conceptual design of grid shell structures*. Massachusetts Institute of Technology (MIT). Retrieved from <http://18.7.29.232/handle/1721.1/82708>
- Burry, J., & Burry, M. (2010). *The new mathematics of architecture*. New York: Thames & Hudson.
- Cassinello, P., & Torroja, J. A. (2010). Félix Candela: His vocational training at the university and his subsequent relationship with the institute founded by Eduardo Torroja. *Journal of the International Association for Shell and Spatial Structures*, 51(163), 87–95.

- Chilton, J. (2000). *The Engineer's Contributions to Contemporary Architecture: Heinz Isler*. (A. Macdonald & R. Pedreschi, Eds.). London: Thomas Telford Publishing.
- Chiorino, M. A. (2012). Art and Science of Building in Concrete: The Work of Pier Luigi Nervi. *Concrete International*, 34(3), 32–40.
- Dickson, M. (1998). Stuttgart digs deep for cathedral of the train. *The Architects' Journal, Concrete Quarterly*, 207, 2–4.
- Dombernowsky, P., & Søndergaard, A. (2009). Three-dimensional topology optimisation in architectural and structural design of concrete structures. In *Proceedings of the International Association for Shell and Spatial Structures (IASS) Symposium, Valencia*.
- Dombernowsky, P., & Søndergaard, A. (2012). Design, analysis and realisation of topology optimized concrete structures. *Journal of the International Association for Shell and Spatial Structures*, 53(174), 209–216.
- Eisenbach, P., Vasudevan, R., Grohmann, M., Bollinger, K., & Hauser, S. (2014). Parapluie - Ultra Thin Concrete Shell Made of UHPC by Activating Membrane Effects. *Proceedings of the International Association for Shell and Spatial Structures (IASS) Symposium 2013*, 55(4), 201–212.
- Eschenauer, H. a, & Olhoff, N. (2001). Topology optimization of continuum structures: A review. *Applied Mechanics Reviews*, 54(4), 331. <https://doi.org/10.1115/1.1388075>
- Faber, C. (1963). *Candela, the shell builder. With a foreword by Ove Arup*. New York: Reinhold Publishing Corporation.
- Flächentragwerke. (1969). *IL 1: Minimalnet*. Institut für Leichte (IL), Universität Stuttgart.
- Flächentragwerke. (1990). *IL 25: Form-force-mass Experiments*. Institut für Leichte (IL), Universität Stuttgart.
- Flager, F., Adya, A., Haymaker, J., & Fischer, M. (2014). A bi-level method for shape and member sizing optimization of frame structures. *Computer and Structures*, 1–11. <https://doi.org/10.1016/j.compstruc.2013.10.004>
- Frattari, L., Dagg, J. P., & Leoni, G. (2013). Conceptual design of a pedestrian bridge by means of topology optimization. In Paulo J.S. Cruz (Ed.), *Proceedings of the second International Conference on Structures and Architecture (ICSA): Concepts, Applications and Challenges* (pp. 229–236). Guimaraes: Taylor & Francis Group.
- Frei Otto. (2005). *Frei Otto complete works: lightweight construction, natural design*. (W. Nerdinger, Ed.). Basel: Birkhäuser.
- Garlock, M. M., & Billington, D. P. (2008). *Felix Candela, Engineer, Builder, Structural Artist*. Yale University Press.
- Goshima, R., Ohmori, H., Hagiwara, N., & Aoki, N. (2011). Investigation of the cross-section of the Pantheon dome through catenary mechanism. *Journal of the International Association for Shell and Spatial Structures: J. IASS*, 52(1), 19–23.
- Greco, C. (1994). Pier Luigi Nervi and ferro-cemento. *Domus*, (766), 80–82.
- Greco, C. (1995). The Ferro-Cemento of Pier Luigi Nervi. the new material and the first experimental building. In *Spatial Structures: Heritage Present and Future* (pp. 309–316).
- Grohmann, M., & Tessmann, O. (2011). Geometry, topology, materiality: The structural parameters in a collaborative design approach. In T. Kocaturk & B. Medjdoub (Eds.), *Distributed Intelligence in Design* (1st ed., pp. 252–260). Wiley-Blackwell. <https://doi.org/10.1002/9781444392395>
- Kicinger, R., Arciszewski, T., & De Jong, K. (2005). Evolutionary computation and structural design: A survey of the state-of-the-art. *Computers and Structures*, 83(23–24), 1943–1978. <https://doi.org/10.1016/j.compstruc.2005.03.002>
- Krog, L., Tucker, A., & Rollema, G. (2011). *Application of Topology, Sizing and Shape Optimization Methods to Optimal Design of Aircraft Components*. Retrieved from www.altairproductdesign.com

- Liang, J., Zhang, M. Y., Xu, X. L., Li, J. W., & Huang, L. Di. (2013). Topology Theory Application in Exhibition Design. *Applied Mechanics and Materials*, 357–360, 289–292. <https://doi.org/10.4028/www.scientific.net/AMM.357-360.289>
- Liang, Q. Q. (2010). Performance-based shape optimization of continuum structures. *IOP Conference Series: Materials Science and Engineering*, 10, 012194. <https://doi.org/10.1088/1757-899X/10/1/012194>
- Lochner-Aldinger, I. (2011). Geometry Studies using parametric Structural Models and Optimization Methods. In *Proceedings of the International Association for Shell and Spatial Structures (IASS)*. London.
- Lochner-Aldinger, I., Karl, J., & Adriaenssens, S. (2015). Biomimetic approach to structural morphology. In *Proceedings of the International Association for Shell and Spatial Structures (IASS): Future Visions*. Amsterdam, Netherlands.
- Lochner-Aldinger, I., & Schumacher, A. (2014). Homogenization method. In S. Adriaenssens, P. Block, D. Veenendaal, & C. Williams (Eds.), *Shell structures for architecture* (pp. 210–223). Routledge.
- López, D. L., Mele, T. Van, & Block, P. (2016). Dieste , González Zuleta and Sánchez del Río : Three approaches to reinforced-brick shell structures. *Structural Analysis of Historical Constructions*, (Dieste 1987), 571–578.
- Lozano-Galant, J. A., & Payá-Zaforteza, I. (2011). Structural analysis of Eduardo Torroja’s Frontón de Recoletos’ roof. *Engineering Structures*, 33(3), 843–854. <https://doi.org/10.1016/j.engstruct.2010.12.006>
- Mendoza, M. (2015). Felix Candela’s first European Project : The John Lewis Warehouse , Stevenage. *Arq : Architectural Research Quarterly*, 19(2), 149–160. <https://doi.org/http://dx.doi.org.proxy.lib.umich.edu/10.1017/S1359135515000251>
- Mungan, I., & Abel, J. (Eds.). (2011). *Fifty years of progress for shell and spatial structures*. Madrid, Spain: IASS (International Association for Shell and Spatial Structures).
- Muttoni, A., Lurati, F., & Fernández Ruiz, M. (2013). Concrete shells - Towards efficient structures: Construction of an ellipsoidal concrete shell in Switzerland. *Structural Concrete*, 14(1), 43–50. <https://doi.org/10.1002/suco.201200058>
- Nervi, P. L. (1956). *Structures*. (G. Salvadori & M. Salvadori, Eds.). New York: McGraw-Hill.
- Nervi, P. L. (1965). *Aesthetics and technology in building*. Cambridge, Massachusetts: Harvard University Press.
- Nervi, P. L., & Joedicke, J. (1957). *Works*. (E. Priefert, Ed.). New York: F. A. Praeger.
- Ney, L., & Adriaenssens, S. (2014). Shaping forces. In S. Adriaenssens, P. Block, D. Veenendaal, & C. Williams (Eds.), *Shell Structures for Architecture* (pp. 15–20). Routledge.
- Ochsendorf, J., & Block, P. (2014). Exploring shell forms. In S. Adriaenssens, P. Block, D. Veenendaal, & C. Williams (Eds.), *Shell Structures for Architecture* (pp. 7–14). Routledge.
- Otto, F. (2005). *Frei Otto complete works*. (W. Nerdinger, I. Meissner, E. Möller, & M. Grdanjski, Eds.). Birkhauser.
- Paolo VI Audience Hall in Vatican City. (n.d.). Retrieved August 5, 2017, from <http://www.arcvision.org/?p=17789&lang=en>
- Pedreschi, R. (2008). Form, Force and Structure: a brief history. *AD Architectural Design*, 78(2), 12–19. <https://doi.org/10.1002/ad.636>
- Pugnale, A., & Sassone, M. (2007). Morphogenesis and Structural Optimization of Shell Structures With the Aid of a Genetic Algorithm. *Journal of the International Association for Shell and Spatial Structures*, 48(3), 161–166.
- Ramm, E. (2011). Heinz Isler shells - The priority of form. *Journal of the International Association for Shell and Spatial Structures*, 52(169), 143–154.
- Richardson, J., Adriaenssens, S., Coelho, R. F., & Bouillard, P. (2014). Discrete topology optimization. In S. Adriaenssens, P. Block, D. Veenendaal, & C. Williams (Eds.), *Shell structures for architecture* (pp. 170–179). Routledge.

- Sasaki, M. (2007). *Morphogenesis of flux structure*. London: AA Publications.
- Sasaki, M. (2014). Structural design of free-curved RC shells: an overview of built works. In S. Adriaenssens, P. Block, D. Veenendaal, & C. Williams (Eds.), *Shell Structures for Architecture* (pp. 259–270). Routledge.
- Schlaich, J. (2014). On architects and engineers. In S. Adriaenssens, P. Block, D. Veenendaal, & C. Williams (Eds.), *Shell structures for architecture* (p. viii). Routledge.
- Solomita, P. (2015). *Pier Luigi Nervi vaulted architecture: towards new structures* (First edit). Bologna: Bononia University Press.
- Tedeschi, A. (2014). *AAD, Algorithms-aided Design: parametric strategies using Grasshopper*. (F. Wirz & S. Andreani, Eds.) (First edit). Brienza: Le Penseur Publisher.
- Torroja, E. (1958). *The structure of Eduardo Torroja: an autobiography of engineering accomplishments*. New York: F. W. Dodge Corporation.
- Veltkamp, M., Basso, P., & Lago, A. (2012). Shape invariant stiffness optimization of shell-like structures. *Journal of the International Association for Shell and Spatial Structures*, 53(174), 247–256.
- Williams, C. (2001). The analytical and numerical definition of the geometry of the British Museum Great Court roof. In M. Burry, S. Datta, A. Dawson, & A. J. Rollo (Eds.), *Mathematics & Design*. Geelong, Victoria, Australia: Deakin University.
- Williams, C. (2014). What is a shell? In S. Adriaenssens, P. Block, D. Veenendaal, & C. Williams (Eds.), *Shell Structures for Architecture* (pp. 21–32). Routledge.
- Winslow, P. (2014). Multi-criteria gridshell optimization. In S. Adriaenssens, P. Block, D. Veenendaal, & C. Williams (Eds.), *Shell structures for architecture* (pp. 180–193). Routledge.

Chapter 4 :

Daylighting in large-span roof systems

Architects in planning rooms today have forgotten their faith in natural light. Depending on the touch of a finger to a switch, they are satisfied with static light and forget the endlessly changing qualities of natural light, in which a room is a different room every second of the day.

-Louis Kahn

4.1 Introduction

Light directly affects the visual experience of architecture by revealing space, form, texture, and color when it shines on surfaces (Baker & Steemers, 2002). Light and vision are interrelated, and the key issue for any lighting installation is to help those using a space see well (Benya, Hesching, McGowan, Miller, & Rubinstein, 2001). Light also acts as a biologically active element, profoundly affecting human life and health (Benya et al., 2001; Webb, 2006). Designers and researchers argue that good lighting results in higher productivity for occupants (Benya et al., 2001). Light is also an energy source, as it changes to heat when it falls on surfaces, thus affecting surface and air temperatures, and indirectly, thermal comfort and air movement (Baker & Steemers, 2002). Therefore, light in architecture relates to an integrated web of aesthetic and functional criteria and cannot be isolated from other design concerns.

Daylighting commonly refers to the use of sunlight, skylight, and diffuse overcast sky illumination to support indoor activities (Reinhart & Selkowitz, 2006). The use of daylight in buildings is an energy-efficient strategy. According to the U.S. Department of Energy (DOE), as of 2015, buildings represent about a 40% share of U.S. primary energy consumption (U.S. Department of Energy, 2015a). The U.S. buildings energy end-use splits by fuel type in 2015 reveal that lighting energy fueled by electricity constitutes 11% of the building energy use (U.S. Department of Energy, 2015b). The use of daylight reduces environmental impacts, as U.S. buildings produced about 40% of total carbon dioxide emissions in 2015 (U.S. Department of Energy, 2015c); of that total, 11% of emissions were from the use of electricity for lighting (U.S.

Department of Energy, 2015d). Finally, daylighting is a major factor in occupants' perception and acceptance of workspaces (Reinhart & Selkowitz, 2006). According to research conducted by Galasiu & Veitch (2006), there is a strong preference for daylight in workplaces, particularly associated with the belief that daylight supports better health.

This chapter focuses on daylighting design in large span roof structures through top daylighting systems. As large span roof systems are designed to cover large spaces, they have the potential to bring daylight into the space to meet the architectural program's needs, to create a dynamic space throughout the day and the year, to connect the interior space with the sky, and to reduce the energy consumption of artificial lighting. However, since the structural role of roof systems is significant, any daylighting mechanism closely relates to the design of the roof's structural system. Therefore, it is important to scrutinize the ways in which structural and daylighting design interact with and affect one another.

The first section of the chapter introduces various passive design strategies. The daylighting design strategies either interlink with other disciplines' engineering design strategies, or are independent and perform within one disciplinary boundary. Examining different daylighting design strategies helps to classify the various levels at which daylight can be controlled. The outcome of this section is a classification of various levels of daylight control, which sets the stage for linking each daylighting design strategy to one or multiple design strategies from other disciplines, in this case, structural design. The daylighting classification diagram, along with the structural design classification diagram from Chapter 3, will ultimately be carried over to Chapter 5 to examine the overlaps of these two disciplines, and to isolate the design strategies that affect both disciplines simultaneously. This will guide the discussion of how to link the two disciplines, considering their linked components to create an interdisciplinary design approach.

The second section of the chapter introduces different metrics that are employed to measure the daylighting performance of a space. Not only does examining different performance metrics review different indices that have been employed by researchers and designers, it also illustrates the rationale used for identifying and choosing the most relevant metrics. The outcome of this phase of the study will be carried over to Chapter 6, where the simulation studies and their results are explained through case studies.

Daylighting developments are rooted in two distinct yet interrelated threads of technological advances: developments around glass as a glazing material, and developments in the design of

structural systems and structural materials. Kittler, Kocifaj, & Darula (2012) review the development of glass from 5000 BCE to 1960 CE. They demonstrate that advances in daylighting started with the design of unglazed windows and atrium houses in 5000 BC, continued with advances in the Romanesque period, when glazed window panes were installed in medieval castles and houses, progressed during the Gothic era, when cathedrals were constructed with clerestory windows and color glazing, and finally entered the era of modern architecture in 1960 (Kittler et al., 2012).

The development of new structural systems and the way in which they affect daylighting can also be tracked. Greek and Egyptian post and beam structures allowed narrow shafts of light to enter buildings. Since public activity took place in large monumental buildings in Roman societies, these column-free spaces had to be flooded with light; thus, effective daylighting strategies to illuminate the activities within involved the inventive use of structure and glass. Larger openings and spaces were created through the construction of arches, vaults, and domes, architectural features that were combined with the use of clear glazing. The Pantheon in Rome is an example of a building that integrates structure, geometry, and daylighting design.

Moving forward in history, Romanesque churches turned into dark and grim spaces because of the massive loadbearing masonry walls and the short spans above their fenestration; in contrast, the flying structural buttresses built during the Gothic era freed walls from supporting structural loads, and these constructions allowed much more daylight to enter the space (Baker & Steemers, 2002). Finally, in the early 20th century, at the dawn of modern architecture, buildings which used to be dark and unhealthy, with massive masonry structures and small windows, began to be constructed with longer spans and larger openings, changes made possible by technological advances (Boubekri, 2014).

Although improvements in technology constantly facilitated the use of daylight in buildings, its importance to building design has fluctuated throughout history. Daylight started out as the primary light source and a significant form-giver before the first part of the 20th century. However, it was largely ignored in the post WWII era with the advancements of fluorescent light, air conditioning, and the availability of cheap energy. Interest in daylighting was renewed after the oil crises of the 1970s, but declined again in the 1980s and 1990s as energy concerns lessened. The quest to use daylight and sunlight in buildings is once more a subject of increased interest for

architects and building owners due to the energy concerns of recent decades, as well as the occupant-centered school of daylighting design (Reinhart & Selkowitz, 2006).

This research focuses on passive daylighting design strategies. Passive strategies are stationary, as opposed to active strategies that move with respect to the daily movement of the sun (Ruck & Smith, 1988). This research focuses on daylighting design in large span roof structures through toplighting systems. Toplighting systems capture light on the roof of a building to channel it into spaces below, whereas side lighting systems employed in facades capture light to redirect it toward the back portion of a room or to the core of a large building (Boubekri, 2014).

Toplighting systems have the potential to bring more light inside a building, since more daylight is available from a roof than walls during an entire year. However, such systems are affected by the time factor; more daylight is available mid-day compared to any other time of the day. They are also affected by changes in seasons, meaning that high sun angles during the summer versus lower sun angles during the winter affect the amount of solar radiation emitted on a horizontal surface (Boubekri, 2014). The next section examines different levels at which light hits the building enclosure and thus the levels at which light can be controlled.

4.2 Levels of daylight control

Daylight can be considered to have two components, namely direct light coming from the sun, and diffuse light coming from the sky and the clouds. Direct light depends on the sun path and its movement, whereas diffuse light can either come directly from the sky, or be reflected from external and/or internal surfaces. Researchers discuss the components of diffuse light in detail, and describe light coming directly from the sky as the Sky Component (SC), light coming from external surfaces, including surrounding buildings, as the “Externally Reflected Component (ERC)”, and light reflected from internal surfaces as the “Internally Reflected Component (IRC)” (Baker & Steemers, 2002, p. 58).

With these two main components of daylight in mind, there are three levels at which daylighting hits the building envelope and can be controlled. These levels correspond with the order in which light hits and enters the building. The first is at its geometry, either globally or locally. Light then hits the second level, namely the glazing. Once passed through the glazing, light either hits a third level of control, namely interior justifications, or enters the interior space directly. Ways of controlling daylight are categorized in accordance with the levels that light hits

the building levels before entering the space. A summary of various levels at which daylight can be controlled is presented in Figure 4.1.

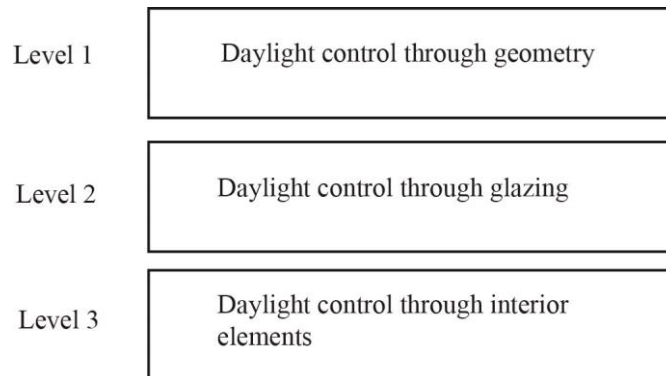


Figure 4.1. Various levels of daylight control

In the following subsections, numerous precedents are used to describe daylight control at different levels. The criteria for choosing the precedents is not bound by a specific country or continent, nor does it focus on those belonging to a specific time period. Rather, the criteria for precedent selection is twofold: first, to represent an example that employs top lighting as the main source of daylight for a space covered either by a large span roof structure, or a continuous building envelope starting as a façade and ending as a roof. Second, the precedents are all located in the Northern hemisphere where North light is considered the reflected skylight, and the sun moves from east to west. Each daylighting control strategy is discussed in depth by examining precedents.

4.2.1 First level of daylight control: global geometry

The role of form and geometry is emphasized in passive daylighting design of spaces (Turrin, von Buelow, Kilian, & Stouffs, 2012). The first level of daylight control is through the geometry of design. The amount of direct incident light admitted to a building can be controlled by changing both the global and the local geometry.

In terms of global geometry, the orientation and curvature of a surface can be varied to affect the amount of daylight admitted to a building (Figure 4.2).

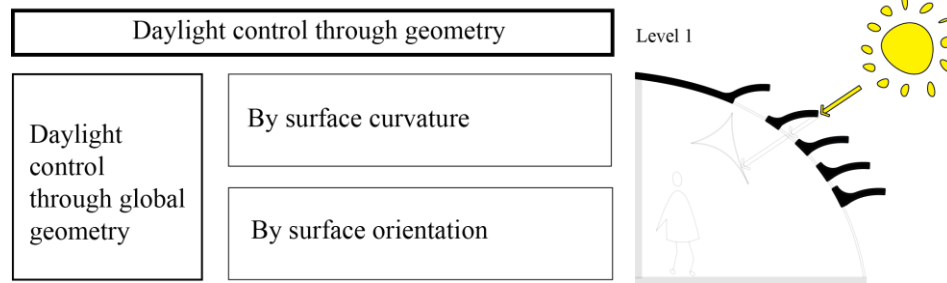


Figure 4.2. Daylight control through global geometry

Direct solar incidence produces high levels of illumination (Munoz, Esquivias, Moreno, Acosta, & Navarro, 2014). Consider a flat roof, fully exposed to direct solar beams; as the roof surface is curved, different sections of the roof are exposed to direct light incidence differently. In addition, a curved surface might self-shadow, preventing direct light beams from hitting a portion of its surface. Therefore, changing the global geometry by varying the surface curvature can be an effective strategy in controlling daylight.

Surface orientation is another important factor in controlling daylight. There is a large body of knowledge on how different facade orientations affect daylighting performance (Caldas, 2008; Carmody, 2004; Gratia & De Herde, 2007; Sherif, El-Zafarany, & Arafa, 2012). In roof systems however, the importance of surface orientation increases as a flat roof transforms into a curved roof. Once a specific curved surface is designed, the way it is oriented with respect to the sun path affects the direct light incident on the surface. Thus, surface orientation affects daylighting in roof systems.

The MyZeil shopping mall is a building with a curved roof system and demonstrates the ways a curved roof affects daylighting performance. Designed by Studio Fuksas in Frankfurt, Germany in 2009, the MyZeil shopping center is a column-free shopping mall realized by a triangular steel grid structure (Knippers & Helbig, 2009). The surface curvature was mainly optimized for structural performance and smoothed out to reduce the bending moments in the steel members (Scheible & Dimcic, 2011). Though its effect was not considered during design, the building shows how surface curvature and orientation affect daylight performance. The freeform surface covering the roof starts as a nearly flat surface on both sides and curves into a valley-shaped surface in the middle, which is shadowed under varying sun angles (Figure 4.3). A diagram (Figure 4.4) demonstrates that depending on how deep the valley curves are, the shadowed area can potentially increase under certain sun angles.

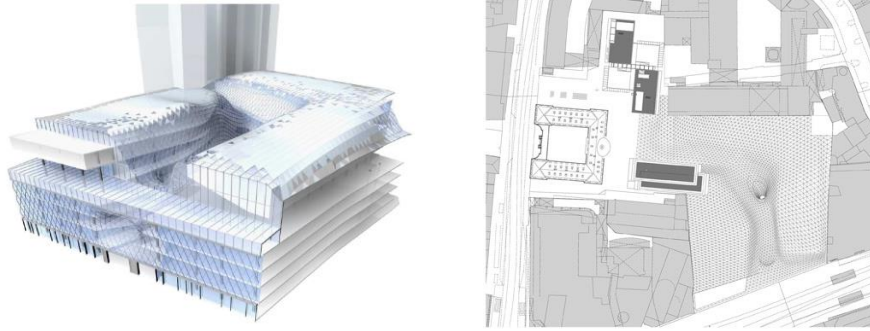


Figure 4.3. MyZeil shopping mall, showing the alternating panels of glass and steel in the roof (Knippers & Helbig, 2009)

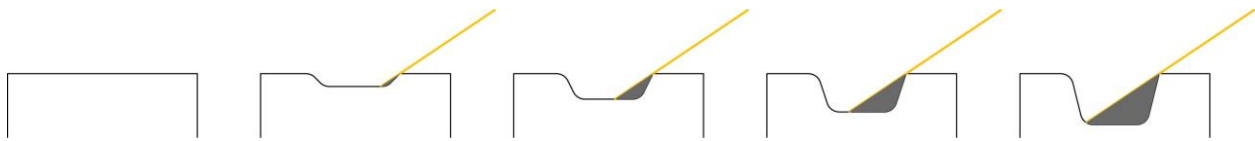


Figure 4.4. The diagram illustrates how a valley with various curvatures can be shadowed differently

The surface curvature can also have different daylighting performances depending on its orientation with respect to the sun path. In the MyZeil roof, when the sun is to the east, the valley is shadowed by the peak surface edge on east, and when the sun is to the west, the valley is shadowed by the peak surface edge on the west. At noon, however, the valley is subject to direct light incident (Figure 4.5).

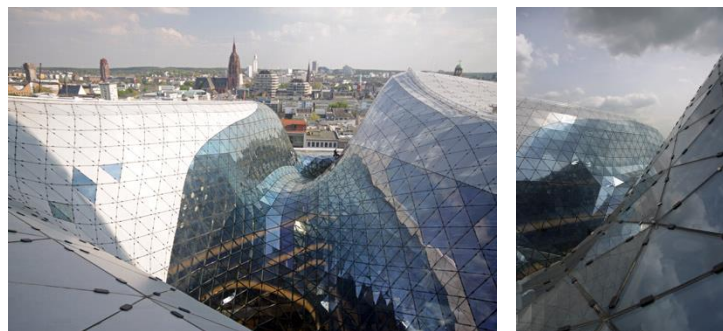


Figure 4.5. The surface shadows the valley differently under various sun angles

The amount of direct light incident admitted into a building can also be controlled by changing the local geometry. Three main groups of design variables are recognized in changing the local geometry in the toplights. The design changes include varying the shape, size, depth, scale, and ultimately the geometry of the openings; varying the orientation and angle of the openings with respect to the sun; and finally, adding external shading devices with various shapes, sizes, angles,

and orientations. These strategies are folded under three main categories, namely *change in shape and size*, *north light orientation* and *adding exterior shadings* (Figure 4.6).

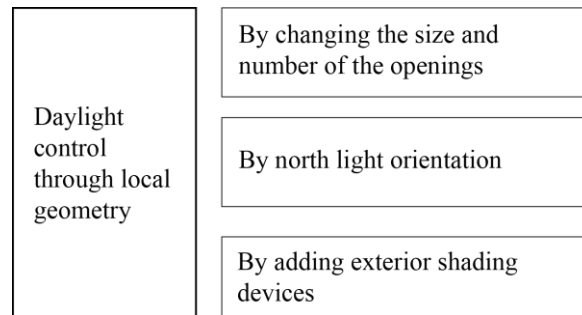


Figure 4.6. Daylight control through local geometry

It should be noted that changes in orientation toward north are represented as a separate category, although they could be folded under the third category as “adding external shading devices.” In fact, the north light orientation is a special case of adding external shading systems that are merged with the building envelope, affecting its structure and material. Thus, it can be considered special case of external shading, since shading systems are primarily designed to block direct sun and admit diffuse light to the space. However, due to the common practice of facing openings to the north in the northern hemisphere to provide a steady, diffuse light, north light orientation is represented as a separate strategy.

Before illustrating each strategy with a related precedent, toplight systems will be studied more in depth. Some of the most commonly used toplight typologies include skylights, monitor roofs, and sawtooth roofs (C. S. Kim & Chung, 2011; Steemers, Baker, & Fanchiotti, 2001). Figure 4.7 demonstrates how changing a design parameter in one typology leads to morphing into one of the other typologies. It also demonstrates the design parameters that can be varied within each typology.

The diagram starts from a *skylight*, represented by a horizontal opening in the roof. The size of the opening and the shape of glazing above it are the variables that can be changed. Afterward, the horizontal glazing is stretched upward while four vertical planes enclose its four sides, forming a *light well*. The depth of the light well is the feature that can be changed. Next, the horizontal transparent plane is replaced with an opaque plane, and the vertical opaque planes are replaced by transparent planes to form a *roof monitor*. Roof depth and roof tilt are two design variables associated with monitor roofs that can be varied. Then, the angle of the monitor roof is changed to

form a closed sloped surface, resulting in a *sawtooth roof*. The shape, angle, orientation, and scale of sawtooth roofs can be changed. Finally, when the vertical glazing is removed, and a horizontal glazing placed above the opening, a “skylight with external shading” is formed. The shape, angle, orientation, and scale of external shadings are the variables in this case.

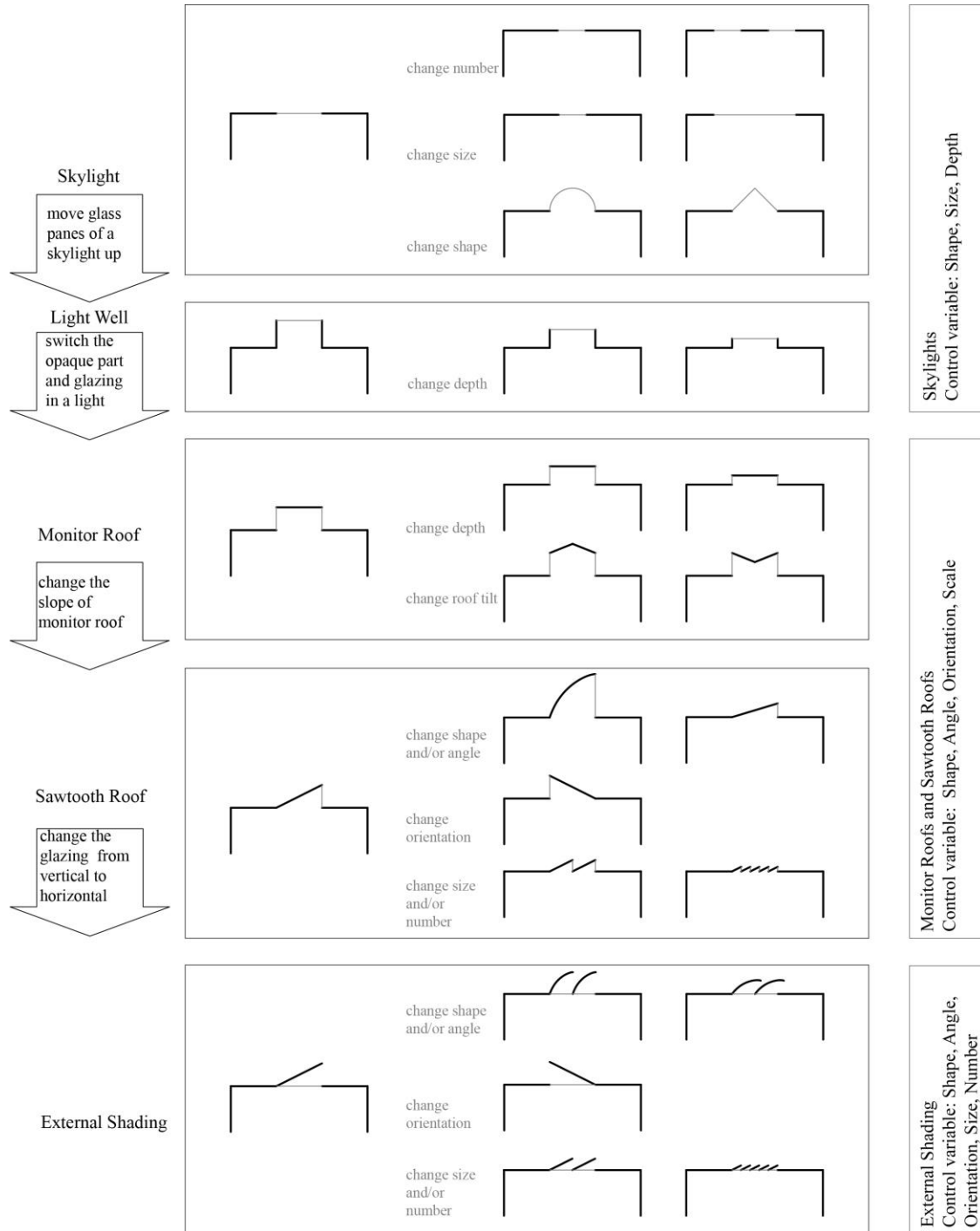


Figure 4.7. Toplighting typologies, showing transformations from one typology to the other

Examining the design variables within each typology, and eliminating the variables related to the glazing, the following variables remain: size and number of the openings, depth of the light well, orientation of the sawtooth, and shape, angle, orientation, size, and number of the external shadings. These variables can be folded under the daylight control strategies through local geometry, summarized as changes in “size and number,” “orientation,” and “external shading devices.”

4.2.1.1 Example of changing the size and number of the openings for daylight control

Changing the size and number of openings is a strategy to control daylight. There is a large body of literature on how changing the size and number of windows affects the window-to-wall ratio (WWR), and thus the daylighting of a space (Echenagucia, Capozzoli, Cascone, & Sassone, 2015). Similar to WWR, there is a skylight-to-roof ratio (SRR), which is the net glazing area of the skylights divided by the roof area.

The Forum at the Eckenberg Academy is a precedent that demonstrates design that makes use of this variable. Ecker Architekten designed the Forum as a central campus hub. The concrete slab is articulated through a variety of cycloidal coffers, some of which accommodate transparent skylights. The coffering’s role is twofold; first, it reduces the actual weight of the slab which is supported by the columns, while it demonstrates the actual depth of the slab. Second, the skylights introduce lighting to the space, on top of their acoustic absorption properties and role in ventilation. These skylights are designed with different radii and thus admit different amount of daylight (Gerfen, 2013) (Figure 4.8).

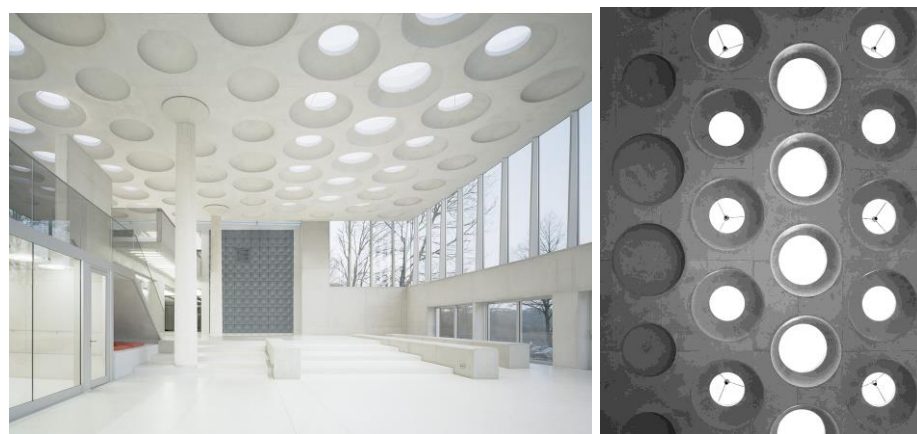


Figure 4.8. Forum at the Eckenberg Academy (Gerfen, 2013)

4.2.1.2 Example of north light orientation for daylight control

North-light orientation for skylights is another method for daylight control in the northern hemisphere, where the apertures in buildings are often oriented towards north to primarily receive diffuse daylight. The Kunsthaus Graz in Austria (Figure 4.9), built in the year 2000, is an example of employing this approach. Designed by Peter Cook and Colin Fournier of spacelab, and structurally engineered by Bollinger and Grohmann, the building lacks any recognizable architectural reference in the envelope. Its biomorphic shape is covered with double-curved acrylic panels and has no windows; instead, daylight is admitted through nozzle-shaped apertures that extrude from the surface of the skin to light the upper exhibition deck (Chaszar, 2006). The prefabricated nozzles were integrated into the hexagonal steel structure of the shell; the steel shell was then sealed off with insulated metal panels. Plexiglass panes were then installed as the final material of the envelope (Bollinger & Grohmann, 2004).

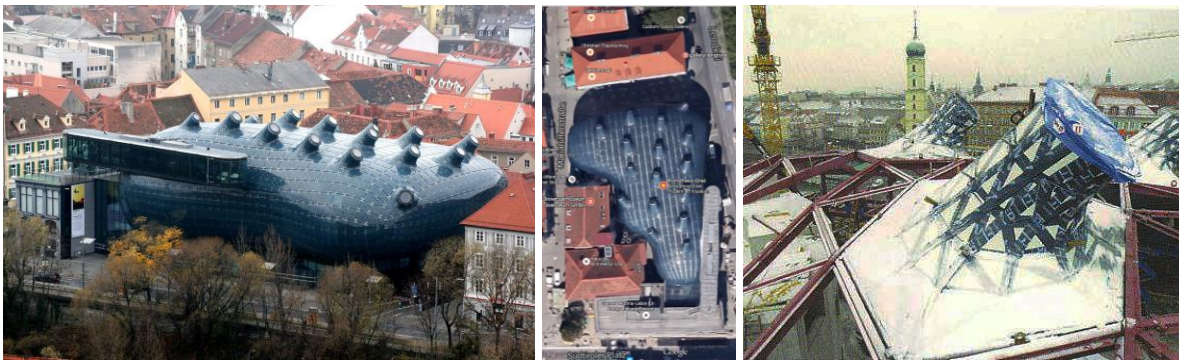


Figure 4.9. perspective view of the Graz musum (a) plan view (b), close-up view of a nozzle (c) (Chaszar, 2006)

4.2.1.3 Example of adding external shading elements for daylight control

Finally, adding exterior shading devices in front of the openings is a strategy to control daylight by blocking direct light incident, improving daylight quality, and controlling the daylight level (Freewan, 2014). External shadings either have a consistent geometry across the building envelope (Karagianni, Turrin, Knaak, & Hordijk, 2016) or are custom-designed for each specific location on the envelope (Bechthold, King, Kane, Niemasz, & Reinhart, 2010).

The Kimbel Art Museum Extension designed by Renzo Piano Building Workshop and Kendall/Heaton Associates is an example of employing external shading louvers over skylights, used to control the amount of daylight entering the gallery spaces (Figure 4.10).



Figure 4.10. Exterior blinds installed on the skylights of the Kimbel Museum extension (Piano, n.d.)

Exterior blinds are not always designed as regular planar surfaces and can have various shapes. As an example, the extension of the High Museum of Art in Atlanta, Georgia, designed by Renzo Piano Workshop with Lord Aeck Sargent, and engineered by Ove Arup company, aimed to use toplighting as a passive daylight control strategy. Light scoops in the shape of sails, which are called *vele* in Italian, were designed and arranged in a 1.2 m by 1 m grid on top of the roof of the pavilion to block direct daylight and capture the northern diffuse light, deflecting it into the galleries (Figure 4.11). The round skylights below the *vele* were cut at an angle, with the lowest point facing north to further control daylight. The design meets the IES recommendations for lighting of 50 lux for sensitive artwork and 200 lux for less-sensitive artwork. The design does not allow any direct sunlight into the galleries; rather, it allows a diffuse UV-filtered light inside (Boubekri, 2014).

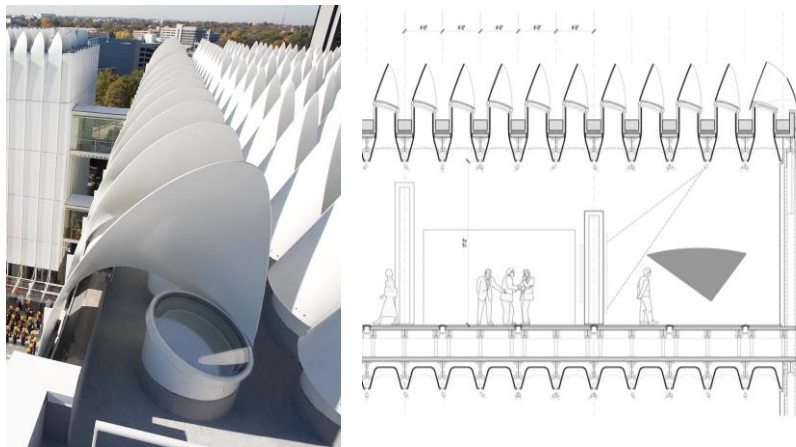


Figure 4.11. Vele on the roof of the museum designed by Renzo Piano

This section demonstrated different methods of changing local geometry to control daylight, including changing the shape and size of the openings, orienting skylights towards north, and adding external shading devices. The next section describes different control strategies applicable once light beams hit the glazing.

4.2.2 Second level of daylight control: glazing

The second level of daylighting control addresses daylight at the glazing level. This section focuses on static glazing, which is referred to glazing that possesses single fixed optical and thermal properties such as U-value, visible transmittance (T_{vis}), or solar heat gain coefficient (SHGC) (Hee et al., 2015). Daylight control through glazing is summarized in Figure 4.12.

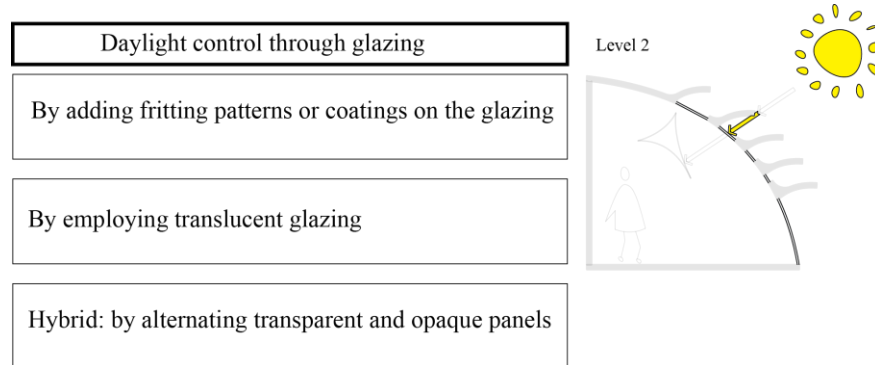


Figure 4.12. Daylight control through glazing

Changing the amount of glazing, glazing tint, glazing thickness, gas infill, and coating are some of the treatments that can be applied to glazing (Cuce & Riffat, 2015). Tinted glass in glazing systems absorbs solar radiation to reduce heat and light transmission (Pfrommer, Lomas, Seale, & Kupke, 1995). Lee, Selkowitz, Inkarojrit, & Kohler (2002) note that the low emissivity (Low-e) coating on glazing reflects a high amount of solar infrared radiations for a visible transmittance, thus transmitting *cooler* daylight. Ceramic frit silk-screened onto glass is another strategy to diffuse daylight and cut down incident solar radiation. Glass fritting enables designers to use patterns on architectural glazing; it also mitigates excessive solar gain, potential visual discomfort and excessive illuminance (Roudsari & Waelkens, 2015). All potential glazing treatments are categorized under *adding fritting patterns and coatings on the glazing* in the categorization.

The second category considers *translucent glazing* as a solar filter. As Ruck (2000), “rooflights are usually not designed for a view to the outside; therefore, obstructing elements such as deep light shafts or non-transparent systems can be applied in rooflight design” (p. 2.16). A research study considered the daylight factor distribution difference between a translucent panel and a tinted double glazing. The results demonstrated that the width of the daylit zone ranges from about 1.1–1.4 meter for translucent façade and 1.8–2.1 meter for tinted glazing (Pfrommer et al., 1995).

Translucent glazing is categorized as a separate category, since it does not provide a clear view to the outside, but is also efficient at diffusing daylight and reducing glare.

Employing a hybrid approach combining transparent, translucent, or opaque panels is another strategy to control the amount of incoming daylight. This strategy is similar to changing the skylight-to-roof ratio, mentioned in section 4.2.1.1 as a design strategy that addresses local geometry. Each strategy is further explained below.

4.2.2.1 Adding fritting patterns and coatings to glass for daylight control

The Cathedral of Christ the Light, in Oakland, California, designed by Skidmore, Owings and Merrill (SOM), employs this strategy (Figure 4.13). They used unitized curtain wall panels consisting of two clear glass layers laminated together. A custom-designed ceramic frit coating is baked on the inner surface of the layer of glass, which modulates daylight. Fritted glass is the only layer of protection before the light beams hit the interior wooden louvers (Sarkisian, Lee, & Long, 2011).



Figure 4.13. Fritting patterns on the glazings of the Cathedral of Christ the Light, California (photo by author)

Another example is the New Elephant House in Copenhagen, designed by Foster and Partners, where a varying fritting pattern is present on the glazing panels of the canopy (Figure 4.14). Through employing this strategy, they achieved solar control, as well as variable lighting that simulates natural condition and shadings of trees. The solar control of the fritting depends on the ratios of transparent to opaque areas (Woodbury, 2010). Figure 4.15 demonstrates the appearance of different frit percentages. It should be noted that in the figure, white patches represent frit, while the black surface represents glass.



Figure 4.14. Interior of the main enclosure in the New Elephant House (a); detail of the frit pattern (b) (Foster, n.d.)

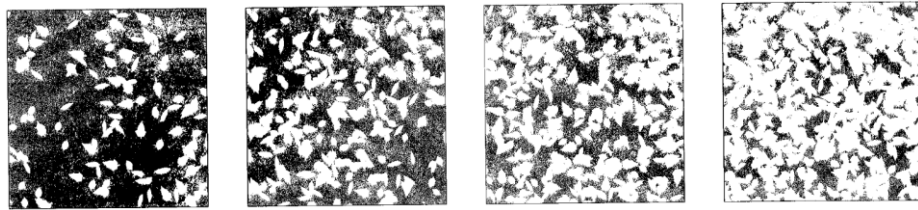


Figure 4.15. 15%, 30%, 45%, 60% frit patterns (Woodbury, 2010)

In the High Museum of Art, designed by Foster and Partners, a low-iron insulated glass with PVB¹ lamination is installed in the skylights to improve the color temperature of the northern light and to filter UVB² radiation (Boubekri, 2014).

4.2.2.2 *Example of translucent glazing for daylight control*

Using all-translucent glazing over skylights is another strategy to control incoming daylight. The Kimbell Art Museum Extension employed this strategy for the roof's glazing to admit natural daylight to the galleries and other spaces (Figure 4.16).

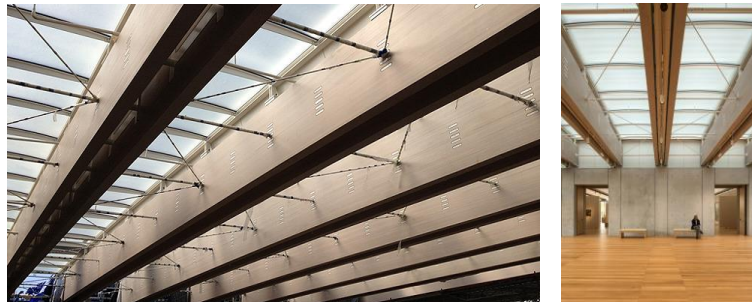


Figure 4.16. Kimbel Art Museum Expansion, showing translucent glazing in the roof (Piano, n.d.)

¹ Polyvinyl butyral

² Ultraviolet B (shortwaves)

4.2.2.3 Alternating panels for daylight control

This is a hybrid strategy that uses two or more types of glazing in one setting. Looking at the New Elephant House, it can be noted that not all of the glazing panels are fritted, but instead are interspersed with some transparent glazing panels (Figure 4.17a). Looking at the MyZeil shopping mall, it can be seen that it is designed with alternating panels of glass and steel (Figure 4.17b).



Figure 4.17. Alternating fritted and transparent panels at the New Elephant House, alternating opaque (a); transparent panels at the MyZeil Shopping Mall (b)

4.2.3 Third level of daylight control: interior elements

The third level of daylight control modulates daylight once it has already passed through glazing and entered the interior space (Figure 4.18). The most effective way to reduce the solar load on building envelopes is to intercept direct radiation from the sun before it reaches the glass; thus, the use of internal blinds and shades has fewer advantages than exterior daylighting controls (D.-W. Kim & Park, 2012; Gratia & De Herde, 2007). However, internal shading elements have the advantage of being protected from outside weather conditions, and in some cases, occupants have the flexibility of changing the shades' state. The use of interior blinds, reflectors, or fabrics are all strategies to diffuse light and reflect it back through the space.

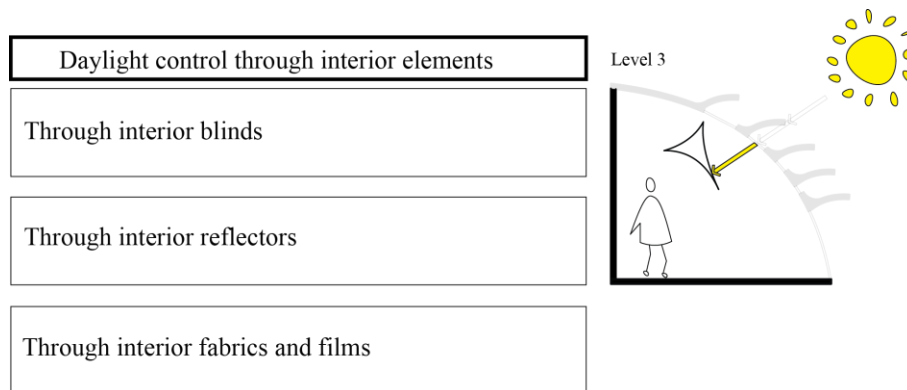


Figure 4.18. Daylight control through the use of interior elements

4.2.3.1 Using interior blinds for daylight control

In the Cathedral of Christ the Light in Oakland, California, interior wooden louvers modulate daylight once it passes the glazing. Other than at night, the cathedral is lit entirely with natural daylight, and the louvers serve an integral role in the casting of natural daylight into the space. The orientation and width of the louvers change over the height of the structure; they are wider with steeper angles near the base, and narrower and flatter near the top. The glued laminated timber louvers play a structural role, interconnecting and providing lateral bracing for inner rib members (Sarkisian et al., 2011). In addition, the interior planar shading devices forming the oculus ceiling are installed under the roof of the skylight (Figure 4.19).

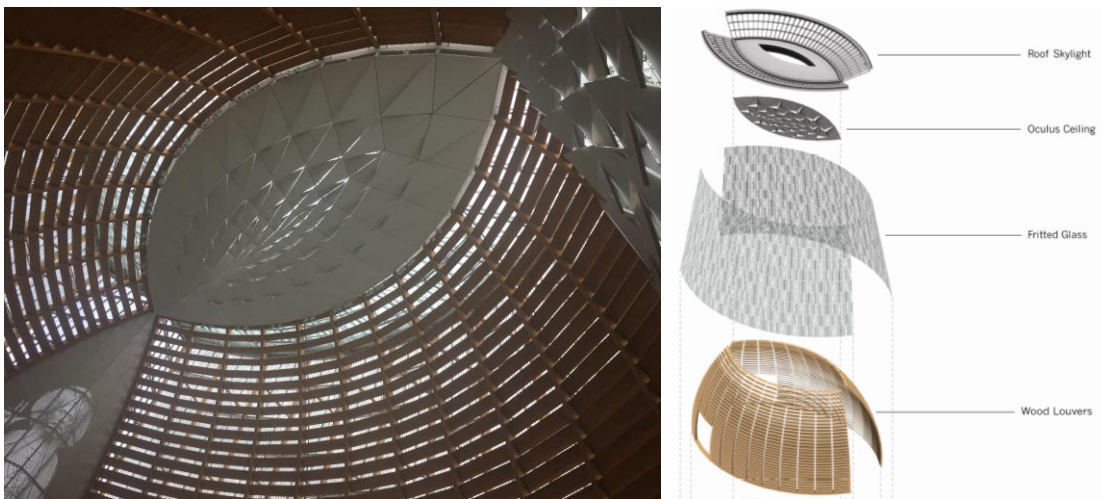


Figure 4.19. Interior blinds and the oculus ceiling of the Cathedral of Christ the Light (a); layers of the envelope from top to bottom include roof skylight, oculus ceiling, fritted glass, and wood louvers (b) (Sarkisian et al., 2011)

4.2.3.2 Interior reflectors for daylight control

The Kimbell Art Gallery designed by Louis Kahn provides an example of the use of interior light reflectors (Figure 4.20). The parallel cylinder concrete shapes are aligned from north to south, which is most efficient for gathering the sun's light. The linear 75 cm (2'6") long roof skylights are then carved out of the top edges of the spanning shapes. The roof skylights admit natural light, and a suspended reflector bounces light onto the concrete ceiling. The very top of the reflector is made of opaque aluminum to eliminate direct sunlight at noon, while the remainder of the reflector is perforated to allow more light into the space. In places where art is not displayed, such as the lobby, the reflector is perforated, allowing the noon light to shine directly into the space (Pierce, 1998).

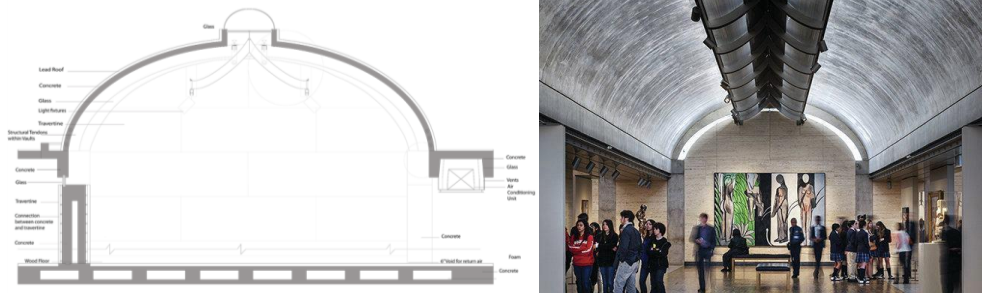


Figure 4.20. Kimbell Art Gallery designed by Louis Kahn

In the previously discussed High Museum of Art, 1.5-m-deep tubular units made of glass fiber-reinforced plaster are installed in the interior spaces, right beneath the skylights, to further diffuse the light (Figure 4.21) (Boubekri, 2014).



Figure 4.21. Dome-shaped coffers fabricated by Georgia-Pacific Gypsum LLC

4.2.3.3 Interior fabrics for daylight control

I. M. Pei designed the German Historical Museum extension (Deutsches Historisches Museum) in Berlin in 2002. As part of the extension, the courtyard of the Zeughaus was enclosed by a great glass skylight for year-round use. The glass roof spanning the square courtyard was designed by Schlaich, Bergermann and Partner from Stuttgart (Schlaich Bergermann Partner (SBP), n.d.). The 14-cm-deep roof grid shell with double curvature glass is point-supported at the four corners and oriented in a diagonal direction—the direction of the flow of forces (Schlaich & Schober, 2005). The courtyard was designed to be used for all kinds of events, but it turned out that the acoustic reverberation time was too long, and floating echo problems manifested due to the lack of sound-absorbing surfaces. Therefore, two layers of MicroSorber films were set at a distance of 15 cm from each other to solve the acoustic problem (BARRISOL, n.d.). These translucent films not only affect the acoustics, but also modulate the incoming daylight (Figure 4.22).



Figure 4.22. The courtyard of the German Historical Museum in Berlin

4.2.4 Summarizing various levels of daylight control in buildings

Multiple daylight control levels were reviewed in previous sections. However, multiple strategies are often combined to perform as a system in buildings. Many of the precedents described implement and combine more than one strategy to control daylight. Figure 4.23 summarizes the precedents used in this section with all the daylight control strategies that are used.

			Myzeil Mall	Forum at the Eckenberg Academy	Graz Museum	High Museum extension	New Elephant House	Kimbel Museum extension	Cathedral of Christ the Light	Kimbel Museum	German Historical Museum courtyard
level 1: geometry	Global geometry	Surface curvature	○								
		Surface orientation	○								
	Local geometry	Size and geometry of the openings		○							
		North light orientation			○	○					
		Exterior shading devices				○		○			
level 2: glazing	Fritting patterns or coatings				○	○		○			
	Translucent glazing							○			
	Hybrid: alternating panels	○									
level 3: interior justifications	Interior blinds							○			
	Interior reflectors				○				○		
	Interior fabrics or films									○	

Figure 4.23. Summary of various levels of daylight control with examples

To summarize, there are three levels at which daylight can be controlled. The first level is control through the geometry of the building. This can be through its global geometry, including building orientations and surface curvature. It can also be done through its local geometry, by altering the geometry and dimension of the openings; by shifting the orientation of the openings away from the direct light towards north; or by blocking direct light incident through adding external shading devices. The second level of daylight control occurs when light beams hit the

glazing, and is accomplished by applying different coatings and/or fritting patterns on the glazing; by employing translucent glazing; or by employing a hybrid strategy that alternates transparent, translucent, and opaque panels. The third level of control is applied when the light beams have already entered the building, where an interior louver, reflector, or fabric further diffuses the light. A diagram of all daylighting control levels is presented in Figure 4.24.

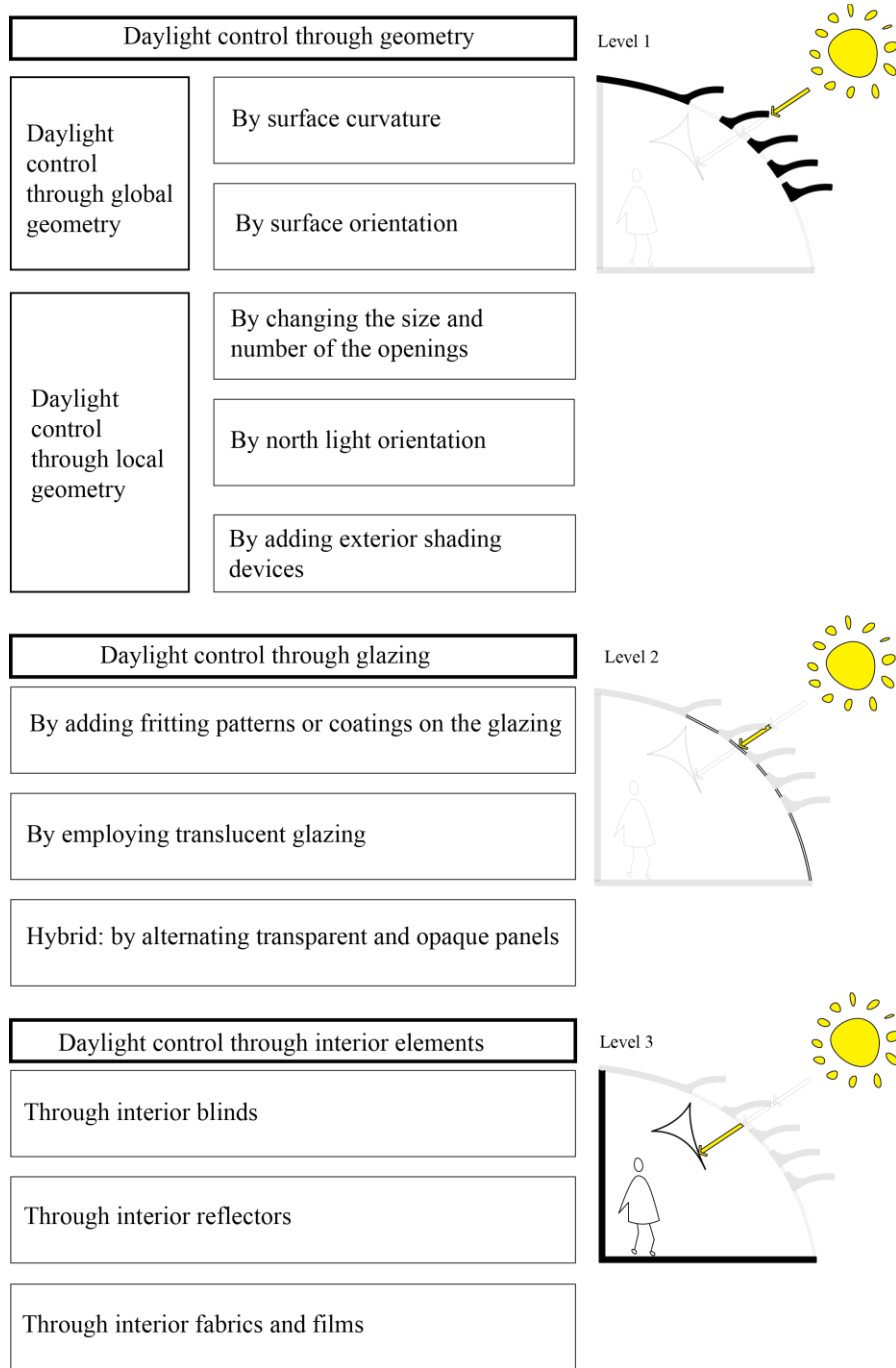


Figure 4.24. Summary of various levels of daylight control in building envelopes

4.3 Daylighting performance and metrics to measure it

According to Hensel (2013, p. 26) two “approaches to the notion of performance in architecture originate largely from the deep-seated debate over the relationship between form and function that has been dominant in its various guises in architectural discourse since the 1930s.” He then defines these two approaches to performance as *formal* and *functional* performance, where the former focuses on the artistic aspect, and the latter is associated with the scientific aspect and, more specifically, with engineering (Hensel, 2013). This section looks at the daylighting performance of a luminous environment from the scientific point of view and describes the metrics that are employed to measure it.

Designers and engineers have different definitions for daylighting, which may place a different emphasis on the spatial and/or technical qualities of daylight. (Reinhart & Wienold, 2011) defined daylit space as “a space that is primarily lit with natural light and that combines high occupant satisfaction with the visual and thermal environment with low overall energy use for lighting, heating and cooling” (p. 387). Based on this definition, three performance categories for daylight are identified, namely daylight availability, visual comfort, and thermal loads (Reinhart & Wienold, 2011). Boyce & KAG Smet (2014) count three objectives for daylighting metrics: characterizing what constitutes good daylighting; providing an estimate of the effect of daylight on the energy consumption of the building; and indicating the likelihood of the occurrence of visual or thermal discomfort. These objectives are in line with Reinhart’s performance categories for a daylit space. Therefore, daylight availability, visual comfort, and thermal loads are three performance categories considered when designing a daylit environment. But what are the best metrics to use for measurement of these criteria?

According to Boyce & KAG Smet (2014) “a metric is a well-defined measure that the designer can use to evaluate a design” (p. 622). He counts the essential characteristics of a metric as being quantitative, having application criteria attached to it, having the potential to be calculated during design and measured after installation, and finally, as having some relation to the desired objective. C. Reinhart & Selkowitz (2006) note that performance metrics range from being very general to being specific. The general metrics usually combine several individual submetrics into a single overall rating and stipulate a pass/fail criterion. They are aimed to draw the attention of the design team towards a specific issue at the early stages of design; however, they are difficult to formulate and are less effective for more qualitative aspects of design. On the other hand, the specific metrics

can be used for comparative studies to guide building design, or to benchmark a building against a pool of other buildings. It is noticeable that setting a specific metric for measuring how good daylighting is largely depends on different professions, as each profession concentrates on a different aspect of daylighting (Reinhart, Mardaljevic, & Rogers, 2006).

In order to categorize related metrics, three questions need to be answered: “what is being measured?” “how it is being measured?” and “how are the data being interpreted?” The following section discusses key performance criteria related to daylighting, including illuminance, uniformity, glare, and directionality. Afterward, different methods to measure illuminance and glare are discussed, along with the related interpretations. Finally, the metrics are compared with each other to extract those that are most relevant.

4.3.1 Performance criteria: illuminance, distribution, glare, and directionality of light

The lighting performance criteria are used to determine if there is good visibility in a space. Generally, good visibility is defined by the presence of an adequate amount of light allowing the occupant to accomplish his tasks (Cantin & Dubois, 2011). The performance criteria that assure good visibility include having an adequate quantity of light for the expected visual tasks, uniform distribution of illuminance and luminance, sufficient directionality, the absence of glare, and sufficient spectral content to render colors accurately (Ruck, 2000). Each criterion is briefly reviewed in the following sections.

4.3.1.1 *Illuminance*

For many years, the metric for lighting design has been based on the *illuminance* of the task measured as candela per square meter, or lux. Illuminance has been a very long-lived criteria: its strength is that it is a well-defined metric, and it has criterion levels for different applications. IESNA has defined the illuminance levels required for various tasks and programs (Illuminating Engineering Society of North America, 2000). Turrin et al. (2012) highlights that “in daylight comfort, the daylight requirements are related to the illumination levels needed according to the visual tasks taking place within the different spaces” (p. 4). In addition, there are several different methods by which illuminance can be calculated, and there are inexpensive meters that can be used for its measurement. However, there are some weakness associated with illuminance; among them, it is only approximately related to how visible a task will be (Boyce & Smet, 2014). Different metrics used for measuring illuminance are discussed in next section.

4.3.1.2 Distribution

The distribution of illuminance indicates how lighting varies from point to point across a plane of surface. Some degree of uniformity across the task plane is desirable, otherwise, if the eye is forced to adapt too quickly to a wide range of light levels, poor visibility and visual discomfort are the result. Uniformity is usually measured on a horizontal work plane for reading tasks. Illuminance and luminance ratios, such as maximum-to-average or average-to-minimum are used to quantify lighting uniformity. Contrast across the immediate task, between the task and background, and between the task and remote surfaces should be around 2.5:1, 3:1, and 10:1, respectively (Ruck, 2000).

4.3.1.3 Glare

According to Wienold & Christoffersen (2006, p. 744) “the aim of a good daylight design is first, to provide fully sufficient visual performance, and second, to ensure a comfortable and pleasing environment appropriate to its purpose. The comfort aspect of a daylight design is closely related to the problem of glare”. *Disability glare* causes the vision to be partly or totally impeded when the eye is forced to adapt to different brightness regions within the field of view, whereas *discomfort glare* is a sensation of annoyance caused by high or non-uniform distributions of brightness in the field of view (Ruck, 2000).

4.3.1.4 Direction

According to Ruck (2000), as the amount of diffuse light increases, less shadowing occurs, which reduces the occupant’s ability to evaluate the depth, shape, and texture of a surface. Therefore, a balance between diffuse and directional light is required. There are no standard performance parameters to evaluate the direction and diffusion of light; however, daylighting systems that rely on sky light will typically produce diffuse omni-directional light. Some daylighting systems can redirect diffuse light, so some directional affects appear even in diffuse light.

Among the criteria discussed here, illuminance and glare are reviewed most extensively, as they are used for daylighting performance assessment in my simulation studies. These factors are affected by the decisions that are made during the early stages of design, such as massing, orientation, and window design, whereas measuring uniformity and direction of the light requires a more detailed description of the interior spaces and furniture layouts. Measuring illuminance and

glare is within the scope of this research, and supports the aim of developing a multi-disciplinary design approach to daylighting at the early stages of architectural design.

4.3.2 Static and dynamic metrics for measuring illuminance

Static metrics measure illuminance at a specific time and day throughout a year. Daylight factor (DF) is a static metric defined as the ratio of the internal illuminance received at a given point to the unobstructed exterior horizontal illuminance. However, daylight is inherently climate-dependent and varies over time; thus a daylighting metric needs to take account of this everyday reality (Cantin & Dubois, 2011).

During the last decade, a series of dynamic daylight metrics have emerged that can serve as an alternative to daylight-factor based approaches. Dynamic computing is based on a time series of illuminances within a room based on solar radiation data for the location of the building, and the calculations can span the entire year (Boubekri, 2014). As Boyce & KAG Smet (2014) explain, some data files of irradiances or illuminances provided by the sky and sun for a given location over a whole year exist. Thus, the illuminances that will be produced at a given point in a space, depending on the prevailing climate, the window or skylight arrangements, and the orientation of the building, can be calculated every hour for a whole year from such records. The annual climate file offered by the U.S. Department of Energy (DOE) includes “hourly data for direct and diffuse irradiances” (Reinhart et al., 2006, p. 8). According to them, the use of dynamic daylighting metrics has increased in both professional and educational environments due to several factors: first, affordable access to enhanced computing power; second, the existence of widespread computer agility and interest in information technology; and third, the availability of enhanced user interfaces for generating three-dimensional building models in CAD systems to carry out simulations (Reinhart et al., 2006)

To develop a dynamic performance metric for a space, a series of choices need to be made. First, the sensor points need to be identified, including their resolution and location. As an example, a grid of 0.5 m x 0.5 m at work plane height (around 0.8 m above the floor) is a typical location for measuring daylight. Second, the time range and time intervals that illuminance is being measured should be specified. Two common approaches in this regard include measuring the *daylight hours during the year*, or the *occupied times of the building over a year* (Reinhart et al., 2006).

Once a dynamic daylight performance metric is calculated for multiple sensor points in a space, it is desirable to come up with one single metric for the space, even though graphical representations such as contour plots and false color maps do exist. Picking a limited number of sensors for reading is one strategy to interpret dynamic daylight performance results. In a research study by Reinhart et al. (2006) a two-person office with a 4 m x 4 m façade and 8 m depth was studied. They assumed that the sensors on the center axis, at 2 m and 6 m from the façade, are most relevant and could be used to represent the DA of the entire space. Another strategy for making sense of the dynamic daylight performance data is to consider all sensors on the work plane and derive a metric based on data from all of them.

The following subsections describe daylight factor (DF), a well-known static metric, and some other illuminance-based dynamic performance metrics, including daylight autonomy (DA), continuous daylight autonomy (DA_{con}), useful daylight illuminance (UDI), and daylight availability. After these descriptions, various approaches to interpreting the results are explained.

4.3.2.1 Daylight factor (DF)

Daylight factor measures the ratio between the indoor illuminance at a reference point and the outdoor global illuminance on an unobstructed horizontal surface (Ruck, 2000). This metric assumes a CIE³ overcast sky which is rotationally symmetric about the vertical axis, and does not take direct sunlight into account (Boyce & Smet, 2014). As an example, if the outside illuminance is about 10000 lux under an overcast sky, and the measured illuminance inside is 200 lux, the corresponding daylight factor is calculated as 200 lux / 10000 lux = 2% (Figure 4.25).

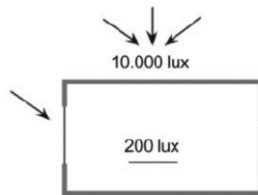


Figure 4.25. daylight factor of 2% when the outdoor global illuminance is 10000 lux (Ruck, 2000)

The advantages of DF include that it is intuitive and easy to communicate predictions within a design team. However, since DF is calculated under an overcast sky, it does not include any direct sun beams. Direct sun beams vary in orientation, as well as in different locations with varying latitudes. Reinhart et al. (2006, p. 10) highlight that DF “was never meant to be a measure of good

³ Commission Internationale de l'éclairage (International Commission on Illumination)

daylighting design, but a minimum legal lighting requirement.” Boyce & KAG Smet (2014) indicates that DF meets the objectives for a good daylighting metric in a limited way, since it is a relatively static measure and ignores the contribution of sunlight. The shortcomings of DF are summarized below:

- “DF does not consider direct light coming from the sun under non-overcast skies
- DF does not evaluate the impact of building/room orientation
- DF does not take building location or differences in climate into account
- The non-horizontal lighting of walls, which is critical for human perception, is not considered in the measurement of horizontal DF” (Cantin & Dubois, 2011).

The aforementioned limitations of DF suggest that shading studies be paired with the DF predictions, either through simulation or scale model measurements. The objective of shading studies is to avoid direct sunlight in the building. The combined approach of weighting daylight factor against unwanted solar gains leads to better energy balance (Reinhart et al., 2006). The major advantage of this combined approach is that it considers building orientation and latitude; however, it still does not address climate, occupant requirements, or the effects of dynamic shading and building type. The characteristics of DF are summarized in Table 4.1.

Table 4.1. Daylight Factor (DF)

Metric to measure illuminance as a daylight parameter	Static or dynamic	Measurement plane	Criterion	Note	Source
Daylight factor (DF)	Static	Horizontal	DF<2%	Electric lighting is necessary	(Ruck, 2000)
			2%<DF<5%	Daylit appearance with the use of electric light in working interiors.	(Reinhart et al., 2006) (Cantin & Dubois, 2011)
			DF>5%	Bright daylit appearance, might be associated with thermal/glare problems	(Boyce & Smet, 2014)

4.3.2.2 Daylight autonomy (DA) and annual sunlight exposure (ASE)

Illuminance-based dynamic performance metrics have become viable alternatives to static performance criteria, e.g. the daylight factor metric. Association Suisse des Electriciens in 1989 defined daylight autonomy (DA) as “the percentage of the year when a minimum illuminance threshold is met by daylight alone” (Reinhart et al., 2006, p. 10). DA uses work plane illuminance as an indicator to determine whether there is sufficient daylight in a space to allow an occupant to work by daylight alone. Sufficiency of daylight for different spaces and tasks is determined from reference documents, such as the IESNA⁴ lighting handbook. The simulation process for a project considers weather information retrieved from the specific geographic location under all sky conditions (Boubekri, 2014).

In 2001, Reinhart and Walkenhorst improved the DA description by redefining it as the “percentage of the occupied times of the year when the minimum illuminance requirement at the sensor is met by daylight alone” (Reinhart et al., 2006, p. 10). For instance, if an office space requires 500 lux on the work plane, and has a DA of 80% for one sensor, it means that the minimum lighting level will be met by daylight alone for 80% of the year at that sensor, and artificial lighting is needed for the remaining 20% of the year.

According to researchers, “an interior area is interpreted to be daylit if it receives at least half the time sufficient daylight compared to an outside point” (Reinhart & Wienold, 2011, p. 388). Therefore, another approach for interpreting data is to calculate the percentage of nodes within a space that have a DA higher than 50%. This means that if a sensor does not receive the target threshold (500 lux for an office space as an example) during at least half of the year, then it is not counted as a daylit sensor. To calculate this, one may count the number of sensors that have a DA higher or equal to 50%, and then divide the result by the total number of sensors.

LEED v4 suggests spatial daylight autonomy (sDA) for spaces where nodes meet the required 300 lux for 50% of the year (sDA_{300/50%}). The building can earn points for a LEED certificate based on the percentage of nodes in a space that meet sDA criteria. If 55% or 75% of the nodes of a regularly occupied floor area meet the criteria, then 2 or 3 points, respectively are earned (U.S. Green Building Council, 2013).

⁴ Illuminating Engineering Society of North America

Another possible approach, when the data for DA performance of all sensors is available, is to calculate the arithmetic average of DA to get the mean daylight autonomy (MDA). The shortcoming of this approach is that some nodes with a high DA may cover for other sensors with a low DA, and still provide a good mean result at the end. In other words, MDA does not illustrate if a room is half dark and half overlit, or fully daylight.

It should be noted that DA has no relevance for assessing visual discomfort caused by glare (Boyce & Smet, 2014), and it does not demonstrate the existence of light oversupply. Therefore, it should be paired with another criterion, the annual sunlight exposure (ASE). The ASE is the percentage of square footage in regularly occupied spaces that have direct sunlight during the year. LEED v4 requires an ASE_{1000,250}, meaning that the illuminance values of 1000 lux and above must not exceed 250 occupied hours during the year (10% of the year), and must not exist in more than 10% of the occupied floor area (U.S. Green Building Council, 2013). These requirements are summarized in Table 4.2.

Table 4.2. Daylight autonomy (DA) and annual sunlight exposure (ASE)

Metric for illuminance as daylight parameter	Static or dynamic	Measurement plane	Criteria	LEED points for regularly occupied floor area	Source
Spatial daylight autonomy (sDA) and annual sunlight exposure (ASE)	Dynamic	Horizontal	sDA _{300/50%} > 55% and ASE _{1000,250} < 10%	2 points	(U.S. Green Building Council, 2013)
			sDA _{300/50%} > 75% and ASE _{1000,250} < 10%	3 points	

4.3.2.3 Continuous daylight autonomy (DA_{con}) and maximum daylight autonomy (DA_{max})

Continuous daylight autonomy (DA_{con}) is proposed in the literature to attribute partial credit to time steps when the daylight illuminance lies below the minimum illuminance level, acknowledging that even a partial contribution of daylight to illuminate a space is beneficial. As an example, an area with a 500 lux requirement that is provided with 400 lux by daylight receives

a partial credit of $400 \text{ lux}/500 \text{ lux} = 0.8$. This index softens the transition between compliance and noncompliance, instead of a presenting a hard binary threshold (Reinhart et al., 2006). A researcher proposed the area percentage of a work plane with a continuous daylight autonomy (DA_{con}) level above 40 percent, 60 percent or 80 percent be reported, and receive either one, two or three LEED credits, respectively (Architectural Energy Corporation, 2006).

DA_{con} is often paired with a second criterion, maximum daylight autonomy (DA_{max}). DA_{max} reports the percentage of occupied hours during which direct sunlight or exceedingly high daylight conditions are present, and its value is related to the likelihood of appearance of glare. DA_{max} is defined as a sliding level equal to ten times the design illuminance target of space. As an example, if a computer lab is designed to have 150 lux illuminance, the DA_{max} is calculated to be 1500 lux (Reinhart et al., 2006). It is worth mentioning that DA_{max} can be employed to assess the illuminance uniformity of the space, and if a high percentage of a space is subject to DA_{max} , it can potentially warn the designer that the light uniformity of the space is poor. According to (Architectural Energy Corporation, 2006) Rogers (2006), the metric requires the space not exceed the DA_{max} threshold for 5% of the workplane. This metric is summarized in Table 4.3.

Table 4.3. Continuous daylight autonomy (DA_{con}) and maximum daylight autonomy (DA_{max})

Metric for illuminance as daylight parameter	Static or dynamic	Measurement plane	Criteria	Note	Source
Continuous daylight autonomy (DA_{con}) and maximum daylight autonomy (DA_{max})	Dynamic	Horizontal	$DA_{con} \Rightarrow 1$	A percentage is calculated by dividing the actual illuminance to the target illuminance, to acknowledge partial credit. Higher percentages indicate that light is evenly distributed.	(Architectural Energy Corporation, 2006)
			$DA_{con} \Rightarrow 0.8$		
$DA_{con} \Rightarrow 0.6$					
$DA_{con} \Rightarrow 0.4$					
			and $DA_{max} < 5\%$	DA_{max} is defined as a sliding level, equal to ten times the design illuminance of a space. DA_{max} considers the likelihood of the appearance of glare.	

4.3.2.4 Useful daylight illuminance (UDI)

Useful daylight illuminance (UDI) is another dynamic daylight performance criterion, also based on work plane illuminances. This metric addresses some shortcomings of daylight autonomy, emphasizing that not every light level that equals or exceeds the light threshold will be useful for the occupant. Nabil & Mardaljevic (2005) define UDI as a daylight level which is neither too dark nor too bright. UDI results are categorized as UDI-underlit, UDI, and UDI-overlit, categories corresponding to the percentages of the occupied times of the year when the lighting levels fall short (<100 lux), are appropriate (100–2000 lux), or are too bright (>2000 lux). The UDI range can further be broken down into a range of 100–500 lux, where daylight illuminance “are considered effective either as the sole source of illumination or in conjunction with artificial lighting,” and a range of 500–2000 lux, values which “are often perceived as desirable or at least tolerable” (Nabil & Mardaljevic, 2005, p. 49). This scale is summarized in Table 4.4.

Table 4.4. Useful daylight illuminance (UDI)

Metric for illuminance as daylight parameter	Static or dynamic	Measurement plane	Criteria	Note	Source
Useful daylight illuminance (UDI)	Dynamic	Horizontal	UDI < 100 lux	Daylight is ignored, and electric lighting is dominant	(Nabil & Mardaljevic, 2005)
			100 < UDI < 500 or 500 < UDI < 2000	Useful daylight for occupants	
			UDI > 2000 lux	Space is likely prone to visual and/or thermal discomfort	

Nabil & Mardaljevic (2005) note that *all* workplace sensors should synchronously fall in the 100–2000 lux range for the lighting to be considered useful. However, such a goal is not always realistic; therefore, they note that the UDI “allows rapid comparative assessment of any number of design variants” (=55). In a study, they calculated the percentage of the working year for which useful daylight illuminances occurred for a case study, to enable them to compare different design scenarios. They state that “a well-daylit space is one where the achieved UDI is maximized at the expense of the other two metrics” (Nabil & Mardaljevic, 2005, p. 50).

Peter Boyce (2014) introduces a four-part illuminance scale, which divides the 100 to 3000 lux range. He notes that daylight less than 100 lux at a point is largely ignored, and daylight more than 3000 lux is not considered useful. The intermediate range is divided into two subranges: the 100 to 300 lux range is where daylight will be noticed but will be considered as supplementary to the electrical lighting, and the 300 to 3000 lux range is where daylight will be considered primary, and electrical lighting is likely to be dimmed or turned off given a responsive control system. This means that only illuminance in the range of 100 to 3000 lux is useful. The weakness of this scale is that it does not deal with discomfort glare (Boyce & Smet, 2014).

4.3.2.5 Daylight availability

Daylight availability is an amalgamate of DA and UDI information into a single figure. In this scale, an overlit area presents an oversupply of daylight for at least 5% of the working year (Reinhart & Wienold, 2011). According to Reinhart, the 5% criterion is selected as an analogue method to thermal assessment methods in British Standard BS EN 15251, where exceeding “several thermal comfort categories by 3-5 percent of occupied times of the year” is defined as the standard threshold level (Reinhart & Wienold, 2011, p. 388). The threshold of daylight oversupply is met if the illuminance level is above ten times more than the target illuminance, which corresponds to the DA_{max} discussed earlier. This scale is summarized in Table 4.5.

Table 4.5. Daylight availability

Metric for illuminance as daylight parameter	Static or dynamic	Measurement plane	Criteria	Note	Source
Daylight availability	Dynamic	Horizontal	$DA > 50\%$ and $DA_{overlit} < 5\%$	DA corresponds with the adequate amount of daylight throughout the year, whereas $DA_{overlit}$ corresponds with the likelihood of visual discomfort when an illuminance level ten times higher than the target level is provided.	(Reinhart & Wienold, 2011)

4.3.3 Static and dynamic metrics for measuring glare

The previous section summarized the annual daylight availability metrics measuring illuminance, followed by a discussion of the metrics that predict visual discomfort. However, these metrics are all measured on a horizontal plane. According to Reinhart & Wienold (2011), “there

is a widely-shared notion that horizontal work plane illuminance is a poor predictor of discomfort glare as the amount of light falling on a working plane area has little in common with a person’s visual experience of a space” (p. 389). Therefore, it is essential to also assess the visual comfort of a space with relevant metrics retrieved from vertical plane measurements.

Glare analysis is based on luminance distribution in the field of view of an observer (Reinhart & Wienold, 2011). Many metrics have been developed to assess glare, and the equations for these ratings draw upon four main physical quantities, including the luminance of the glare source (L_s); the general field of luminance, also called the background luminance (L_b); the solid angle subtended by the source (ω_s); and the angular displacement (ψ) of the source from the observer’s line of sight (Wienold & Christoffersen, 2006). The glare constant, G , expresses the subjective sensation, and the letters e , f , and g are weighting components.

$$G = \left(\frac{L_s^e \omega_s^f}{L_b^g f(\psi)} \right)$$

The following sections review two commonly used metrics for assessing glare, namely the point-in-time daylight glare probability (DGP) and the annual DGP.

4.3.3.1 Daylight glare probability (DGP)

Some metrics used to assess glare include the British glare index (BGI), the discomfort glare index (DGI), the CIE glare index (CGI), the CIE’s unified glare rating system (UGR), the visual comfort probability (VCP), the discomfort glare probability (DGP), the predicted glare probability (PGSV), and the Osterhaus’ subjective rating (SR) (Carlucci, Causone, De Rosa, & Pagliano, 2015; Clear, 2012). Of all these metrics, daylight glare probability (DGP), developed by Wienold and Christoffersen, is discussed in the most depth.

In their studies, DGP is defined as a function of the vertical eye illuminance as well as the glare source luminance, and other parameters (Wienold & Christoffersen, 2006). Human subjects in Wienold’s study rated the glare within their field of view as imperceptible, perceptible, disturbing, or intolerable, a scale known as daylight glare rating (DGR) (Wienold & Christoffersen, 2006, p. 949) (Figure 4.26).

Glare rating	avg	RSMD	SE	95%-confidence interval	
				lower limit	upper limit
imperceptible	0.33	0.098	0.010	0.314	0.352
perceptible	0.38	0.112	0.011	0.356	0.398
disturbing	0.42	0.148	0.015	0.390	0.448
intolerable	0.53	0.181	0.031	0.464	0.590
avg	0.39	0.098	0.010	0.314	0.352

Figure 4.26. Human subjects' rating of the DGP

DGP intervals in response to glare ratings are categorized as below:

If $DGP < 0.35$, DGR is imperceptible glare

If $0.35 \leq DGP < 0.4$, DGR is perceptible glare

If $0.4 \leq DGP < 0.45$, DGR is disturbing glare

If $DGP \geq 0.45$, DGR is intolerable glare

4.3.3.2 Annual daylight glare probability

Evaluations of glare on an annual basis have been carried on by researchers in search of an efficient method. According to Reinhart et al. (2006), it is necessary to repeat point-in-time glare analysis for all hours of the year, using site specific climate data to evaluate the overall appearance of discomfort glare at a workspace over the course of the year. Another researcher discusses three methods for calculating the annual glare, including a timestep-by-timestep calculation, a simplified DGP based on vertical eye illuminance, and a simplified DGP calculation based on vertical eye illuminance and simplified images (Wienold, 2009). He points out that an hour-by-hour calculation for a dynamic metric is very time consuming; thus, the enhanced simplified method that uses daylight coefficient-based vertical eye illuminance and simplified images is proposed as more appropriate for calculating annual DGP profiles.

4.3.4 Summarizing static and dynamic metrics for measuring illuminance and glare

The metrics for measuring illuminance on a horizontal plane and glare based on vertical eye luminance are summarized in Table 4.6 and Table 4.7 respectively. These are not an exhaustive list of metrics, as there are existing research studies with a comprehensive list of metrics with their underlying equations (Carlucci et al., 2015). Rather, these tables present the commonly-used metrics for assessing the daylighting performance of a space, while they summarize *what is being measured, how it is being measured, and how the results are being interpreted*. These tables also

allow consideration of whether one metric should be paired with another to allow the user to draw a more comprehensive conclusion from the performance criteria.

Table 4.6. Metrics for measuring illuminance on a horizontal plane

Metric for illuminance	Criteria	Note	Source
Daylight factor (DF) (Static)	DF < 2%	Electric lighting is necessary	(Ruck, 2000)
	2% < DF < 5%	Daylit appearance with the use of electric light in working interiors.	(Reinhart et al., 2006)
	DF > 5%	Bright daylight appearance, might be associated with thermal/glare problems	(Cantin & Dubois, 2011) (Boyce & Smet, 2014)
Spatial daylight autonomy (DA) + annual sunlight exposure (ASE) (Dynamic)	sDA _{300/50%} > 55% and ASE _{1000,250} < 10%	2 points	(U.S. Green Building Council, 2013)
	sDA _{300/50%} > 75% and ASE _{1000,250} < 10%	3 points	
Continuous daylight autonomy (DA_{con}) + maximum daylight autonomy (DA_{max}) (Dynamic)	DA _{con} => 1	A percentage calculated by dividing the actual illuminance to the target illuminance to acknowledge partial credit. Higher percentages indicate that light is evenly distributed.	(Architectural Energy Corporation, 2006)
	DA _{con} => 0.8		
	DA _{con} => 0.6		
	DA _{con} => 0.4		
	and DA _{max} < 5%	DA _{max} is defined as a sliding level equal to ten times the design illuminance of space. DA _{max} considers the likely appearance of glare.	
Useful daylight illuminance (UDI) (Dynamic)	UDI < 100 lux	Daylight is ignored and electric lighting is dominant	(Nabil & Mardaljevic, 2005)
	100 < UDI < 500	Useful daylight for occupants	
	or 500 < UDI < 2000		
	UDI > 2000 lux	Space is likely to prone to visual and/or thermal discomfort	
Daylight availability (Dynamic)	DA > 50% and DA _{overlit} < 5%	DA corresponds with the adequate amount of daylight throughout the year, whereas DA _{overlit} corresponds with the likelihood of visual discomfort when an illuminance level ten times higher than the target level is provided.	(Reinhart & Wienold, 2011)

Table 4.7. Metrics for measuring glare

Metric for glare	Criteria	Note	Source
Daylight glare probability (DGP) (static metric)	$DGP < 0.35$	imperceptible glare	(Wienold & Christoffersen, 2006)
	$0.35 \leq DGP < 0.4$	perceptible glare	(Wienold, 2009)
Annual daylight glare probability (dynamic metric)	$0.4 \leq DGP < 0.45$	disturbing glare	
	$DGP \geq 0.45$	intolerable glare	

4.4 Discussion and summary in the context of large span roof systems

In the first section of this chapter, different daylighting design strategies were examined to classify the various levels at which daylight hits the building envelope and can be controlled. The classes are defined as the *geometry level*, *glazing level*, and *interior level*. This classification set the ground for linking each daylighting design strategy to one or multiple design strategies of other disciplines, in this case, the discipline of structural design. This classification will ultimately be carried over to Chapter 5, where it will be used to examine the overlaps between daylighting and structural disciplines to help to isolate the design strategies that simultaneously affect both disciplines. This will ultimately provide guidance on how the two disciplines can be linked via their linked design parameters with the aim of developing an interdisciplinary design approach.

The second section of the chapter introduced the different metrics that are employed to measure the daylighting performance of space. The metrics for measuring illuminance on a horizontal plane as well as glare were discussed. According to three overall performance categories, expressed as daylight availability, visual comfort, and thermal loads (Reinhart & Wienold, 2011), the metrics presented in Table 4.8 were selected for measuring daylighting availability and visual comfort, in addition to the lighting, heating, and cooling energy loads for a space. The outcome of the second phase of the study will be carried over to Chapter 6, where the simulation studies and their results will be explained through case studies.

Table 4.8. Metrics for daylighting performance assessment

Metric	criterion
Spatial daylight autonomy (sDA) of 300 lux for at least 50% of the year should be met by 55% of the surface area	$sDA_{300/50\%} > 55\%$
The maximum amount of daylight autonomy (DA) is 10 times more than the target daylight: $DA_{max} = 10 * DA = 10 * 300 \text{ lux} = 3000 \text{ lux}$. A DA of 3000 lux is considered oversupply and should not occur more than 5% of the year.	$DA_{oversupply} \leq 5\%$ of the year
Daylight glare probability (DGP) should not be intolerable or disturbing.	$DGP < 0.04$
Lighting, cooling and heating energy loads	[kW-h]

On a final note, the space that the roof is covering is defined as a hypothetical courtyard where the surrounding walls are adiabatic and opaque, and the roof is the only possibility of admitting daylight into the space. The target required light level of 300 lux on the horizontal plane is set as the lighting level for the courtyard. This is used for simulations explained in Chapter 7.

4.5 References

- Architectural Energy Corporation. (2006). *Daylighting metric development using daylight autonomy calculations in the sensor placement optimization tool*. CHPS Daylighting Committee. Boulder, Colorado.
- Baker, N., & Steemers, K. (2002). *Daylight design of buildings*. London: James & James.
- BARRISOL. (n.d.). Microsorber EFTE product for Berlin German Historical Museum. Retrieved April 12, 2017, from <http://microsorber.net/uk/references/films/berlin-german-historical-museum/#details>
- Bechthold, M., King, J., Kane, A., Niemasz, J., & Reinhart, C. (2010). Integrated Environmental Design and Robotic Fabrication Workflow for Ceramic Shading Systems. In *Proceedings of the 28th Conference of the International Association for Automation and Robotics in Construction* (pp. 70–75).
- Benya, J., Hesching, L., McGowan, T., Miller, N., & Rubinstein, F. (2001). *Advanced Lighting Guidelines*. (J. Roberts, Ed.). New Buildings Institute.
- Bollinger, K., & Grohmann, M. (2004). *Workflow: Struktur - Architektur, Architecture - Engineering*. (P. C. Schmal, Ed.). Basel: Birkhauser. Retrieved from <http://mirlyn.lib.umich.edu/Record/004930250>
- Boubekri, M. (2014). *Daylighting design : planning strategies and best practice solutions*. Basel: Birkhäuser.
- Boyce, P., & Smet, K. (2014). LRT symposium 'Better metrics for better lighting' - a summary. *Lighting Research & Technology*, 46, 619–636.
- Caldas, L. (2008). Generation of energy-efficient architecture solutions applying GENE_ARCH: An evolution-based generative design system. *Advanced Engineering Informatics*, 22(1), 59–70. <https://doi.org/10.1016/j.aei.2007.08.012>

- Cantin, F., & Dubois, M. (2011). Daylighting metrics based on illuminance, distribution, glare and directivity. *Lighting Research & Technology*, 43(3), 291–307.
- Carlucci, S., Causone, F., De Rosa, F., & Pagliano, L. (2015). A review of indices for assessing visual comfort with a view to their use in optimization processes to support building integrated design. *Renewable and Sustainable Energy Reviews*, 47(7491), 1016–1033. <https://doi.org/10.1016/j.rser.2015.03.062>
- Carmody, J. (2004). *Window systems for high-performance buildings*. New York: Norton (1st ed.). New York.
- Chaszar, A. (Ed.). (2006). *Blurring the Lines: Computer-Aided Design and Manufacturing in Contemporary Architecture*. Great Britain: John Wiley & Sons.
- Clear, R. D. (2012). Discomfort glare: What do we actually know? *Lighting Research and Technology*, 45(2), 141–158. <https://doi.org/10.1177/1477153512444527>
- Cuce, E., & Riffat, S. B. (2015). A state-of-the-art review on innovative glazing technologies. *Renewable and Sustainable Energy Reviews*, 41, 695–714. <https://doi.org/10.1016/j.rser.2014.08.084>
- Echenagucia, T. M., Capozzoli, A., Cascone, Y., & Sassone, M. (2015). The early design stage of a building envelope: Multi-objective search through heating, cooling and lighting energy performance analysis. *Applied Energy*, 154, 577–591. <https://doi.org/10.1016/j.apenergy.2015.04.090>
- Foster, N. (n.d.). Foster and Partners. Retrieved from <https://www.fosterandpartners.com/>
- Freewan, A. A. Y. (2014). Impact of external shading devices on thermal and daylighting performance of offices in hot climate regions. *Solar Energy*, 102, 14–30. <https://doi.org/10.1016/j.solener.2014.01.009>
- Galasiu, A. D., & Veitch, J. A. (2006). Occupant preferences and satisfaction with the luminous environment and control systems in daylit offices: a literature review. *Energy and Buildings*, 38(7), 728–742. <https://doi.org/10.1016/j.enbuild.2006.03.001>
- Gerfen, K. (2013). Eckenberg Gymnasium. *Architect*, 102(October), 108–117. Retrieved from www.architectmagazine.com
- Gratia, E., & De Herde, A. (2007). The most efficient position of shading devices in a double-skin facade. *Energy and Buildings*, 39(3), 364–373. <https://doi.org/10.1016/j.enbuild.2006.09.001>
- Hee, W. J., Alghoul, M. A., Bakhtyar, B., Elayeb, O., Shameri, M. A., Alrubaih, M. S., & Sopian, K. (2015). The role of window glazing on daylighting and energy saving in buildings. *Renewable and Sustainable Energy Reviews*, 42, 323–343. <https://doi.org/10.1016/j.rser.2014.09.020>
- Hensel, M. (2013). *Performance-oriented Architecture: rethinking architectural design and the built environment* (First edit). John Wiley & Sons Ltd.
- Illuminating Engineering Society of North America. (2000). *The IESNA lighting handbook* (9th ed.). New York.
- Karagianni, L., Turrin, M., Knaak, U., & Hordijk, T. (2016). Additive Manufacturing for daylight Towards a customized shading device. In R. Attar, A. Chronics, S. Hanna, & M. Turrin (Eds.), *Symposium on Simulation for Architecture and Urban Design (SimAUD)* (pp. 69–76). London: Society for Modeling & Simulation International (SCS).
- Kim, C.-S. S., & Chung, S.-J. J. (2011). Daylighting simulation as an architectural design process in museums installed with toplights. *Building and Environment*, 46(1), 210–222. <https://doi.org/10.1016/j.buildenv.2010.07.015>
- Kim, D.-W., & Park, C.-S. (2012). Comparative control strategies of exterior and interior blind systems. *Lighting Research and Technology*, 44(3), 291–308. <https://doi.org/10.1177/1477153511433996>
- Kittler, R., Kocifaj, M., & Darula, S. (2012). *Daylighting science & daylighting technology*. (J. Roberts, Ed.). New York: Springer. <https://doi.org/10.1007/978-1-4419-8816-4>
- Knippers, J., & Helbig, T. (2009). The Frankfurt Zeil Grid Shell. In A. Domingo & C. Lazaro (Eds.), *Proceedings of the International Association for Shell and Spatial Structures (IASS) Symposium* (pp. 1367–1378). Valencia, Spain.

- Lawrence Berkeley National laboratory, (LBNL). (2002). *High-Performance Commercial Building Façades*. Retrieved from <http://gaia.lbl.gov/hpbf/main.html>
- Munoz, C. M., Esquivias, P. M., Moreno, D., Acosta, I., & Navarro, J. (2014). Climate-based daylighting analysis for the effects of location, orientation and obstruction. *Lighting Research & Technology*, 46(3), 268–280. <https://doi.org/10.1177/1477153513487005>
- Nabil, A., & Mardaljevic, J. (2005). Useful daylight illuminance: a new paradigm for assessing daylight in buildings. *Lighting Research & Technology*, 37(1), 41–59. <https://doi.org/10.1191/1365782805li128oa>
- Pfrommer, P., Lomas, K. J., Seale, C., & Kupke, C. H. R. (1995). The Radiation Transfer Through Coated and Tinted Glazing. *Solar Energy*, 54(5), 287–299.
- Piano, R. (n.d.). Renzo Piano Building Workshop (RPBW). Retrieved from <http://www.rpbw.com/>
- Pierce, G. (1998). Natural Lighting at the Kimbell Museum. *A86th CSA Annual Meeting and Technology Conference*, 89–93.
- Reinhart, C., Mardaljevic, J., & Rogers, Z. (2006). Dynamic daylight performance metrics for sustainable building design. *LEUKOS - Journal of Illuminating Engineering Society of North America*, 3(1), 7–31. <https://doi.org/10.1582/LEUKOS.2006.03.01.001>
- Reinhart, C., & Selkowitz, S. (2006). Daylighting-Light, form, and people. *Energy and Buildings*, 38(7), 715–717. <https://doi.org/10.1016/j.enbuild.2006.03.005>
- Reinhart, C., & Wienold, J. (2011). The daylighting dashboard - A simulation-based design analysis for daylight spaces. *Building and Environment*, 46(2), 386–396. <https://doi.org/10.1016/j.buildenv.2010.08.001>
- Roudsari, M. S., & Waelkens, A. (2015). A New Approach to Modeling Frit Patterns for Daylight Simulation. In H. Samuelson, S. Bhooshan, & R. Goldstein (Eds.), *Proceedings of the Symposium on Simulation for Architecture & Urban Design (SimAUD)* (pp. 183–188). Washington D.C.
- Ruck, N. (2000). *Daylight in Buildings: a source book on daylighting systems and components*. International Energy Agency (IEA) Solar Heating and Cooling Programme, Energy Conservation in Buildings & Community Systems. Retrieved from <http://www.iea-shc.org>
- Ruck, N., & Smith, S. C. J. (1988). The Passive Daylighting of Building Interiors. *Architectural Science Review*, 31(3), 87–98. <https://doi.org/10.1080/00038628.1988.9696634>
- Sarkisian, M., Lee, P., & Long, E. (2011). A Celebration of Structure as Architecture - The Cathedral of Christ the Light. In D. Ames, T. L. Droessler, & M. Hoit (Eds.), *Structures Congress* (pp. 2044–2055). American Society of Civil Engineers (ASCE).
- Scheible, F., & Dimcic, M. (2011). Parametric Engineering Everything is Possible. In *Proceedings of the International Association for Shell and Spatial Structures (IABSE-IASS) Symposium : Taller, Longer, Lighter*. London. Retrieved from http://programmingarchitecture.info/publications/ScheibleDimcic_IASS_2011.pdf
- Schlaich Bergemann Partner (SBP). (n.d.). Schlüterhof Roof, German Historical Museum. Retrieved April 12, 2017, from <https://www.sbp.de/en/offices/new-york/>
- Schlaich, J., & Schober, H. (2005). Freeform glass roofs. In *Structures Congress*. American Society of Civil Engineers (ASCE).
- Sherif, A., El-Zafarany, A., & Arafa, R. (2012). External perforated window Solar Screens: The effect of screen depth and perforation ratio on energy performance in extreme desert environments. *Energy and Buildings*, 52, 1–10.
- Stemers, K., Baker, N., & Fanchiotti, A. (2001). *Daylighting in architecture, a European reference book*. James & James.
- Turrin, M., von Buelow, P., Kilian, A., & Stouffs, R. (2012). Performative skins for passive climatic comfort. *Automation in Construction*, 22, 36–50. <https://doi.org/10.1016/j.autcon.2011.08.001>
- U.S. Department of Energy. (2015a). Buildings Energy Data Book. Retrieved April 4, 2017, from <http://buildingsdatabook.eren.doe.gov/TableView.aspx?table=1.1.3>

- U.S. Department of Energy. (2015b). Buildings Energy Data Book. Retrieved April 4, 2017, from <http://buildingsdatabook.eren.doe.gov/TableView.aspx?table=1.1.5>
- U.S. Department of Energy. (2015c). Buildings Energy Data Book. Retrieved April 4, 2017, from <http://buildingsdatabook.eren.doe.gov/TableView.aspx?table=1.4.1>
- U.S. Department of Energy. (2015d). Buildings Energy Data Book. Retrieved April 4, 2017, from <http://buildingsdatabook.eren.doe.gov/TableView.aspx?table=1.4.3>
- U.S. Green Building Council. (2013). LEED BD+C, v4. Retrieved April 16, 2017, from <http://www.usgbc.org/credits/healthcare/v4-draft/eqc-0>
- Webb, A. R. (2006). Considerations for lighting in the built environment: Non-visual effects of light. *Energy and Buildings*, 38(7), 721–727. <https://doi.org/10.1016/j.enbuild.2006.03.004>
- Wienold, J. (2009). Dynamic daylight glare evaluation. In *Eleventh International IBPSA Conference: Building Simulation* (pp. 944–951). Glasgow, Scotland. <https://doi.org/citeulike-article-id:11069372>
- Wienold, J., & Christoffersen, J. (2006). Evaluation methods and development of a new glare prediction model for daylight environments with the use of CCD cameras. *Energy and Buildings*, 38(7), 743–757. <https://doi.org/10.1016/j.enbuild.2006.03.017>
- Woodbury, R. (2010). *Elements of Parametric Design* (First edit). New York: Routledge.

Chapter 5 :

Parameters

“Nothing is as dangerous in architecture as dealing with separated problems. If we split life into separated problems, we split the possibilities to make good building art.”

-Alvar Alto

5.1 Introduction

This chapter first discusses the notion of integrated design and the scope of its application in the dissertation. Integrated design is implemented through parametric and performance-oriented design, while taking into account the structural and daylighting disciplines at the early stages of design discussed in Chapter 2. Chapter 3 reviewed shell structures as roof systems and discussed topology, shape, and sizing design in shell structures. Chapter 4 discussed principles of daylighting and categorized daylight control strategies in roof systems into three levels, namely control at the geometry, the glazing, and the interior level. The structural and daylighting classifications from Chapter 3 and 4 are meshed together to isolate design parameters that link and affect both disciplines, for an integrated design approach. The parameters that are common in the two disciplines are identified, and once discussed in depth, an alternative naming convention is introduced. The common design parameters are the cornerstones of the computational model that will be created. Chapter 6 will discuss the methodology used for implementing an integrated design framework for the large span roof systems with openings, Chapter 7 will describe the case studies, and results are discussed in Chapter 8.

Diversification and segregation of professions in the building industry has helped designers and other participants in the design and build process to embrace projects with a high level of complexity and information content. However, since professional silos generate disconnected information, problems related to the dispersed nature of the industry arise. *Integrated design* is the term for a proposed method whose implementation aims to narrow the gaps between disciplines and ultimately to bridge them. Although different researchers frame this concept differently, the

definitions can be classified into three main categories based on the core issue that each is addressing. Integrated design can be defined as:

- 1- Integrating form and performance
- 2- Integrating multiple disciplines such as structure, environmental design, and acoustics
- 3- Integration at the tool level, where interoperability becomes the focus.

The first definition of integrated design revolves around the combination of form with performance during design. Michael Hensel, in his book entitled *Performance-oriented architecture: rethinking architectural design and built environment*, discusses how the notion of performance was brought into architecture from theatrical performances and how it is perceived in architecture (Hensel, 2013). Koleravic (2014) discusses how a growing emphasis on sustainability led environmental performance to become an important factor in architectural design. A researcher defines integrated design by redefining form “not as the geometric representation of a material object alone, but a multitude of effects and behavior, where the dualism of form and function is transformed to a synergy that aspires integral design solutions” (Fasoulaki, 2008, p. 28). Integration can be taken to a level where performance leads the design, called performance-based design, as briefly described in Chapter 2.

In the case of shell structures, the form-finding strategies and experiments reviewed in Chapter 3 are examples of integrating structural performance in design. In fact, the form is created due to structural forces. As stated by Oxman & Oxman, “form finding is a significant concept that changes the traditional meaning of performance by integrating formation and generation processes” (Oxman & Oxman, 2014). Associations between form and performance can take different arrangements. Either form has priority and performance is assessed once the form is finalized; or performance has priority and it dictates form; or form and performance are integrated, a case in which performance is assessed frequently to help the designer make informed decisions (Figure 5.1).

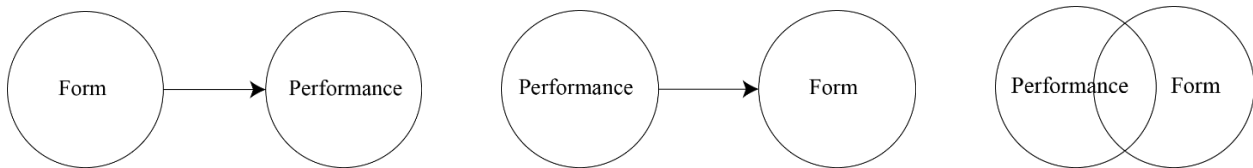


Figure 5.1. Form has a priority (a); performance dictates form (b); integrating form and performance (c)

The second definition of integrated design focuses on integrating multiple disciplines together. Dominik Holzer points to the importance of arriving at solutions which are a result of an integrative approach by stating that “integrated solutions are the best way forward to address the plethora of requirements design teams face on projects” (Holzer, 2009, p. 52). Michela Turrin identifies two design approaches to design in the architecture, engineering, and construction (AEC) industry, *mono-disciplinary* and *multi-disciplinary* design approaches (Turrin, 2014). In her description, a mono-disciplinary approach to design evaluates the performance of modularized building systems in each discipline in a manner detached from other disciplines, and sometimes in a hierarchical order. However, decision making for coupled building systems, in which performance in one field largely affects the performance of other fields, requires a multi-disciplinary design approach. Another researcher studies building systems and has categorized them into *modularized* and *coupled* systems. In modularized systems, the component systems can be analyzed and synthesized independently since their performance and design do not interact or affect one another. In coupled building systems, however, the component systems do interact and influence one another (Fasoulaki, 2008). She describes integrated design as “the integration of interrelated and diverse building performances involving multiple disciplines” (Fasoulaki, 2008, p. 3).

The concept of integrating multiple disciplines can be extended to collaborations among multiple disciplines, leading to an interdisciplinary design approach. Kiel Moe extends the definition of integrated design from disciplines to participants: “Depending upon the context, integrated design may mean that a building’s spatial, construction, energy, and system’s logic are intertwined. It may also mean that a building is the product of new social relationships amongst architects, clients, developers, builders, communities, and consultants. Integrated design means many things to different practices depending on the context” (Moe, 2008). Dominik Holzer conducted a research action observing the dynamics among different disciplines within the firm Arup for three years. He defined three areas of importance regarding multi-disciplinary design collaboration, including “1-knowledge capture, 2- trade-offs in multidisciplinary design, and 3-common geometry” (Holzer, 2009, p. 120). His findings emphasize the importance of capturing knowledge from one discipline and communicating it with others; understanding the trade-offs between multiple disciplines upon decision making; and finally, having a common geometry as the means of communication between disciplines. Another researcher points to the evolving definition of integrated design and expresses that “the definition of integrated practice is still

developing, but what is common in most examples of such practice is an attempt to reduce the barriers and hurdles for communication between disciplines. It can mean having more interdisciplinary meetings with communal goal settings and exploration rather than parallel studies and results sharing. This is especially relevant at the conceptual design stage where many fundamental but often less well-founded decisions are made” (Tsigkari et al., 2013, p. 155).

In the context of shell structures, integrated design regarding multiple disciplines can be translated into a design approach that not only considers structural performance, but also considers environmental performance when the continuous shell is perforated, or when a grid shell is used. This mode of integration is illustrated in Figure 5.2.

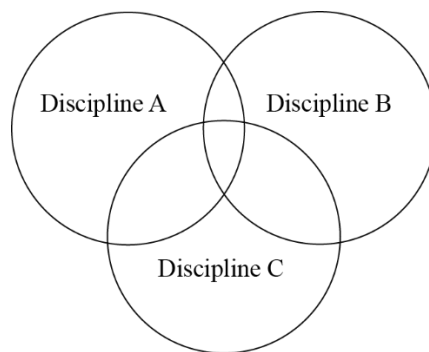


Figure 5.2. Integrating performance from multiple disciplines

The third definition addresses integrated design at the tool level. It focuses on *how* multiple disciplines can be integrated and how collaboration between multiple professionals can be facilitated. Interoperability becomes the focus of this definition. Some research studies have been conducted on the *Interoperability of Building Modeling (IBM)*, or tool interoperability, meaning that one model is created to be directly operatable in various disciplinary platforms. Once the model is transferred to a specific platform, it can then be further developed according to disciplinary requirements. Many architects are trying to create design tools that offer better connectivity by developing plugins for software platforms such as Grasshopper by McNeel, Generative Components (GC) by Bentley, and Dynamo by Autodesk.

A more recent approach to resolving the interoperability issue focuses on storing the model’s data in the cloud, where multiple disciplines can have access to it. Recently, a tool that facilitates interoperability, named Flux, has been introduced.¹ Each Flux project becomes the hub for data

¹ <https://flux.io>

interchange between tools and team members. In this case, once data is updated in one platform, those changes are synced across the team’s connected tools. With this method, file-based data exchange is no longer in use; rather, data exchange occurs through interconnected platforms.

In addition to Flux, there is another software platform, named Project Quantum, under development by Autodesk Inc. at the time of drafting this dissertation (September 2017). Autodesk has announced that Project Quantum aims to address interoperability and integration issues in the AEC industry. Their goal is to transfer data between multiple disciplines while all participants are interconnected, to bridge the gap between design, engineering, and construction (Figure 5.3). By keeping the shared data on cloud servers, the file-based mode of collaboration shifts towards a data-based mode of collaboration.

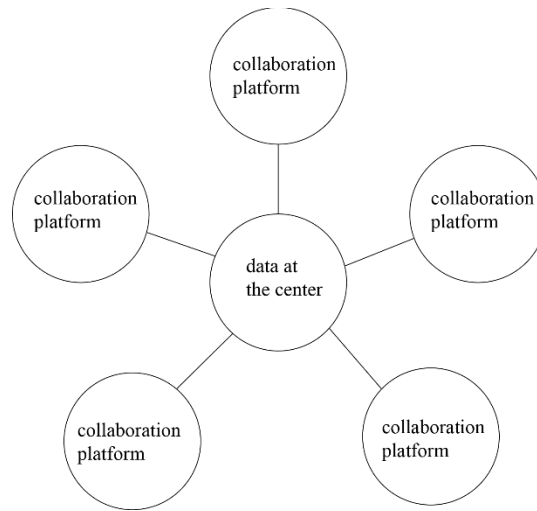


Figure 5.3. interoperability at the tool level among disciplines

It should be noted that interoperability is not the focus of this dissertation. However, creating a parametric model that is meaningful for multiple disciplines and can potentially be translated and connected to disciplinary platforms is an objective. Therefore, integrated design is used in its first and second definition.

Many researchers in the field of architectural design have conducted studies on integrated design approaches. Focusing on integrating form and performance, they have integrated form generation with structural or environmental performance. These studies are single-objective or multi-objective in one discipline. It should be noted that environmental design is considered as a discipline that encompasses energy use, daylight availability, indoor air quality, and the like. In the structural design discipline, researchers have used different tools and methodologies to

integrate design with structural performance, such as integrating parametric modeling with structural performance (Danhaive & Mueller, 2015), implementing multi-objective design optimization using genetic algorithms (Evins et al., 2012), integrating NURBS modeling with FEM structural analysis in Oasys GSA (Dimcic & Knippers, 2012), using a generative structural design system named eifForm, by using GenerativeComponents and then implementing it through the use of XML models in roof trusses (Shea, Aish, & Gourtovaia, 2005). The same methodology is observed in the discipline of environmental design. As an example, a group of researchers report a technique for multi-criteria assessment of building designs by implementing a computer program named ENER-RATE to compare the energy use, indoor air quality, thermal comfort, operating plant load, financial costs, and other environmental degradation of design alternatives (Soebarto & Williamson, 2001). Others have integrated heating, cooling, and lighting energy performance at the early stages of design (Brown, Tseranidis, & Mueller, 2015) (Tomás Méndez Echenagucia, Capozzoli, Cascone, & Sassone, 2015). Integration of design with simulation has been implemented in practice as well. As an example, a group of designers at Foster and Partners report on how they integrate simulation in their design practices (Tsigkari et al., 2013).

There is a large body of literature focusing on integrating multiple disciplines, referred to as multi-disciplinary design. Either a single objective or multiple objectives are considered in these studies. In one example, researchers compared multidisciplinary design, analysis (MDA) and optimization (MDO) processes in the AEC and aerospace industries based upon case data gathered on recent projects in each industry (Flager & Haymaker, 2007). Multi-objective multi-disciplinary analysis has been employed in large-scale buildings such as sports building envelopes (Yang, Sun, Turrin, Buelow, & Paul, 2015; Yang, Turrin, Sariyildiz, & Sun, 2015), and small-scale design projects, such as classroom design, considering the project's structural and energy performance (Flager, Welle, Bansal, Soremekun, & Haymaker, 2009). Structural design has been integrated with energy-related design aspects including solar radiation control (Adriaenssens et al., 2014), and with acoustics by employing genetic algorithms (Tomas Mendez Echenagucia, 2013). A plethora of design and performance assessment tools, as well as workflows, have been employed by researchers. As an example, Alfaris & Merello (2008) created a framework for building a generative multi-performance design system in CATIA environment, and demonstrated its applicability through a fictional design case of spatial components within a grid of cells, where the objective requirements were adjacency, area, real-estate, proportion, thermal, and daylighting.

Another researcher has discussed *optioneering* as a computational framework that has been implemented in DesignLink, to assist designers and consultants to resolve design problems through integrated analysis across disciplines in the early stages of design (Holzer, 2010).

As the body of studies on multi-objective, multi-disciplinary design approaches is growing, there is a developing parallel body of literature on ways in which the results can be explored. One example is a study on multi-attribute decision making (MADM) and a data visualization method for comparing different alternatives (Abraham, Flager, Macedo, Gerber, & Lepech, 2014).

Finally, there is a body of literature that examines interoperability of design and performance assessment platforms. A group of researchers report on supporting optimization within a single computational design system employing SMART Form for form finding, Robot Structural Analysis for structural performance assessment, and Ecotect for building performance assessment by using DesignScript (Aish, Fisher, Joyce, & Marsh, 2012). Another group of researchers discuss how engineering software should be developed in a way that it enables seamless integration, rather than seeking to integrate existing packages. They focus on developing *live* or *real-time* structural analysis applications in which user interaction, visualization, and computation appear to occur simultaneously, towards developing an intuition for the effects that design modifications have on structural performance (Clune, Connor, Ochsendorf, & Kelliher, 2012). Another researcher incorporated a prototype tool named H.D.S. Beagle to combine parametric modeling with multi-objective optimization through an integrated platform for enabling rapid iteration and trade-off analysis across the domains of design, energy use intensity, and finance (Gerber & Lin, 2013a; Gerber & Lin, 2013b; Lin & Gerber, 2014).

Each of the aforementioned studies in the AEC discipline develop a case study considering one or multiple disciplines for performance assessment, followed by employment of a methodology for the generation and assessment of multiple alternatives. In addition, some researchers have explored post-processing data exploration techniques to better understand the results. The gaps that exists in the current literature are listed below. It should be noted that some studies include some but not all of them which are essential for creating a parametric model for a multi-disciplinary study.

1. *Identify disciplinary design parameters*: existing studies do not discuss which design parameters professionals in each discipline consider in the design phase before conducting a multi-disciplinary performance assessment study.

2. *Identify overlapping design parameters between disciplines:* existing studies do not discuss if each design parameter is rooted in only one discipline, or if it exists in multiple disciplines.
3. *Explain why and how the overlapping (and non-overlapping) parameters are included in the parametric model:* even if key design parameters and overlapping parameters in each discipline are identified, existing studies do not discuss how and why some design parameters are included in or excluded from the model. The rationale behind creating the model is not formalized beyond explaining the technical modeling processes.
4. *Explain how implementing the parameters in the parametric model bounds the design space:* once design parameters are implemented using a parametric model, some opportunities are created, while some limitations are imposed. In other words, a design-space is created. The boundaries of the design space, including the extreme possibilities, are not discussed in depth regarding multiple disciplines in existing studies.
5. *Explain the expected relationship between implemented parameters and performance in multiple disciplines:* it is expected that parameters affect performance, but not all parameters affect performance in every discipline. Having an understanding of their possible relationship will greatly assist in understanding the results.
6. *Results are bound to specific case studies:* in a majority of existing studies, the implementation process is discussed in depth, and its application to a case study is explored. However, the results remain restricted to that specific case study and have not been extended to scrutinize possible applications of the approach to other relevant cases.

The objectives of this research are summarized in Chapter 1, which also aim to address the gaps outlined above.

On a separate note, to have consistency in terminology, *parameter* is used to describe an *independent variable* that designers can implement in their model. Many times, one independent variable may translate directly to a design parameter; other times, the combination of multiple independent variables creates a design parameter. Parameters can be quantified and recorded or be expressed as ratios, and may or may not be a cause to an effect.

On the other hand, *performance* is used to describe any *dependent variable* with a value that changes based on the change in the parameter. Performance can also be quantified and measured,

and it can be tested against certain criteria, or disciplinary metrics. The evaluation criteria of performance is generally fixed (such as strength limits), but sometimes may be compared to a baseline case.

5.2 Overlapping parameters in structure and daylighting disciplines

Chapter 3 discussed the topics of topology, shape, and sizing in structural design, and then replicated the categorization in the context of continuous and grid shell structures. Chapter 4 classified various levels at which daylight can be controlled based on the order in which light beams hit various levels of a building envelope, namely the geometry, glazing, and interior levels, by focusing on continuous shell structures. These two classifications are placed side by side to identify the parameters that link the two disciplines (Figure 5.4).

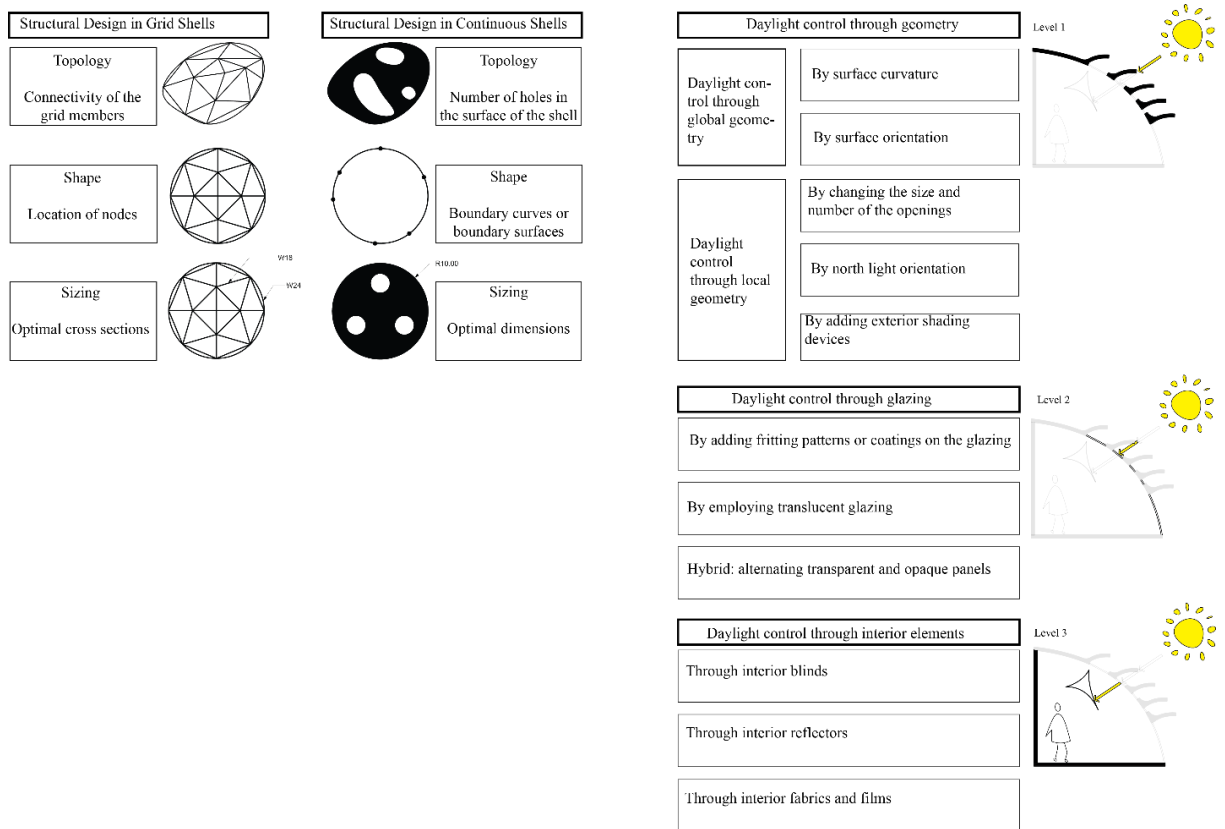


Figure 5.4. Placing the structural and daylighting categorization side by side

After reviewing the two diagrams, the second and third level of daylight control can be eliminated, since neither the glazing type nor the interior justifications interact with topology, shape, or sizing design in the structural discipline of continuous shell structures. These are the parameters that only affect daylighting performance; thus, they are eliminated from the

comparison. It is worth noting that different glazing materials or any added layer in the interior space that is structurally supported by the roof system will impose an added weight to the structure. But this weight can be considered as a dead load applied to the system in a more detailed structural consideration, which is not within the scope of an interdisciplinary design approach at the early stages of design. After removing the second and third levels of daylight control, two categories are left, presented side by side in Figure 5.5.

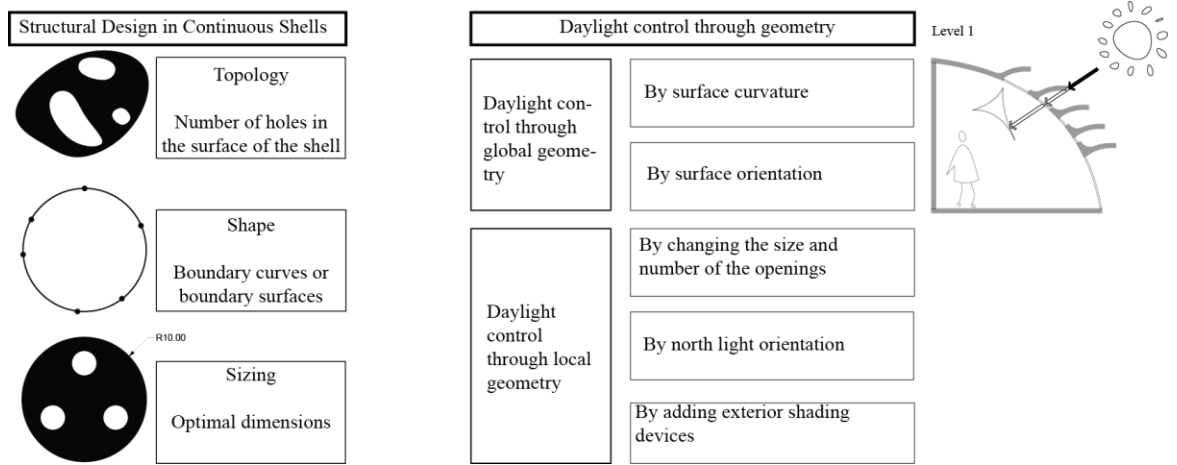


Figure 5.5. Placing the structural and daylighting design stages side by side

By looking at the two classifications, the first parameter that appears in both disciplines is the *number of openings*, noted as topology in structural design, and under local geometry in the daylighting design category (Figure 5.6).

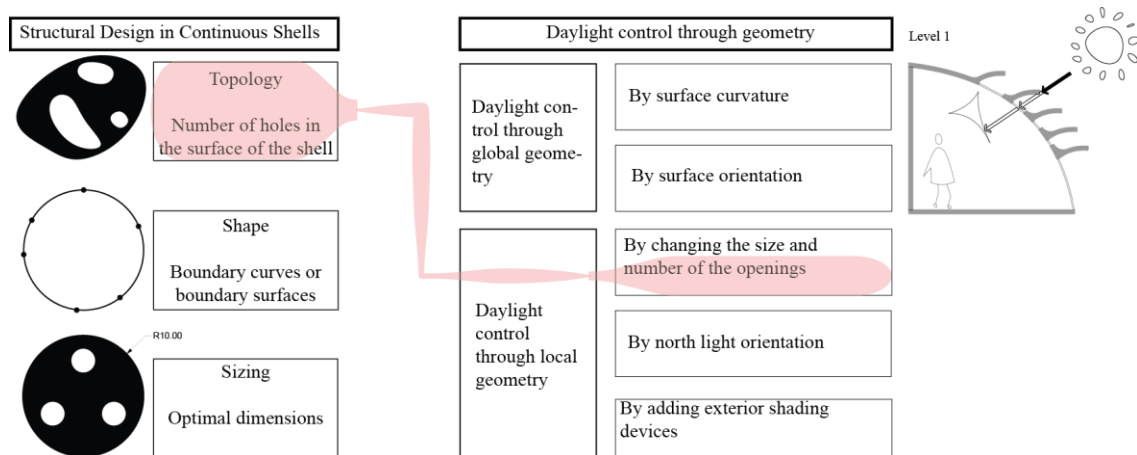


Figure 5.6. *Number of openings* as the first parameter that is common in two disciplines

The second parameter that overlaps both disciplines is the *size of the openings*, noted as sizing in structural design, and under local geometry in the daylighting design (Figure 5.7).

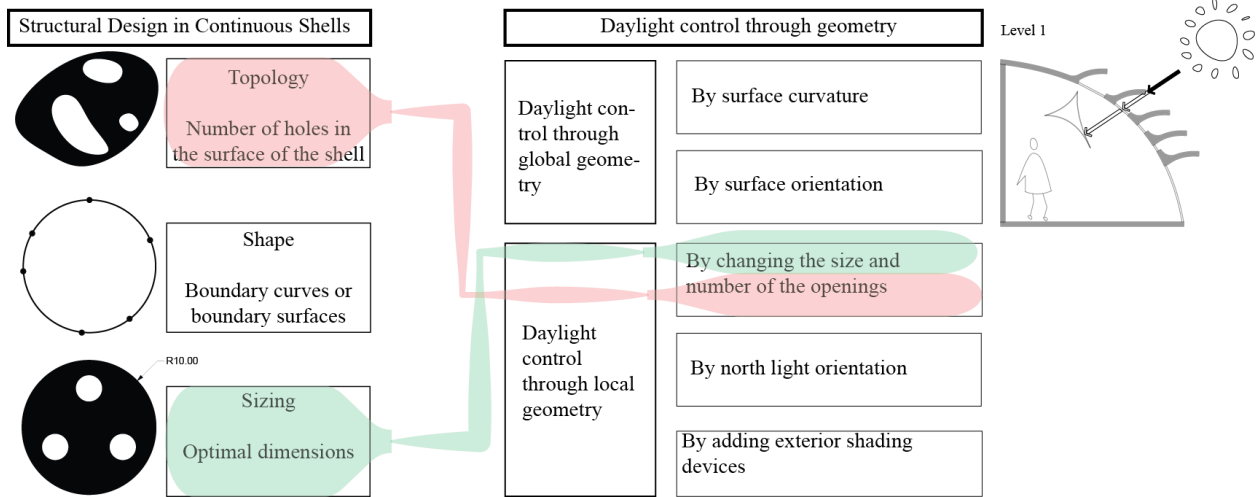


Figure 5.7. *Size of the openings* as the second parameter that is common in two disciplines

The third parameter that overlaps the two disciplines is *surface curvature*, noted as boundary curves in structural discipline, and framed under daylight control through global geometry in the daylighting design category (Figure 5.8).

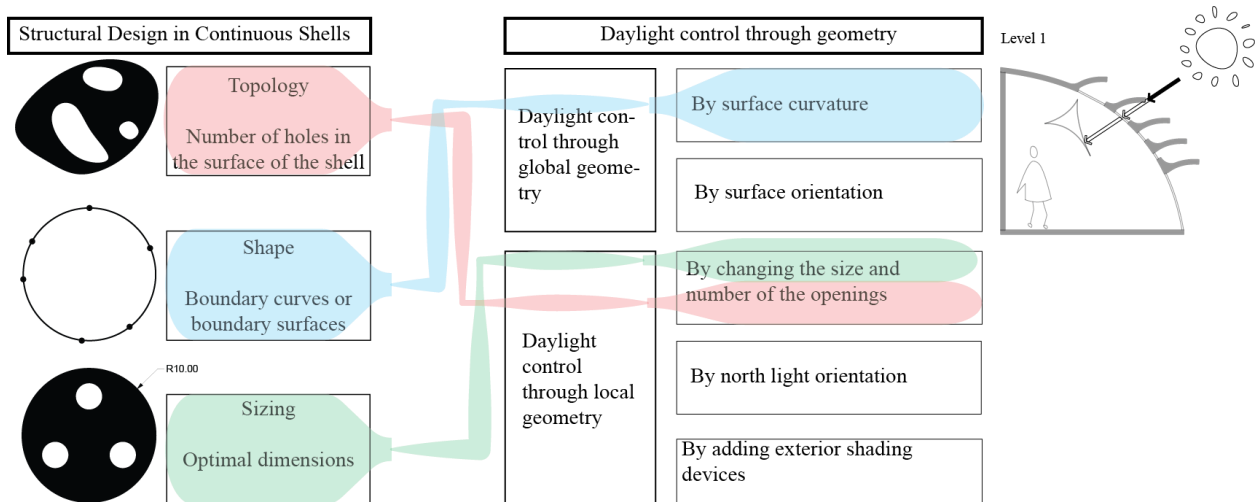


Figure 5.8. *Surface curvature* as the third parameter that is common in two disciplines

Therefore, the overlapping parameters are identified as:

- The size of the openings,
- number of openings, and
- surface curvature

Although the overlapping parameters are identified, it is worth discussing the parameters that are not on this list, especially those from the daylighting discipline. Three parameters are not considered as overlapping parameters:

- The surface orientation,
- north light orientation, and
- addition of exterior shading devices

The first two parameters are concerned with orientation, which is important only for daylighting. Orientation of a form does not affect its structural performance and design, unless the wind load is concerned. To consider wind load in structural design, since the wind's directionality is not predictable, a form is usually tested against multiple wind directions and the worst case is selected as the basis for design. There is also another design strategy that takes into account prevailing wind conditions based on statistical observations; thus, there are design systems that have used this approach with dominant wind loads in a particular direction. This study assumes the former approach, and so does not consider orientation as a common parameter.

The third parameter that is not considered as a linking parameter is *adding exterior shading devices*. Similar to adding interior devices, this can be calculated as an added dead load applied to the structure and does not necessarily overlap with topology and shape design.

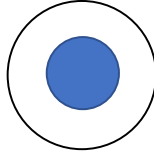
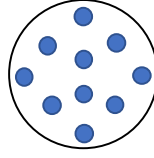
5.2.1 Perforation Ratio, Granularity, and Bias

Once the interrelated parameters between two disciplines are identified, they can be investigated in depth and be interpreted for design implementation. The number and size of the openings is captured through different ratios. A common parameter that is widely used in façade and roof studies for daylighting design is the perforation ratio, which is calculated using the size and number of the openings. Perforation ratio is calculated through the following equation.

$$\text{Perforation ratio (PR)} = \frac{\Sigma(\text{number of the opening} \times \text{size of the opening})}{\text{surface area}}$$

Although the perforation ratio is widely used, it does not describe the granularity of the openings, which ultimately affects the quality of daylight. In other words, PR does not communicate how big or small the perforations are. A simple comparative case is illustrated in Table 5.1, demonstrating how two cases with the same PR can potentially provide two different lighting qualities. Therefore, other indices must be calculated alongside PR.

Table 5.1. Inefficiency of Perforation Ratio (PR) in describing the size of the openings in the daylighting discipline

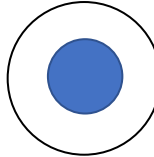
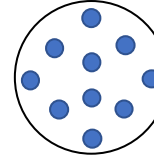
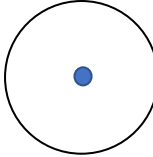
	case 1	case 2
		
Area of one opening	50	5
Number of openings	1	10
Area of roof surface	100	100
Perforation ratio (PR)	0.5	0.5

To address the inadequacy of PR as a parameter, the structural discipline is scrutinized as a source of inspiration. Structural design quantifies the number of openings in a surface under topological design, and through the genus, or g-value, while quantifying the size of the openings under sizing design. Drawing upon this perspective, a new parameter is introduced to be used by designers alongside PR, named granularity (GR), used to describe how fine the openings are. Granularity can be defined as the number of the perforations relative to the surface area.

$$Granularity (GR) = \frac{\Sigma(\text{number of openings})}{\text{surface area}}$$

Within a constant perforation ratio, there might be only one large hole, or 100 small holes; granularity is the parameter that can quantify the difference between these two cases. It should be noted that granularity is meaningful only when combined with PR. As seen in Table 5.2, two cases with the same granularity (GR) can have dramatically different perforation ratios.

Table 5.2. Granularity can be used alongside perforation ratio for a more comprehensive analysis

	case 1	case 2	case 3
			
Area of one opening	50	5	10
Number of openings	1	10	1
Area of roof surface	100	100	100
Perforation ratio (PR)	0.5	0.5	0.1
Granularity (GR)	0.01	0.1	0.01

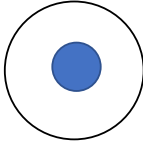
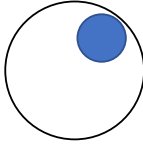
Once the perforation ratio and granularity of a design are identified, a third parameter can be considered. All the predictions above are made based upon the assumption that the openings are equally distributed across any surface, and the distribution of openings is evenly spread. Both

structural and daylighting performance can be affected by the placement of the openings. Neither Perforation ratio nor granularity can predict the effect that the location of an opening can have on the daylighting and structural performance of a structure. Therefore, there is a need to quantify a third parameter, bias. Bias quantifies how the extent to which an opening deviates from the center of a given geometry.

$$\text{Bias} = \text{deviation of an opening from the center}$$

Table 5.3 demonstrates an example that differentiates a geometry with a central opening versus a geometry with a biased opening.

Table 5.3. importance of considering bias as well as perforation ratio and granularity

	case 4	case 5
		
Area of one opening	25	25
Number of openings	1	1
Area of roof surface	100	100
Perforation ratio (PR)	0.25	0.25
Granularity (GR)	0.01	0.01
Bias	center	skewed

In an effort to quantify bias, various possible approaches are scrutinized. The goal is to arrive at a method that can capture the effect of bias yet is simple enough to be easily applied to multiple cases. For this goal, a square is used as a simple symmetric geometry to demonstrate various approaches of defining bias.

The simplest approach is to divide the square into 4 equal parts and determine if an opening is located in a specific zone. Different zones can be indexed as 1, 2, 3 and 4, where a coordinate system is mapped on the lower left corner of the square (Figure 5.9).

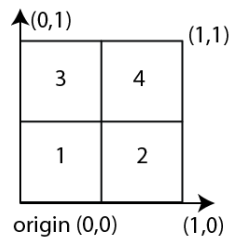


Figure 5.9. Dividing a square into four equal sections to quantify bias

A series of hypothetical cases are created using the four-zone division (Figure 5.10). To quantify bias, it is assumed that if an opening spread over a specific region, the bias is expressed as the zone index. In the case that an opening is spread over two regions, the region that houses the greater portion of the opening's area is expressed as the bias. If an opening is equally spread over two or more zones, one strategy to define bias is to express it as a combination of more than one zone. For example, if an opening is equally mapped on zone 1 and 2, the Bias can be expressed as $\frac{1}{2}$ zone 1 + $\frac{1}{2}$ zone 2.

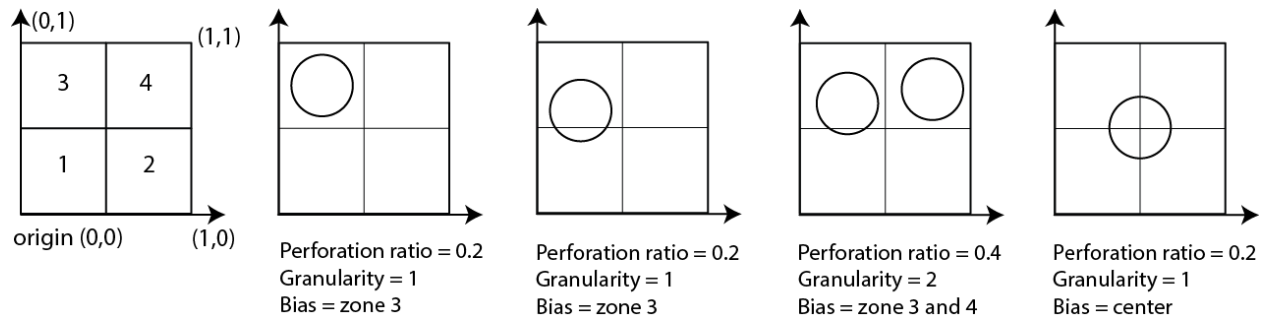


Figure 5.10. Dividing a square into four equal sections to quantify Bias

Although these assumptions facilitate using a four-division map, it does not accommodate the very basic case with an oculus at the center. Therefore, the division can become finer in the next iteration. The next iteration divides the same square into 9 equal zones. A coordinate system is mapped on the lower left corner of the square, and different zones are indexed as 1 through 9 (Figure 5.11).

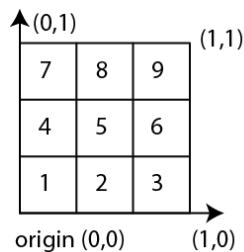


Figure 5.11. Dividing a square into nine equal sections to quantify bias

Having a total of 9 zones easily captures the case where an opening is placed at the center. Again, when an opening spread over two regions, it is assumed that the region that is housing the greater portion of the opening's area is the indicator of bias. This case, along with other hypothetical cases, is demonstrated in Figure 5.12.

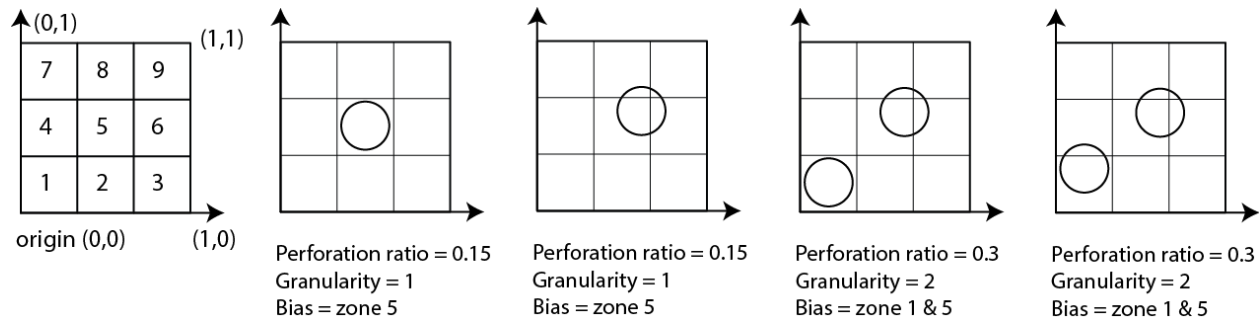


Figure 5.12. Dividing a square into nine equal sections to quantify bias

A 9-zone division is still simple to adopt. It should be noted that as the division of the square become finer and finer, it can give a more accurate description of the placement of the openings, but it becomes more complex to adopt (Figure 5.13). In addition, deciding on the number of divisions depends on the specific geometry at hand, with the relevant factors including its scale and symmetry, to name a few.

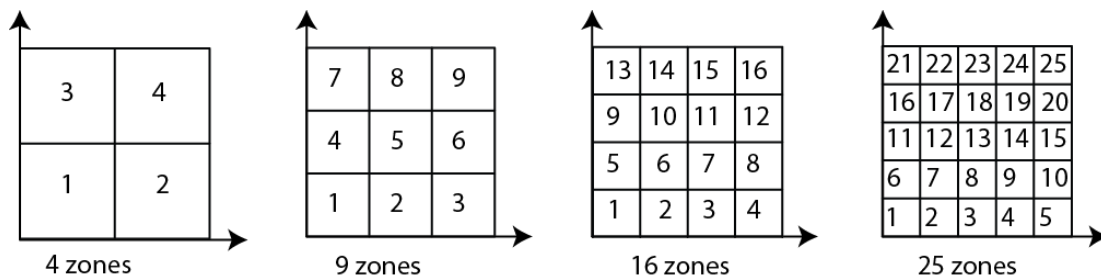


Figure 5.13. As the divisions become finer, the accuracy of quantifying bias increases but the process becomes more complex

5.2.2 Surface Curvature

The third parameter that overlaps the two disciplines is *surface curvature*, noted as boundary curves in structural discipline, and framed under daylight control through global geometry in the daylighting discipline. It is essential to first review the concept of surface curvature mathematically before describing it in the context of shell structures. As previously noted, shells have a small thickness in one axis compared to the dimensions in the other two axes.

According to Blaauwendraad & Hoefakker (2014), if point A is defined on a smooth surface, there will be a tangent plane at that point, where the normal to the surface is defined to be normal to the tangent plane. There are an infinite number of plane curves at point A, but one of them has a minimum curvature and another has a maximum curvature. These two plane curves are called

the *principal sections*, and their curvatures are called the *principal curvatures*, denoted by k_1 and k_2 (Figure 5.14). Curvature is the inverse of the radius.

$$\text{Curvature} = \frac{1}{\text{Radius}}$$

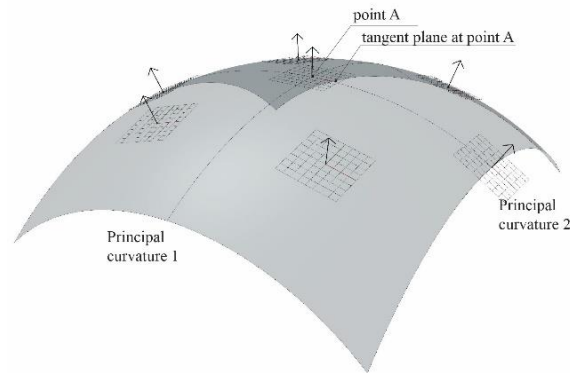


Figure 5.14. A tangent plane can be passed through the points on the surface to draw principal curvatures

The product of the two principal curvatures, $k_g = k_1 \times k_2$, is called the Gaussian curvature of the surface at a point. A surface can be comprised of many curvatures at different points. The Gaussian curvature can be positive, negative, or zero. If it is positive, k_1 and k_2 have the same sign and the resultant surface is synclastic or dome-shaped. If the Gaussian curvature is negative, k_1 and k_2 have opposite signs, and the surface is anticlastic or saddle-shaped. If either k_1 or k_2 is zero, their product is zero; thus, the surface has a single curvature or is vault-shaped (Blaauwendraad & Hoefakker, 2014). This overall definition is used to differentiate different shapes, while the maximum and minimum curvature can be used for a more detailed analysis.

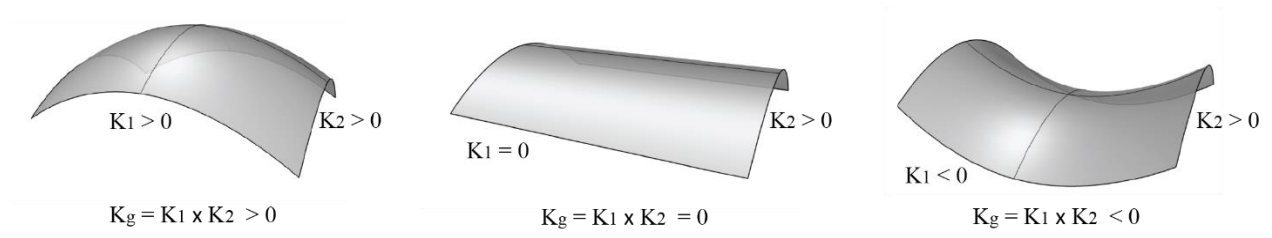


Figure 5.15. Synclastic, single curvature, and anticlastic forms with a positive, zero, and negative Gaussian curvature, created after (Blaauwendraad & Hoefakker, 2014)

5.3 Constructing a design space for shells

Reviewing the concept of shape change in shell structures, the shape of a shell can transform from a dome to a barrel vault and then to a saddle. Thus, it can be said that the boundary curves

can change continuously so that the product of curvatures changes from positive to zero and then to a negative value. The spectrum of shape change is illustrated in Figure 5.16.

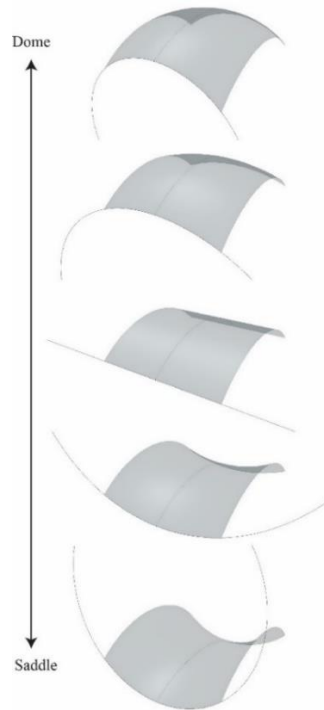


Figure 5.16. Change in the shape of a shell from a dome to a vault and then to a saddle

From another point of view, topology change in shell structures is considered a spectrum, where a continuous shell can be perforated to such an extent that it becomes a grid shell, as discussed in Chapter 3. Figure 5.17 is reiterated from Chapter 3. This spectrum can potentially accommodate changes in design parameters, including perforation ratio, granularity, and bias.

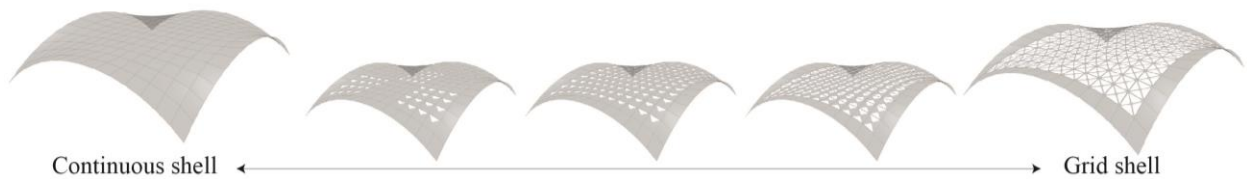


Figure 5.17. Potential change in perforation ratio, granularity, and bias in the spectrum of continuous to grid shells

Combining the two spectrums, one ranging from continuous to discrete shells, addressing perforation ratio, granularity, and bias in the x-axis; and the other addressing shape change in the y-axis, a two-dimensional design space for shell structures can be constructed. Different shell structures can potentially be mapped onto this design space (Figure 5.18).

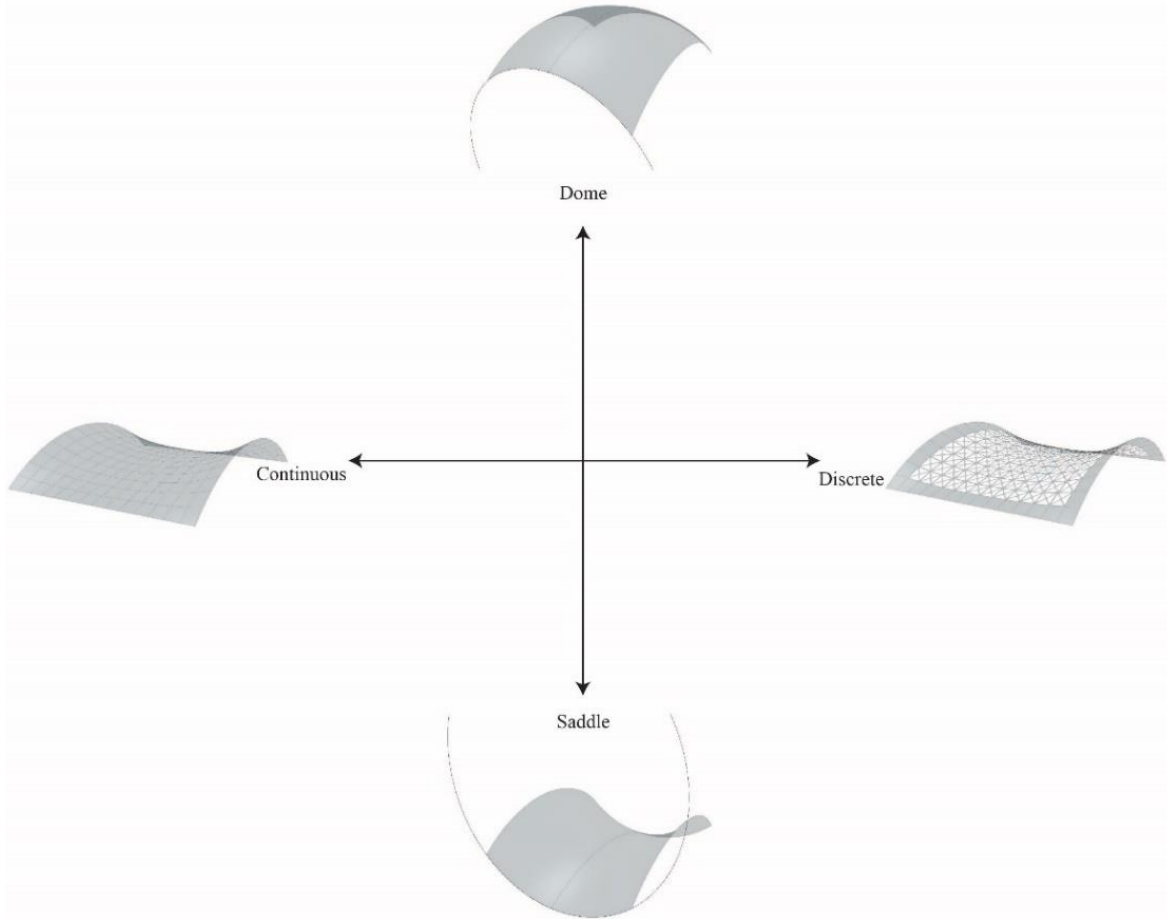


Figure 5.18. Shell design space, spanning continuous to grid shells with varying shapes

Once the design space is constructed including the design parameters rooted in the structural and daylighting discipline, a parametric model can be constructed to create a search space leading to the generation of solutions.

5.4 Discussion

In the first section of this chapter, the notion of integrated design in architectural discipline and the scope of its application in the dissertation is discussed. Then the structural and daylighting classifications from Chapter 3 and 4 are meshed together to isolate design parameters that link and affect both disciplines, moving towards an integrated design approach. This strategy can be a *design method* employed by architects and designers for an interdisciplinary design approach (Figure 5.19). This design method is described in detail for a hypothetical case (Figure 5.20).

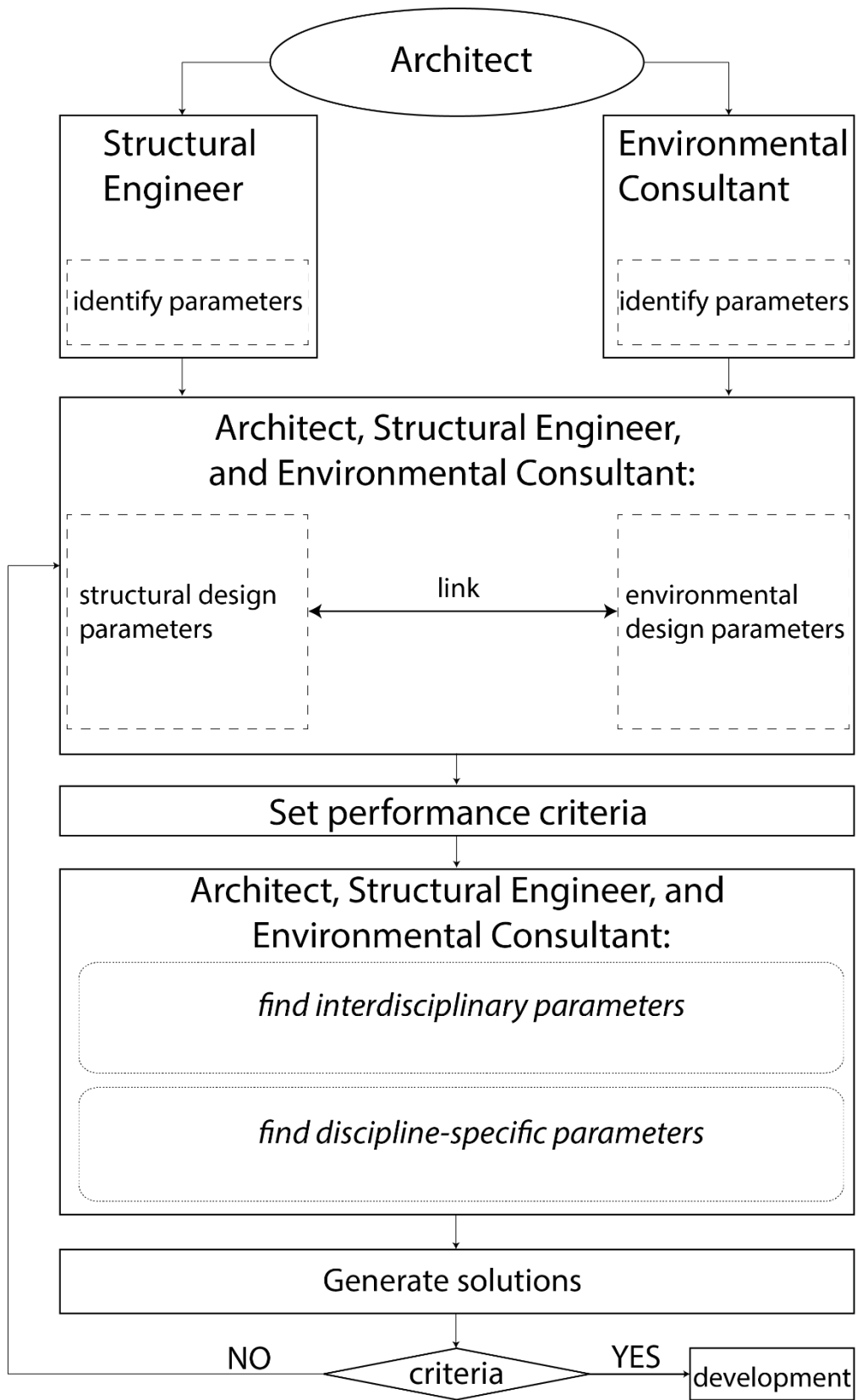


Figure 5.19. Roadmap for designers for identifying the interdisciplinary design parameters

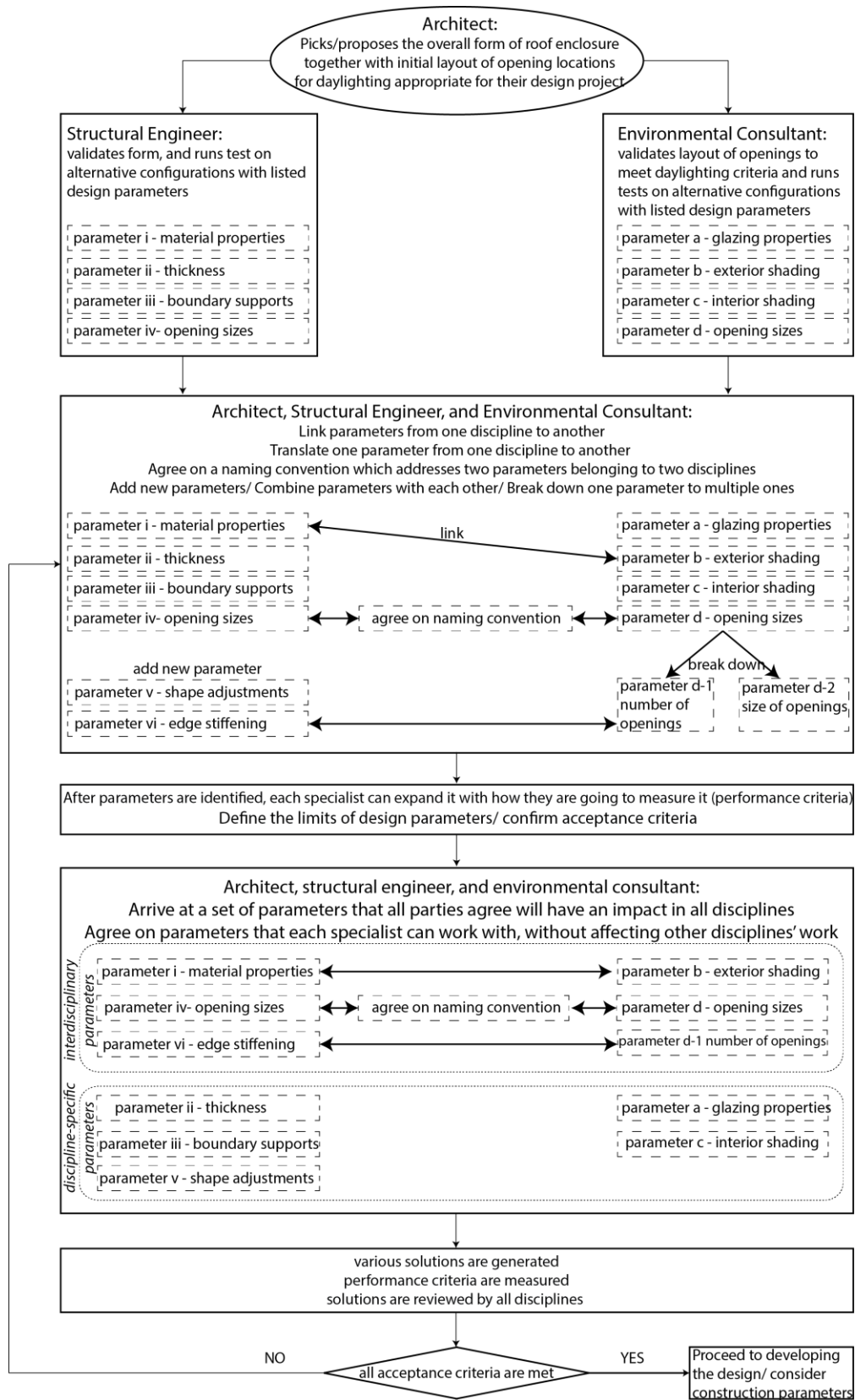


Figure 5.20. Design method described in detail for a hypothetical case

In shell structures, the parameters that overlap two disciplines include *the size of the openings*, *the number of openings*, and *the surface curvature* for shell structures. Once the common design parameters are identified, the parameters and ratios that capture the design parameters are discussed. Although perforation ratio is a common parameter used in environmental design analysis, it does not capture how fine the openings are. Therefore, another parameter, granularity, is suggested for use with perforation ratio. Finally, since the placement of the perforations affects daylighting and structural performance, a third parameter, bias, is introduced to be employed by designers alongside perforation ratio and granularity. Surface curvature is another design parameter that is quantified by its global shape, as a dome, vault, or saddle. On the basis of the common design parameters, a conceptual design space for shell structures is constructed.

In addition, a two-dimensional design space for shell structures is developed with a varying topology component in one axis and a varying shape component in the other axis. This diagram illustrates the underlying conceptual model for developing a parametric model.

The next chapter discusses the methodology that is employed for implementing an integrated design approach for designing perforated concrete shell structures with consideration of their structural and daylighting performance.

5.5 References

- Abraham, K., Flager, F., Macedo, J., Gerber, D., & Lepech, M. (2014). Multi-Attribute Decision-Making and Data Visualization for Multi-Disciplinary Group Building Project Decisions. In *Engineering Project Organization Conference*.
- Adriaenssens, S., Rhode-Barbarigos, L., Kilian, A., Baverel, O., Charpentier, V., Horner, M., & Buzatu, D. (2014). Dialectic Form Finding of Passive and Adaptive Shading Enclosures. *Energies*, 7(8), 5201–5220. <https://doi.org/10.3390/en7085201>
- Aish, R. (Autodesk), Fisher, A. (Buro H., Joyce, S. (University of B., & Marsh, A. (Autodesk). (2012). Progress towards Multi-Criteria Design Optimisation using DesignScript with SMART Form , Robot Structural analysis and Ecotect building performance analysis. In *ACADIA* (Vol. II, pp. 47–56).
- Alfaris, A., & Merello, R. (2008). The Generative Multi-Performance Design System. In *Silicon Skin Biological Processes and Computation Proceedings of the 28th Annual Conference of the Association for Computer Aided Design in Architecture ACADIA* (pp. 448–457).
- Blaauwendraad, J., & Hoefakker, J. H. (2014). *Structural Shell Analysis Understanding and Application*. (G. M. L. Gladwell, Ed.) (Vol. 200). New York: Springer. <https://doi.org/10.1007/978-94-007-6701-0>
- Brown, N., Tseranidis, S., & Mueller, C. (2015). Multi-objective optimization for diversity and performance in conceptual structural design. In *Proceedings of the International Association for Shell and Spatial Structures (IASS) Symposium "Future Visions."* Amsterdam, Netherlands.
- Clune, R., Connor, J. J., Ochsendorf, J. a., & Kelliher, D. (2012). An object-oriented architecture for extensible structural design software. *Computers and Structures*, 100–101, 1–17. <https://doi.org/10.1016/j.compstruc.2012.02.002>
- Danhaive, R. A., & Mueller, C. T. (2015). Combining parametric modeling and interactive optimization for high-

- performance and creative structural design. In *Proceedings of the International Association for Shell and Spatial Structures (IASS) Symposium "Future Visions."* Amsterdam, Netherlands.
- Dimcic, M., & Knippers, J. (2012). Integration of FEM, NURBS and Genetic Algorithms in Free-Form Grid Shell Design. *Computational Design Modelling*.
- Echenagucia, T. M. (2013). *Computational Search in Architectural Design*. Politecnico di Torino.
- Echenagucia, T. M., Capozzoli, A., Cascone, Y., & Sassone, M. (2015). The early design stage of a building envelope: Multi-objective search through heating, cooling and lighting energy performance analysis. *Applied Energy*, 154, 577–591. <https://doi.org/10.1016/j.apenergy.2015.04.090>
- Evins, R., Joyce, S. C., Pointer, P., Sharma, S., Vaidyanathan, R., & Williams, C. (2012). Multi-objective design optimisation: getting more for less. *Proceedings of the Institution of Civil Engineering (ICE)*, 165(5), 5–10. <https://doi.org/10.1680/cien.11.00014>
- Fasoulaki, E. (2008). *Integrated Design: A Generative Multi-Performative Design Approach*. Massachusetts Institute of Technology (MIT).
- Flager, F., & Haymaker, J. (2007). A comparison of multidisciplinary design, analysis and optimization processes in the building construction and aerospace industries. In *24th international conference on Information technology in construction* (pp. 625–630).
- Flager, F., Welle, B., Bansal, P., Soremekun, G., & Haymaker, J. (2009). Multidisciplinary process integration and design optimization of a classroom building. *Electronic Journal of Information Technology in Construction*, 14(14), 595–612.
- Gerber, D. J., & Lin, S.-H. (2013a). Geometric complexity and energy simulation. In *Open Systems: Proceedings of the 18th International Conference on Computer-Aided Architectural Design Research in Asia (CAARDIA)* (pp. 87–96). Hong Kong.
- Gerber, D. J., & Lin, S.-H. E. (2013b). Designing in complexity: Simulation, integration, and multidisciplinary design optimization for architecture. *Simulation*, 90(8), 936–959. <https://doi.org/10.1177/0037549713482027>
- Hensel, M. (2013). *Performance-oriented Architecture: rethinking architectural design and the built environment*. John Wiley & Sons Ltd.
- Holzer, D. (2009). *Sense-making across collaborating disciplines in the early stages of architectural design*. School of Architecture and Design. Royal Melbourne Institute of Technology (RMIT).
- Holzer, D. (2010). Optioneering in Practice Optioneering in Collaborative Design Practice. *International Journal of Architectural Computing*, 08(02), 165–182.
- Koleravic, B. (2014). Computing the performance. In R. Oxman & R. Oxman (Eds.), *Theories of the digital in architecture* (pp. 103–111). Routledge.
- Lin, S.-H., & Gerber, D. J. (2014). Evolutionary energy performance feedback for design: Multidisciplinary design optimization and performance boundaries for design decision support. *Energy and Buildings*, 84, 426–441. <https://doi.org/10.1016/j.enbuild.2014.08.034>
- Moe, K. (2008). *Integrated design in contemporary practice*. New York: Princeton Architectural Press.
- Oxman, R., & Oxman, R. (2014). Performance/ Generation: from analysis to informed synthesis. In R. Oxman & R. Oxman (Eds.), *Theories of the digital in architecture* (pp. 97–102). Routledge.
- Shea, K., Aish, R., & Gourtovaia, M. (2005). Towards integrated performance-driven generative design tools. *Automation in Construction*, 14(2 SPEC. ISS.), 253–264. <https://doi.org/10.1016/j.autcon.2004.07.002>
- Soebarto, V. I., & Williamson, T. J. (2001). Multi-criteria assessment of building performance: theory and implementation. *Building and Environment*, 36(6), 681–690. [https://doi.org/10.1016/S0360-1323\(00\)00068-8](https://doi.org/10.1016/S0360-1323(00)00068-8)
- Tsigkari, M., Chronis, A., Joyce, S. C., Davis, A., Feng, S., & Aish, F. (2013). Integrated design in the simulation process. *Symposium on Simulation for Architecture and Urban Design (SimAUD)*, 153–160.
- Turrin, M. (2014). *Performance Assessment Strategies: A computational framework for conceptual design of large*

roofs. Architecture and the Built Environment.

- Yang, D., Sun, Y., Turrin, M., Buelow, P. von, & Paul, J. (2015). Multi-objective and multidisciplinary design optimization of large sports building envelopes : a case study. In *Proceedings of the International Association for Shell and Spatial Structures (IASS) Symposium "Future Visions."* Amsterdam, Netherlands.
- Yang, D., Turrin, M., Sariyildiz, S., & Sun, Y. (2015). Sports Building Envelope Optimization Using Multi-objective Multidisciplinary Design Optimization (M-MDO) Techniques Case of Indoor Sports Building Project in China. In *IEEE Congress on Evolutionary Computation (CEC)* (pp. 2269–2278). IEEE.

Chapter 6 :

Methodology

“As to methods there may be a million and then some, but principles are few. The man who grasps principles can successfully select his own methods. The man who tries methods, ignoring principles, is sure to have trouble.”

- Ralph Waldo Emerson

6.1 Introduction

This chapter discusses the theoretical and computational methodologies for implementing an integrated computational design approach for the design and search of high-performance perforated shell structures regarding their structural and daylighting performance. There is a distinction between optimization, used in engineering disciplines, and optioneering, a word that researchers suggest for use in architectural research and practice. Both disciplines seek to balance multiple competing objectives. However, some methods are more suited to architecture than others. The introduction of this chapter reviews optimization concepts with a focus on *a posteriori* heuristic algorithm, and then discusses optioneering, which is rooted in these concepts. The second section reviews ParaGen, a computational framework in use at the University of Michigan’s Hydra Lab. Finally, the methodology for conducting the research is described in detail in the third section. The case studies using this methodology and their results are discussed in Chapter 7.

Since the mid-1990s, computer scientists have been seeking ways to progress from single-objective problems to multi-objective problems. The process of multi-objective optimization (MOO) has been defined as “the process of optimizing systematically and simultaneously a collection of objective functions” (Marler & Arora, 2004, p. 369). It should be noted that these multiple objectives can exist in one discipline, or in multiple disciplines. Therefore, the term multi-disciplinary optimization (MDO) is also used in the literature. The distinction between multi-objective and multi-disciplinary optimization is illustrated in Figure 6.1.

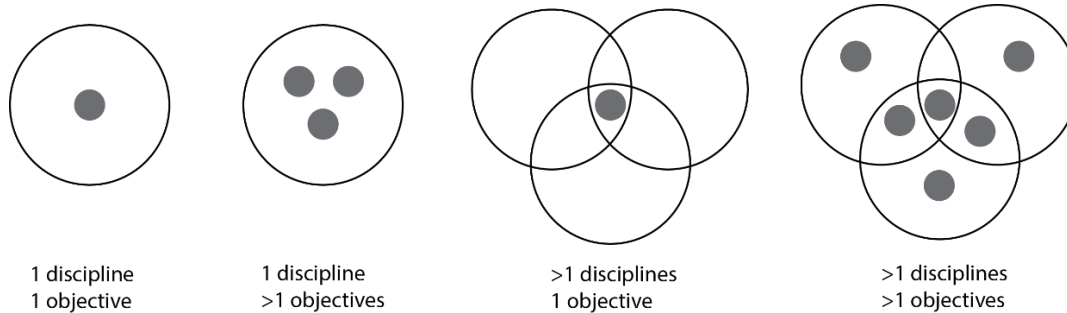


Figure 6.1. Multi-objective optimization (MOO), and Multi-disciplinary optimization (MDO), after (Yang, Sun, Turrin, Buelow, & Paul, 2015)

Marler and Arora (2004) explain that there are some available methods for current continuous nonlinear Multi-Objective Optimization (MOO) problems. These methods are categorized in approaches with *a priori* articulation of preferences, *a posteriori* articulation of preferences, and *problems with no articulation of preferences*. The *a priori* articulation of preferences implies that the user indicates the relative importance of the objective functions or desired goals before running the optimization algorithm by creating a composite weighted objective function at the outset. In some cases, however, “it is difficult for a decision-maker to express an explicit approximation of the preference function. Therefore, it can be effective to allow the decision maker to choose from a pallet of solutions” (Marler & Arora, 2004, p. 380). Using *a posteriori* optimization articulation of preferences is suited for the latter category of problems. This entails selecting a single solution from a set of mathematically equivalent solutions, where the designer chooses from among a number of near-optimal designs after an optimization has been run. They also mention a quote from Messac and Mattson’s article that the methods with *a posteriori* articulation of preferences are called “cafeteria or generate-first-choose-later approaches” (Marler & Arora, 2004, p. 380). Finally, the *progressive articulation of preferences* is an interactive articulation of preferences, where the designer gives input while the algorithm is running. This research focuses on *a posteriori* optimization methods for multi-objective, multi-disciplinary design problems.

As noted, *a posteriori* articulation of preferences entails selecting a single solution from a set of mathematically equivalent solutions, also called the Pareto set. Pareto optimality is an important concept in MOO. Pareto optimization is currently the leading multi-objective search technique, which is based on the work of French-Italian economist and sociologist, Vifredo Pareto (Diwekar, 2008). Other researchers explain that “In contrast to single-objective optimization, a solution to a multi-objective problem is more of a concept, than a definition. Typically, there is no

single global solution, and it is often necessary to determine a set of points that all fit a predetermined definition for an optimum. The predominant concept in defining the optimal point is that of Pareto optimality” (Marler & Arora, 2004, p. 371). Other researchers describe Pareto in multicriteria optimization as “a point in the design space if no feasible point exists that would reduce one criterion without increasing the value of one or more of the other criteria” (Papalambros & Wilde, 2015, p. 17). Another description is that “a point is Pareto optimal if there is no other point that improves at least one objective function without determinant to another function” (Marler & Arora, 2004, p. 371).

Trade-off is an important concept in MOO. Trade-off “represents the increment in objective function j resulting from a decrement in objective function i ” (Marler & Arora, 2004, p. 372). In other words, trade-off represents the relation among contrasting objectives, and how improving performance in one objective is accompanied with decreasing performance in the other. As Evins et al. explain, “it is often not possible to say in advance where on the trade-off front it is most desirable to be. Exploration of the shape of the trade-off front allows informed decision-making regarding marginal benefits” (Evins et al., 2012, p. 6).

Dominance is another important concept in MOO. Mendez highlights the non-dominant set by stating, “the Pareto-front, also called trade-off set or non-dominant set, is the set of all non-dominated solutions in a given group” (Echenagucia, Capozzoli, Cascone, & Sassone, 2015, p. 3). Dominance and the non-dominant set are further described in Figure 6.2. In it, Objectives 1 and 2 are both targeted for minimization. Solution B has a smaller value for both Objectives compared to Solution D. Therefore, Solution B is *dominating* Solution D. On the other hand, Solution B is not dominating Solution A, nor is A dominating B.

From a different standpoint, solution A is presenting a smaller value for Objective 1, whereas Solution C has a smaller value for Objective 2. There is no other solution in the feasible space that offers a result better than Solution A’s Objective 1 or Solution C’s Objective 2. Therefore, Solution A and C, as well as the previously discussed solution B, belong to the *non-dominant set*, and there is a trade-off between A, B, and C. The A-B-C line presented in Figure 6.2 is the Pareto set consisting of non-dominant solutions.

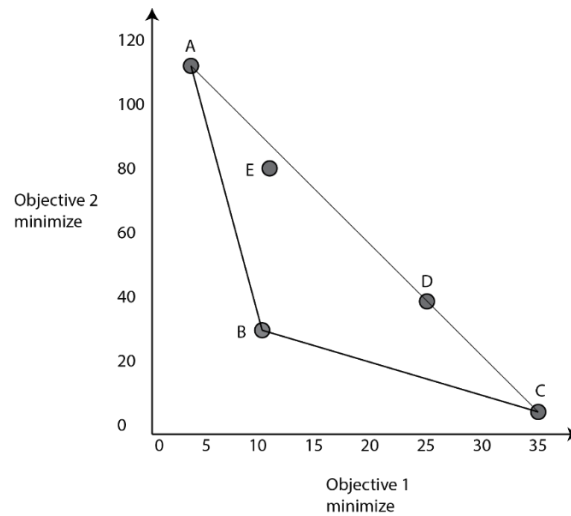


Figure 6.2. Describing non-dominant solutions falling in the Pareto set

In general, there are three important factors in any multi-objective optimization problem:

- 1- System boundaries
- 2- Methods that provide the Pareto optimal set
- 3- Methods that identify a single solution

System boundaries, including defining the variables and the constants, is crucial in any multi-objective problem. Researchers emphasize that subsystems need to be selected carefully to avoid arriving at a complex solution. One group of researchers express this by stating that “applying multi-objective optimization methods requires careful consideration of the system in question. It is not practical to consider all sub-systems and variables simultaneously; the formulation of system boundaries such that some things are varied while others are held constant is of critical importance. The system to be optimized is defined by objectives, variables to adjust, and constraints that must be maintained” (Evins et al., 2012, p. 5).

From another point of view, an algorithm needs to be used to determine a representation of the Pareto optimal set, and then a strategy needs to be employed to explore the Pareto optimal set to come to a final selection. As some researchers describe, “for any given problem, there may be an infinite number of Pareto optimal points constituting the Pareto optimal set. Therefore, one must distinguish between methods that provide the Pareto optimal set or some portion of that set, and methods that seek a final single point” (Marler & Arora, 2004, p. 372).

Regarding the methods that provide a Pareto optimal set, heuristic algorithms are widely used. These algorithms trade accuracy with speed and find an approximate solution by ranking the

alternatives at each branching step based on available information, towards deciding which branch to follow. One group of researchers states that “heuristic methods such as evolutionary algorithms tend to be superior when applied to problems with non-linear, stochastic or chaotic component” (Flager, Welle, Bansal, Soremekun, & Haymaker, 2009, p. 597). There exists an array of evolutionary algorithms; nevertheless, genetic algorithm (GA) is one of the most popular types of multi-objective algorithms. As a researcher describes, “the most well-known [algorithm type] is Genetic Algorithm, a form of evolutionary computation. Other methods operate along similar lines, for example, differential evolution, evolutionary strategies and genetic programming” (Evins et al., 2012). As Park (2005) states, GA uses probabilistic transition rules (taking random choices to guide the search) towards regions of most likely improvement in the search space, to guide its search. He further explains that “GA provides some potential solutions to a given problem, with the choice of the final solution being left to the user” (Park, 2005, p. 98). This is useful for identifying alternative solutions where a particular problem does not have one individual solution. Discussing the suitability of GA for searching discontinuous design spaces, one group states that “Genetic Algorithms utilize processes analogous to natural selection to search stochastically for the best designs. Since they do not require objective or constraint gradient information, genetic algorithms can search discontinuous and noisy design spaces effectively” (Flager et al., 2009, p. 602). Another researcher explains that “the search space is a space of coded solutions (genotype) to the problems while the solution space is the actual solutions (phenotype)” (Park, 2005, p. 96). Search space versus solution space is conceptually illustrated in Figure 6.3.

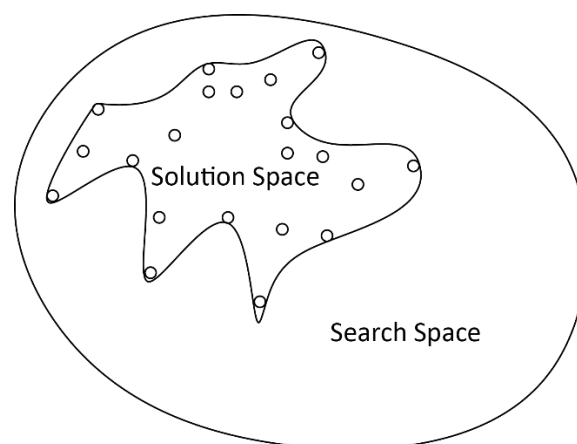


Figure 6.3. Search space versus solution space

Finally, there are a range of methods to seek a solution from the Pareto optimal set. According to Holzer (2009) Multi-Criteria Decision Analysis (MDDA) allows for the evaluation of complex

problems where decisions need to be taken with a high degree of uncertainty. It serves to “evaluate and choose among alternatives based on multiple criteria using systematic analysis to overcome the limitations of unstructured individual or group decisions” (Holzer, 2009, p. 212). Another group of researchers refer to multi-criteria-decision-making (MCDM) methods as ones that “structure and model the imprecise goals of multi-dimensional decision problems in terms of a set of individual decision criteria where each criterion characterizes a single dimension of the problem to be evaluated” (Abraham, Flager, Macedo, Gerber, & Lepech, 2014, p. 2). The majority of MCDM methods studied in the building design and construction are value-based techniques that are a normative method. “Value or utility theory approaches ask decision makers to develop a numerical score or value for each decision alternative and choose the alternative with the highest value” (Abraham et al., 2014, p. 2). The decision maker would need qualitative support once the essential information for early decision-making process is considered. One may not expect to find singular optimum solutions in multi-criteria decision-making processes, but rather *satisficing* (satisfice = satisfy + suffice).

Other researchers have done a post-Pareto analysis to acquire a wider understanding of the actual meaning of the solutions. Echenagucia et al. (2015) performed a statistical analysis and used a box-plot representation of the Pareto optimal set to investigate the statistical variation of the values. The aim was to understand how the values of the design parameters spread within the Pareto front solutions. Their results showed that “[v]ariables characterized by a very low spread represent those inputs for which there is a low degree of freedom in selection of their values,” and thus can be almost constant for the solution to belong to the Pareto front. On the other hand, “variables that had a great variability within the Pareto front solutions are those that may be the most important to optimize” (Echenagucia et al., 2015, p. 14). Simple additive weighting (SAW) is another technique that weights the contributions from each attribute, according to the decision maker’s preference (Abraham et al., 2014).

Visualization techniques are other tools that play an important role in the decision-making process. Classic decision models include decision tables, decision trees, and influence diagrams. More complex decision methods, such as two-dimensional Pareto fronts, Level Graphs, and other multi-dimensional Pareto representations may also be employed. However, as others explain, visualization tools are required to be situated in context with a quantitative decision support, as

“simply adopting decision support tools does not strictly improve decision-making” and “ a smart combination of tools to aid decision-making is required” (Abraham et al., 2014, p. 13).

One of the engineering disciplines that utilizes Pareto optimal as a design exploration tool is the aerospace industry. They have used the technology to quickly create, represent and analyze design options from the perspective of multiple disciplines. In 1998, Boeing began a project to design a hypersonic vehicle with the mission requirement of taking off from a commercial airport and delivering a payload to the upper stratosphere. Using model-based approaches, and after six years of working, the team was unable to produce a design that meets the mission requirements (Flager & Haymaker, 2007). Therefore, in 2002, Boeing adopted a suite of technologies and methodologies to support multi-disciplinary analysis. This was performed by using “product models, among them parametric geometry definition, integrated design schemas, automated discipline analysis, and multi-disciplinary optimization” (Flager & Haymaker, 2007, p. 625), which led to improved product performance. In short, Boeing used an in-house tool called *General Geometry Generator (GGG)* for the parametric geometry generation, *Phoenix Integration’s Model Center and Analysis Server* for the automatic exchange of model-based information, *Boeing’s Design Explorer* for Design of Experiment (DOE), and building Response Surface Models (RSM) to perform the optimization (Flager & Haymaker, 2007).

Irrespective of the multiple ways that a Pareto optimal set can be generated and then explored, the process can be applied to various disciplines to find solutions for design problems. Architects are facing design problems which are ill-defined and wicked. There is no single optimal solution for wicked design problems, but “an array of possible design options that can be explored to find a suitable solution” (Holzer, 2009, p. 210). These options can be evaluated with different priorities and from a plurality of disciplines participating in a design project. Hence, the design options need to be explored across disciplines in an informed manner. In general, designers utilize different design strategies to solve problems, including problem-driven design, solution-driven design, information-driven design, and knowledge-driven design (Kruger & Cross, 2006). Others state that “solution driven design and computational processes provide a general framework for understanding multi-disciplinary design optimization” (Basbagill, Flager, & Lepech, 2014, p. 138).

In the architecture, engineering and construction (AEC) industry, the engagement of multiple stakeholders often causes complex problems with multiple conflicting objectives. Holzer found

that a *decision support-environment* is missing in current practice; it combines different sets of analysis from the architecture, structural engineering, façade engineering, acoustics, and environmental design sectors. Such an environment enables design teams to test design options across disciplines in a *what-if* manner (Holzer, 2009, p. 121)

There have been advances in modeling and analysis tools in the AEC industry that now allow performance simulation in the early stages of projects. Holzer (2009) proposes *optioneering* as a term to be used for multi-disciplinary multi-objective search in architectural problems. Optioneering is a hybrid between *option* + *engineering*. It implies the creation of options through a process similar to that applied to engineering processes. This includes informed decision making based on a level of scientific rigor similar to engineering processes. According to Holzer, this term is being used in everyday practice at Arup, to describe an approach where multiple variations of design are proposed, and then they are evaluated regarding their diverse performance criteria. Optioneering can facilitate lateral thinking between design professions (Holzer, 2009). Therefore, design options can be created by manually drawing CAD models, or by retrieving design alternatives driven by parametric interrelations. The performance of the options can also be assessed on a one-by-one basis or in an automated manner.

Optioneering is a method that allows for a better structure for decision-making processes. Holzer (2009) suggests that processes guided through optioneering do not necessarily need to consider design-criteria across multiple disciplines. Optioneering is well suited to address multi-criteria optimization within the boundaries of a single, or a selected few disciplines. Optioneering can establish a network of connections across disciplines thus facilitate lateral thinking between design professions. This will be based on the specific requirements of a design project. The criteria for evaluation, scoring, weighting, viewing, and analyzing results depends upon understanding the design priorities and the performance targets of various disciplines.

Optioneering is in line with the partial list of requirements for applying MDO to AEC projects that Flager et al. (2009) identifies, and which is summarized below.

- a. Rapidly generate design alternatives: This is the ability to investigate a large number of design alternatives in a flexible and user-friendly environment, which is critical to finding successful designs.

- b. Rapidly analyze design alternatives: Once an alternative is generated, designers must be able to assess the performance of the alternative across a wide range of criteria to make an informed decision.
- c. Integrate conventional CAD/CAE tools: Practitioners need to be able to use tools they trust. Thus, the MDO method should support the effective automation and exchange of information between tools of the practitioner's choice. Such interoperability may occur through data models (such as industry foundation class) or direct access to application programming interfaces (API).
- d. Customize optimization strategies: The selection of optimization algorithm depends upon the formulation of the problem, including objective, constraints, and their number and type (discrete versus continuous).
- e. Visualize trade spaces: The interaction of human expertise and computer-based exploration is essential for the process to be successful. To understand general performance trends and variable sensitivities, the use of advanced plotting tools that enable multi-dimensional data visualization is crucial. Pareto and parallel coordinates plots have proven useful for this purpose.
- f. Communicate process and information dependencies: Practitioners must be able to understand the steps and information flow between process tasks. This is important to improve the re-usability of the process for future projects.

The ParaGen computation framework developed at the University of Michigan's Hydra Lab (von Buelow, 2012) corresponds with the requirements for applying optioneering to AEC projects, as identified by Flager et al. (2009) and Holzer (2009). ParaGen allows rapid generation and evaluation of design alternatives that are created through parametric modeling. It allows integration of commercial CAD/CAE and simulation tools into the process. In addition, there is a visualization environment integrated with the framework that allows the user to search the solutions qualitatively. The next section explains the ParaGen computational framework. Then, the research methodology, and the ways in which ParaGen fits into the study aim of implementing an interdisciplinary design approach, are discussed.

6.2 ParaGen framework

ParaGen is a computational framework under development at the University of Michigan's Hydra Lab. ParaGen supplies geometric variations, along with their performance data, in an interactive environment, providing a means of searching the design space. It employs a GA, an evolutionary algorithm suited for exploration, to search for well-performing geometric solutions for architectural problems at the early phases of design. The geometric solutions are generated using parametric design tools, and commercial software can be used for performance assessment. Solutions are stored in an online SQL database, and the genetic algorithm uses the performance values of the solutions as a guide to search for good solutions. According to von Buelow, "The ParaGen process makes use of a web server and a cluster of Windows PCs which run the parametric and analysis software. In addition, there is an open web interface that can be accessed throughout the design process by any web browser. Together this provides the designer with an effective means to explore large, complex design spaces typical in parametric design" (von Buelow, 2011, p. 2).

An interactive webpage is connected to the SQL database, which allows the user to explore the design space both quantitatively and qualitatively by browsing, filtering, and sorting the solutions. Each solution can be scrutinized by clicking on it to read its detailed design parameters and performance criteria. Design space exploration provides the opportunity to compare multiple solutions with each other based on their performance in multiple disciplines, as well as qualitatively. Therefore, a design option which is performing well in multiple disciplines can be recognized as distinct from a solution which offers excellent performance in only one discipline and poor performance in the other. The interactive webpage provides the opportunity to plot Pareto front graphs to show a better landscape of the alternatives' performance. Numerous publications provide a comprehensive explanation of the framework (von Buelow, 2011, 2014, 2017). Figure 6.4 illustrates ParaGen's general workflow.

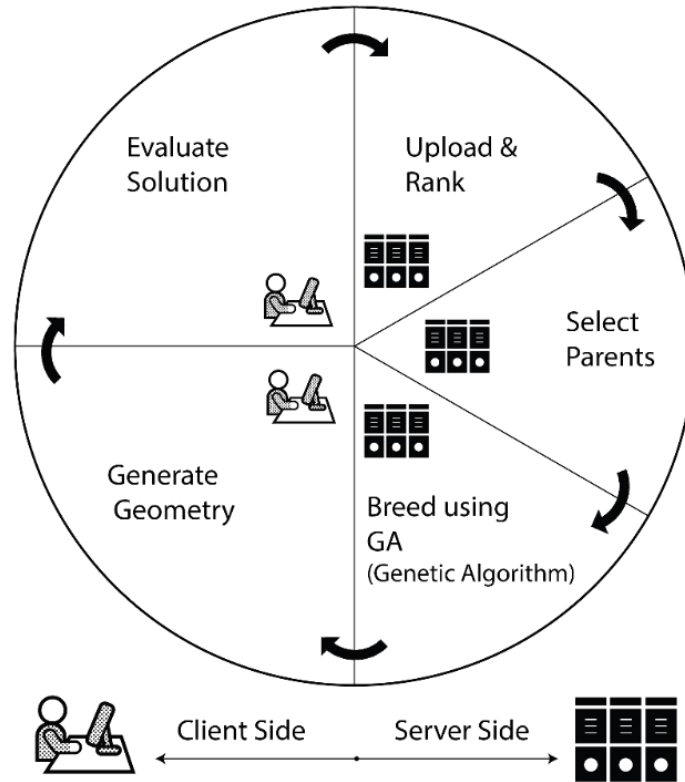


Figure 6.4. ParaGen framework, after von Buelow (2011)

As noted, ParaGen allows integration of commercial software systems suited for various projects into the framework. Rhinoceros by McNeal and the Grasshopper plugin for parametric design are used in this study for geometry generation, along with Python scripting and the Weaverbird plugin. Once the geometry is generated, the structural, daylighting, and energy performance of the shells are assessed using the Karamba, DIVA, and Archsim plugins for Grasshopper, respectively.

Karamba is a Finite Element Method (FEM) simulation engine, whereas DIVA and Archsim use Radiance and Energy Plus engines respectively. Ghowl, a plugin for Grasshopper, is used to read and write the input and output data to an excel file. ParaGen is used to automate the cycle of generation and evaluation by using AutoHotkey to script the sequence of steps. The commercial software systems used in this study and the way in which they are integrated into the ParaGen framework is illustrated in Figure 6.5.

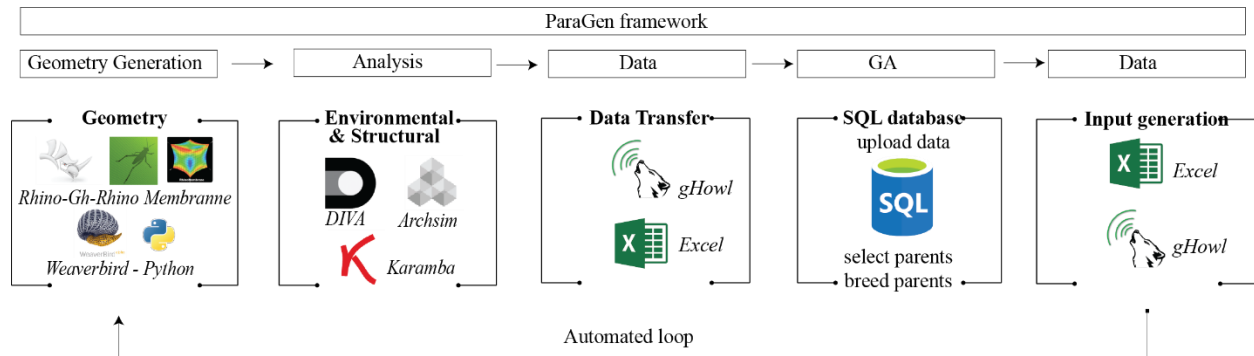


Figure 6.5. The commercial software systems used in the ParaGen framework for this study

6.3 Research methodology

This research aims to propose methodology for implementing an integrated design approach regarding multiple disciplines in the AEC industry. The methodology consists of the following steps:

- Identifying the overlapping design parameters between two disciplines (parameter)
- Conceptualizing the computational design space of the building typology based on the identified design parameters (search space)
- Employing a computational framework for rapid generation and performance assessment of the alternatives in the design space (performance)
- Exploring the solution space to understand the effect of parameters on and performance, and to explore the tradeoffs between performance in multiple disciplines (solution space exploration)
- Choosing built case studies and exploring if they can be mapped onto the solution space

This research employs statistical analysis, namely analysis of variance (ANOVA), to determine the significance of parameters' influence on performance criteria. It also maps real-world case studies onto the solution space to verify if connections can be drawn between the performance of generated shells in the solution space with the performance of other shell typologies represented by built case studies.

The first step is to identify the common design parameters between two disciplines. This is built based on an understanding of design principles within each discipline through their own lens first. Chapters 3 and 4 categorize various design steps in structural and daylighting design, respectively. Once there is a formalized understanding of design principles in each discipline, along with the design parameters that are considered by the professionals, two disciplines can be

meshed together. Chapter 5 meshes the two disciplines and isolates the overlapping design parameters.

The second step is to conceptualize a potential design space that entails the overlapping design parameters for a multi-objective multi-disciplinary analysis. The goal is to include only the overlapping design parameters in the design space and avoid introducing additional complexity. This is in line with the process that Evins et al. (2012) suggested, saying that subsystems need to be selected carefully to avoid arriving at a complex solution. This research methodology emphasizes that the overlapping parameters need to be understood by the designer as well as by specialists from various disciplines in order to enhance an interdisciplinary design approach.

The third step consists of using a computational design framework for rapid generation and performance assessment of alternatives in the solution space, based on a parametric design model created based on the conceptualized design space. ParaGen is the framework that is employed in this study. The advantages that make ParaGen stand out are: first, easy integration of commercial software systems into the framework based on the needs of each project; second, storage of all the generated solutions, along with their quantitative performance, in an online SQL database which can be explored through an interactive webpage; third, availability of qualitative as well as quantitative exploration through the interactive webpage, as each solution is connected to the stored images of the solutions. In addition, a GA is implemented in ParaGen to lead the search for finding well-performing alternatives either systematically, randomly, or through breeding high-performance parents.

The fourth step in conducting this research consists of Pareto-front exploration and statistical analyses, aimed at validated the effect of parameters (independent variables or control variables) on the performance (dependent variables or response variables). ANOVA is conducted for each parameter in two different disciplines, structure and daylighting, respectively. This step also consists of computationally modeling built case studies, simulating their structural and daylighting performance, and mapping the case studies onto the solution space to find matches. Mapping built shells based on their simulated analysis helps to understand if the solution space can predict the performance of other shell typologies. The methodology workflow is illustrated in Figure 6.6.

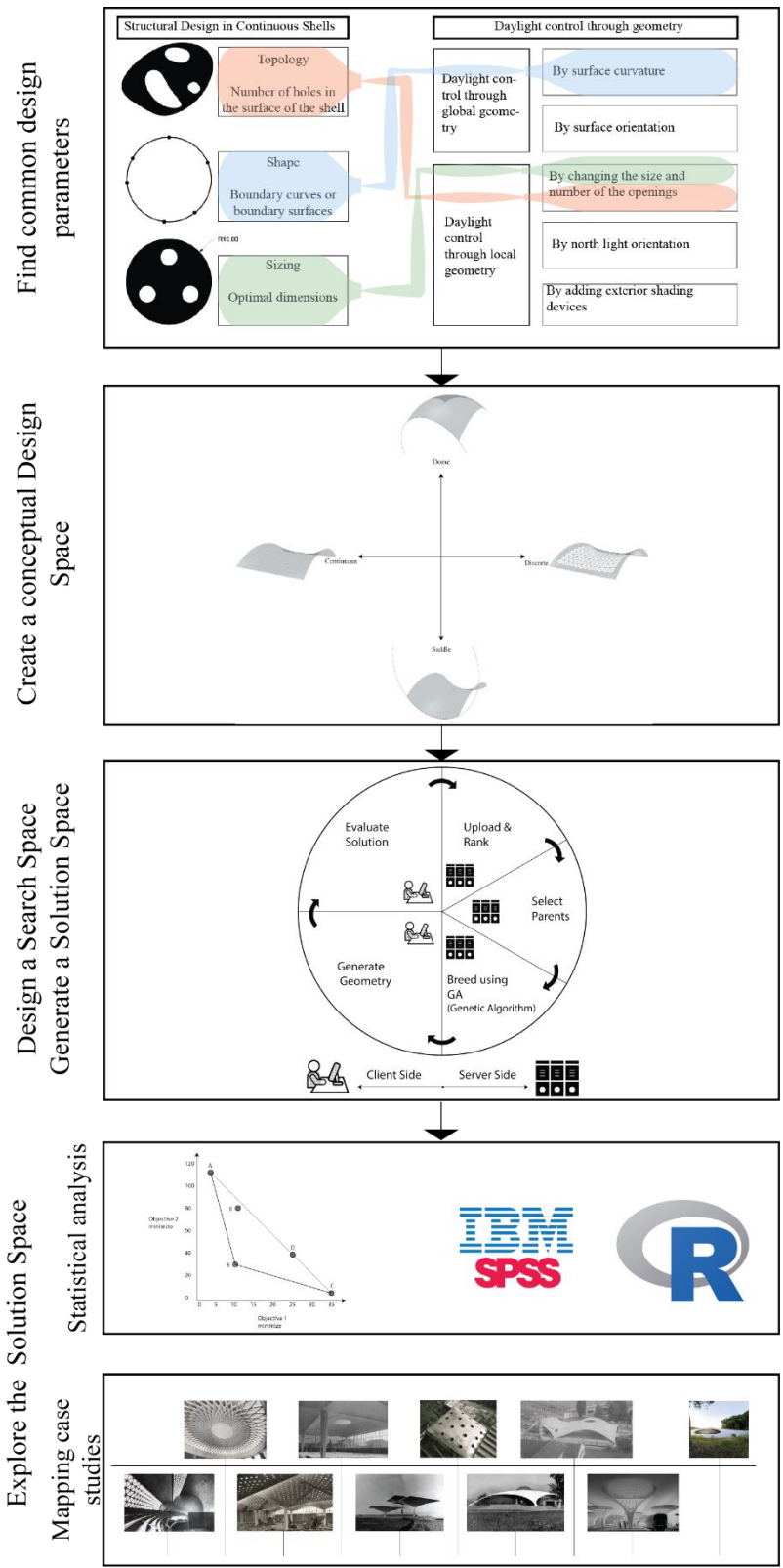


Figure 6.6. Research methodology workflow

6.4 Discussion

This chapter explains the research methodology that is employed for conducting the research described in later chapters. It is built on the previous chapters and ties them together to paint a clear image of the methodological framework. The hypothesis of the research is that to build an effective multidisciplinary design approach, each discipline must be first understood, and then the overlapping design parameters need to be identified. The methodology offers formalized steps for an integrated design approach to architectural problems. The methodology is composed of four main steps: first, identifying the common design parameters between disciplines; second, conceptualizing the limits of the design space, along with the possibilities and limitations; third, creating a parametric model to make a search space and generating the solution space through computational design and simulation tools; and fourth, exploring the solution space through trade-off analysis, rigorous statistical analysis, and mapping case studies onto the solution space. The next chapter explains the solution space exploration.

6.5 References

- Abraham, K., Flager, F., Macedo, J., Gerber, D., & Lepech, M. (2014). Multi-Attribute Decision-Making and Data Visualization for Multi-Disciplinary Group Building Project Decisions. In *Engineering Project Organization Conference*.
- Basbagill, J. P., Flager, F. L., & Lepech, M. (2014). A multi-objective feedback approach for evaluating sequential conceptual building design decisions. *Automation in Construction*, 45, 136–150. <https://doi.org/10.1016/j.autcon.2014.04.015>
- Diwekar, U. (2008). *Introduction to Applied Optimization*. (P. Pardalos, Ed.) (2nd ed., Vol. 22). Springer. <https://doi.org/10.1007/978-0-387-76635-5>
- Echenagucia, T. M., Capozzoli, A., Cascone, Y., & Sassone, M. (2015). The early design stage of a building envelope: Multi-objective search through heating, cooling and lighting energy performance analysis. *Applied Energy*, 154, 577–591. <https://doi.org/10.1016/j.apenergy.2015.04.090>
- Evins, R., Joyce, S. C., Pointer, P., Sharma, S., Vaidyanathan, R., & Williams, C. (2012). Multi-objective design optimisation: getting more for less. *Proceedings of the Institution of Civil Engineering (ICE)*, 165(5), 5–10. <https://doi.org/10.1680/cien.11.00014>
- Flager, F., & Haymaker, J. (2007). A comparison of multidisciplinary design, analysis and optimization processes in the building construction and aerospace industries. In *24th international conference on Information technology in construction* (pp. 625–630).
- Flager, F., Welle, B., Bansal, P., Soremekun, G., & Haymaker, J. (2009). Multidisciplinary process integration and design optimization of a classroom building. *Electronic Journal of Information Technology in Construction*, 14(14), 595–612.
- Holzer, D. (2009). *Sense-making across collaborating disciplines in the early stages of architectural design*. School of Architecture and Design. Royal Melbourne Institute of Technology (RMIT).
- Kruger, C., & Cross, N. (2006). Solution driven versus problem driven design: strategies and outcomes. *Design Studies*, 27(5), 527–548. <https://doi.org/10.1016/j.destud.2006.01.001>
- Marler, R. T., & Arora, J. S. (2004). Survey of multi-objective optimization methods for engineering. *Structural and*

Multidisciplinary Optimization, 26(6), 369–395. <https://doi.org/10.1007/s00158-003-0368-6>

- Papalambros, P. Y., & Wilde, D. J. (2015). *Principles of Optimal Design Modeling and Computation* (Third edit). Cambridge University Press.
- Park, H.-J. (2005). *A Quantification of Proportionality Aesthetics in Morphological Design*. University of Michigan.
- von Buelow, P. (2011). Genetically Enhanced Parametric Design for Performance Optimization. *7th International Seminar of the IASS Structural Morphology Group*.
- von Buelow, P. (2012). ParaGen: Performative Exploration of Generative Systems. *Journal of the International Association for Shell and Spatial Structures*, 53(4), 271–284.
- von Buelow, P. (2014). Using Database Storage to Improve Explorative Optimization of Form Critical Structures. In *Proceedings of IASS-SLTE Symposium “Shells, Membranes and Spatial Structures: Footprints.”* Brasilia, Brazil. <https://doi.org/10.13140/2.1.3568.3840>
- von Buelow, P. (2017). Choosing parents to produce better performing children : a comparison of selection methods used for evolutionary search. In A. Bögle & M. Grohmann (Eds.), *Proceedings of the IASS Annual Symposium 2017 “Interfaces: architecture . engineering . science.”* Hamburg, Germany.
- Yang, D., Sun, Y., Turrin, M., Buelow, P. von, & Paul, J. (2015). Multi-objective and multidisciplinary design optimization of large sports building envelopes : a case study. In *Proceedings of the International Association for Shell and Spatial Structures (IASS) Symposium “Future Visions.”* Amsterdam, Netherlands.

Chapter 7 : Analysis and application through case studies

“A great building must begin with the immeasurable, must go through measurable means when it is being designed, and in the end, must be unmeasured.”

-Louis Kahn

7.1 Introduction

Chapter 2 reviewed parametric and performance-oriented design in building envelopes, whereas Chapter 5, being built on top of Chapters 3 and 4, demonstrated integration of structural and daylighting disciplines through their overlapping design parameters. Chapter 6 explained the research methodology as well as the computational design framework that is employed for rapid generation and evaluation of the design alternatives.

Two key terms that are briefly touched upon in Chapter 6 are reiterated and explained here. Park (2005) explains that the *search space* is a space of coded solutions (genotype) to problems, while the *solution space* is a space of actual solutions (phenotype). A parametric model that is created inspired by the overlaps between the two disciplines creates a search space which is bound to the limits of its governing parameters. However, not all possible alternatives will be generated, since an exhaustive combination of all parameters takes a lot of time and computational power. Therefore, only some subset of possible combinations is generated, creating a solution space. This chapter refers to the generated shells that are stored in a database as the solution space.

This chapter starts by explaining the parametric model that is used for creating a search space. First, the ParaGen computational framework is employed to generate and evaluate shells with the aim of creating the solution space. The generated shells are stored in a database along with their parameters and performance criteria. Second, the performance values are statistically analyzed to better understand the relationship between design parameters and performance criteria in the structural and daylighting disciplines. The results of this analysis are used to validate whether the identified parameters are controlling performance. The statistical results are summarized as a heatmap. A heatmap, which is also called a shading matrix, is a graphical representation of data

in which the individual values in a matrix are represented with colors. The heatmap is further explored using surface plots and scatterplots to explore their meanings. Scatter plots are graphs in which values of two variables are plotted along two axes as data points, and the pattern of the resulting points reveals any present correlation. On the other hand, surface plots are diagrams of three-dimensional data where a functional relationship between two independent variables (x and y) and a designated dependent variable (z) is shown. The process and details of the statistical analysis are described in Appendix E. Third, two case studies are selected to be mapped onto the solution space. The dimensions and boundary conditions of these case studies are adjusted as needed to mimic the dimensions and boundary conditions of the generated shells in the solution space as closely as possible. The structural and daylighting performance of the case studies is then used to filter the solution space to validate if the shells it contains can predict the performance of other case studies. The workflow is summarized in Figure 7.1.

Section 7.2 explains the parametric model that is used for generating a solution space, and then explains the performance criteria that are considered. This phase is labeled as *data generation* in Figure 7.1.

Section 7.3 summarizes the results of statistical analysis computed on the generated data. It explores the correlation between design parameters and performance limits in two disciplines. Heatmaps and surface plots are used for data visualization. This phase is marked as *validation phase 1* on Figure 7.1.

Sections 7.4 and 7.5 explain the chosen case studies that are adjusted and then mapped onto the solution space. This phase is marked as *validation phase 2* on Figure 7.1.

It should be noted that validation phase I and II are independent from each other. The results of the statistical analysis explain how change in the parameter affects performance, whereas case study mapping demonstrates how different typologies can be mapped onto a generated solution space.

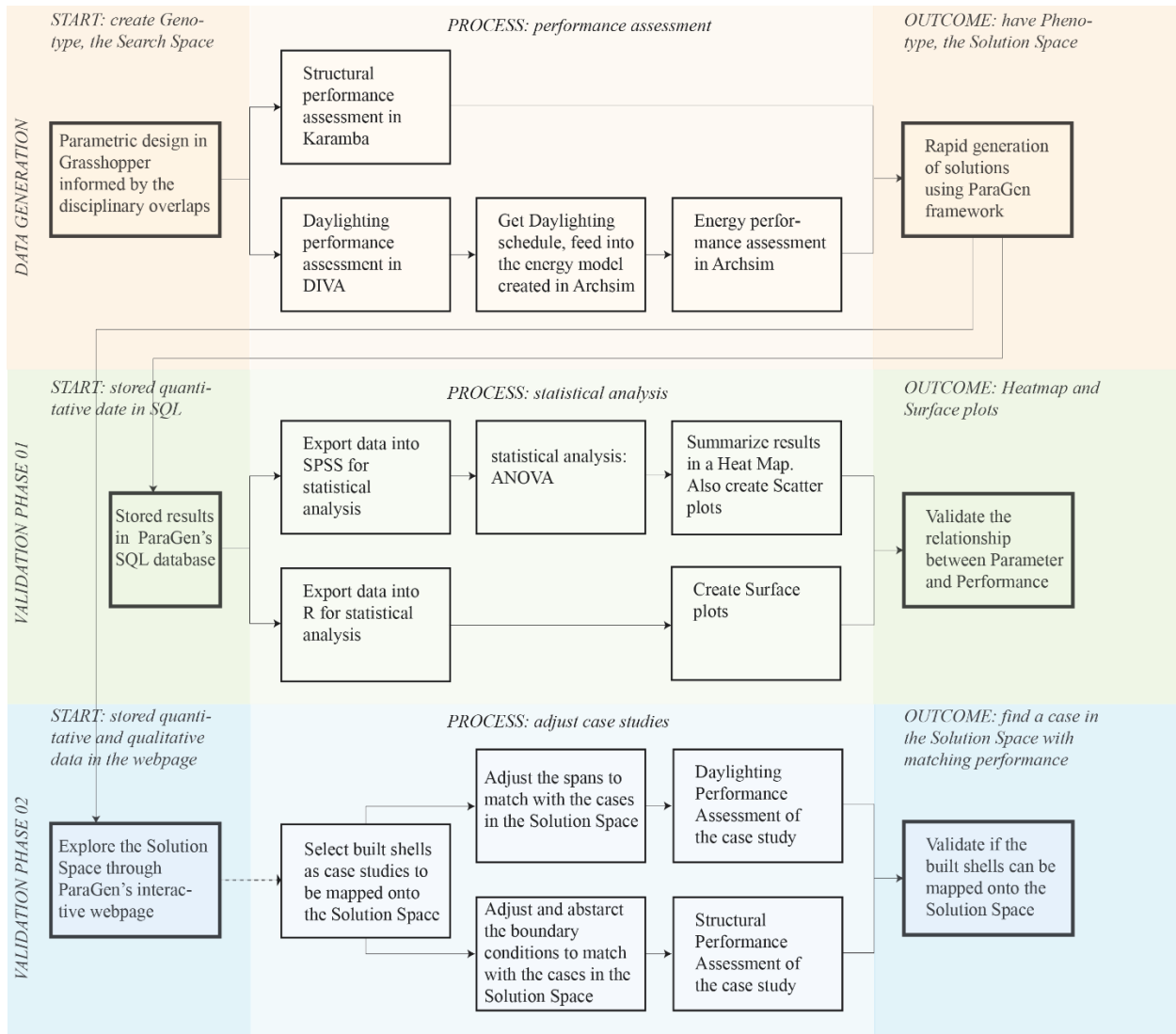


Figure 7.1. Computational design, performance assessment and validation framework

7.2 Parameter and performance

A conceptual design space for shells is proposed in Chapter 5, where the topology of the shell is changing in one axis, and the shape of the shell is changing in the other axis (Figure 7.2). Using this conceptual design space, a parametric model is created using Rhino NURBS modeling software and Grasshopper visual programming add-on to create a search space.

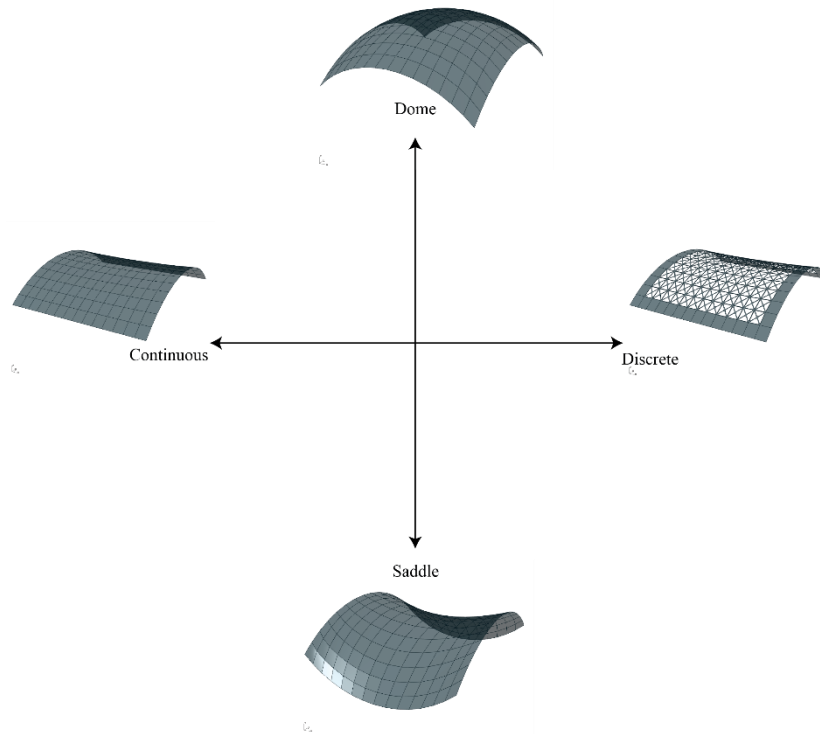


Figure 7.2. Conceptual design space for shells, reiterated from Chapter 5

Based on the conceptual design space, a parametric model is created to facilitate creation of an actual search space. The plugins used, and the sequence of their use, are described in Chapter 6. First, the edge curves are generated, so that a surface is constructed within the edge curves. Then, RhinoMembrane, a form finding plugin in Grasshopper, is used to form a minimal surface. Afterward, Weaverbird, another plugin for Grasshopper, is used for triangulating the mesh. The triangulation pattern is the basis for subtracting perforations. An algorithm implemented in Python systematically subtracts apertures from the shell surface to make it perforated in various zones. This creates a range of possible shell topologies ranging from a continuous to a grid shell. Before explaining the variables that define the parametric model in the following sections, I explain two limitations of the employed strategy for geometric modeling which I noticed towards the end of the process.

The first limitation, that I recognized after completing the statistical analysis and upon mapping the adjusted case studies onto the solution space, is that the *internal pressure*, which is one of the Rhino Membrane settings, has not been adequate to create vaults or synclastic surfaces. In fact, all

of the solutions are generated by using the same internal pressure¹ and the results are anticlastic shells, even though their boundary curves have positive–positive, positive–zero, or positive–negative Gaussian curvatures. The actual search space for the shells resulting from the parametric model is illustrated in Figure 7.3. After exploring the model, I noticed that I should have used three different values for pressure in Rhino Membrane to obtain three different typologies apart from the shape of their boundary curvatures.² On a separate note, this modeling limitation also explains the high deflection value evident for some shells, since some surfaces receive insufficient curvature, and when loaded, the low curvature leads to bending rather than membrane stresses.

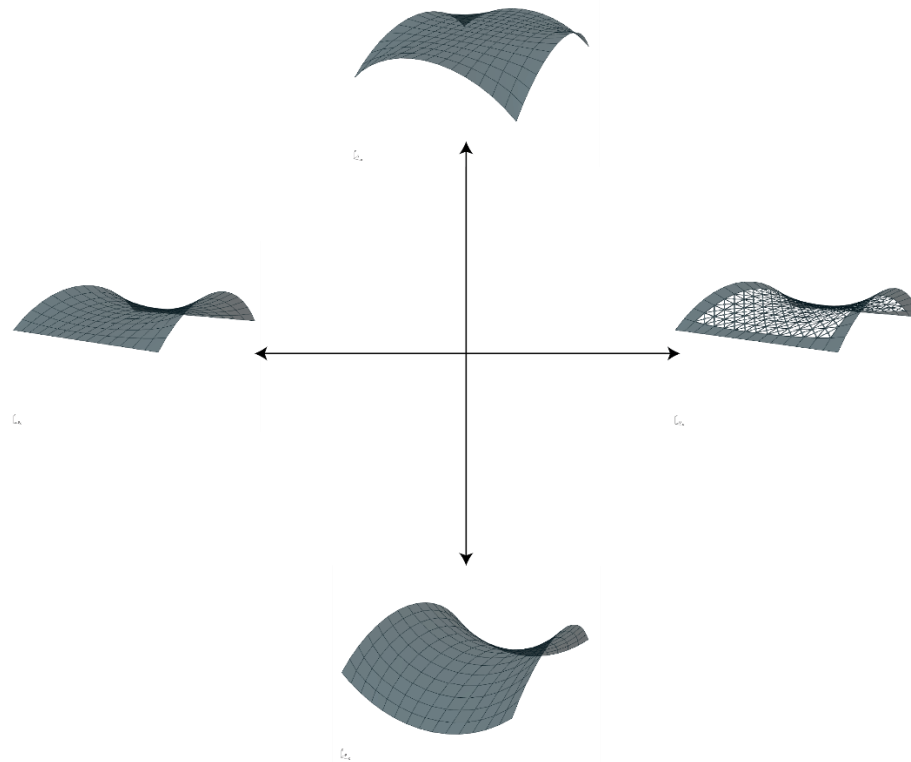


Figure 7.3 . The actual search space created by the parametric model

Based on this understanding, I created a second solution space using an increased internal pressure, which generates only synclastic shells, and later used this second solution space to map cases that have a synclastic surface. The goal is to demonstrate how case studies can be mapped onto a solution space that contains relevant cases. The statistical analysis describing the trends in *saddles* only are explained only in the conclusion.

¹ An internal pressure of 0.04 is used for all shell typologies generated.

² A pressure of 0.35 for synclastic surfaces, 0.2 for barrel vaults, and 0.04 for anticlastic.

Second, although *Bias* is proposed in Chapter 5 as one of the potential design parameters, it is not considered in this model. The method that the Python program uses to subtract zones is explained in depth in the next subsection, 7.2.2. In short, it is a systematic method of combining zones and then putting them in a list³ with a varying length from one to nine, where at least one zone can be subtracted, and at most all nine zones can be subtracted. Although this process is not random, and each combination can be retrieved by its index, the index does not imply whether or not there is a bias in geometric arrangement of various zones. Currently, it should be manually explored to see if any bias is present, which is an exhaustive trial-and-error type exploration (Figure 7.4). A different coding approach could have addressed this by identifying a group of cases that result in a distributed versus biased subtraction pattern.

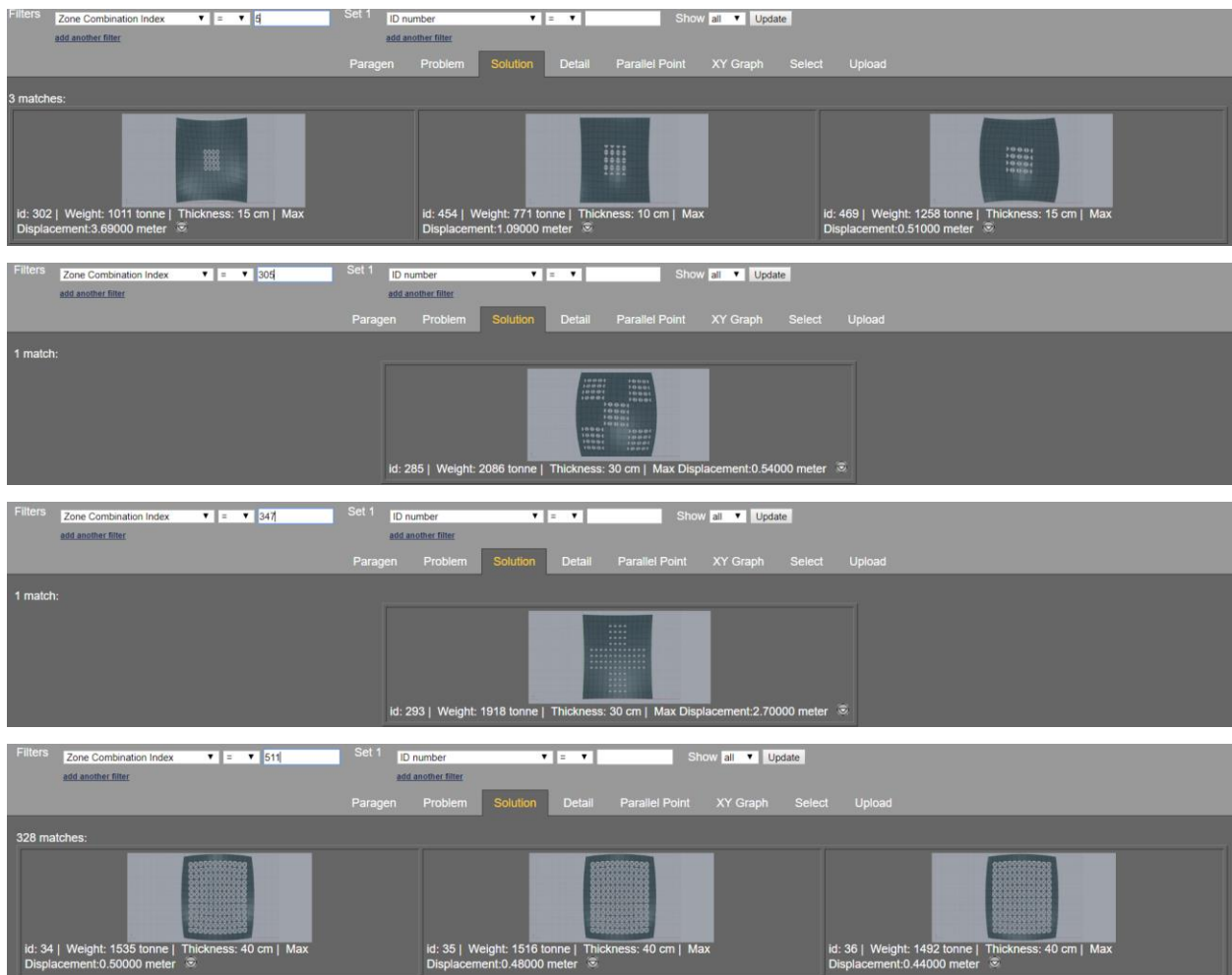


Figure 7.4. Matches for zone combination index of 5, 305, 347, and 511 which result in symmetric opening patterns

³ In Python it is called a list, whereas other programming languages such as C++ call it an array

There are a total of eight variables in the parametric model that can be altered to generate different geometries. Five variables change the global geometry by controlling the boundary curves, and three variables change the local geometry by controlling the location and percentage of perforations, as well as by changing the shell thickness. An overview of the eight variables can be found in Figure 7.5. The constants and variables are introduced in Table 7.1, and each design variable is explained in depth in the following subsections.

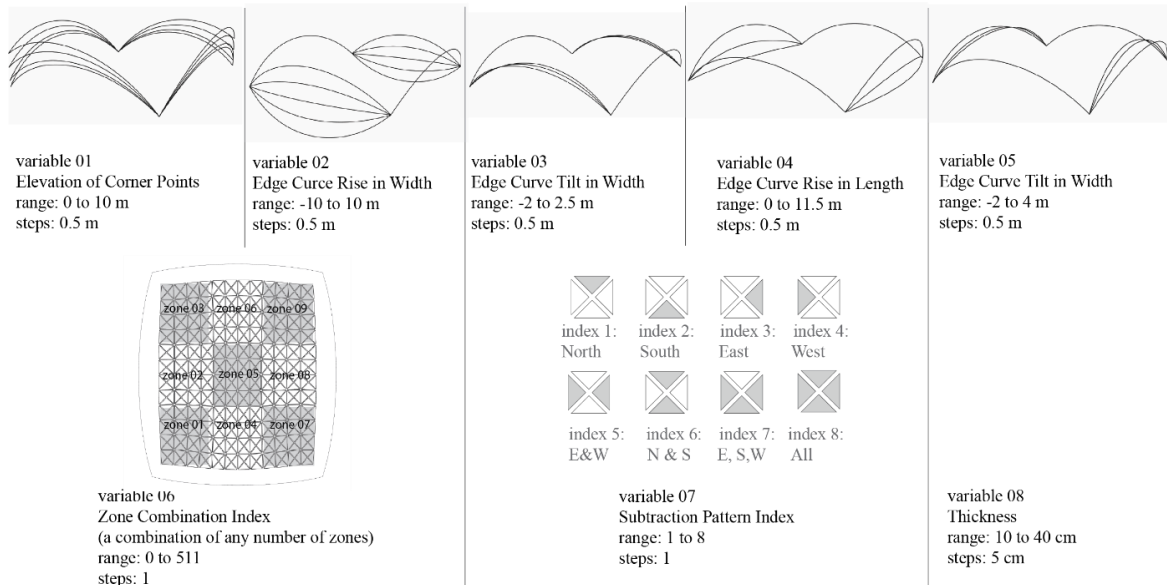


Figure 7.5. The variables that control the parametric geometry generation in Grasshopper

Table 7.1. Constants and variables in the parametric model

Parameter	Constant / Variable	Acceptable interval	Number of possible values
Floor plan dimensions	Constant	50 m wide by 60 m long	1
Minimum height	Constant	15 m	1
Elevation of corner point	Variable	[0 to 10] step 0.5 m	20
Edge Curve Rise in Width	Variable	[-10 to 10 m] step 1 m	21
Edge Curve Tilt in Width	Variable	[-2 to 2.5] step 0.5 m	10
Edge Curve Rise in Length	Variable	[0 to 10 m] step 1 m	11
Edge Curve Tilt in Length	Variable	[-2 to 4 m] step 0.5 m	13
Zone combination index	Variable	[0 to 511] step 1	511
Subtraction pattern index	Variable	[1 to 8] step 1	8
Thickness	Variable	[10 to 40 cm] step 5 cm	7
Triangulation subdivision	Constant	Divided by a 14 by 14 grid	1

7.2.1 Variable 01 to 05: controlling the boundary curves of the roof geometry

The first five variables control the global geometry of the shell by changing the edge conditions. The edge curves are constructed between three points: the start, mid, and endpoint. By moving the endpoints of the curves in the z-direction, the corner of the shell is elevated (Figure 7.6). By moving the mid-point of the curve in the z-direction, the curvature of the constructed curve is varied (Figure 7.7). By moving the midpoint outward or inward in the x or y-direction, the curves are tilted outward or inward (Figure 7.8 and Figure 7.9).

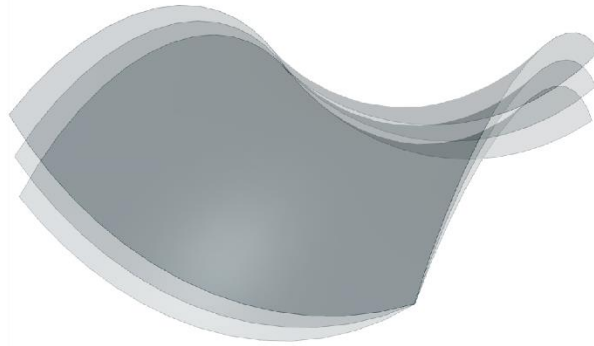


Figure 7.6. Variable 01 is elevation of edge corners which affect the global geometry

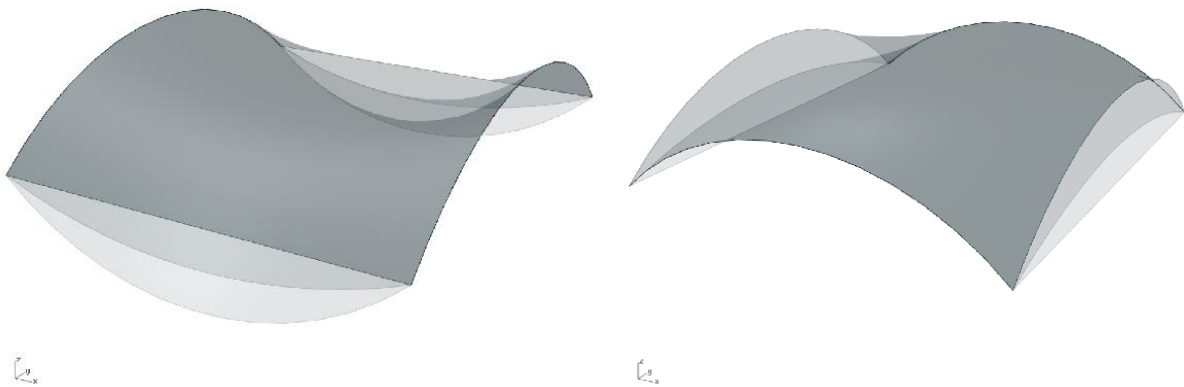


Figure 7.7. Variable 02 is the rise of edge curve in width (a); Variable 03 is the rise of edge curve in length (b)



Figure 7.8. Variable 04 is the tilt of edge curves in width

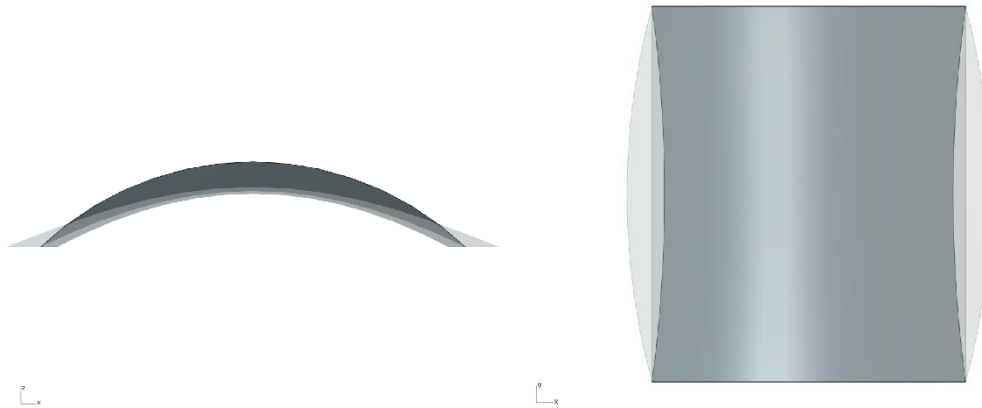


Figure 7.9. Variable 05 is the tilt of edge curve in length

Once a surface is constructed between the boundary curves, the Rhino Membrane plugin for Grasshopper is used to relax the surface. Rhino membrane creates the surface by applying stress in warp and weft (x and y) directions, while adding an upward or downward pressure.

7.2.2 Variable 06: zone combination index

After the global geometry is found using the Rhino Membrane plugin, the surface is triangulated using the Weaverbird plugin. The shell surface is subdivided using a triangular grid pattern (Figure 7.10-a). Then, using a Python script, a margin is isolated along the edges of the surface so that no meshes can be subtracted (Figure 7.10-b). This approach creates solid edge beams, which are helpful for structural analysis and will prevent large deformations from happening at the edges.

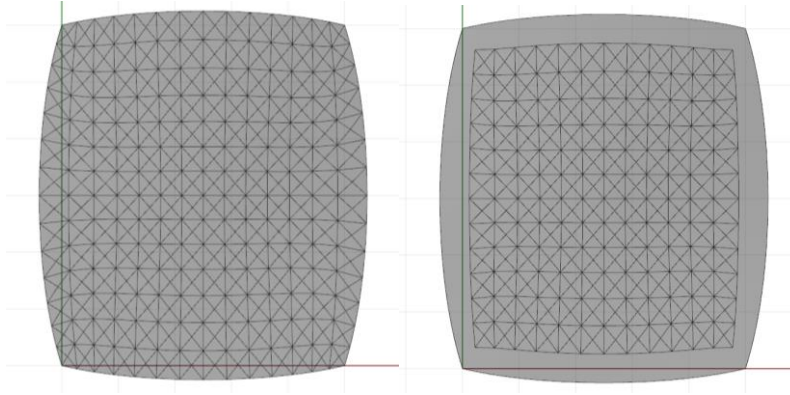


Figure 7.10. Triangular pattern (a); isolating the triangular divisions at the edges for future structural analysis (b)

The remaining triangular modules are then offset inward to create bands for placing concrete reinforcement (Figure 7.11-a). Finally, the triangle's corners are filleted to avoid solutions that create high local stresses at the sharp corners of the triangles (Figure 7.11-b).

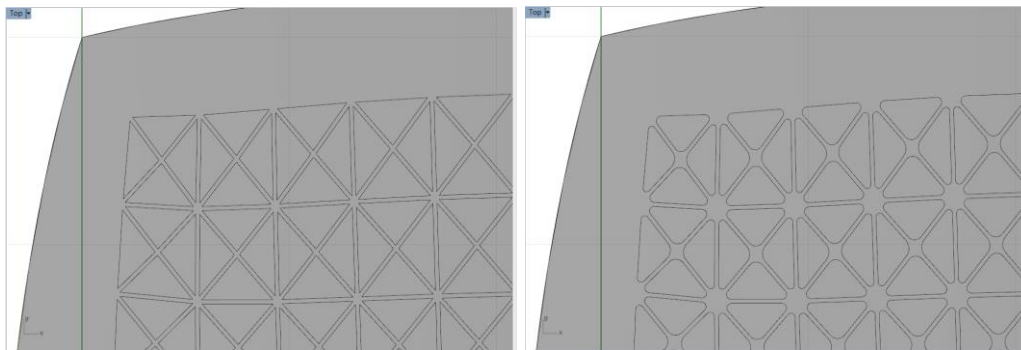


Figure 7.11. Offsetting the triangular grid inward (a); and then filleting the corners to avoid high local stresses (b)

Once the triangulated pattern is processed, a Python algorithm implementation clusters the triangulated patterns into nine zones (Figure 7.12). These zones are each associated with an index, starting from 1 to 9, that will be used to select and combine the zones with each other. Therefore, the *zone combination index* is one of the variables that controls the perforation ratio.

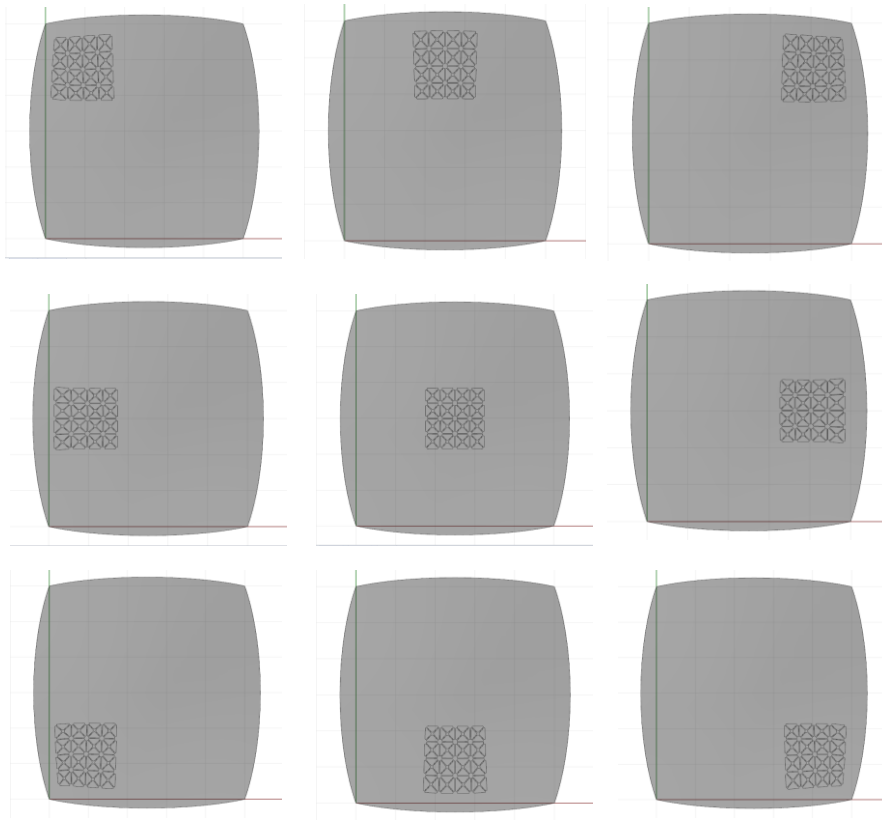


Figure 7.12. The python algorithm implementation clusters triangulated divisions into nine zones

Knowing that there are 9 total zones, and by using the combination formulas (Equation 1), the algorithm can choose any number of zones and combine them together. As an example, if only one zone out of nine is to be chosen, stated as *choose 1 from 9*, there are nine possible options, including *zone 1, or zone 2, or... zone 9* (Equation 2); whereas if nine zones out of nine are to be chosen, stated as *choose 9 from 9*, there is only one possible combination including *zone 1 and zone 2 and ... zone 9* (Equation 3). In each combination, changing the order of the zones doesn't change the combinations. As an example, if two zones out of nine zones are to be chosen, stated as *choose 2 from 9*, two possible combinations with similar members are *zone 1 and zone 2*, and *zone 2 and zone 1*. The algorithm does not allow both to happen; and it considers them to be equivalent. It should be noted that the effect of changing the zone number on the daylighting performance is explored through independent simulations summarized in Appendix F.

The number of total zone combinations are calculated as 511 (Equation 4). In the extreme case where all zones are selected and all apertures are subtracted, an open grid mesh is retrieved.

$$C(n,r) = \frac{n!}{r!(n-r)!} \quad (1)$$

$$C(9,1) = \frac{9!}{(1!(9-1)!)} = 9 \quad (2)$$

$$C(9,9) = \frac{9!}{(9!(9-9)!)} = 1 \quad (3)$$

$$C(9,0) + C(9,1) + C(9,2) + C(9,3) + C(9,4) + C(9,5) + C(9,6) + C(9,7) + C(9,8) + C(9,9) = 511 \quad (4)$$

7.2.3 Variable 07: perforation pattern

Once any number of zones are chosen and combined, another python Algorithm implementation controls subtraction patterns at a micro level. Not all of the apertures of the selected zone are subtracted; rather a 25%, 50%, 75% or 100% perforation ratio facing various orientations is selected as the subtraction pattern (Figure 7.13).

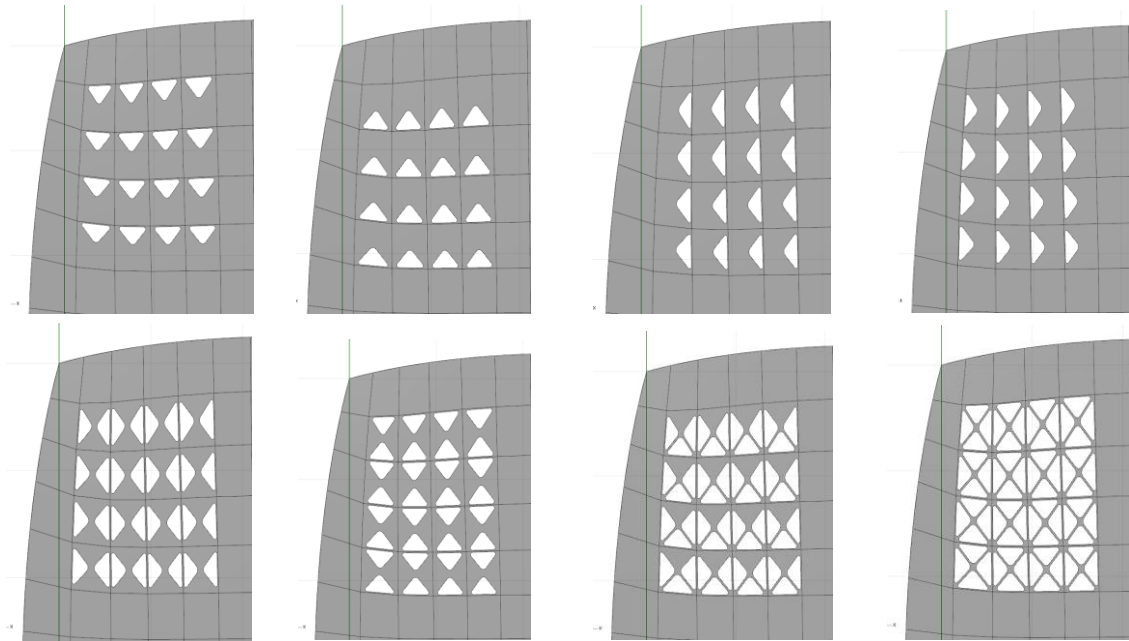


Figure 7.13. Possible perforation patterns mapped onto the pattern

7.2.4 Variable 08: thickness

Finally, the thickness of the shell varies from 10 to 40 cm (4 inches to 16 inches) in 5 cm (2 inch) increments.

7.2.5 Exploring the size of the search space based on the variables

Based on the number of possible values for each variable according to its range and step-variable described in Table 7.1, the total possible number of permutations in the search space can be calculated by multiplying them:

Possible number of permutations = $1 \times 1 \times 20 \times 21 \times 10 \times 11 \times 13 \times 511 \times 8 \times 7 \times 1 = 17,186,769,600$

There are $17E+9$ possible permutations in the search space. Each run took about 1 hour on one laptop of common computational power.⁴ Therefore, $17e9$ hours is needed if one wants to run all the cases on one machine of similar power, equal to $716e6$ days, or $196e4$ years. If 100,000 machines with the same computational power are clustered, 19.6 years are still required to run the full factorial permutations.

Given the available time and computational resources, 1176 cases were generated, simulated, and stored in the database. This solution space contains about 7E-8% of all possible permutations of the search space. Random generation of the first 500 cases is a method to find data points that are as widely spread as possible in the search space to get a population in the solution space that is representative of the search space. After completing the process and by looking at it through a fresh lens, I noticed that setting the range and steps for the variables is critical, as it directly affects the size of the search space. In addition, avoiding duplication of parameters can vastly help to minimize the size of the search space. Finally, not all parameters will affect performance; eliminating the irrelevant ones or those that have little or no impact can help in constructing a better search space. Statistical analysis and a case study simulation, discussed in sections 7.3 and 7.4, respectively, help to identify the most significant variables, as well as the variables that can be eliminated or reduced.

Although design variables 06 and 07 (zone combination index and perforation pattern index respectively) suggest that there might be some repetitive outcomes due to their symmetric patterns, the number of possible permutations is so large that it is highly unlikely that two cases with the *exact* same properties, while having symmetric perforation patterns, can be found among the 1176 runs. However, *similar* results in different symmetrical orientations could have been found. The possibility of duplicated cases could have been eliminated, though. At the time of creating the parametric model, it was assumed that curvature will have an impact on the daylighting performance of the shells, and therefore having the perforations in zone 1 versus zone 9 will make a difference. However, after seeing the results, I noticed that the difference is in performance due to the varied location of the same number of zones is negligible. The same assumption was also

⁴ Windows 8.1 Pro 64/ 4th generation Intel® Core™ i7-4800MQ Processor/NVIDIA® GeForce® 840M Graphics with 2048 MB of dedicated video memory/16GB DDR3 System Memory (2 DIMM)/ 1TB 5400 rpm Hybrid Hard Drive

made for variable 07, the perforations patterns index, and the same conclusion was drawn. By considering the symmetry of these patterns, the number of possible values for variable 05 and variable 06 will be reduced to 8 and 4 from 511 and 8 respectively. The elevation of corner point (20 possibilities), the tilt of curve in width (10 possibilities), and the tilt of curve in length (13 possibilities), could also have been eliminated. This would have reduced the number of possible permutations from $17e9$ to $5e4$ (51744). Increasing the step changes between other parameters from 0.5 m to 1 m could also further reduce the total number of possibilities.

The goal of employing this computational framework is to explore the search space by sampling possible solutions. The goal of this research is to explore shell design space, spanning from continuous to discrete on one axis and from a dome to a saddle on a second axis. Therefore, the designed parametric model is designed in a way that ensures it creates a large number of possibilities. Based on the goal of a particular study, different computational models with different scopes can be created. In fact, once a large region of possibilities is explored, the designer can create a second model and repeat the process with the goal of exploring a magnified region more fully.

7.2.6 Parameter

The previous sections described the design variables that are implemented in the parametric model. It should be noted that sometimes a variable is directly translated into a design parameter. As an example, *thickness* is a variable in the parametric model which matches with the design parameter. However, not all the variables match a design parameter; rather, combination of two or more variables create a design parameter. As an example, a combination of edge curves having different curvatures in width and length combined with surface curvature can describe different roof geometries, e.g. a dome, barrel vault, or saddle. The former are variables whereas the latter is called a parameter. The limitation of not having a synclastic or a barrel vault is explained in section 7.2. Although the terms dome or vault are no longer applicable literally, they are still used for consistency with the coded solutions in the database, and with the statistical analysis, which is based on geometric groupings. The terms *dome* and *vault* in this chapter (and in Appendix E) refer only to the boundary curvatures and not the surface curvature. The design parameters are summarized in Table 7.2, while Appendix E explains the design parameters in depth.

Table 7.2. Design parameters

	possibilities	Driving variable
Roof geometry	Dome/Vault/Saddle	Variable 1 to 5
Perforation ratio	0 to 60%	Variable 6 and 7
Thickness	10 to 40 cm	Variable 8

7.2.7 Performance

From a different perspective, performance of the shells is assessed in the structural and daylighting disciplines. The metrics that are measured in the structural discipline include weight, maximum deflection, von Mises stress levels, and structural costs (including the costs of material and formwork). Boundary conditions set up for the structural model is explained in Appendix B.

Similarly, the performance of the shells is assessed regarding their daylighting and energy performance. The metrics measured include spatial daylight autonomy, daylight oversupply, total energy consumption (including lighting, heating, and cooling), and total operational costs. These metrics are explained in depth in Chapter 4. The model setup for the daylighting and energy simulations in DIVA and Archsim are explained in Appendices C and D, respectively. Table 7.3 summarizes the performance criteria in the structural and daylighting disciplines.

Table 7.3. Performance criteria in two disciplines

	Discipline	Criterion	Constraint or goal?
Weight	Structure	Minimize weight	Goal
Maximum displacement	Structure	Deflection limits (dead load + live load) < 0.3 m	Constraint
Von Mises stress at Q3	Structure	Stress limits: von Mises < 30 MPa	Constraint
Material and formwork cost	Structure	Minimize cost	Goal
Spatial daylight autonomy (sDA)	Daylighting	Daylighting limits of acceptability: sDA > 55%	Constraint
Daylight oversupply	Daylighting	Limits on maximum daylight: DAv oversupply < 0.05	Constraint
Total energy	Daylighting	Minimize total energy	Goal
Total operational costs	Daylighting	Minimize operational costs	Goal

It should be noted that total energy consumption and total operational costs are categorized under the discipline of daylighting in this study, since the role of daylight in affecting the total energy performance and operational costs is studied in this research. In fact, the daylighting schedule is retrieved after daylighting simulation is completed and then is fed into the energy

simulation engine. Thus, the reduction in the electricity costs by the availability of daylight will be considered.

With the identified parameters and performance criteria, and by using ParaGen framework, more than thousand solutions are generated. All the alternatives are associated with their performance criteria and can be interactively explored. Subsection 7.2.5 explains the size of the solution space and ways in which it could have been reduced. A screenshot of the interactive website displaying the generated cases is presented in Figure 7.14.

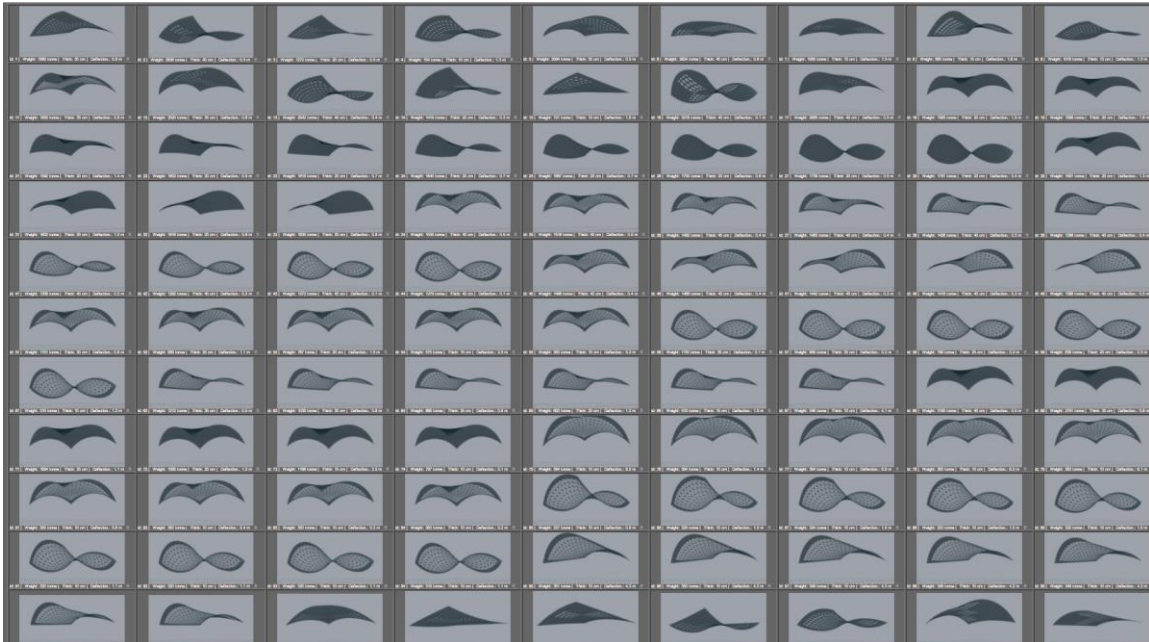


Figure 7.14. Screenshot of the interactive webpage connected to the online SQL database as part of the ParaGen framework

This interactive webpage can be explored quantitatively and qualitatively by the user (Figure 7.15), to understand the relationship between a parameter and a performance, or to understand the tradeoffs between multiple performance criteria. The concept of tradeoff is explained in the introduction of Chapter 6.

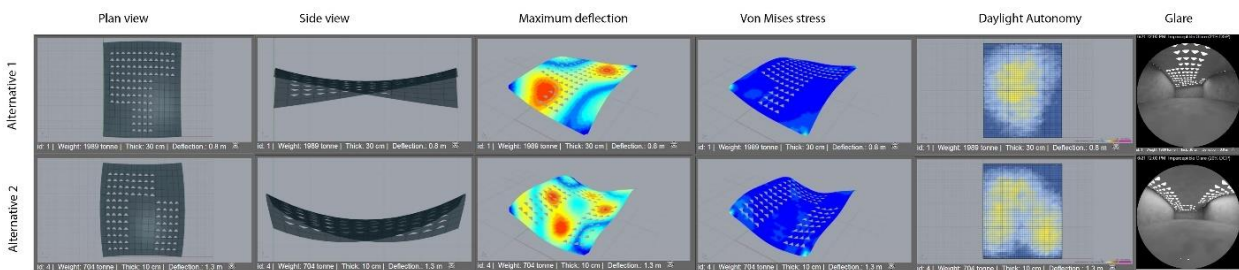


Figure 7.15. Different alternatives can be explored qualitatively and quantitatively with regard to their multiple performance criteria

This research aims to take a rigorous quantitative approach to analyzing the results, and to validating if the identified overlapping design parameters are affecting the structural and daylighting performance in the shells. Therefore, ANOVA, an analysis of variance, is computed to statistically determine the relevance of one parameter to multiple performance criteria, while keeping all other parameters constant. The process is repeated for all eight performance criteria. The research also seeks to map the built case studies onto the solution space, to understand if the behavior of the generated shells can be matched with the simulation results of the abstracted case studies. The approach, involving a first validation phase through statistical analysis, and a second validation phase through case study mapping, is explained in Sections 7.3, 7.4 and 7.5. The detailed processes are summarized in Appendices E and F.

7.3 Statistical analysis

ANOVA statistically determines the relevance of one parameter to multiple performance criteria, while keeping all other parameters constant. A heat map presented in Table 7.4 summarizes the ANOVA results, and the correlations between parameters and performance criteria. Only significant p-values (p-values less than 0.05) are color-coded. The green color indicates a positive correlation, whereas the orange color indicates a negative correlation. The intensity of the color represents the significance of the correlation: a pale color indicates weak correlation, and a vibrant color indicates strong correlation. Surface plots are also presented, to visually demonstrate the trend of change in performance criteria when the design parameters are changing. The effect of the design parameters on each performance criterion is also explained.

Table 7.4. Heat map summarizing the correlation between parameters and performance

	Dome		Vault		Saddle	
	Perforation ratio	Thickness	Perforation ratio	Thickness	Perforation ratio	Thickness
DV-1 :Weight						
DV-2: Deflection						
DV-3: von Mises stress						
DV-4: Structural cost						
DV-5: Spatial daylight autonomy						
DV-6: Light oversupply						
DV-7: Total energy						
DV-8: Total energy costs						

legend		
positive correlation	negative correlation	
lowest	lowest	p < 0.05
		p < 0.01
highest	highest	p < 0.001

7.3.1 Performance: weight

Looking at the first performance criterion, *DV-1: Weight* on the heatmap, it is noticed that as thickness increases, the increase in the weight of vaults and saddles is significant. On the other hand, as perforation Ratio increases, the decrease in weight of saddles is significant. The surface plots in Figure 7.16 also demonstrate the overall trend of increased weight in thicker shells with less holes. This is one of the most straight-forward and intuitive correlations.

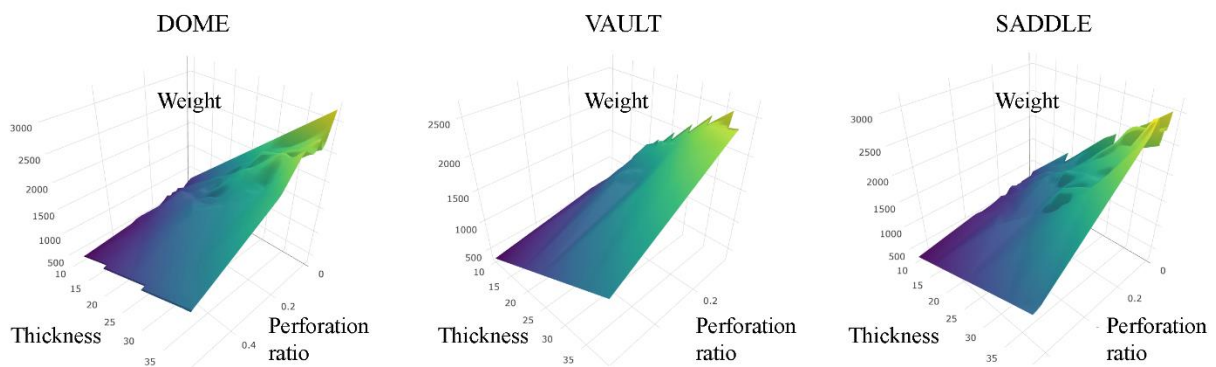


Figure 7.16. Surface plots for DV-1 (weight) plotted on the z-axis; perforation ratio and thickness are plotted on the x- and y-axes, respectively

The detailed statistical analysis is described in Appendix E; however, the outcomes are summarized here (in italics). Interpreting the coefficients for these predictors for saddles, I find that:

- *A one-unit increase in perforation ratio results in a 14.76 unit expected decrease in weight, holding the other predictors fixed.* This means that when perforation ratio changes from 1% to 0% for example, the shell that is covering the 50 by 60-meter space will weigh 14.76 t less, keeping the thickness constant.
- *A one-unit increase in thickness results in a 63.89 unit expected increase in weight, holding the other predictors fixed.* This means that when thickness is increased from 10 cm to 15 cm, for example, the weight increases by 63.89 t, when perforation ratio is kept constant.

Having a p-value less than 0.005 for both variables means that these are both significant. Table F.7 in Appendix F includes the coefficients and interactive plots.

7.3.2 Performance: maximum deflection

Looking at the second performance criterion, *DV-2: Deflection* on the heatmap, I noticed that as thickness increases, the decrease in maximum deflection is significant in saddles. It should be noted that on one hand, increasing the thickness makes the shell stiffer; on the other hand, by increasing the thickness, the self-weight of the shell, and thus its dead load (D.L.), is increased. Under constant live load (L.L.), the increased thickness seems to be making the shell stiffer since maximum deflection is reduced. It can be noticed that as perforation ratio increases, the decrease in maximum deflection is significant in saddles. The surface plots are presented in Figure 7.17.

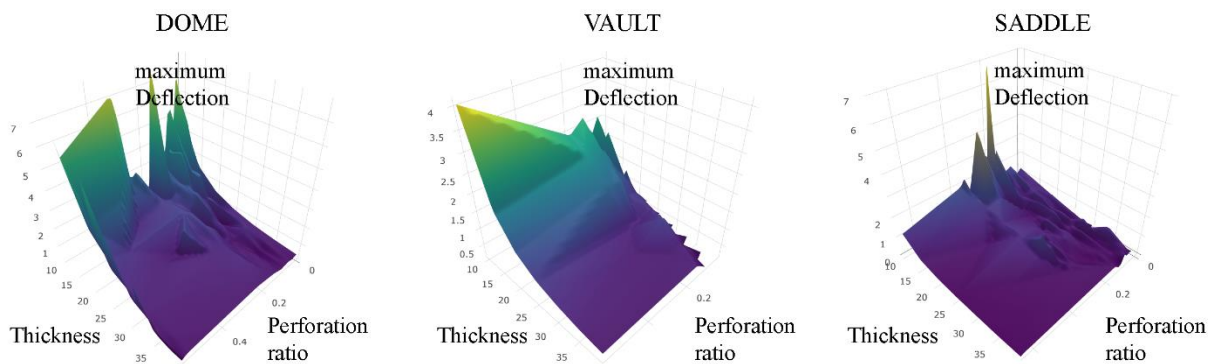


Figure 7.17. Surface plots for DV-2 (maximum deflection) plotted on the z-axis, with perforation ratio and thickness plotted on the x- and y-axes, respectively

This correlation between perforation ratio and deflection is questionable, as it is expected that not having holes in the surface increases its stiffness, and thus reduces stress. Therefore, this correlation is explored further. By looking at a scatter plot (Figure 7.18) of data for saddles, where perforation ratio is plotted on the x-axis and deflection is plotted on the y-axis, the overall trend matches the statistical results. However, after clicking on individual data points, it is observed that although all cases are saddles, they each possess different curvatures. Therefore, the statistical results of this parameter and the retrieved coefficients cannot be generalized. Future statistical analysis will need to control for curvature as one of the independent variables.

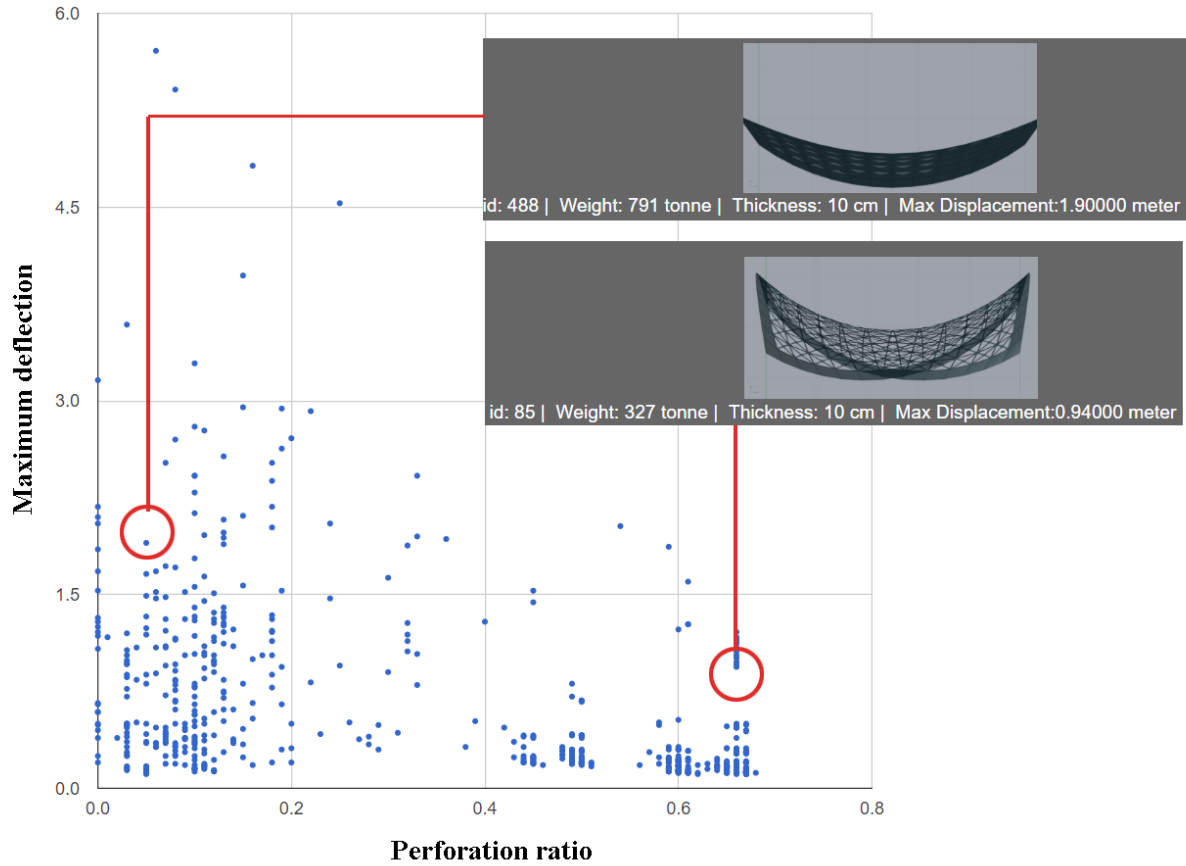


Figure 7.18. Although deflection is reduced by increasing perforation ratio in saddles, since the statistical analysis is not controlling for curvature, the results cannot be generalized

7.3.3 Performance: von Mises stress

Looking at the third performance criterion, *DV-3: von Mises stress* on the heatmap, it can be noticed that as thickness increases, the decrease in von Mises stress levels is significant in saddles and domes. Added thickness creates added geometric stiffness, which helps to reduce the stress levels. On the other hand, as perforation ratio increases, the decrease of von Mises stress is significant in domes, vaults, and saddles. It should be noted that the size of the holes is constant and only the number of holes and their locations are varied in shells with different perforation ratios. The surface plots are presented in Figure 7.19.

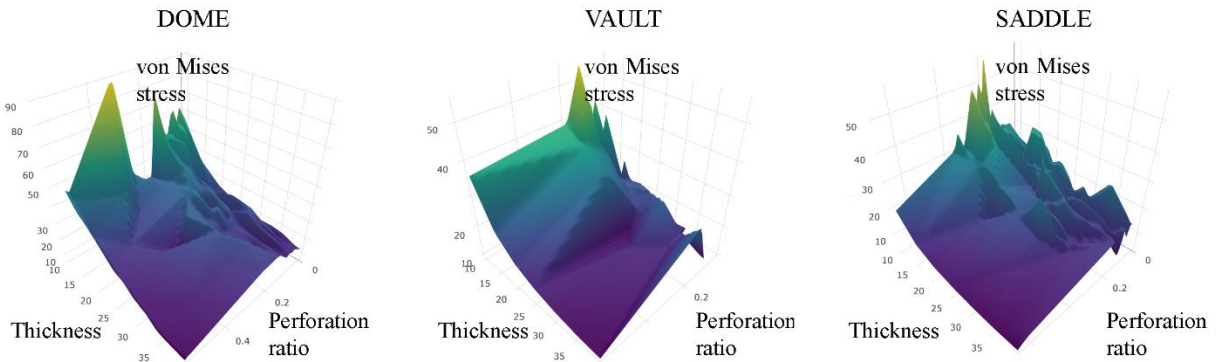


Figure 7.19. Surface plots for DV-3 (von Mises stress at Q3) plotted on the z-axis, with perforation ratio and thickness plotted on the x- and y-axes, respectively

The detailed statistical analysis is described in Appendix E; however, the outcome is summarized here (in italics). The results are compared with a base case (a saddle with perforation ratio of 0, and thickness of 20 cm, represented by id 27 in the solution space).⁵ Interpreting the coefficients of these predictors for saddles, I find that:

- *a one-unit increase in perforation ratio results in a 0.021-unit decrease in expected von Mises stress levels, holding the other predictors fixed.* This means that if the perforation ratio is increased from 0% to 1%, for example, the von Mises stress is expected to decrease by 0.18⁶ percent of the von Mises stress levels of the solid shell while other parameters are kept constant.
- *a one-unit increase in thickness results in a 0.078-unit decrease in expected von Mises stress levels, holding the other predictors fixed.* This means that if the thickness is increased from 10 cm to 15 cm, for example, the von Mises stress is expected to decrease by 0.6⁷ percent of the von Mises stress levels of the solid shell if other parameters are kept constant.

Although it is common sense that less material should increase stress (stress = Load/Area), the statistical results show that as the shell becomes more perforated meaning that as the surface area decreases, von Mises stress also decreases. Therefore, this is further explored by analysis of a scatter plot (Figure 7.20). In that plot, which contains data for saddles, perforation ratio is plotted on the x-axis and von Mises stress is plotted on the y-axis; the overall trend matches the statistical

⁵ Von Mises stress of this case is 11.6 MPa

⁶ $0.021/11.6 = 0.0018$

⁷ $0.078/11.6 = 0.006$

results. However, after examining individual data points, it is observed that although all cases are saddles, they have different curvatures. Therefore, the statistical results of this parameter and the retrieved coefficients cannot be generalized. Just as for the correlation between deflection and perforation ratio, future statistical analysis will need to control for curvature as one of the independent variables.

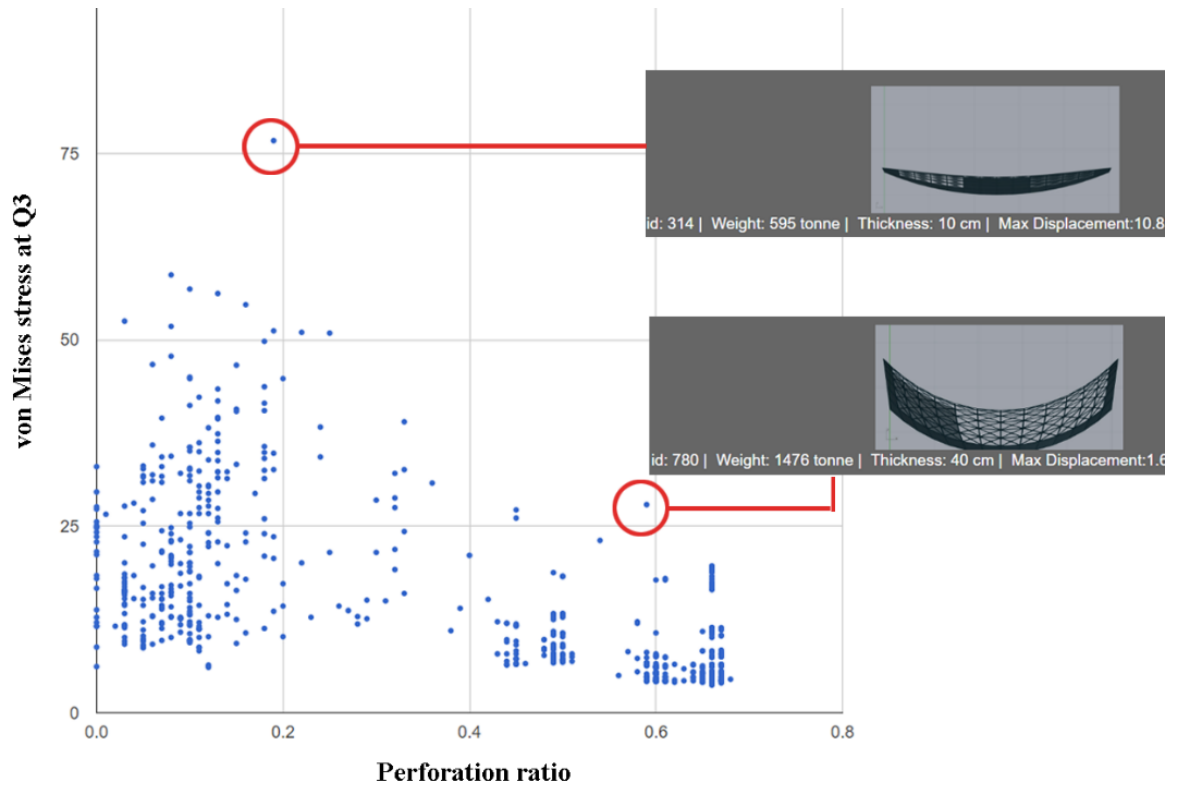


Figure 7.20. Von Mises stress is reduced as the shells become more perforated

7.3.4 Performance: total structural costs

Looking at the fourth performance criterion, *DV-4: total structural costs*, on the heatmap, as thickness increases, the increase in total structural costs is significant in domes, vaults, and saddles. It is intuitive that using more material, increases costs. Also, as perforation ratio increases, the decrease of total structural costs is significant in domes and saddles. At first look, this makes sense, since construction of a perforated shell uses less material. However, total structural costs consist of both material and formwork costs. The detailed process of calculating the costs is summarized in Appendix C. In short, the material cost is calculated first; for a solid shell, the formwork cost is calculated with a 1 to 1 ratio; for a grid shell, the formwork cost is calculated with a 3 to 1 ratio; and for other shells, lying between solid and grid shells, the ratio varies between 1 and 3. Later in

the process, I noticed that this method of calculation would have worked for shells with constant thickness. With thickness and perforation ratio both changing, a 10-cm thick solid shell could have been using the same amount of material as a 40-cm thick grid shell, and thus the increased ratio for formwork costs for a 10 cm shell can be canceled out by the higher material costs of a solid shell. Future research needs to address this by using a more accurate calculation method. Currently, the results are limited to material costs for concrete and plywood used as formwork. The ratio applied to shells with higher perforation ratio is assumed to be used for more detailed local reinforcement around the holes. The surface plots are presented in Figure 7.21.

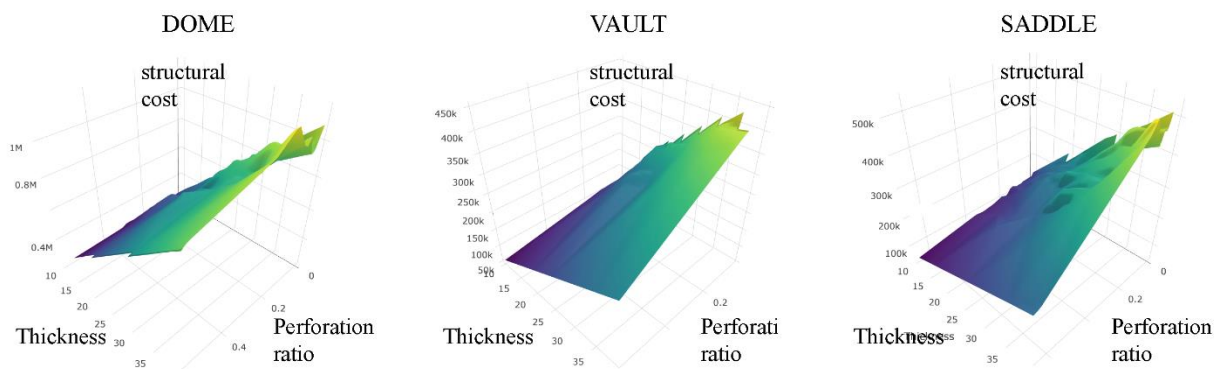


Figure 7.21. Surface plots for DV-4 (material and formwork costs) plotted on the z-axis, with perforation ratio and thickness are plotted on x- and y-axes, respectively

The detailed statistical analysis is described in Appendix F; however, the outcome is reiterated here (in italics). The results are compared with a base case (a saddle with perforation ratio of 0, and thickness of 20 cm, represented by id 27 in the solution space).⁸ Interpreting the coefficients for these predictors for saddles, we find that:

- *a one-unit increase in perforation ratio results in a 1.75 unit in one thousand expected decrease in structural costs, holding the other predictors fixed.* This means that if perforation ratio is increased from 0% to 1%, the total structural costs decrease by 0.29%⁹ of the structural costs of the solid shell if other parameters are kept constant.
- *a one-unit increase in thickness results in a 26 unit in one thousand expected increase in structural costs, holding the other predictors fixed.* This means that if thickness is increased

⁸ Total structural costs for this case are calculated as \$590,978

⁹ $1750/590978 = 0.0029$

from 10 cm to 15 cm, total structural costs are increased by 4.3%¹⁰ of the structural costs of the solid shell if other parameters are kept constant.

7.3.5 Performance: spatial Daylight Autonomy

Looking at the fifth performance criterion, *DV-5: spatial daylight autonomy*, on the heatmap, thickness does not have a significant effect on performance. However, with an increase in perforation ratio, spatial daylight autonomy increases significantly in domes and saddles. This makes sense, as the presence of more holes in the shells allows more daylight to enter the space. However, by looking at the surface plots presented in Figure 7.22, a kink in all surface plots is recognized. In other words, the curvature of the surface plots changes abruptly when perforation ratio hits a certain threshold.

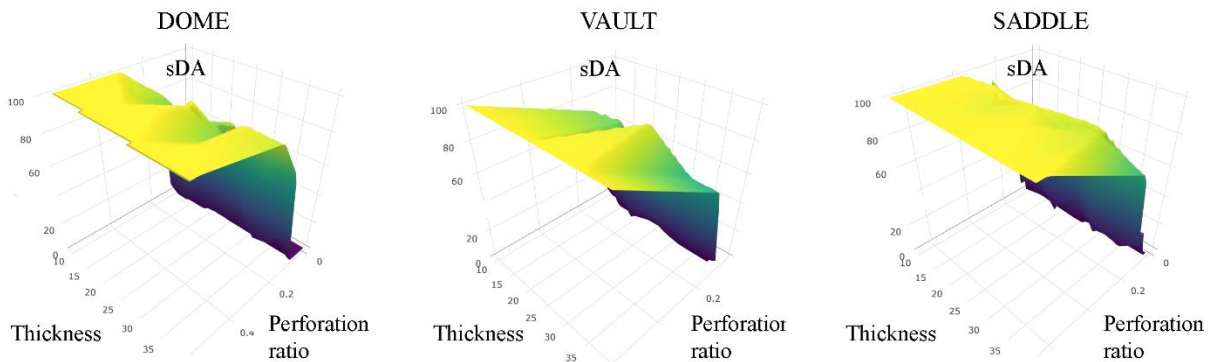


Figure 7.22. Surface plots for DV-5 (spatial daylight autonomy) plotted on the z-axis, while perforation ratio and thickness are plotted on x- and y-axes, respectively

Figure 7.23 is a plot of perforation ratio versus spatial daylight autonomy. It confirms that sDA is nearly zero when perforation ratio is less than 10%, and then it starts to spike up until it hits 100% at 30% perforation ratio. If the perforation ratio increases beyond 30%, sDA no longer increases since it has already reached its maximum amount. This means that perforation ratios less than 10% do not provide adequate daylight, and increasing the perforation ratio beyond 30% does not provide any additional daylight for the space. It should be noted that translucent glazing has been used in the simulations.

¹⁰ $26000/590978 = 0.043$

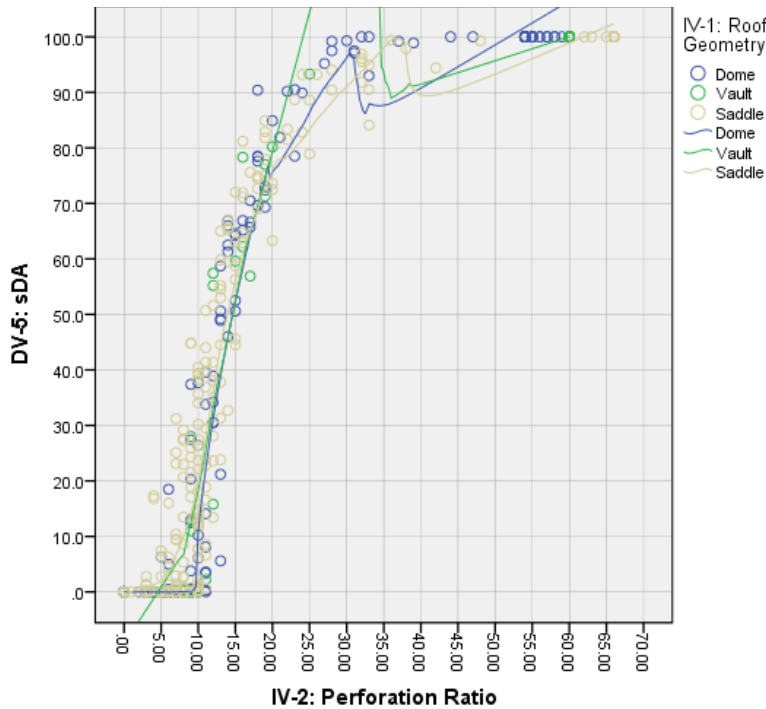


Figure 7.23. Perforation ratio versus spatial daylight autonomy (sDA)

7.3.6 Performance: light oversupply

Looking at the sixth performance criterion, *DV-6: Light oversupply* on the heatmap, increase of perforation ratio significantly increases light oversupply. In other words, as there are more holes in the surface, lighting levels beyond what is needed are provided, as seen in the surface plots in Figure 7.24. Again, a kink in the surface plots is noticed, which is analyzed further below.

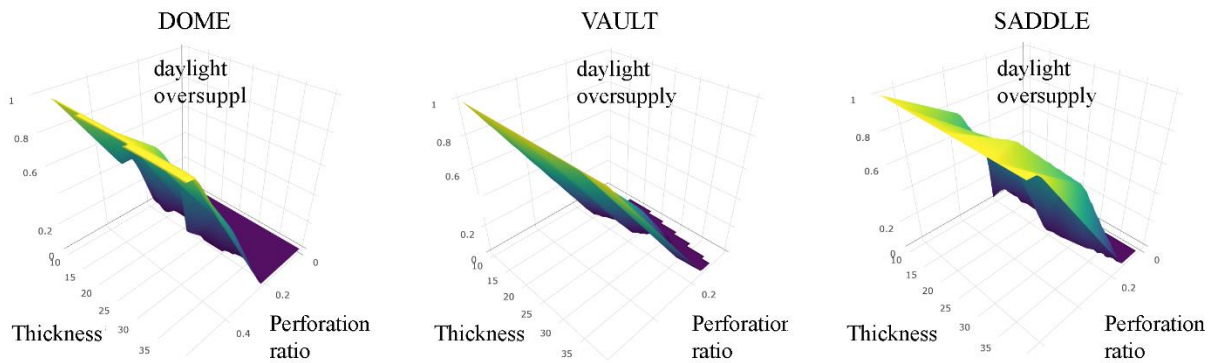


Figure 7.24. Surface plots for DV-6 (Light oversupply) plotted on the z-axis, where perforation ratio and thickness are plotted on x and y-axis

The scatter plot illustrates the perforation ratio versus spatial daylight autonomy (Figure 7.25). When the perforation ratio is about 20%, the light oversupply is zero (which is desirable). Once

the perforation ratio increases beyond 20%, light oversupply starts to spike. It should be noted that high percentages of light oversupply increase the chances of discomfort glare.

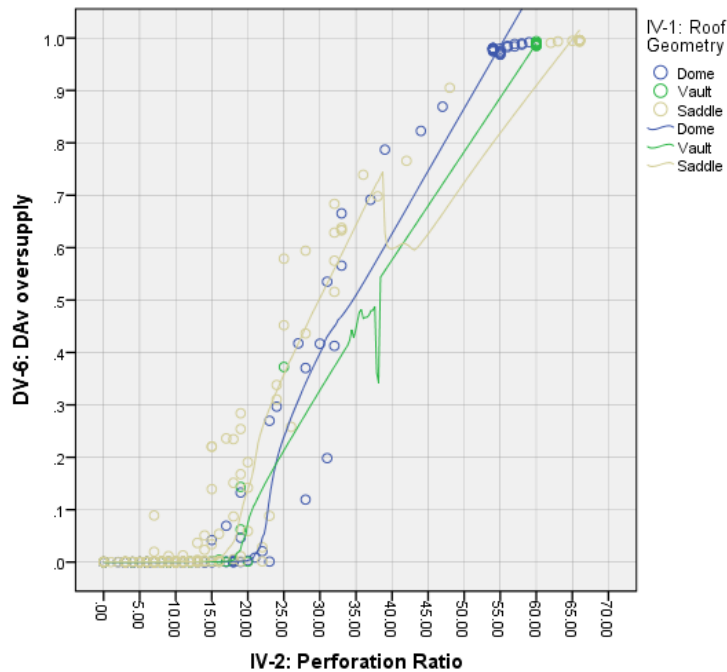


Figure 7.25. Perforation ratio versus light oversupply (DAv)

Reviewing scatterplots in Figure 7.20 and 7.22 side by side shows that a perforation ratio between 10% and 20% provides adequate sDA without light oversupply. It should be noted that these percentages are retrieved using translucent glazing without any exterior or interior shading devices.

7.3.7 Performance: total operational energy

Looking at the seventh performance criterion, *DV-7: Total operational energy* on the heatmap, as thickness increases, the total operational energy (including heating, cooling, and lighting) decreases in saddles. In other words, thicker shells consume less operational energy. On the other hand, as perforation ratio increases, the total energy costs increase significantly in saddles. The surface plots in Figure 7.26 demonstrate this and are followed by an analysis of the results.

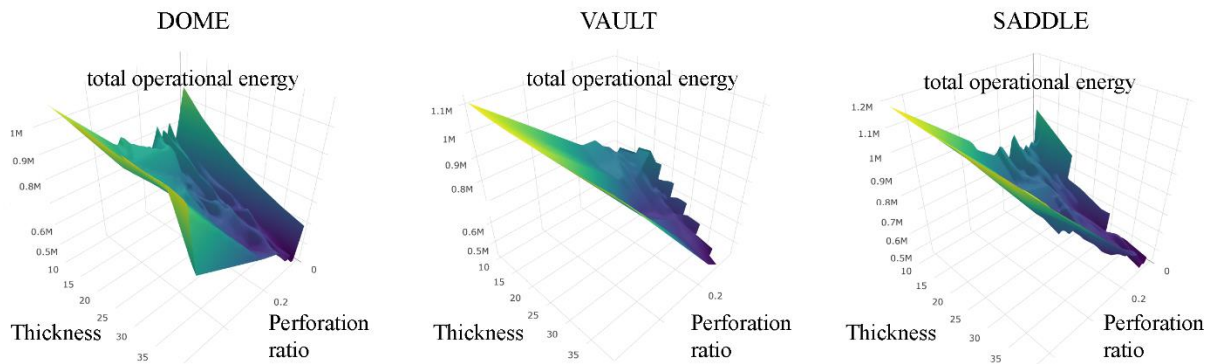


Figure 7.26. Surface plots for DV-7 (Total operational energy) plotted on the z-axis, with perforation ratio and thickness plotted on x- and y-axes, respectively

The multinomial regression model that is computed is demonstrated in Appendix E, showing that *increases in perforation ratio significantly increase the odds of having total energy higher than 800, and between 600 and 800, relative to total energy less than 600, relative to saddles. In other words, the odds of getting a worse total energy increase as the perforation ratio increases.* This is explored more to ensure that this increased operational energy is due to increased heat gain which ultimately increases cooling loads in the summer months.

The model also revealed that increases in thickness significantly decreases the odds of having total energy higher than 800 MWh/m³, and between 600 and 800 MWh/m³, relative to higher than 1200 MWh/m³, relative to saddles. In other words, the odds of getting a better total operational energy increases as the thickness increases. This suggests that increased concrete thickness offers insulating properties, leading to reduced heating loads.

From a different perspective, although the effect of thickness and perforation ratio on the *total operational energy* is considered, it is important to know if it is heating, cooling, or lighting energy that is driving the results. It should be noted that Boston, a heating-dominated climate, is used for simulations. By looking at the scatter plots in Figure 7.27, thickness and perforation ratio are both affecting heating loads. However, thickness is not affecting cooling or lighting loads, while perforation ratio is affecting both cooling and lighting loads (Figure 7.28 and Figure 7.29).

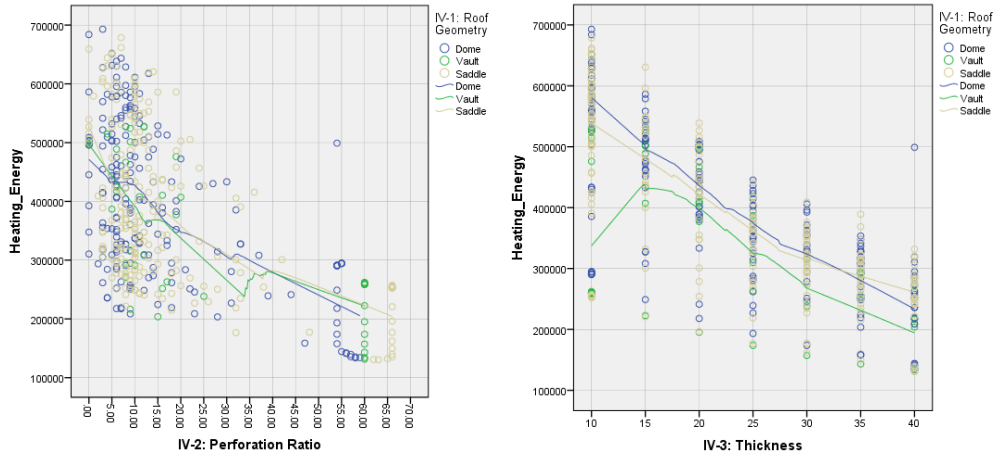


Figure 7.27. By creating more holes, heating energy decreases (a); by making the shells thicker, heating energy decreases (b)

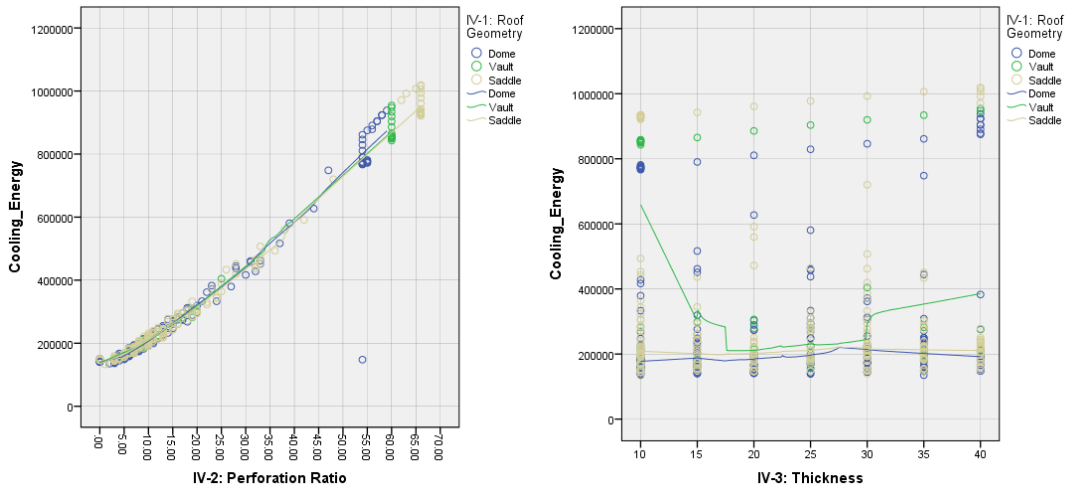


Figure 7.28. By creating more holes, cooling loads increase (a); thickness does not seem to affect cooling loads (b)

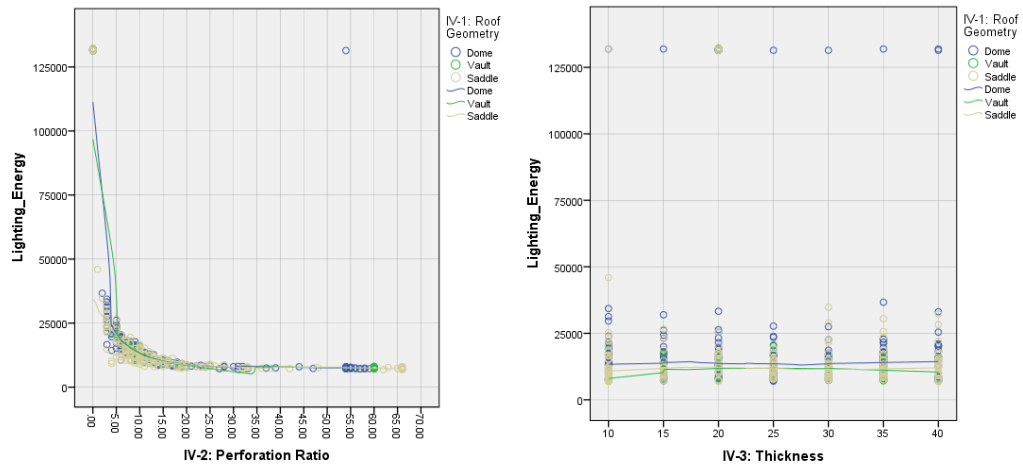


Figure 7.29. Lighting energy reaches a plateau when the perforation ratio is more than 20% (a); thickness does not seem to affect lighting loads (b)

7.3.8 Performance: total energy costs

Looking at the eighth performance criterion, *DV-8: Total energy costs* on the heatmap, it can be observed that energy costs increase significantly as perforation ratio increases and decrease when shells become thicker. Thickness does not have an effect on this performance criterion. The overall trend is similar to that observed for total operational energy. The surface plots presented in Figure 7.30 demonstrate the trend.

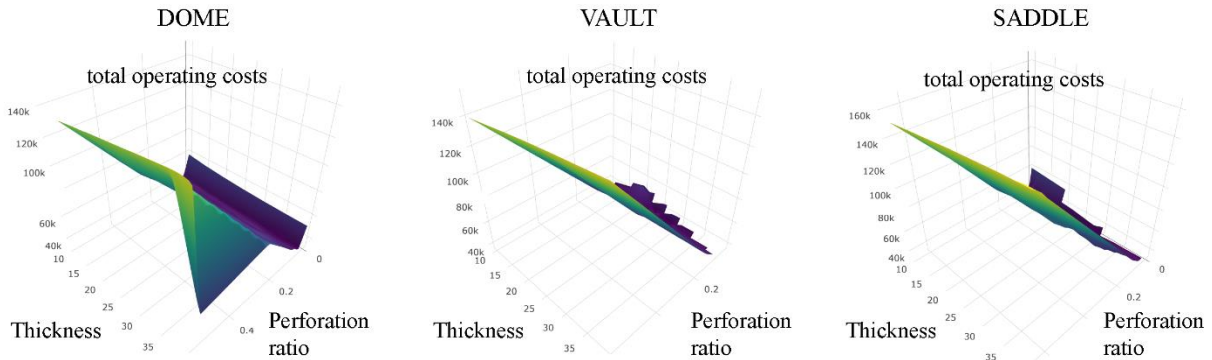


Figure 7.30. Surface plots for DV-8 (total energy costs) plotted on the z-axis, with perforation ratio and thickness plotted on x- and y-axes, respectively

By running an Ordinal Logistic Regression model (described in Appendix E), *predictor perforation ratio* was found to increase the probability of a higher-valued category (category 3: total operational costs >\$4 k) significantly. In other words, the probability of higher energy costs or worse outcomes increase as this predictor, perforation ratio, increase by one unit.

Predictor thickness was found to decrease the probability of a higher-valued category (category 3: total operational costs > \$45k) significantly. In other words, the probability of higher energy costs, or worse outcome decrease as this predictor, thickness, increase by one unit. There is no evidence of significant interaction.

7.3.9 Tradeoff between performance

The statistical analysis unfolds the relationship between parameters and performance. In fact, almost all of the design parameters that were identified as common parameters between the two disciplines are found to affect performance in both disciplines. The statistical results suggest that the methodology for identifying overlaps between disciplines is effective.

Once the relationship between parameter and performance is investigated, the tradeoffs between performance in multiple disciplines can be investigated. The heat map is a good starting

point for this, as contrasting colors for the same parameter for two different performance criteria suggests there is a tradeoff between those performance criteria when considering that parameter.

As an example, two contrasting parameters are marked on the heat map illustrated in Figure 7.31, and the scatterplot illustrated in Figure 7.32 further explores this tradeoff. It demonstrates that in thinner shells, with a thickness of 10 or 15 cm, the total operating costs for one year are dominating, whereas the effect of material cost is negligible. However, as the shells get thicker, the tradeoff between the two increases. These two performance criteria are both expressed in unit cost, and therefore are selected for review. Other tradeoffs have different units on the two axes.

	Dome		Vault		Saddle	
	Perforation Ratio	Thickness	Perforation Ratio	Thickness	Perforation Ratio	Thickness
DV-1 :Weight						
DV-2: Deflection						
DV-3: von Mises						
DV-4: Structural Cost						
DV-5: Spatial Daylight Autonomy						
DV-6: Light oversupply						
DV-7: Total Energy						
DV-8: Total energy costs						

Figure 7.31. Identifying contrasting colors on the heat map

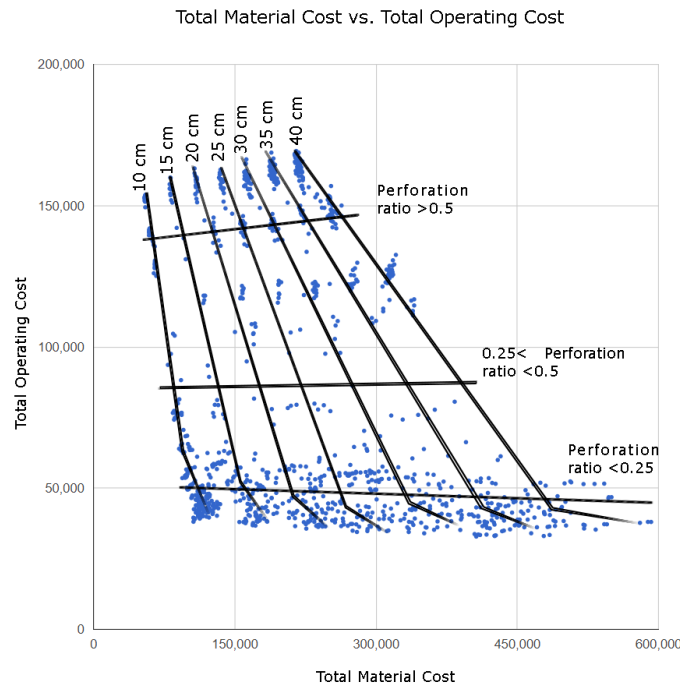


Figure 7.32. Tradeoff between two performance criteria: structural cost versus operating costs

The next phase of the research seeks to map case studies of actual structures onto the solution space generated by ParaGen, to understand if the behavior of the generated shells can be matched

with the simulation results of the abstracted built shells. The first case study is the High Life Textile Factory designed by Candela with distributed perforations. The second case study is the COOP Warehouse designed by Heinz Isler. It should be noted that not all case studies have the same typology as the generated shells; thus, some abstraction is necessary to create similar boundary conditions.

7.4 Case study 01: High Life Textile Factory

This section explains the first case study, High Life Textile Factory, designed and build by Candela. The first subsection describes Candela's design and construction techniques and the original dimensions of the umbrella shell. The second subsection explains how the dimensions of the umbrella shell are adjusted for daylighting simulations to match the boundary conditions of the shells generated using ParaGen to allow a comparative study. The goal is to compare shells that are covering the same floor area of 3000 m² (50 by 60 m), with roof perforations as the only source of daylight. The third subsection explains how the structural boundary conditions are abstracted to match the boundary condition of the generated cases in the solution space. The adjustment procedure before mapping the performance of the High Life Textile Factory onto the solution space is presented in Figure 7.33.

The purpose of a case study is usually to replicate the simulated results with as-built condition. However, the dimensions and boundary condition of the case studies are adjusted in this research to reach a slightly different goal: this study aims to study what happens after a solution space is created and see if the results will be limited to the specific typology that has been generated or can it be used as an inspiration and/or information source for designing other typologies different from the ones generated in the solution space. In other words, the case study adjustment seeks to answer questions, such as what would Felix Candela do if he wanted to design an umbrella shell that covers a 50 by 60 m space, supported on four edges using his umbrella shell typology? Or how would the bubble shell designed by Heinz Isler for the COOP warehouse perform if it was supported on only four corners? The adjustments that have been made to these case studies reveal how different typologies can be adjusted to be comparable with a specific generated typology stored in the solution space. Ultimately, it demonstrates how the results retrieved from a solution space can be expanded to other design problems that do not necessarily have the exact same boundary conditions. This goal justifies adjusting the case studies' boundary conditions and

dimensions, to see how closely they can be matched with the dimensions and boundary conditions of the cases in the solution space.

On a separate note, and as explained in section 7.2.5, it was noticed that the Rhino Membrane pressure should have been increased to get a synclastic surface. Based on this understanding, a new solution space is populated with all dome-shaped shells. This new solution space is used to map case studies onto, referred as *ParaGen ii* or *new solution space* in the following sections.

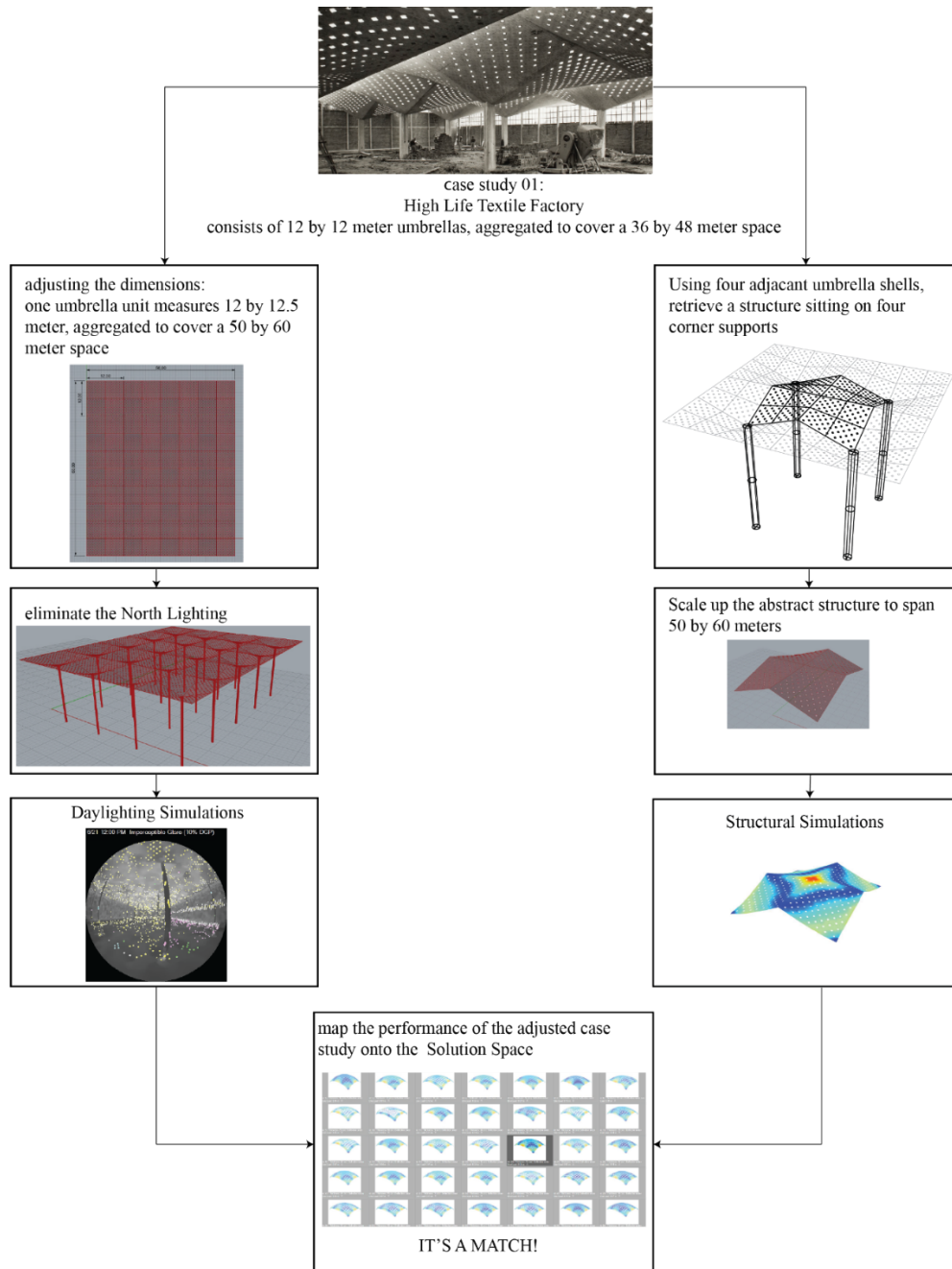


Figure 7.33. The process of adjusting the case studies for mapping onto the solution space

It should be noted that by making these adjustments, I am not strictly comparing the analysis results with the actual as-built structures. I am using the adjustment as a basis for geometric reference only to fit the model sizes of the new solution space. In the daylighting discipline, the north lighting is eliminated, while the number of sequenced umbrellas is increased from 12 umbrellas covering a 36 by 48 m space, to 20 umbrellas covering a 50 by 60 m space. It is expected that the overall daylight availability of the space is reduced by eliminating the north light. However, it is expected that after north light is eliminated, changing the overall dimension of the space from a rectangle with a 4 by 3 ratio (48 by 36 m) to a rectangle with a 6 to 5 ratio (60 by 50 m) while keeping the perforation ratio and the distribution of the holes constant, will not make a huge difference.

In the structural discipline however, scaling up or down can have huge structural implications to the end results. The goal is to support shells on four corners without any intermediate supports or columns. However, the limitation of this approach may be recognized: the shell thickness of the as-built project cannot be compared with the simulation results, as there may be other parameters that cannot be compared.

7.4.1 The original design of the High Life Textile Factory

One of the shells designed and built by Candela is the High Life Textile Factory (now the Cavalier Industries Factory) in the Coyoacán section of Mexico City (Figure 7.34). The umbrella shells are tilted to present a sawtooth profile, are perforated, and glass bricks are installed in the perforations. After the factory was used as a sewing and ironing shop, overheating problems arose; thus, the glass bricks were covered with heavy asphalt paper and tar to reduce the overheating of the interior (Garlock & Billington, 2008). A recent research paper assessed the structural as well as the daylighting performance of the shells in their original state as well as the current state (Emami, Giles, & von Buelow, 2018). This shell is selected as a case study to be computationally simulated and compared with the shells in the new solution space. The geometry is created in Rhino and Grasshopper, and then its daylighting and structural performance is assessed using the DIVA and Karamba plugins for Grasshopper.



Figure 7.34. High Life Textile Factory with perforations (Garlock & Billington, 2008)

Before analyzing the case study, Felix Candela's design and construction methods are discussed more. As noted in Chapter 3, Candela used hyperbolic paraboloids, also called hypars, in the design of his shells. As shown in Figure 7.35, a straight-edge hypar consists of four areas, one shaded in white. This section is then used to create an umbrella structure (Garlock & Billington, 2008).

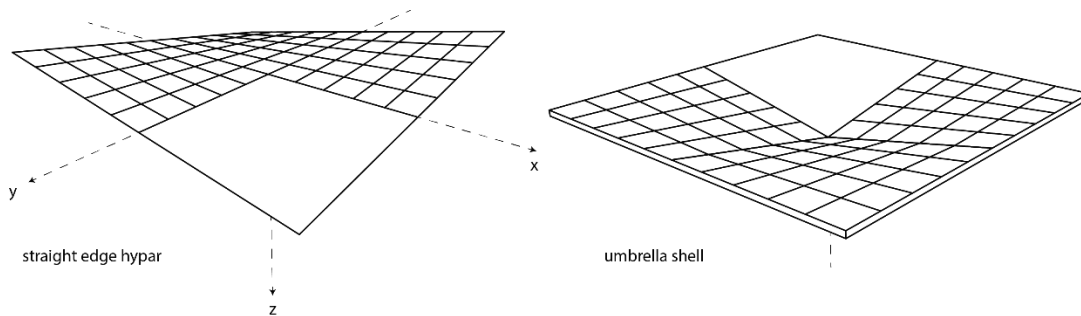


Figure 7.35. Straight-edge hypar with an area identified in white (a) an umbrella shell comprised of four areas (b), after (Garlock & Billington, 2008)

The advantage of hyperbolic paraboloids is that while they are doubly curved, they can be formed from straight lines. The construction of Candela's shells required scaffolding to support the form boards and then to mold the concrete. Once the forms were placed, steel reinforcing was added. Candela then placed a layer of cement grout over the form boards to obtain a smooth interior surface before the concrete was poured. The concrete was typically 4 cm (1.5 inch) thick. His hypar structures were innovative not only in terms of their form, but also because of his use of an umbrella-shaped foundation, as well as elimination of stiffening arches and edge beams in the

structure. In addition, he placed additional steel reinforcement in the edges that work in tension (Garlock & Billington, 2008).

In many design projects, Candela placed multiple umbrellas in sequence to create large roof coverings. He introduced daylight to the spaces that were covered with multiple umbrellas either by tilting the umbrellas to create a sawtooth roof (Figure 7.36), by varying the height of umbrellas in each row, or even by piercing the shell with glass bricks (Garlock & Billington, 2008). In the cases in which the umbrellas were tilted, they “were grouped horizontally and isolated by flat ribbons of light. Every three feet or so, slender struts connect their edges, adding rigidity to the shells, guarding against sway” Faber (1963, p.111). Each pavilion is a huge cantilever which is self-supporting under symmetric loading, but very unstable under local patterned loading that would cause instability all the way back to the supporting perimeter walls.

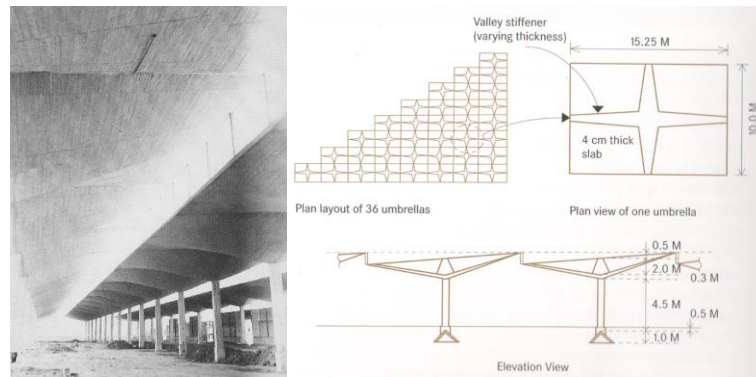


Figure 7.36. Plan and section drawings of Rio's Warehouse with tilted umbrellas (Garlock & Billington, 2008)

Candela's first umbrella built in 1952, was measured 10 by 10 m (33 by 33 foot) with a rise of 1 m (3 feet 4 inches), and a thickness of 4 cm (1½ inch). His second experimental umbrella was built in 1953 and measured 8 by 8 m (25 by 25 feet), with a rise of 0.75 m (2 feet 4 inches), and a thickness of 8 cm (¾ inch). After building these two experimental umbrellas, he built Rio's Warehouse in 1954 (Figure 7.36), consisting of umbrellas measuring 10 by 15 m (32 by 49 feet) with a 2-m (6½ foot) rise. Rio's Warehouse “initiated the umbrella shell as Candela's trademark for low-cost industrial construction” (Garlock & Billington, 2008, p.102). The features of these umbrella structures are summarized in Table 7.5.

Candela later mentions that the optimum rise depends on the area covered by the umbrella, and his rule of thumb was that the rise is roughly equal to 0.015 times the area (rise = 0.015 x area) (Garlock & Billington, 2008, p.100). He also notes that umbrellas have a coverage size limitation

of 185 m² (2000 square feet), and if the area of the umbrella, and thus its rise, increases, controlling deflections will be difficult.

The High Life Textile Factory was built after Rio's Warehouse, in 1954–55 in the Coyocan section of the Mexico City. The then-44-year-old Candela designed and built his first perforated umbrella shell which also presents a saw-tooth profile. The square-shaped perforations in this shell are rotated 45 degrees in the direction of straight-line generators. To understand the reason behind the rotation of the perforations, the placement of reinforcement in the shell needs to be examined. Candela analyzed the umbrella shells using the membrane theory, and noticed that the direction of tension and compression forces along the umbrella structure acts at 45 degrees in the direction of the straight-line generators (Figure 7.37-a). He then placed steel reinforcement in a matching layout, which can be seen in a picture from the construction of one of his umbrella shells (Figure 7.37-b). The practical placing of the reinforcement distribution in the shell explains the 45-degree rotation of square perforations so they fit in the grid created between the intersecting reinforcements (Figure 7.38).

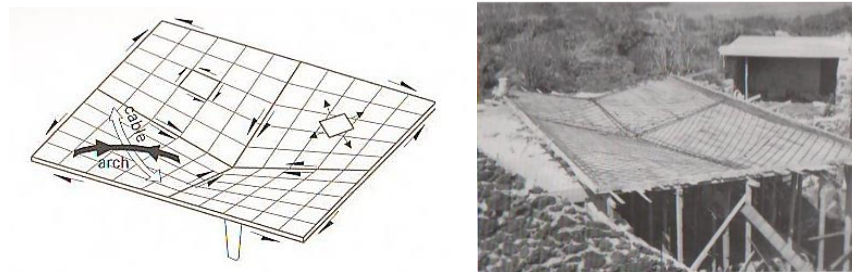


Figure 7.37. Force flow in the umbrella shell (a); reinforcement placement in the shell (b) (Garlock & Billington, 2008)

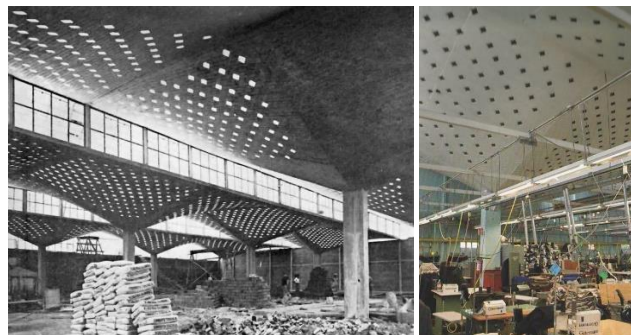


Figure 7.38. The 45-degree rotation of perforations (a); factory in use (b) (Garlock & Billington, 2008)

The dimensions of the factory are not found in the examined literature. However, it can be measured using Google Maps (Decimal Degrees = 19.354074, -99.162826), and its width and

length measured as 12 by 12 m. Looking at the site plan, an array of 4 by 3 umbrellas is recognized (Figure 7.39-a). It is noticeable that the sawtooth roof is facing north (Figure 7.39-b). The High Life Textile Factory’s rise and thickness is assumed to be similar to Rio’s Warehouse, which has a rise of 2 meters and a thickness of 4 cm. Since the perforations are currently covered, their dimensions could not be measured. For that purpose, old photographs of the building are scrutinized, and the square perforations assumed to be 15 by 15 cm (6 by 6 inches). The plan view of the High Life Textile Factory is reproduced using the measured dimensions (Figure 7.40).

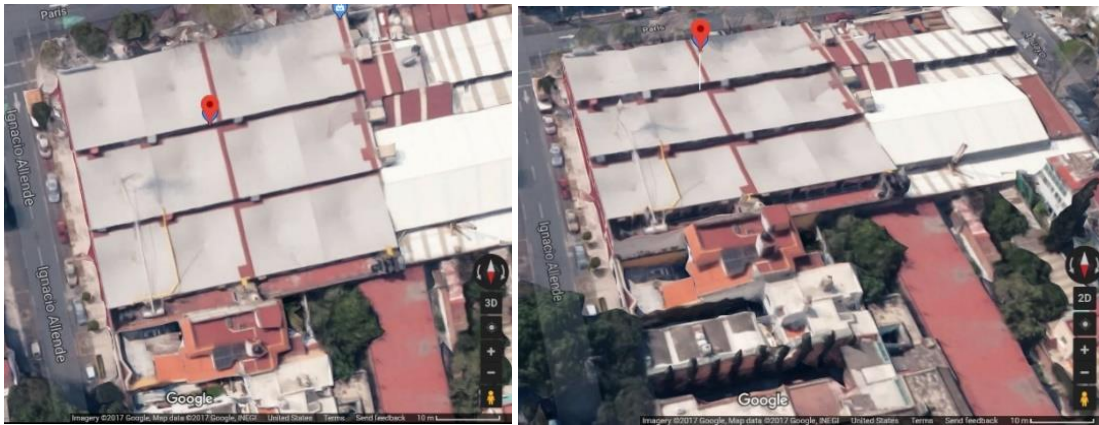


Figure 7.39. Site plan (a); 3d view (b) of the High Life Textile Factory captured from Google Maps

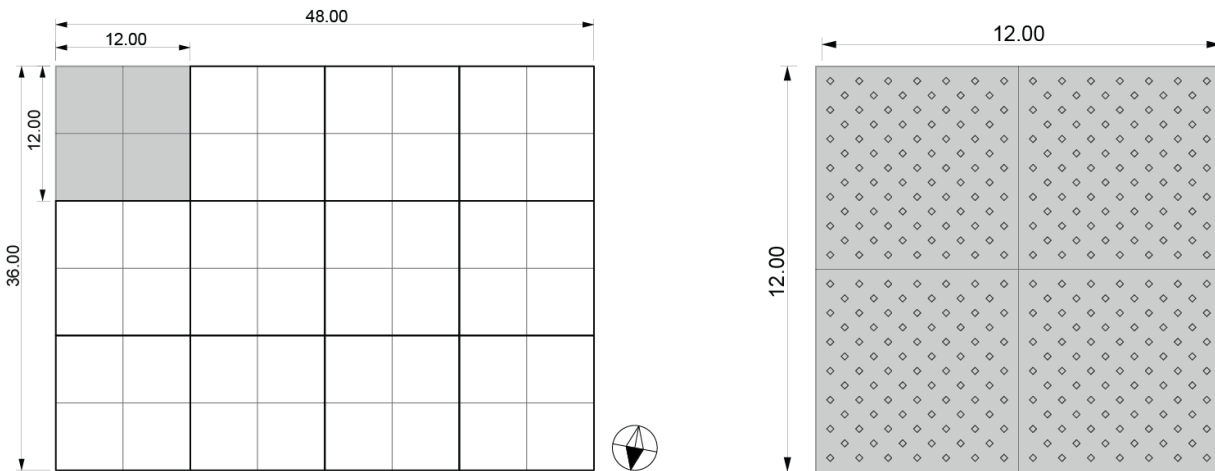


Figure 7.40. The plan view of High Life Textile Factory recreated in Rhino based on the measured dimensions (a); the magnified drawing of one umbrella unit with the assumed dimensions for the perforations (b)

A summary of the dimensions of the two experimental umbrella shells, Rio’s Warehouse, as well as the measured dimensions of the High Life Textile Factory, are summarized in Table 7.5. The rise/area ratio is calculated for each shell, to be compared to Candela’s suggested rule of thumb of 0.015.

Table 7.5. comparing dimensions and thickness of the first umbrellas built by candela

	Length [m]	Width [m]	Area (limit 185 m ²)	Rise [m]	Rise/Area ratio (optimal 0.015)	Thickness [cm]
First experimental umbrella (1952)	10	10	100	1	0.01	4
Second experimental umbrella (1953)	8	8	64	0.75	0.011	8
Rio's Warehouse (1954)	10	15	150	2	0.013	4
High Life Textile Factory (1954–55)	12	12	144	2	0.013	4

* The length and the width are measured from Google Maps, while the rise and the thickness are assumed to be similar to Rio's Warehouse.

7.4.2 Adjusted High Life Textile Factory for daylighting simulation


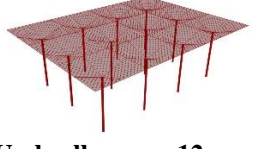
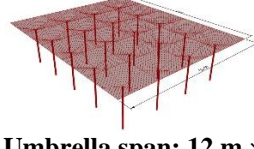
The shells that are generated in the new solution space do not have any side lights; perforations are the only source of daylighting. Therefore, the tilt of the umbrellas, and thus the north lighting, is eliminated to create a case more directly comparable with other cases. In addition, the dimensions of each umbrella unit are changed from 12 by 12-m to 12.5 by 12-m, and instead of being arrayed in a 4 by 3 grid covering a 48 by 36-meter space, arrayed in a 4 by 5 grid to cover a 50 by 60-m space. The final assembly dimensions correspond with the shells' dimensions in the new solution space covering a 50 by 60-m space. The original shell, as well as the adjusted variations, are summarized in Figure 7.41.



Figure 7.41. As-built High Life Textile Factory (a); eliminating North light (b); adjusting the size of each umbrella unit and arraying them in a 4 by 5 grid to cover a 50 by 60-m space (c)

It is important to understand how eliminating the side lights and then changing the dimensions of the space affects the daylighting performance of the space. Therefore, a comparative simulation study has been conducted for the as-built shell and the adjusted shells. The DIVA plugin for Grasshopper is used for daylighting analysis. Single pane clear glazing, as well as translucent glazing, which is similar to the shells in the database, is used in the simulations, and Boston is used as the location. The results are summarized in Table 7.6, and a false-color image of the simulation result for an arrayed set of umbrellas covering a 50 by 60-m space using clear glazing is presented in Figure 7.42.

Table 7.6. Comparing daylighting performance of the built shell with the adjusted variations

	 Umbrella span: 12 m × 12 m Coverage 48 m × 36 m With clerestory	 Umbrella span: 12 m × 12 m Coverage 48 m × 36 m No clerestory	 Umbrella span: 12 m × 12.5 m Coverage 60 m × 50 m No clerestory
sDA*	60%	6%	6%
DAv-over 300 lux*	74%	62%	65%
DAv-over 3000 lux*	25%	27%	27%
DAv-under 300 lux*	0	9%	6%
Daylight Glare Rating*	Imperceptible	Imperceptible	Imperceptible
sDA**	0	0	0
DAv-over 300 lux**	0	1%	2%
DAv-over 3000 lux**	0	0	0
DAv-under 300 lux**	1	99%	97%
Daylight Glare Rating**	Imperceptible	Imperceptible	Imperceptible

*glazing-single pane-88

** generic translucent panel_20

***location is set as Boston, the same location as the shells in the generated solution space

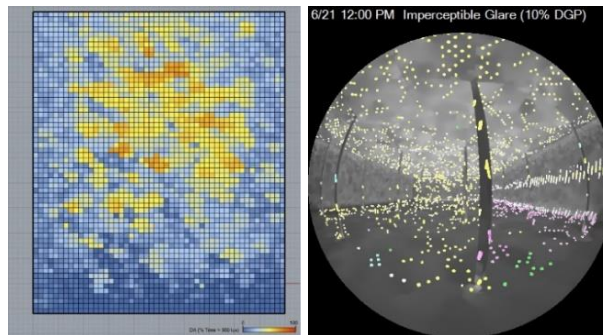


Figure 7.42. Spatial daylight autonomy distribution and light oversupply of the High Life Textile Factory

7.4.3 Adjusted High Life Textile Factory for structural simulation

The Karamba plugin for Grasshopper is used for structural analysis, where maximum deformation, von Mises stress levels, weight, and material costs are recorded. Setting the boundary conditions for structural analysis requires careful consideration, since the original design of the High Life Textile Factory has interior columns that are supporting the umbrellas every 12 m in width and in length. When compared to a shell spanning a 60 by 50-m space without any interior columns and only supported at its corners, the closely spaced umbrellas outperform the shells. Therefore, the umbrella shells are abstracted to allow a comparable structural analysis to be conducted.

In the first phase of analysis, as illustrated in Figure 7.43, four umbrellas measuring 12 by 12 m (the original size of the umbrellas) are placed to form a square shape, and then the inner assembly sitting on four columns is extracted. This assembly, which is resting on corner supports, is analyzed structurally; the results are summarized in Table 7.7.

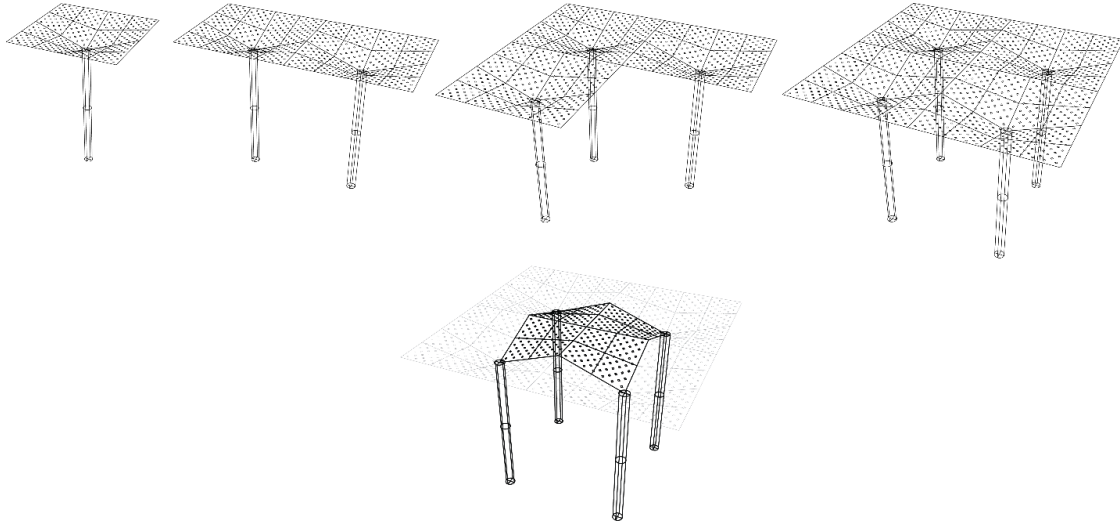
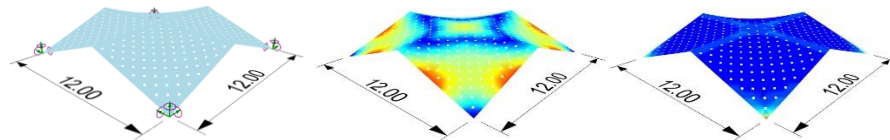


Figure 7.43. (top row) 12.5 by 12-meter umbrellas are assembled to shape a larger square; (bottom row) four central sections at the intersection of the umbrellas are isolated and scaled up for structural analysis

Table 7.7. Structural performance assessment of a 12 by 12-m assembly



Width [m]	12
Length [m]	12
Rise	2.16
Rise/Area ratio	0.015
Hypar surface area [m²]	150
Perforation ratio	0.047
Hypar thickness [cm]	5
D.L. Deflection [cm]**	0.27
L.L. Deflection [cm]**	0.27
Total deflection [cm]	0.52
Von Mises stress at Q-3 [MPa]	1.11
Weight [tones]	16.8
Concrete price [\$]	2858
sDA of this unit arrayed*	6%

* without north light, using clear glazing. Comprehensive results are summarized in Table 7.6

**D.L. stands for dead load, and L.L. stands for live load

In the second phase, this assembly is scaled up to cover a 50 by 60-m space for comparative structural analysis. The inherent limitations of scaling, which are explained in section 7.4, need to

be recognized. The objective of scaling up is to speculate on how the umbrella shell typology would perform if it was designed to cover a 50 by 60-m space and only supported by four corner supports. For the purpose of scaling up, the dimensions of the umbrella units are changed from 12 by 12-m to 12.5 by 12-m since this module's dimensions allow the 50 by 60-m space to be fully covered with whole umbrella units. The abstract assembly is then scaled up, while having Candela's efficient rise-to-area ratio of 0.015 in mind. As noted before, Candela mentions that umbrellas have a coverage size limitation of 185 m² (2000 square feet), and if the area of the umbrella, and thus its rise, increases, controlling deflections will be difficult.

Maintaining the 0.015 rise-to-area ratio, the 12.5 by 12-m assembly unit with a rise of 2.25 m becomes a 50 by 60-m assembly unit with a rise of 45 m, labeled Morphology-A (Figure 7.40-a). Since this shell has a height much greater than the 15-m height limit of the courtyard of all other shells in the solution space, a second rise-to-area ratio of 0.005 is applied to arrive at Morphology-B, with a rise of 15-meters (Figure 7.44-b). Finally, a third ratio of 0.003 is applied to arrive at Morphology-C, with a rise of 9-m (Figure 7.44-c). The geometric properties of the shell morphologies are summarized in Table 7.8.

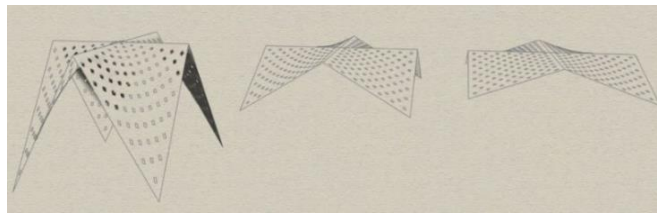



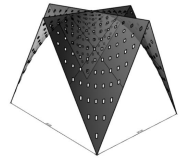
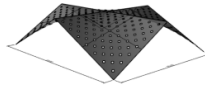
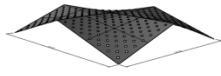
Figure 7.44. Abstract morphology-A with a rise of 45 m (a); Abstract morphology-B with a rise of 15 m (b); Abstract morphology-C with a rise of 9 m (c)

Table 7.8. Dimensions of the scaled-up hypars

	Original umbrella	Abstract morphology-A	Abstract morphology-B	Abstract morphology-C
Width [m]	12.5	50	50	50
Length [m]	12	60	60	60
Area [m²]	150	3000	3000	3000
Rise	2.25	45	15	9
Rise/Area ratio	0.015	0.015	0.005	0.003
Thickness [cm]	5	In the range of 5 to 35	In the range of 5 to 35	In the range of 5 to 35

In the third phase, the effect of scaling up is explored. When a 12 by 12.5-m assembly is scaled up to become a 50 by 60-m assembly, the dimensions of the shell and its thickness is being multiplied by 5. Following this, deflection of the initial 5-cm thick assembly as well as the three morphologies with a thickness of 25 cm summarized in Table 7.9 are analyzed.

Table 7.9. Structural performance comparison of 5 cm shell with its scaled-up versions

	Original umbrella 	A-25 	B-25 	C-25 
	12.5 × 12 m	50 × 60 m	50 × 60 m	50 × 60 m
Rise	2.25	45	15	9
Rise/Area ratio	0.015	0.015	0.005	0.003
Thickness [cm]	5	25	25	25
Dead load deflection [cm]	0.3	22	5.2	6.7
Live load deflection [cm]	0.26	4	0.93	1.2
Total deflection [cm]	0.57	27	6.1	7.9

Comparing the initial 12 by 12.5-m assembly with Morphology A-25, when the perforation ratio is constant while dimensions and thickness are multiplied by 5, D.L. deflection is increased by a factor of 73 (22/0.3), whereas L.L. deflection is increased by a factor of 15 (4/ 0.26). In other words, after scaling up the structure, the effect of dead loads is huge compared to the constant live loads.

Comparing the initial 12 by 12.5-m assembly with C-25, when perforation ratio is constant but the dimensions and thickness are multiplied by 5 and the rise-to-area ratio is decreased to 0.003, D.L. deflection is increased by a factor of 22.3 (6.7/0.3), whereas L.L. deflection is increased by a factor of 4.6 (1.2 / 0.26) in C-25. Again, the effect of dead loads becomes huge compared to live loads when the structure is scaled up.

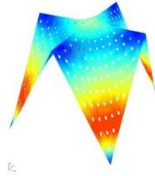
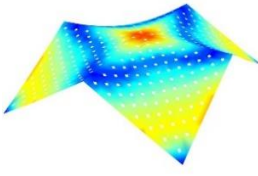
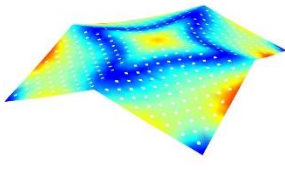
This analysis makes the point that after scaling up the structural system the results can no longer be expanded to the original case study; however, the objective of case study in this research is to explore how this shell typology would have performed if it was built with certain boundary conditions, to later be compared with other shell typologies stored in a solution space.

In the fourth phase, each umbrella morphology is structurally simulated using different thicknesses, ranging from 5 cm to 35 cm in 5-cm increments. As an example, when Morphology

A with a thickness of 5 cm is simulated, it is denoted *A-5*, whereas *B-30* indicates Morphology B with a thickness of 30 cm. The values for maximum deflection, von Mises stress levels, weight, and concrete cost are then recorded for each variation. Afterward, three geometries, each belonging to one of the morphology groups that have matching performance criteria are selected. The criteria for choosing the matching cases is that first, they hit the criteria limit; and second, they have close, if not matching, performance values.

The first criterion for choosing the performative cases is that deflection under L.L. should ideally be less than 2.5 cm (1 inches) and not more than 5 cm (2 inches). Three morphologies were selected that meet this limit while having similar performance values. *A-30*, *B-15*, and *C-15* are 30-cm, 15-cm, and 15-cm thick morphologies, respectively, with corresponding L.L. deflections of 2.7, 2.8, and 3 cm (Table 7.10). Other performance criteria, such as von Mises stress, are then checked to make sure they meet the criteria (as explained in Appendix B, von Mises at Q3 < 15 MPa). All cases have a von Mises stress value about 4 MPa, which is within limits and thus is not a controlling factor. It should be noted that daylighting performance is based on the assembly of smaller umbrella units and the performance values are discussed in the previous section.

Table 7.10. Selected hypar iterations with various rise/area ratios that have matching performance

	A-30	B-15	C-15
			
Width [m]	50	50	50
Length [m]	60	60	60
Rise	45	15	9
Rise/Area ratio	0.015	0.005	0.003
Hypar surface area [m²]	4935	3286	3107
Perforation ratio	0.056	0.056	0.056
Hypar thickness [cm]	30	15	15
D.L. Deflection [cm]*	18	9.4	10
L.L. Deflection [cm]*	2.7	2.8	3
Total deflection [cm]	21	12	13
Von Mises stress at Q-3 [MPa]	3.35	2.89	3.62
Weight [t]	3,287	1,092	1,034
Concrete price [\$]	558,931	185,966	175,811
sDA**	10.4%	10.4%	10.4%

*D.L. stands for dead loads and L.L. stands for live loads

**sDA stands for spatial daylight autonomy. The sDa values are retrieved from simulating the original geometry of the High Life Textile Factory, explained in the previous section (Table 7.5).

Knowing that all three cases presented in Table 7.10 meet the performance criteria limits and have similar performance values, they can be compared with each other in terms of their economic performance (cost). C-15, with the lowest weight and concrete price, is superior to the other three; thus, it is selected to be mapped onto the solution space (Figure 7.45).

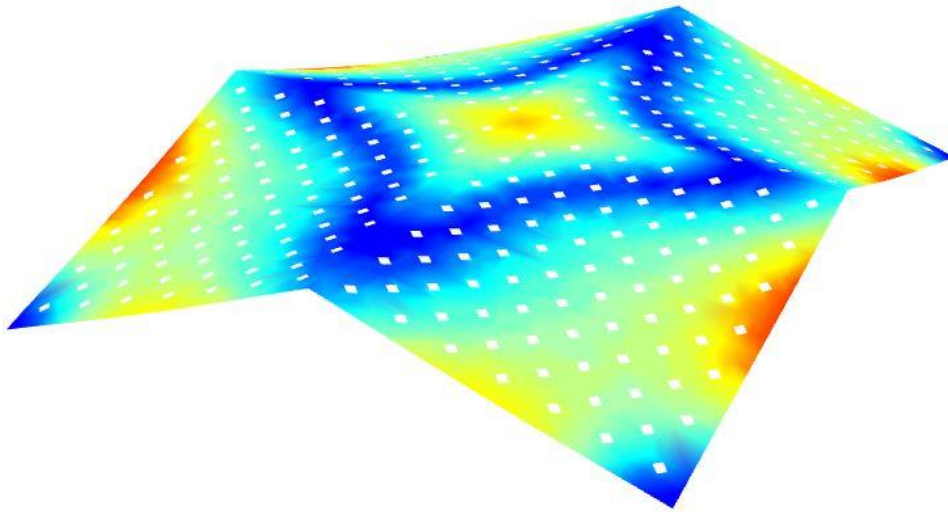


Figure 7.45. C-15, the abstract model of Candela's umbrella shell. Its structural performance will be mapped onto the ParaGen design space.

7.4.4 Mapping the abstract High Life Textile Factory onto the new solution space

Once three hypars with similar performance values are identified, the most economical one, C-15, is identified. Its performance values are then used to explore and filter the new solution space with the goal of finding a different shell typology that has matching performance criteria. The criteria used for exploring the new solution space are summarized below:

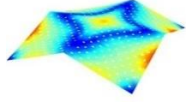
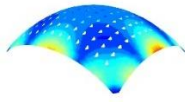
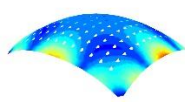
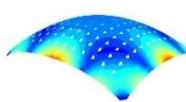
$$\text{Perforation ratio} \leq 0.06 \text{ and } \geq 0.05$$

$$\text{Shell thickness} = 15 \text{ cm}$$

$$\text{L.L. deflection} \leq 4.5 \text{ cm (0.045 m)}$$

After applying these filters to the new solution space, three shells with matching performance criteria are selected (Table 7.11).

Table 7.11. Hypars' performance mapped onto shells generated with ParaGen to find matching shells

	C-15	Id-01 (ParaGen ii*)	Id-38 (ParaGen ii)	Id-43 (ParaGen ii)
				
Rise in width [m]	9	9	7.5	7
Rise in length [m]	9	9	7	7
Rise/Area ratio	0.003	0.003	0.0025	0.0023
Perforation ratio	0.056	0.06	0.05	0.05
Thickness [cm]	15	15	15	15
D.L. Deflection [cm]**	10	14.3	13.9	12.1
L.L. Deflection [cm]**	3	4.3	4.1	3.6
Total deflection [cm]	13	19	18	16
Von Mises stress at Q-3 [MPa]	3.62	2.8	3	2.9
Weight [t]	1034	1201	1141	1137
Concrete price [\$]	175,811	204226	194037	193358
sDA***	6% (clear glazing) 0% (translucent glazing)	11.7% (clear glazing)	3.7% (clear glazing)	0% (translucent glazing)

*A second solution space is generated using ParaGen to populate more dome-shaped typologies with adjusted form finding pressure in the Rhino Membrane. The glazing can alternate between clear and translucent in this database.

** D.L. stands for dead load, and L.L. stands for live load.

*** sDA (spatial daylight autonomy) values may be based on either translucent or clear glazing.

By examining the properties of the matching shells from the new solution space it can be observed that their rise/area ratio is in the range of 0.0016 to 0.0026, close to that of case C-15. The abstracted version of Candela's hyper (C-15) with a thickness of 15 cm seems to be superior in terms of weight compared to the matching generated shells in the new solution space. The L.L. deflection for C-15 is also slightly smaller than that of the generated shells.

7.5 Case study 02: COOP Warehouse, a bubble shell with multiple openings

This section explains the second case study, COOP Warehouse, designed and built by Heinz Isler. The first sub-section describes Isler's design and construction techniques, with a focus on bubble shells that either have single or multiple openings, followed by an in-depth discussion of the COOP Warehouse. The second and third sub-sections explain how the boundary conditions are adjusted for daylighting and structural performance for a comparative study. The goal is to compare shells that cover the same floor area of 3000 m² (50 by 60 m), and also to arrive at boundary conditions that are as close as possible to those of the shells in the new solution space.

The fourth sub-section explains how the case study is mapped on to the new solution space that was generated. This process is summarized in Figure 7.46.

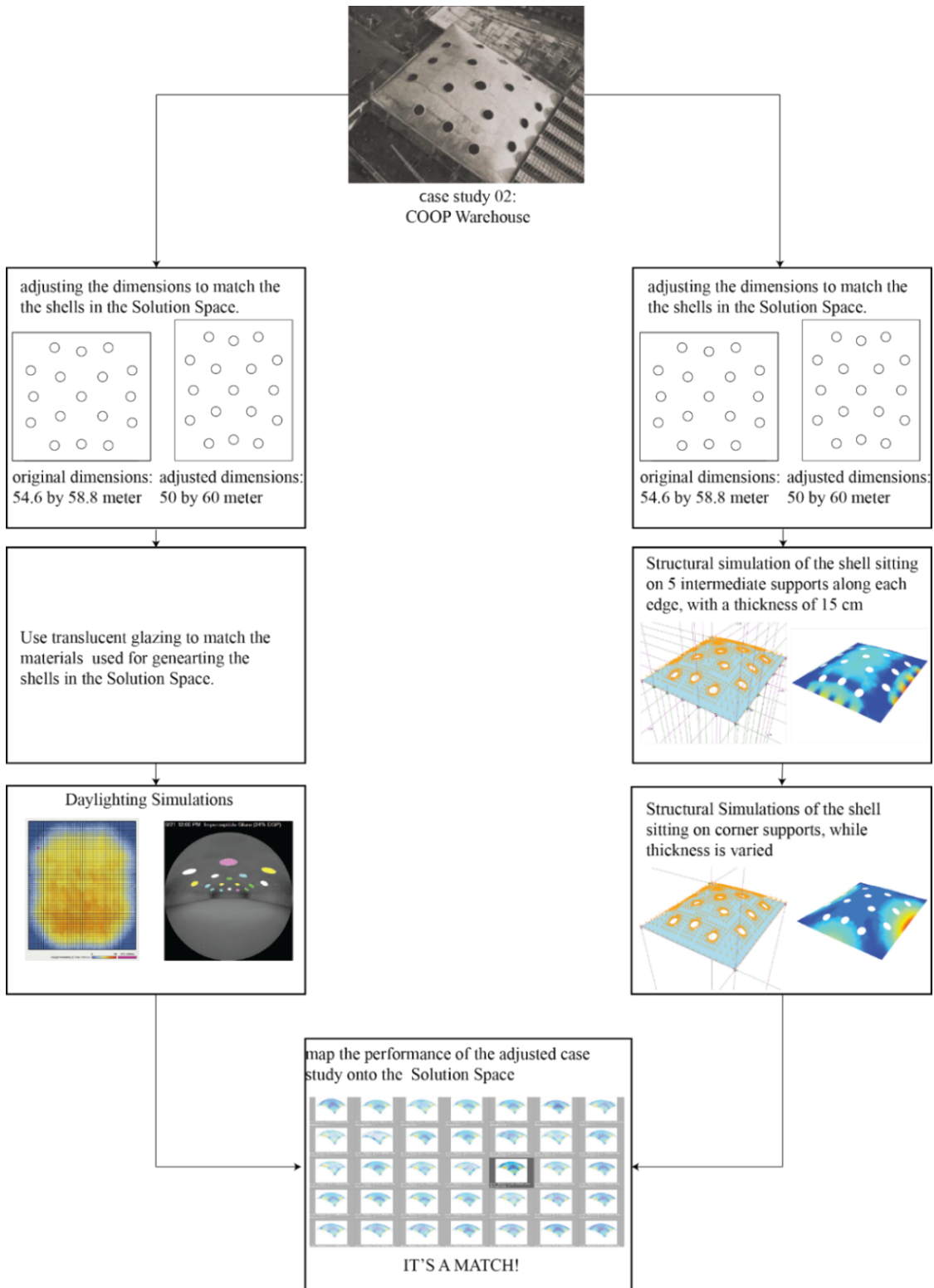


Figure 7.46. The process of adjusting the case studies for structural and daylighting simulations

7.5.1 The Original Design of the COOP Warehouse

The largest of Isler's early bubble shells is a distribution facility for the COOP in Wangen bei Olten built in 1960 (Figure 7.47).

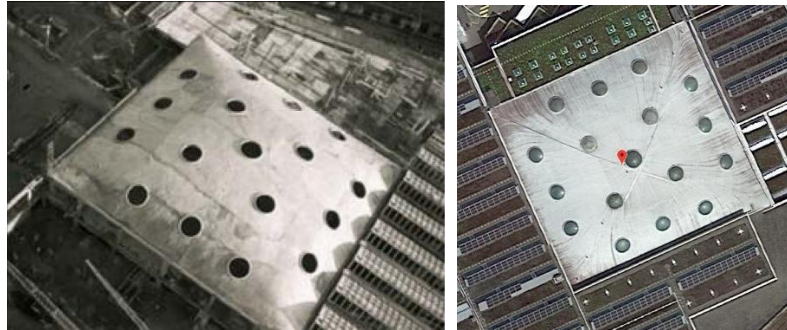


Figure 7.47. The COOP storage and distribution center by Heinz Isler (Ramm, 2011) (a); Google maps (b) ($47^{\circ} 20' 20.70''$ N, $7^{\circ} 51' 50.78''$ E)

The COOP Warehouse is the largest bubble shell that Isler built, and is still in use (Figure 7.48). The 54.6 by 58.8-m shell has an approximate thickness of 150 mm in the critical areas. It has six intermediate supports along each edge of the shell, resulting in a column-free area of over 3200 m². The highest point of the shell is 15 m above the ground; 6.63 m is from the height of the perimeter columns and 9 m is the rise of the shell itself. The shell contains 17 circular openings, including the 4.0 and 4.5-meter diameter openings that represent 4% of the total roof area (Figure 7.49). Isler constructed a 1:50 scale model of this design from polyester in his laboratory. He noticed that “the loads are carried in arch-like sections of the shell, from corner to corner along the diagonals and these arches lean against each other” (Chilton, 2000, p.5). He placed the holes in the shell in a way that the corner to corner arching of the shell is not interrupted.

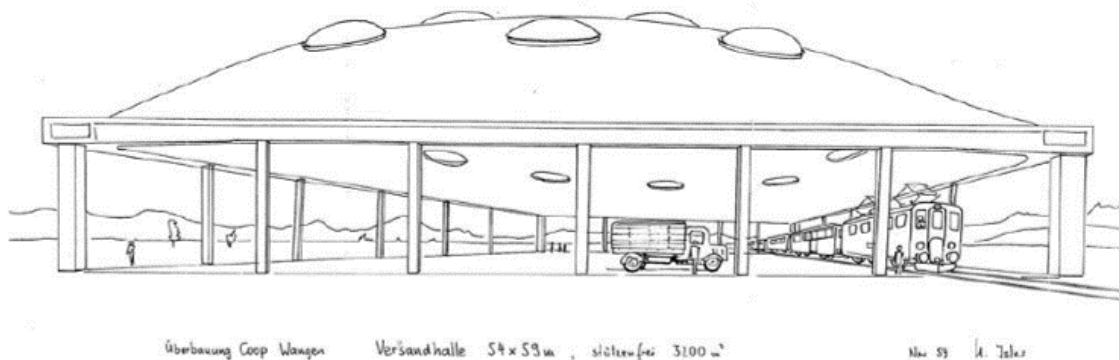


Figure 7.48. Isler's sketch for COOP Warehouse, (Bösiger, 2011)

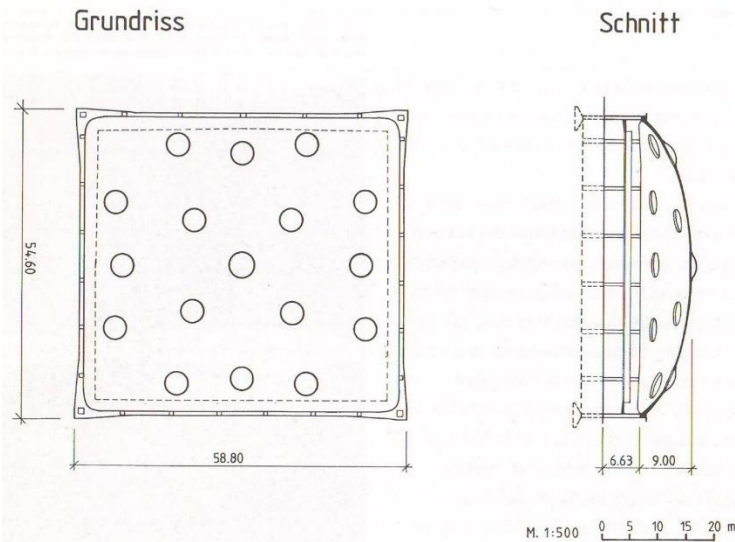


Figure 7.49. Plan and section of COOP Warehouse (Chilton, 2011)

Reviewing Isler’s different bubble shells, the typical span and rise of these shells are summarized in Table 7.12.

Table 7.12. Comparing dimensions and thickness of the first umbrellas built by Isler

	Length	Width	Area (limit 185 m ²)	Rise [m]	Span/Rise ratio	Thickness [cm]
Bubble shells with one central skylight	20 m	20 m	400	2.6	7.69	8 - 10 *
Bubble shells with multiple openings	39 m	39 m	1521	5	7.8	8 - 10*
COOP Warehouse (1960)	54.6 m	58.8 m	3210	9	6.5 m	15 cm**

*Ramm, 2011: 52

**Ramm, 2011:56

The next section explains how the boundary conditions of the COOP Warehouse are adjusted for daylighting and structural analysis to be comparable with the shells in the solution space.

7.5.2 COOP Warehouse adjusted for daylighting simulation

The dimensions of the COOP Warehouse are changed from 54.6 by 58.8 m to 50 by 60 m to match the shells generated in the solution space. Other than the measurements, the relative placement of the openings is unchanged in the adjusted shell. The radius of the openings is 2 m, and as in other cases, translucent glazing is used for simulation. The plan view of spatial daylight autonomy and the fish-eye image of the glare analysis are illustrated in Figure 7.50, while the performance values are summarized in Table 7.13.

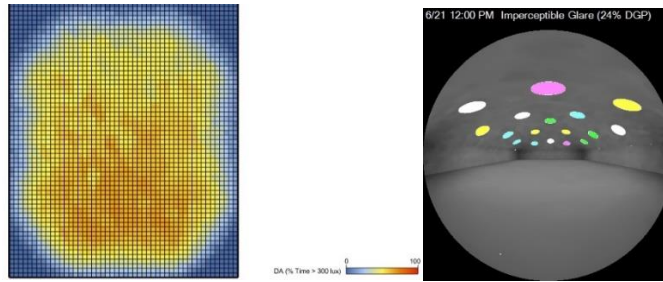


Figure 7.50. Spatial daylight autonomy distribution and light oversupply of the COOP Warehouse

Table 7.13. Daylighting performance of the adjusted COOP warehouse

Spatial daylight autonomy (translucent glazing)	45%
DA_v* oversupply (translucent glazing)	0.27
Daylight glare rating at noon on June 21st (translucent glazing)	Imperceptible glare

*DA_v stands for daylight availability, and DA_v oversupply indicates if the light that is 10 times more than the required threshold (300 lux x 10 = 3000 lux) is present more than 5% of the time.

7.5.3 COOP Warehouse adjusted for structural simulation

The dimensions of the COOP Warehouse are changed from 54.6 by 58.8 to 50 by 60 meters to match the dimensions of the generated shells in the solution space. Placing the supports for structural simulation requires careful consideration, as the original building has six intermediate supports, while the generated shells in the solution space have only corner supports. Therefore, first the original boundary conditions are used for structural simulation of the 15-cm-thick shell resting on five intermediate supports along each edge (Figure 7.51).¹¹ The size and number of the openings is not varied. The performance of the shell is summarized in Table 7.14.

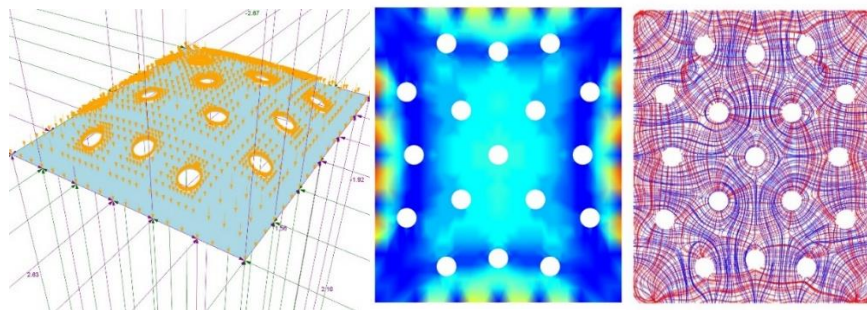


Figure 7.51. structural supports along the edge (a); maximum deflection (b); principle stress lines, blue representing compression and red representing tension (c)

¹¹ Although the original shell has six intermediate support, since the dimensions are adjusted from 54.6 by 58.8 m to 50 by 60 m, the number of intermediate supports is reduced to five.

Once the performance of the shell with the original boundary conditions is assessed, the boundary condition is changed to four corner supports (Figure 7.52), while the thickness is varied from 15 to 35 cm in 5 cm increments. The goal is to find a case with corner supports with performance that matches the performance of the shell with five intermediate supports along each edge.

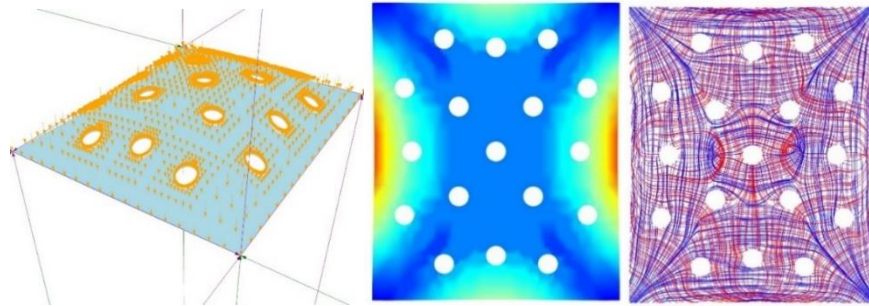


Figure 7.52. Structural supports at the corners (a); maximum deflection (b); principle stress lines, blue representing compression and red representing tension (c)

Table 7.14 summarizes the performance of the COOP warehouse resting on five intermediate supports, as well as the same shell resting on corner supports only with increased thickness. The live load deflection in the latter case is way greater than a shell with intermediate supports. Therefore, thickness is increased to a point that the live load deflections are only within the limits.

Table 7.14. Performance values for the COOP warehouse with adjusted dimensions of 50 by 60 meter

	Adjusted COOP Warehouse boundary condition: five intermediate supports along each edge	Adjusted COOP Warehouse boundary condition: corner supports only
Rise in width [m]	9	9
Rise in length [m]	9	9
Rise/area ratio	0.003	0.003
Perforation ratio	7%	7%
Thickness [cm]*	15	35*
D.L. Deflection [cm]**	0.67	26
L.L. Deflection [cm]**	0.21	3
Total deflection [cm]	0.88	29
Von Mises stress at Q-3 [MPa]	1.21	7.79
Weight [t]	1074	2507
Concrete price [\$]	182,657	426,201
sDA (with translucent glazing)**	45%	45%

*Thickness was varied from 15 to 40 cm, and the case with an acceptable (not matching) L.L. deflection is selected

** D.L. stands for dead load, L.L. stands for live load, and sDA stands for spatial daylight autonomy

7.5.4 Mapping the COOP Warehouse onto the shells generated using ParaGen

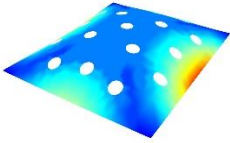
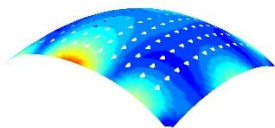
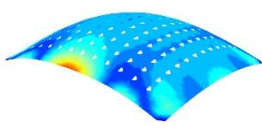
Once the adjusted COOP shell is identified, its performance values are used to explore and filter the solution space with the goal of finding a different shell typology that offers similar performance. The criteria used are summarized below:

$$\text{Perforation ratio} \leq 0.07 \text{ and } \geq 0.06$$

$$\text{L.L. deflection} \leq 3 \text{ cm and } \geq 2 \text{ cm}$$

After applying these filters to the new solution space, two shells are found, as summarized in Table 7.15. These cases have a perforation ratio that is close to that of the case study, but they have lower deflection under live loads.

Table 7.15. Hypars' performance mapped onto ParaGen's generated shells to find matching shells

	Adjusted Warehouse structural supports	COOP corner	Id-192 (ParaGen ii*)	Id-202 (ParaGen ii*)
				
Rise in width [50 m]	9		4.5	3
Rise in length [60 m]	9		8.5	5.5
Span-to-rise ratio in width	5.5		11.1	16.7
Span-to-rise ratio in length	6.6		7.06	10.91
Perforation ratio	7%		6%	6%
Thickness [cm]	35		20	10
D.L. deflection [cm]*	26		10.5	6
L.L. deflection [cm]*	3		2.3	2.7
Total deflection [cm]	29		13	9
Von Mises stress at Q-3 [MPa]	7.79		2.7	3.1
Weight [t]	2507		1497	745.4
Concrete price [\$]	426201		254595	126711
sDA *	45% (with clear glazing)		0 (translucent glazing)	0 (translucent glazing)

*A second solution space is generated using ParaGen to populate dome-shaped typologies with adjusted form finding pressure in the Rhino Membrane. The glazing can alternate between clear and translucent in this database.

** D.L. stands for dead load, L.L. stands for live load, and sDA stands for spatial daylight autonomy

7.6 Discussion

The interrelation between parameter and performance, as well as performance in the two disciplines is discussed in this section. Figure 7.53 graphically represents this interrelation.

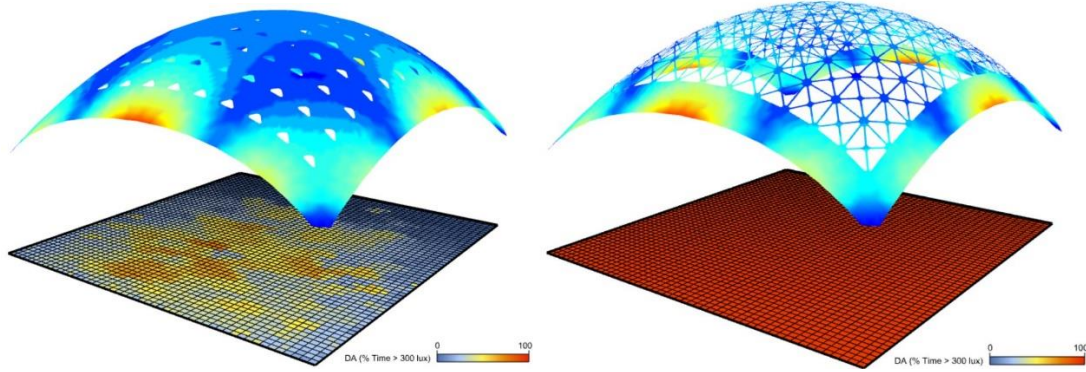


Figure 7.53. An image that graphically shows the simulation results from two different disciplines such as structures (stress plots) and daylighting (spatial daylight autonomy plots)

The statistical analysis elucidates the relationship between parameters and performance. In fact, almost all of the design parameters that were identified as common parameters between the two disciplines are found to affect performance in both disciplines. The statistical results suggest that the methodology for identifying the overlapping disciplines is effective. Looking at the heatmap presented in Table 7.4, the green color represents positive correlation, and the orange color represents negative correlation. The results are computed and explained for anticlastic surfaces (saddles).

7.6.1 Summarizing statistical results

- *Perforation ratio* and *weight* are negatively correlated, as shown by the general linear regression model (GLM). For example, when perforation ratio changes from 1% to 0%, the shell that is covering the 50 by 60-meter space weighs 14.76 tonnes less when other parameters are kept constant.
- *Thickness* and *weight* are positively correlated, as shown by the GLM. For example, when thickness is increased from 10 cm to 15 cm, the weight increases 63.89 tonnes when other parameters are kept constant.
- The results relating to *perforation ratio* and *deflection* cannot be generalized because the statistical analysis does not control for curvature at a micro level, which affects the geometric stiffness, and thus the performance values.
- *Thickness* and *deflection* are negatively correlated, as shown by the multinomial logistic model. It should be noted that on one hand, increasing the thickness makes the shell stiffer; however, on the other hand, increasing the thickness, increases the self-weight of the shell,

and thus its dead load. Under constant live load, an increase in thickness makes the shell stiffer, since its maximum deflection is reduced.

- Like the results for deflection, the results relating to *perforation ratio* and *von Mises stress* cannot be generalized because the statistical analysis does not control for curvature at a micro level, which affects the geometric stiffness, and thus the performance values.
- *Thickness* and *von Mises stress* are negatively correlated, as shown by the GLM. For example, if the thickness is increased from 10 cm to 15 cm, the von Mises stress is expected to decrease by 0.6% of the von Mises stress level of the base case when other parameters are kept constant.
- *Perforation ratio* and *structural costs* are negatively correlated, as shown by the GLM. It should be noted that in this analysis structural costs include concrete, formwork, and reinforcement costs. For example, if the perforation ratio is increased from 0% to 1%, the total structural costs decrease by 0.29% of the structural costs of the base case when other parameters are kept constant.
- *Thickness* and *structural costs* are positively correlated, as shown by the GLM. For example, if thickness is increased from 10 cm to 15 cm, total structural costs are increased by 4.3% of the structural costs of the solid shell when other parameters are kept constant.
- *Perforation ratio* and *sDA* are positively correlated, as shown by the ordinal logistic regression model. Using translucent glazing, a perforation ratio of 10% to 30% provides adequate daylight levels without reaching daylight oversupply.
- The ordinal logistic regression model does not show a correlation between *thickness* and *sDA*. This is counter-intuitive, as it is expected that an increase thickness, resulting in a deeper shaft, should diffuse daylight. The low settings for the radiance daylight simulations in DIVA may have caused this result, a hypothesis which requires further examination.
- *Perforation ratio* and *light oversupply* are positively correlated, as shown by the multinomial logistic regression model. Using translucent glazing, a perforation ratio of 20% or less does not create light oversupply. Considering the correlation of perforation ratio and sDA, as well as this correlation, a perforation ratio of 10% to 20% with translucent glazing seems to provide adequate daylight without light oversupply.

- The multinomial logistic regression model does not show a correlation between *thickness* and *light oversupply*. Once more, the caveat is that the simulation settings may cause this result, and it will require further exploration.
- *Perforation ratio* and *total operational energy* are positively correlated, as shown by a multinomial regression model. Adding more holes to the surface of the shell increases cooling loads in a heating-dominated climate such as Boston, which drives the total operational energy loads.
- *Thickness* and *total operational energy* are negatively correlated, as shown by a multinomial regression model. This suggests that increased concrete thickness offers insulation properties that lead to reduced heating loads, which drives the total operational energy loads.
- *Perforation ratio* and *energy costs* are positively correlated, as shown by an ordinal logistic regression model. The trend follows operational energy loads, and by adding more holes to the surface of the shell, cooling loads and thus the costs of cooling, increase.
- *Thickness* and *energy costs* are negatively correlated, as shown by an ordinal logistic regression model. The trend follows operational energy loads, and by increasing thickness, heating loads are reduced, which offers savings on heating costs.

I find that perforation ratio is the most significant parameter that affects both disciplines and a number between 10% to 20% is the recommended limit for shell structures when translucent glazing is installed; values in this range lead to adequate daylight without light oversupply. From an interdisciplinary standpoint, I studied the sensitivity of structural performance in this 10 to 20% range. By filtering the solution space using these values for perforation ratio, a trend line can be created to indicate correlation with structural criteria. By further limiting the results the working scenarios can be identified.

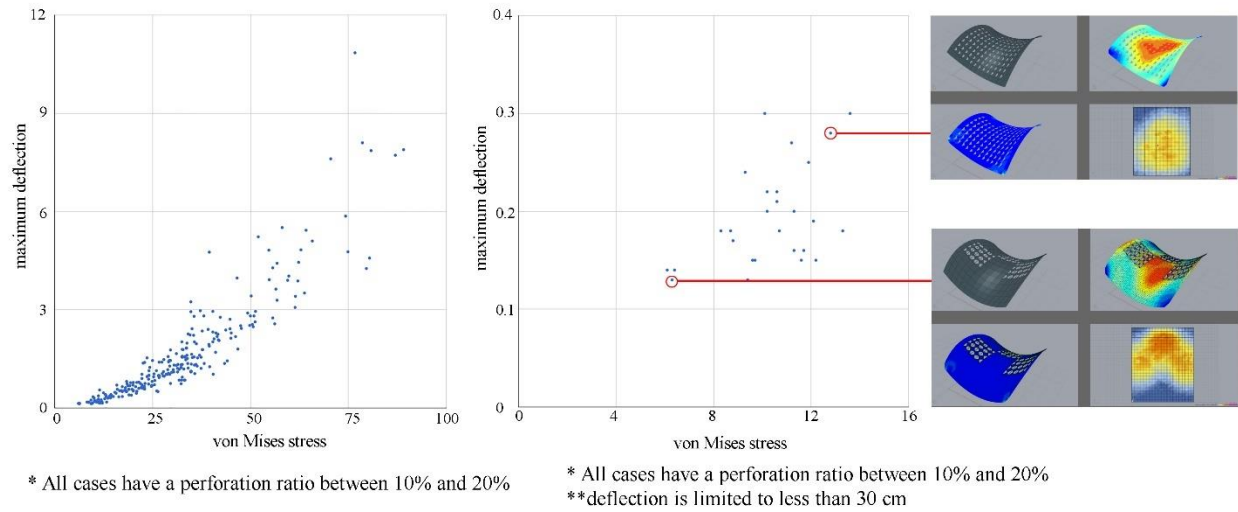


Figure 7.54. Cases that have an acceptable perforation ratio are filtered for their structural performance

7.6.2 Opportunities and limitations

One of the opportunities created by case study mapping and abstracting the boundary conditions is explained here. Morphology-A, which is retrieved by scaling up one of the umbrella units of the High Life Textile Factory, is used by Candela in one other building, the Church of Our Miraculous Lady, in Mexico City. The dimensions of the end module, which is the largest span measured on Google Maps, are 25 by 25 m. The end module is not perforated, and the edge beams are visible in the church. This example makes the point that scaling up a geometric entity requires different structural design strategies (Figure 7.55).

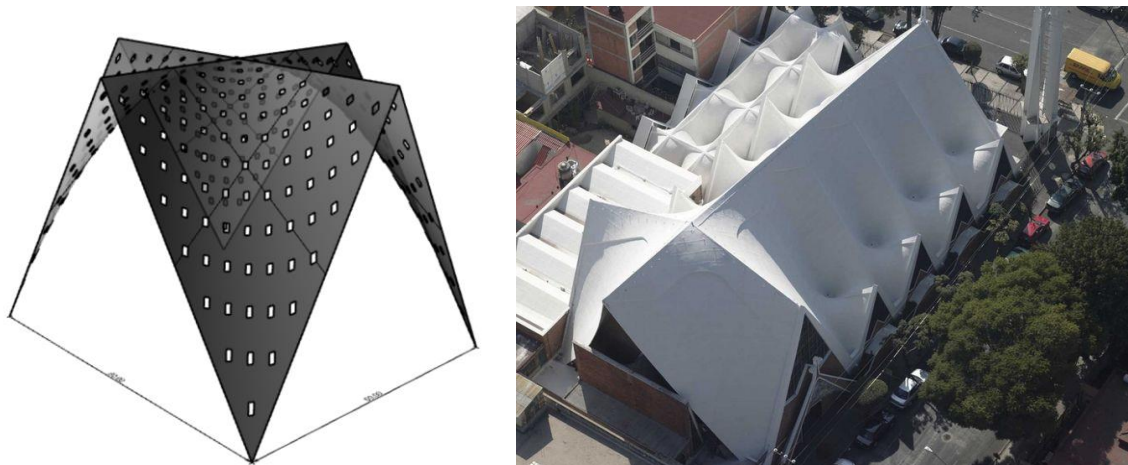


Figure 7.55. Morphology-A retrieved by scaling up the units (a) is seen in Church of Our Miraculous Lady (b) ¹²

¹² Coordinates on Google Maps are 19.379461,-99.157307

The limitations of this study can be described as falling into four categories, namely limitations of parametric modeling, scale-up, simulation settings, and statistical analysis.

Considering the limitations in parametric modeling, the *first* shortcoming is the use of only a single internal pressure for form finding using the Rhino Membrane plugin. This was realized toward the end of the process and upon trying to map case studies onto the solution space. An adjusted model was then created to populate a second solution space with adjusted internal pressure to create synclastic surfaces. The higher-level takeaway of this process demonstrates the dilemma of using parametric modeling and how the results are bound to the possibilities of the parametric model that is initially created by the designer.

The *second* modeling limitation is seen in the modeling of the boundary curves. These are modeled as fixed lines to make a shape; the curves are not allowed to be moved or optimized by the Rhino Membrane plugin. Realizing this *edge stiffening effect*, which acts as a limitation in the form-finding of surfaces, explains the flat areas generated in some shells that then go through large deformations under loading.

The *third* modeling limitation is lack of any stiffening edge beam. The parametric model does not allow for creation of a deep edge beam, and the thickness is assumed to be constant across the shell. However, many built shells employ some sort of design feature to make the edges stiffer, either by use of beams or increased thickness and reinforcement.

The limitations that were realized upon mapping case studies onto the solution space are twofold. *First*, some cases, such as Candela's umbrellas, includes an array of multiple units that create a continuity effect, resulting in a stiffened edge. If one unit is extracted, extra stiffness must be added to the edges of the isolated unit in the simulation to account for this effect.

Second, both High Life Textile Factory and the COOP warehouse have shells with straight edges, whereas the shells in the solution space have curved edges. This demonstrates that each solution space is limited to certain case studies and not every case can be mapped onto it. The designer needs to be very experienced to be able to foresee all possibilities to incorporate them in the parametric model.

The limitation in daylighting simulation caused by using low radiance settings affected the accuracy of the results where the correlation between thickness and sDA is not identified. This shows the tradeoff between accuracy and speed at the early stages of design and illustrates how this tradeoff may affect the results.

Finally, the limitation in statistical analysis needs to be addressed. Boundary curvature, which was assumed to create a dome, barrel vault, or a saddle, has been controlled in the statistical analysis, as well as thickness, and perforation ratio. However, the amount of curvature should have been controlled too. Future research will need to limit the range of change in the curvature to coarse steps to limit it to a deep dome, a shallow dome, one barrel-vault, a shallow saddle, and a deep saddle only, and focus on including the effect of curvature on structural performance.

7.7 References

- Bösiger, H. (2011). The building of Isler shells. *Journal of the International Association for Shell and Spatial Structures*, 52(169), 161–169.
- Chilton, J. (2000). *The Engineer's Contributions to Contemporary Architecture: Heinz Isler*. (A. Macdonald & R. Pedreschi, Eds.). London: Thomas Telford.
- Chilton, J. (2011). Heinz Isler: Shells for two churches. *Journal of the International Association for Shell and Spatial Structures*, 52(169), 173–183.
- Emami, N., Giles, H., & von Buelow, P. (2018). Performative perforations: structural and daylighting performance assessment of Candela's High Life Textile Factory. In C. Mueller & S. Adriaenssens (Eds.), *Proceedings of the IASS Symposium "Creativity in Structural Design."* Boston: International Association for Shell and Spatial Structures (IASS).
- Faber, C. (1963). *Candela, the shell builder. With a foreword by Ove Arup*. New York: Reinhold Publishing Corporation.
- Garlock, M. M., & Billington, D. P. (2008). *Felix Candela, Engineer, Builder, Structural Artist*. Yale University Press.
- Park, H.-J. (2005). *A Quantification of Proportionality Aesthetics in Morphological Design*. University of Michigan.
- Ramm, E. (2011). Heinz Isler shells - The priority of form. *Journal of the International Association for Shell and Spatial Structures*, 52(169), 143–154.

Chapter 8 :

Conclusion and future work

“The time to begin writing an article is when you have finished it to your satisfaction. By that time you begin to clearly and logically perceive what it is that you really want to say.”

-Mark Twain, *Notebook, 1902-1903*

This chapter first reviews the problem statement, gaps, and research methods employed in this dissertation. It then summarizes its contributions in three different categories along with the starting research question and objectives leading to the contribution. The limitations of and future work in each area are also summarized at the end of each section.

8.1 Problem statement

A building needs to stand up and needs to be illuminated; thus, the structural and daylighting disciplines are intimately associated with the fundamental purposes of architectural design. To have an effective building design, the designer needs to consider the interaction between disciplines, where making a decision in one field affects the other. Previous researchers have mainly clustered climate-related issues such as heating, cooling, daylighting, and ventilation, or structure-related issues such as structural topology, shape, sizing, and material design. However, consideration of multiple disciplines and their interaction is key for an interdisciplinary design approach. Moreover, there is no previous formalized method for integrating multiple disciplines towards employing an interdisciplinary design approach in architecture.

My research hypothesis is that:

- The structural and daylighting disciplines can be integrated with each other through their common *design parameters*.
- The structural and daylighting *performance* should play an active role as a design driver, rather than considered and designed as independent components, since they could all influence each other.

- There needs to be integrated considerations in building design since one disciplines can affect the other, conducted interactively, resulting in certain trade offs in arriving at the final solution. It is the job of the designer to make the necessary value judgments on the trade offs which cannot always been objectified; rather is an evaluation that might include other factors such as costs, aesthetics, time, etc.

8.2 Contributions, and future work related to interdisciplinary design

The gaps which lead to contributions to interdisciplinary design identified in Chapter 5 are reiterated below:

Gap a-1: Identify disciplinary design parameters: many studies do not discuss the design parameters that professionals in each discipline consider in the design phase, before they conduct a multi-disciplinary performance assessment study.

Gap a-2: Identify design parameters common to multiple disciplines: it is not often discussed that each design parameter is rooted in only one discipline, or exists in multiple disciplines.

Gap a-3: Explain why and how the common (and discipline-specific) parameters are included in the parametric model: even if key design parameters and common parameters in each discipline are identified, the reasons how and why some design parameters are (and are not) included in a model are not commonly discussed. The rationale behind creating a model is not formalized beyond explaining the technical modeling processes.

It is expected that by carefully identifying the common and discipline-specific design parameters, a more accurate parametric model can be constructed, which may lead to meaningful conclusions.

This dissertation demonstrates interconnections between two disciplines (daylighting and structural engineering) in relation to shell structures. Although shell structures are used in the process, the ambition of the study is to apply the process to other forms, while considering other disciplines, such as acoustics.

One of the research questions of this study is:

Research question a: How can the designer identify the design parameters that are shared between the discipline of architecture and an engineering discipline?

Research objectives:

Objective a-1: To formalize an interdisciplinary design approach regarding structural and daylighting disciplines. To this end, the design parameters that are relevant in both disciplines, as well those that are limited to affecting performance in only one discipline, are identified. Then, a design approach in which common design parameters are implemented in the model is proposed.

Objective a-2: To rationalize how the overlapping design parameters in engineering disciplines can be translated into architectural design parameters to be implemented in architectural models. This includes analyzing the design space that will be created, as well as the opportunities and restrictions offered by the parametric model.

8.2.1 Contributions

One of the most significant contributions of this research is its methodological approach, which uses a formalized framework for categorizing design parameters in the structural and daylighting disciplines and then identifying overlapping design parameters. This *design method*, presented as a roadmap at the end of Chapter 5, is the fundamental new component arising from this research.

8.2.2 Future work

More work in this area can advance this design process to a product which can be applied based on the specific design case. A software platform or a website can be developed where designers and engineers can share their knowledge of the field by breaking down the design parameters that they use in their field. After finding the common parameters and discipline-specific parameters, they can identify the key parameters that will affect more than one of them, and the parameters which they can vary independently without affecting other disciplines.

8.3 Results, contributions, and limitations related to the field of shell structures

One of the gaps that is identified in Chapter 5 is:

Gap b: Explain the expected relationship of implemented parameters with performance in multiple disciplines. It is expected that some parameters affect performance, (not necessarily all). Identifying which are the most influential during the design, will greatly assist in arriving at an integrated and most elegant or optimal solution.

As noted in Chapter 1, by adopting an interdisciplinary design approach using computational design and simulation tools, while considering shell structures as a special case for large span roofs, I ask:

Research question b: What are the design *parameters* that co-exist in the structural and daylighting design disciplines? How may these parameters be used by designers? How do the design *parameters* affect *performance* in structural and daylighting discipline? What is the tradeoff between performance in structural and daylighting design?

The research objectives pursued in order to answer this research question are:

Objective b-1: To understand how the design parameters in shells affect performance across multiple disciplines.

Objective b-2: To study shells as an integrated design problem, by exploring how continuous and grid shells are related.

By considering a wide spectrum of possible typologies, these can simply be categorized between the extremes of continuous and grid typologies. This categorization is based on their material and construction method, where masonry and concrete shells belong to the former, and wood and steel shells belong to the latter. The range of typologies using concrete as the building material comprises a spectrum of shells from continuous to grid shells.

8.3.1 Results

In this research, I answered these questions by first finding the parameters common to both disciplines. Thickness, perforation ratio, and surface curvature are the three design parameters found in both disciplines and used in the parametric model. Next, I demonstrated the correlation between parameters and performance in both structural and daylighting disciplines, through extensive statistical analysis. The detailed statistical results are summarized in the conclusion section of Chapter 7 and Appendix E.

Perforation ratio:

I find that perforation ratio is the most significant parameter that affects both disciplines and a number between 10% to 20% is the recommended limit for shell structures when translucent glazing is installed; values in this range lead to adequate daylight without light oversupply.

The statistical results related to perforation ratio and performance criteria are summarized in the following.

- *Perforation ratio* and *weight* are negatively correlated, as shown by the general linear regression model (GLM).
- The results of this study relating to *perforation ratio* and *deflection* cannot be generalized because the statistical analysis does not control for curvature at a micro level, which affects the geometric stiffness, and thus, the performance values.
- Like deflection, the limitations of the statistical analysis mean the findings of this study relating to *perforation ratio* and *von Mises stress* cannot be generalized.
- *Perforation ratio* and *structural costs* are negatively correlated, as shown by the GLM. It should be noted that in this analysis structural costs include concrete, formwork, and reinforcement costs.
- *Perforation ratio* and *sDA* are positively correlated, as shown by the ordinal logistic regression model. When using translucent glazing, a perforation ratio of 10% to 30% provides adequate daylight levels without daylight oversupply.
- *Perforation ratio* and *light oversupply* are positively correlated, as shown by the multinomial logistic regression model. When using translucent glazing, a perforation ratio of 20% or less does not create light oversupply. When the correlation of perforation ratio and sDA is considered in this context, a perforation ratio of 10% to 20% with translucent glazing seems appropriate to provide adequate daylight without light oversupply. It should be noted that using external or internal shading devices will allow a perforation ratio greater than 20%.
- *Perforation ratio* and *total operational energy* are positively correlated, as shown by a multinomial regression model. Adding more holes to the surface of the shell increases cooling loads in a heating-dominated climate such as Boston, which drives the total operational energy loads.
- *Perforation ratio* and *energy costs* are positively correlated, as shown by an ordinal logistic regression model. The trend follows operational energy loads; upon adding more holes to the surface of the shell, cooling loads, and thus the costs of cooling, increase.

Thickness:

I find thickness effective in the structural performance but not the daylighting performance. Reviewing the daylighting simulation settings, I found a caveat in the model setup. The limitation in daylighting simulation caused by using low radiance settings affected the accuracy of the results where the correlation between thickness and sDA is not identified. This limitation also demonstrates the tradeoff between accuracy and speed in computational simulations at the early stages of design, and the ways in which this tradeoff may affect the results. The statistical results related to thickness and performance criteria are summarized in the following:

- *Thickness* and *weight* are positively correlated, as shown by the GLM.
- *Thickness* and *deflection* are negatively correlated, as shown by the multinomial logistic model. It should be noted that on one hand, increasing the thickness makes the shell stiffer; however, on the other hand, increasing the thickness, increases the self-weight of the shell, and thus its dead load. Under constant live load, an increase in thickness makes the shell stiffer, since its maximum deflection is reduced.
- *Thickness* and *von Mises stress* are negatively correlated, as shown by the GLM.
- *Thickness* and *structural costs* are positively correlated, as shown by the GLM.
- The ordinal logistic regression model does not show a correlation between *thickness* and *sDA*. This is counter-intuitive, as it is expected that an increase in thickness, resulting in a deeper shaft, should diffuse daylight. The low settings for the radiance daylight simulations in DIVA have affected this result, which requires further examination.
- The multinomial logistic regression model does not show a correlation between *thickness* and *light oversupply*. Once more, the caveat is that the simulation settings may have caused this result.
- *Thickness* and *total operational energy* are negatively correlated, as shown by a multinomial regression model. This suggests that increased concrete thickness offers insulation properties that lead to reduced heating loads, which drives the total operational energy loads.
- *Thickness* and *energy costs* are negatively correlated, as shown by an ordinal logistic regression model. The trend follows operational energy loads: by increasing thickness, heating loads are reduced, which offers savings on heating costs.

Surface curvature:

The shells are categorized by surface curvature as dome, barrel vault, and saddle shells for analysis. As discussed in Chapter 7, the internal form finding pressure has not been adequate to generate proper forms for all three categories, and thus the results are only applicable to anticlastic (saddle-shaped) surfaces. The results of this study related to surface curvature cannot be generalized.

I demonstrated the tradeoff between disciplines by summarizing the results in a heatmap, where the tradeoff between performance in various disciplines can be understood by designers. The tradeoff between structural and energy costs was significant, which led me to investigate the Pareto front. In thinner shells, the total operating costs for one year dominate, whereas the effect of material cost is negligible. However, as shells get thicker, the tradeoff between the two increases.

8.3.2 Contributions

This research demonstrates how daylighting performance can be affected in the design of shell structures, a typology that is mainly driven by its structural design criteria in the literature. Also important is its demonstration of how a continuous shell can be perforated to the point at which becomes a grid shell; therefore, continuous and grid shells are two ends of a spectrum rather than two distinct structural typologies. A high-level significance of this dissertation is its marriage of the structural and daylighting disciplines and demonstration of how the two are closely related in shells by the perforation ratio.

8.3.3 Limitations

- Considering limitations in the parametric modeling of the shells, the *first* shortcoming is the use of only a single internal pressure for form finding using the Rhino Membrane plugin. An adjusted model was then created to populate a second solution space with adjusted internal pressure to create synclastic surfaces. This shortcoming affected the performance of synclastic shells; they did not possess adequate curvature, and when loaded, exhibited bending rather than membrane stresses. The higher-level takeaway of this process demonstrates the dilemma of using parametric modeling: the results are bound to the possibilities of the parametric model initially created by the designer.

- The *second* modeling limitation is seen in the modeling of the boundary curves of the shells. These are modeled as fixed lines to make a shape; the curves are not moved or optimized by the plugin. This *edge stiffening effect* limits the form-finding of surfaces and explains the flat areas generated in some shells that experience large deformations under loading.
- The *third* modeling limitation is the lack of any stiffening edge beam in the parametric model; thickness is assumed to be constant across the shell. However, many built shells employ some sort of design feature, using either beams or increased thickness and reinforcement to make the edges stiffer.

8.3.4 Future work

Regarding computational design of the search space, symmetrical patterns for structural analysis could have been considered to reduce the number of possible permutations. In the future, the size of the search space should be taken into account from the beginning. It may be beneficial to first explore the search space at a lower resolution with larger step sizes for the parameters to gain an understanding of their effects on performance, and then increase the resolution on selected parameters to explore a certain aspect of the design. To put this in the context of this study, a good strategy could have been creating three typologies (one dome, one barrel-vault, and one saddle) with the optimized internal pressure thus membrane stress first and understand the effect of perforation ratio and thickness on these typologies. The next exploration step could have been exploring various surface curvature in a synclastic or anticlastic surface.

Although perforation ratio is the most significant parameter bridging the two disciplines in shell structures, there are still gaps in considering relevant parameters. *Material properties* are an important parameter especially if energy evaluations are considered in interdisciplinary research.

This dissertation introduces and theoretically explores two new parameters for daylighting performance assessment in roofs and facades in Chapter 5, namely granularity and bias. Granularity was considered constant for all the shells that were designed and assessed, and bias was not considered in the analysis. Further research in this area can investigate how changes in granularity and bias affect structural and daylighting performance.

8.4 Results and contribution to solution space exploration

The identified gaps in Chapter 5 which lead to contributions to solution space exploration are reiterated below:

Gap c-1: Explain how implementing the parameters in the parametric model bounds the design space: once design parameters are implemented using a parametric model, some opportunities are created and some limitations are imposed; in other words, a search space is created. The boundaries of the design space, including the extreme possibilities, are not commonly discussed in depth regarding multiple disciplines.

Gap c-2: Results are bound to specific case studies: in most studies, the implementation process is discussed in depth, and its application to a case study is explored. However, the results remain restricted to that specific case study and are not extended to scrutinize their possible application to other cases.

These gaps lead to

Research question c: How can the results of a specific design case be useful for application to other design cases that do not necessarily have the same boundary conditions?

The research objective pursued in order to answer the research questions is:

Objective c: To consider other perforated shell structures and try to map them on to the generated solution space. Investigate the effects of abstracting and changing the boundary conditions and determine how effective the resulting comparisons are.

8.4.1 Contributions

Addressing this objective explores how a generated solution space may become useful for other design projects which do not necessarily have the exact same boundary conditions. By abstracting the boundary conditions of new projects to match those in the solution space, the designer can examine possibilities and compare how making a decision in one field may affect performance in other fields.

8.4.2 Limitations

- There are huge limitations when abstracting the structural boundary conditions. When the geometry is scaled up, structural performance criteria do not change linearly. In other words, by changing the geometric proportions of an object, an operation which is easily

accessible in parametric design tools, structural considerations change. However, changing the scale of the objects can be a source of inspiration for designers.

- The parametric model that is used to create the solution space must be designed in a way that accommodates not only geometric variation, but also varying structural edge stiffening effects. This approach will greatly extend the applicability of the method, even if it does not reveal any great impact on interdisciplinary interactions.
- Each solution space is limited to certain case studies, and not every case can be mapped onto it. The designer needs to be very experienced to be able to foresee all possibilities to incorporate them in the parametric model.

8.4.3 Future work

Future studies can include parametric modeling of structural boundary conditions and various stiffness values in the parametric modeling in addition to geometric variations. This will greatly extend the applicability of the method.

8.5 Impact

The impact of this research is its creation of a new interdisciplinary design approach for use in the AEC industry. While new computational tools are being developed to facilitate interdisciplinary design approach and collaboration, identifying parameters that are common to multiple disciplines remains key. This dissertation demonstrates how a formalized methodological approach can open opportunities for designers for interdisciplinary design approach, by differentiating the design parameters bound to one discipline from the design parameters that also affect performance in other disciplines interactively with other disciplines while considering tradeoffs.

Appendix A:

Structural validation of Karamba with ANSYS and numerical calculations

A.1 Boundary conditions

Karamba is a FE (Finite Element) structural simulation plugin used in Rhino NURBS modeling software. The plugin is benchmarked with numerical calculations and another FE software, ANSYS, which is very well-known and reliable. The validation has been conducted for flat plates with and without perforations, as well as curved surfaces. Material properties has remained unchanged throughout the simulations. There are cases where the boundary conditions are changed to observe any difference. SI units are used consistently, but the equivalent imperial units are also provided.

Table A.1. Global geometrical properties

	SI units	Imperial units
Plate dimension	10 by 10 [meter]	32.8 by 32.8 [foot]
Plate thickness	0.3 [meter]	11.8 [inch]

Table A.2. Loading

	SI units	Imperial units
Pressure in the negative y axis	1000 [Pa]	20.88 [Psf] or [Pound-force/ft2]

Table A.3. Material Properties defining *concrete*

	SI units	Imperial units
density	2000 [kg/m ³]	124.85 [lb/ft ³] or [PLF]
E (Young's Modulus)	2.10e+10 [N/m ²] or [Pa]	3045 [ksi]
Shear Modulus	8.75e+09 [Pa]	1269 [ksi]
Poisson ratio	0.2	0.2
Compressive Yield Strength(fy)	2.80e+07 [Pa]	4.06 [ksi]
Tensile Yield Strength	2.80e+06 [Pa]	0.4 [ksi]
alpha T (co-efficient of thermal expansion)	1.20e-05 [strain/°C]	0.66e5 [strain/°F]

zero-thermal-strain	22 [°C]	71.6 [°F]
Compressive Ultimate Strength	2.80e+07 [Pa]	4.06 [ksi]
Tensile Ultimate Strength	2.80e+06 [Pa]	0.4 [ksi]

Table A.4. Global geometrical dimensions

	SI units	Imperial units
Planar dimensions	10 by 10 [meter]	32.8 by 32.8 [foot]
Plate/shell thickness	0.3 [meter]	11.8 [inch]

Table A.5. Global geometrical properties

Case 01: square plate	10 by 10 [meter], thickness of 0.3 [meter]
Case 02: square plate	10 by 10 [meter], thickness of 0.3 [meter]
Case 03: square plate	10 by 10 [meter], thickness of 0.3 [meter]
Case 04: square perforated plate	10 by 10 [meter], thickness of 0.3 [meter]
Case 05: square perforated plate	10 by 10 [meter], thickness of 0.3 [meter]
Case 06: square perforated plate	10 by 10 [meter], thickness of 0.3 [meter]
Case 07: square shell	10 by 10 [meter], thickness of 0.3 [meter], rise of 1.5 [meter] at edges, rise of 3.09 [m] at center

Table A.6. Local geometrical properties

	SI units	Imperial units
Case 01: no holes in the plate	—	—
Case 02: no holes in the plate	—	—
Case 03: no holes in the plate	—	—
Case 04: 1 hole in the plate	Diameter of 3 [meter]	Diameter of 9.84 [foot]
Case 05: 4 holes in the plate	Diameter of 1.5 [meter]	Diameter of 4.92 [foot]
Case 06 :9 holes in the plate	Diameter of 1.0 [meter]	Diameter of 3.2 [foot]
Case 07: no holes in the shell	—	—

A.2 Validation of a solid 10 by 10-meter plate

The first section explains the validation process for a solid concrete plate measuring 10 by 10 meter using numerical calculations, Ansys FEM software, and Karamba plugin for Grasshopper.

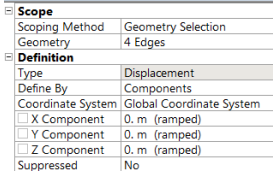
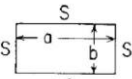

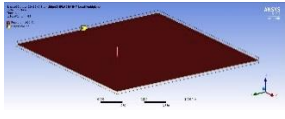
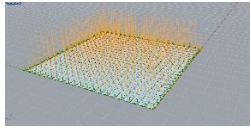
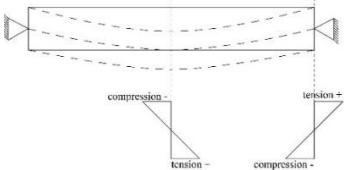
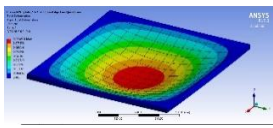
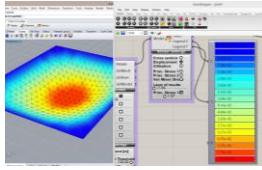
Table A.7. Comparing Ansys simulation results with numerical calculations

<p style="text-align: center;"><u>Case 01: a solid 10-meter by 10-meter plate</u> <u>Compares: Ansys vs. Numerical calculation</u> <u>Boundary condition: Fixed edge surface supports, (x-component=0, y-component = 0, z-component=0)</u> <u>Modeling: Two 10x10 m 0.15m thick plates were modeled touching each other. Then, the 4 surface edges on each plate were selected as supports, having a total number of 8 supporting faces. The midplane is loaded.</u></p>																						
	Ansys	Numerical Calculation ¹																				
Case01: Support		<p>8. Rectangular plate, all edges fixed</p> <p>(page 508)</p>																				
Case01: Load		<p>8a. Uniform over entire plate</p>																				
Bending shape																						
Case01: Maximum deformation		<p>(At center of long edge) $\sigma_{\max} = \frac{-\beta_1 q b^2}{t^2}$</p> <p>(At center) $\sigma = \frac{\beta_2 q b^2}{t^2}$ and $y_{\max} = \frac{\alpha q b^4}{Et^3}$</p> <table border="1"> <thead> <tr> <th>a/b</th> <th>1.0</th> <th>1.2</th> <th>1.4</th> <th>1.6</th> </tr> </thead> <tbody> <tr> <td>β_1</td> <td>0.3078</td> <td>0.3834</td> <td>0.4356</td> <td>0.4680</td> </tr> <tr> <td>β_2</td> <td>0.1386</td> <td>0.1794</td> <td>0.2094</td> <td>0.2286</td> </tr> <tr> <td>α</td> <td>0.0138</td> <td>0.0188</td> <td>0.0226</td> <td>0.0251</td> </tr> </tbody> </table>	a/b	1.0	1.2	1.4	1.6	β_1	0.3078	0.3834	0.4356	0.4680	β_2	0.1386	0.1794	0.2094	0.2286	α	0.0138	0.0188	0.0226	0.0251
a/b	1.0	1.2	1.4	1.6																		
β_1	0.3078	0.3834	0.4356	0.4680																		
β_2	0.1386	0.1794	0.2094	0.2286																		
α	0.0138	0.0188	0.0226	0.0251																		
	0.025 [cm]	0.024 [cm]																				
Case01: Stress at center	-1.39e5 [Pa], compression on top (min Princ. σ) +1.39e5 [Pa], tension on bottom (max Princ. σ)	1.54 e5 [Pa]																				
Case01: Stress at edge	+3.43e5 [Pa], tension on top (max Princ. σ) -3.43e5 [Pa], compression on bottom (min Princ σ)	-3.4e5 [Pa]																				
Equivalent stress	Min: 1.716 e3 Max: 2.7 e5	NA																				

*the results perfectly match

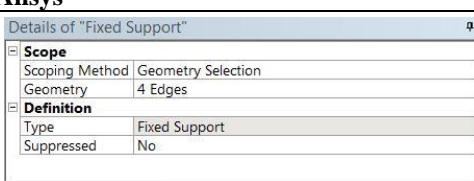

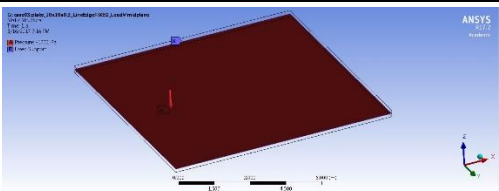
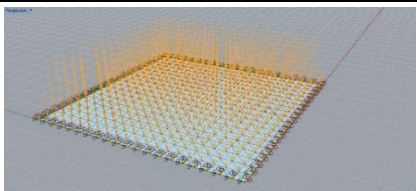
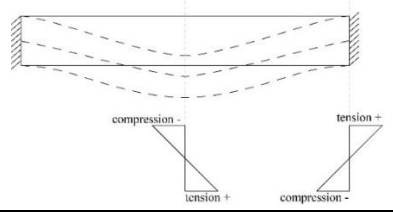
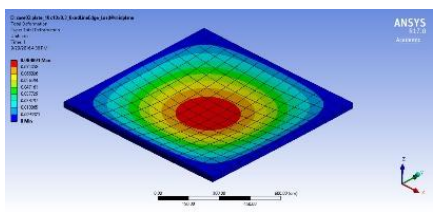
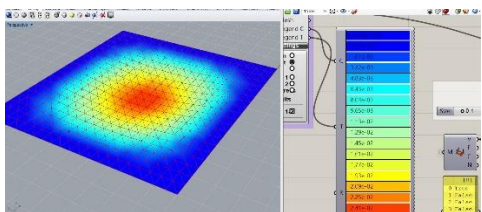
¹ Warren C. Young, Richard G. Budynas, *Roark's formulas for stress and strain*, 2002, McGraw-Hill Companies Inc.

Table A.8. Comparing Ansys simulation results with numerical calculations and Karamba results

Case 02: a solid 10-meter by 10-meter plate Compares: <i>Ansys</i> vs. <i>Numerical calculation</i> vs. <i>Karamba</i> Boundary condition: <i>Simply Supported edge lines</i> , (Displacement support in Ansys, with x-y-z component = 0) Modeling: Two 10x10 m 0.15m thick plates were modeled touching each other. Then, the 4 edge lines are selected as displacements with 0 rotation in three axis in Ansys. The midplane was loaded.																											
	Ansys	Numerical Calculation	Karamba																								
Case02: Support		1. Rectangular plate; all edges simply supported  (page 502)																									
Case02: Load		1a. Uniform over entire plate																									
Bending shape																											
Case02: Maximum deformation		$\text{(At center)} \quad \sigma_{\max} = \sigma_b = \frac{\beta q b^2}{t^2} \quad \text{and} \quad y_{\max} = \frac{-\alpha q b^4}{Et^3}$ $\text{(At center of long sides)} \quad R_{\max} = \gamma q b$ <table border="1" style="margin-left: auto; margin-right: auto;"> <thead> <tr> <th>a/b</th> <th>1.0</th> <th>1.2</th> <th>1.4</th> <th>1.6</th> <th>1.8</th> </tr> </thead> <tbody> <tr> <td>β</td> <td>0.2874</td> <td>0.3762</td> <td>0.4530</td> <td>0.5172</td> <td>0.5688</td> </tr> <tr> <td>α</td> <td>0.0444</td> <td>0.0616</td> <td>0.0770</td> <td>0.0906</td> <td>0.1017</td> </tr> <tr> <td>γ</td> <td>0.420</td> <td>0.455</td> <td>0.478</td> <td>0.491</td> <td>0.499</td> </tr> </tbody> </table>	a/b	1.0	1.2	1.4	1.6	1.8	β	0.2874	0.3762	0.4530	0.5172	0.5688	α	0.0444	0.0616	0.0770	0.0906	0.1017	γ	0.420	0.455	0.478	0.491	0.499	
a/b	1.0	1.2	1.4	1.6	1.8																						
β	0.2874	0.3762	0.4530	0.5172	0.5688																						
α	0.0444	0.0616	0.0770	0.0906	0.1017																						
γ	0.420	0.455	0.478	0.491	0.499																						
	0.084 [cm]	0.078 [cm]	0.083 [cm]																								
Case02: Stress at center	-3.16 e5 [Pa], compression on top (min Princ. σ) +3.15 e5 [Pa], tension on bottom (max Princ. σ)	3.1 e5 [Pa]	-2.95 e5 [Pa], compression on top (Princ. σ 2 at layer +1) +2.95 e5 [Pa], tension on bottom (Princ. σ 1 at layer -1)																								
Case02: Stress at edge	0.016 e5 [Pa], tension on top (max Princ. σ) -0.014 e5 [Pa], compression on bottom (min Princ. σ)	0.04 e5 [Pa]	+3.69 e4 [Pa], tension on top (Princ. σ 1 at layer +1) -3.6 e4 [Pa], compression on bottom (Princ. σ 2 at layer -1)																								
Equivalent stress	Min: 1.641 e3 [Pa] Max: 4.9 e5 [Pa]	NA	Min: 4.1 e4 [Pa] Max: 3.8 e5 [Pa]																								

* Deformation and stress at center is consistent. Stress at support is inconsistent. Ansys and numerical calculation show nearly zero stress at support (since the simple supported edge line can rotate when loaded). Karamba, however, is presenting higher stress values at edges.

Table A.9. Comparing Ansys results with numerical calculation with fixed supports

<p style="text-align: center;"><u>Case 03: a solid 10-meter x 10-meter plate</u> <u>Compares: Ansys vs. Numerical calculation</u> <u>Boundary condition: Fixed edge lines</u>, (fixed support in Ansys) <u>Modeling: Two 10x10 m 0.15m thick plates were modeled touching each other. Then, the 4 edge lines are selected as fixed supports in Ansys. The midplane was loaded. In Karamba, multiple points on the edge lines are chosen as supports as it does not provide other options.</u></p>		
	Ansys	Karamba
Case03: Support		
Case03: Load		
		
Case03: Maximum deformation	 <p style="text-align: center;">0.084 [cm]</p>	 <p style="text-align: center;">0.0257 [cm]</p>
Case03: Stress at center	<p>-3.16e5 [Pa], compression on top (min Princ. σ)</p> <p>+3.15e5 [Pa], tension on bottom (max Princ. σ)</p>	<p>-1.71e5 [Pa], compression on top (Princ. σ 2 at layer +1)</p> <p>+1.37e5 [Pa], tension on bottom (Princ. σ 1 at layer -1)</p>
Case03: Stress at edge	<p>+0.016e5 [Pa], tension on top (max Princ. σ)</p> <p>-0.014e5 [Pa], compression on bottom (min Princ. σ)</p>	<p>+2.73e5 [Pa], tension on top (Princ. σ 1 at layer +1)</p> <p>-2.73e5 [Pa], compression on bottom (Princ. σ 2 at layer -1)</p>
Equivalent stress	<p>Min: 1.641 e3 [Pa]</p> <p>Max: 4.9 e5 [Pa]</p>	<p>Min: 1.5 e4 [Pa]</p> <p>Max: 2.5 e5 [Pa]</p>

* Karamba results does not correspond with Ansys results with the abovementioned settings, however, Karamba is more corresponding with Ansys results with settings provided in case 1 although only a line is fixed and not a surface. Stress at center and edges are also closer to values related to case 01.

Table A.10. Comparing Ansys with Karamba results with fixed edges

<p><u>Case 01 and case 03 combination</u>: a solid 10-meter x 10-meter plate</p> <p><u>Compares</u>: <i>Ansys from case 01</i> vs. <i>Karamba from case 03</i></p> <p><u>Boundary condition</u>: <i>Fixed edges</i></p> <p><u>Modeling</u>: Two 10x10 m 0.15m thick plates were modeled touching each other. Then, the 4 surface edges on each plate were selected as supports, having a total number of 8 supporting faces. The midplane was loaded. In Karamba, multiple points on the edge lines are chosen as supports as it does not provide other options.</p>		
	Ansys (from case 01)	Karamba (from case 03)
Case 01 & 03 combo: Support		
Case 01 & 03 combo: Load		
Case 01 & 03 combo: Maximum deformation	<p style="text-align: center;">0.025 [cm]</p>	<p style="text-align: center;">0.0257 [cm]</p>
Case 01 & 03 combo: Stress at center	<p>-1.39e5 [Pa], compression on top (min Princ. σ)</p> <p>+1.39e5 [Pa], tension on bottom (max Princ. σ)</p>	<p>-1.71e5 [Pa], compression on top (Princ. σ 2 at layer +1)</p> <p>+1.37e5 [Pa], tension on bottom (Princ. σ 1 at layer -1)</p>
Case 01 & 03 combo: Stress at edge	<p>+3.43e5 [Pa], tension on top (max Princ. σ)</p> <p>-3.43e5 [Pa], compression on bottom (min Princ. σ)</p>	<p>+2.73e5 [Pa], tension on top (Princ. σ 1 at layer +1)</p> <p>-2.73e5 [Pa], compression on bottom (Princ. σ 2 at layer -1)</p>
Equivalent stress	<p>Min: 1.716 e3 [Pa]</p> <p>Max: 2.7 e5 [Pa]</p>	<p>Min: 1.5 e4 [Pa]</p> <p>Max: 2.5 e5 [Pa]</p>

* The results retrieved from Karamba and Ansys correspond well. Karamba seems to slightly underestimate stress at edges perhaps because of the difference in modeling.

- The plate with edge-surfaces set as displacements restrained in x, y and z-direction in Ansys yields results that correspond with numerical calculations for a plate with fixed edges (case 01).
- The plate with edge-lines set as displacements restrained in x, y and z-direction in Ansys yields results that correspond with numerical calculations for a plate with simply supported edges (case 02).
- Karamba supports restricted in T_x , T_y and T_z represent simple support, and the yielded results match the ones from Ansys with edge-lines set as displacements restrained in x, y and z-direction and numerical calculations, except for the stress values at edges which is overestimated by Karamba (case 02).

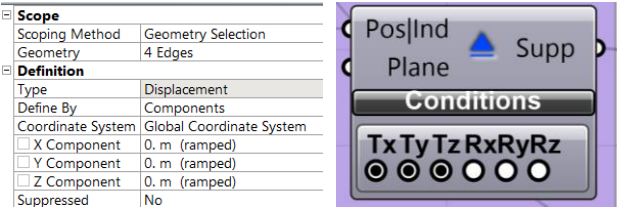


Figure A.1. Ansys and Karamba corresponding support representing a simple support

- In a variation, fixed lines in Ansys were compared with a support in Karamba which is restrained in T_x , T_y and T_z as well as R_x , R_y and R_z . The results did not correspond (case 03).
- It was noticed that the results retrieved from the Karamba model with fixed supports corresponds with the Ansys model where the edge surfaces are fixed (case 01 and case 03).

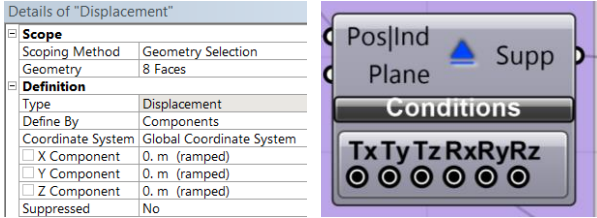


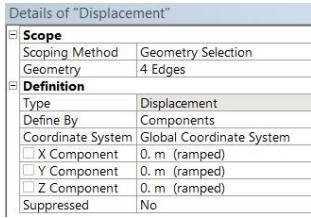

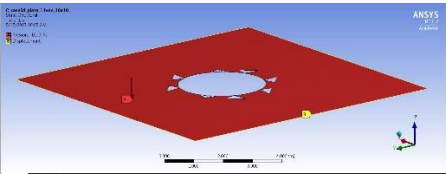
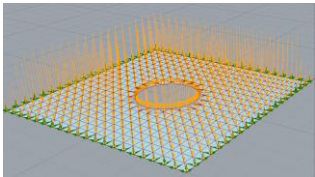
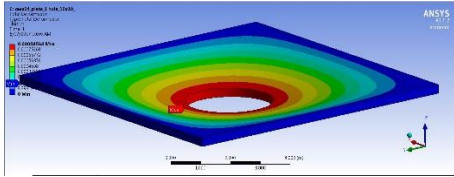
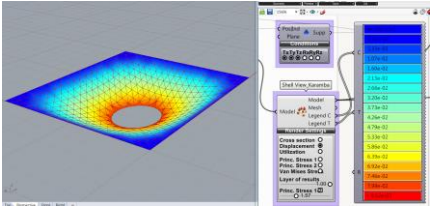
Figure A.2. Ansys and Karamba corresponding support representing a fixed support

- In conclusion, Karamba results with simple supports and fixed supports corresponds with results for a displacement edge-line and displacement edge-surface in Ansys respectively. The deformation, von Mises stress and principle stress levels at center all correspond well. The principle stress levels at edges is overestimated in Karamba model with simple supports and underestimated in Karamba model with fixed supports. This can be explained by pointing to the fact that Karamba allows point supports only rather than any line selected as supports.

A.3 Validation of a hollowed 10 by 10-meter plate

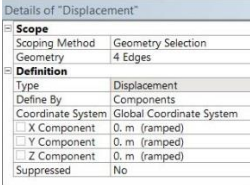

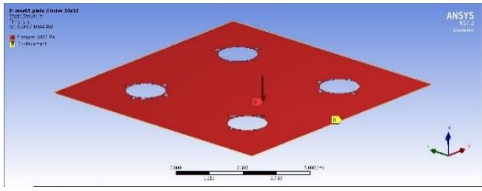
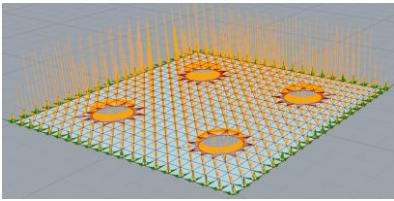
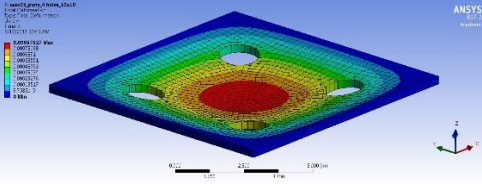
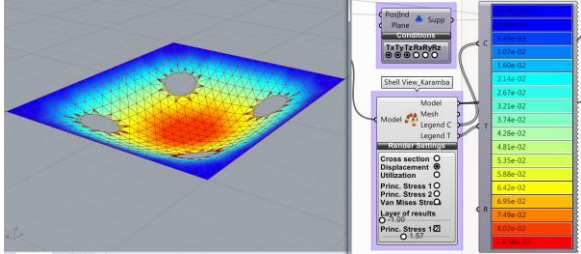
This section explains the validation process for a hollowed concrete plate measuring 10 by 10 meter using Ansys FEM software, and Karamba plugin for Grasshopper.

Table A.11. Comparing Ansys with Karamba results for a plate with one hole

<p>Case 04: a 10-meter x 10-meter plate with a hole that has a diameter of 3 m Compares: <u>Ansys</u> vs. <u>Karamba</u> Boundary condition: <u>Fixed edge lines</u> a simple support is selected for the comparison since principal stress levels at edge are zero and other values can be compared. Modeling: A surface as an <i>stl</i> file type was imported to Ansys and then extruded. In Karamba, multiple points on the edge lines are chosen as supports as it does not provide other options.</p>		
	Ansys	Karamba
Case 04: Support		
Case 04: Load		
Case 04: Maximum deformation	 <p style="text-align: center;">0.0845 [cm]</p>	 <p style="text-align: center;">0.0852 [cm]</p>
Case 04: Stress at center	<p>-4.5 e5 [Pa], compression on top (min Princ. σ)</p> <p>+4.5 e5 [Pa], tension on bottom (max Princ. σ)</p>	<p>-4.67 e5 [Pa], compression on top (Princ. σ 2 at layer +1)</p> <p>+4.67 e5 [Pa], tension on bottom (Princ. σ 1 at layer -1)</p>
Case 04: Stress at edge	<p>+0.0 [Pa], tension on top (max Princ. σ)</p> <p>-0.0 [Pa], compression on bottom (min Princ. σ)</p>	<p>+2.1 e-11 [Pa], tension on top (Princ. σ 1 at layer +1)</p> <p>-7 e-11 [Pa], compression on bottom (Princ. σ 2 at layer -1)</p>
Equivalent stress	<p>Min: 2.01 e4 [Pa]</p> <p>Max: 4.6 e5 [Pa]</p>	<p>Min: 3.8 e4 [Pa]</p> <p>Max: 4.3 e5 [Pa]</p>

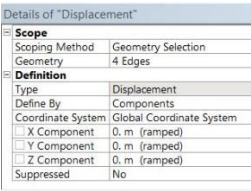

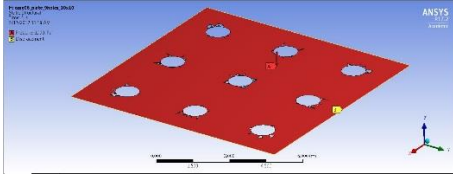
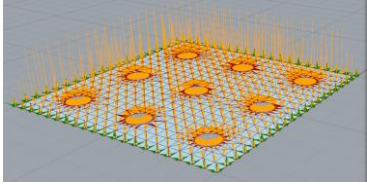
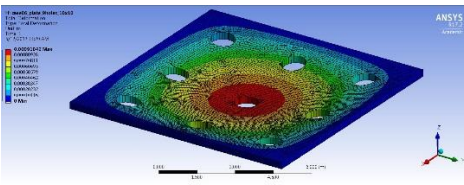
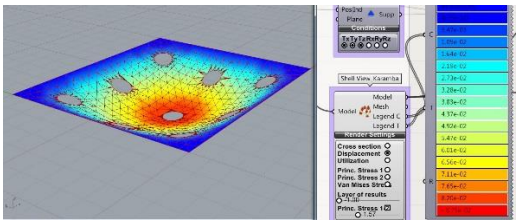
*Conclusion: The deformation, principal stresses and von Mises stress levels correspond well.

Table A.12. Comparing Ansys with Karamba results for a plate with four holes

<p>Case 05: a 10-meter x 10-meter plate with four holes that have a diameter of 1.5 m</p> <p>Compares: <u>Ansys</u> vs. <u>Karamba</u></p> <p>Boundary condition: <u>Fixed edge lines</u> a simple support is selected for the comparison since principal stress levels at edge are zero and other values can be compared.</p> <p>Modeling: A surface as an <i>stl</i> file type was imported to Ansys and then extruded. In Karamba, multiple points on the edge lines are chosen as supports as it does not provide other options.</p>		
	Ansys	Karamba
Case 05: Support		
Case 05: Load		
Case 05: Maximum deformation		
	0.0878 [cm]	0.08555 [cm]
Case 05: Stress at center	<p>-2.97 e5 [Pa], compression on top (min Princ. σ)</p> <p>+2.99 e5 [Pa], tension on bottom (max Princ. σ)</p>	<p>-2.95 e5 [Pa], compression on top (Princ. σ 2 at layer +1)</p> <p>+2.6 e5 [Pa], tension on bottom (Princ. σ 1 at layer -1)</p>
Case 05: Stress at edge	<p>0.0 [Pa], tension on top (max Princ. σ)</p> <p>0.0 [Pa], compression on bottom (min Princ. σ)</p>	<p>+4.2 e-11 [Pa], tension on top (Princ. σ 1 at layer +1)</p> <p>-8.5 e-11 [Pa], compression on bottom (Princ. σ 2 at layer -1)</p>
Equivalent stress	<p>Min: 1.88 e4 [Pa]</p> <p>Max: 5.3 e5 [Pa]</p>	<p>Min: 3.7 e4 [Pa]</p> <p>Max: 4.7 e5 [Pa]</p>

*Conclusion: The deformation, principal stresses and von Mises stress levels correspond well.

Table A.13. Comparing Ansys with Karamba results for a plate with nine holes

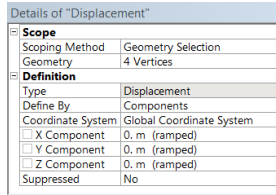
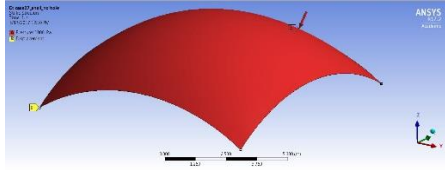
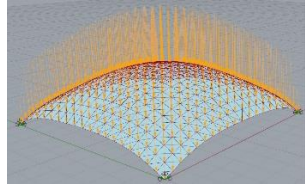
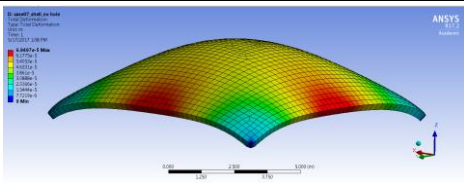
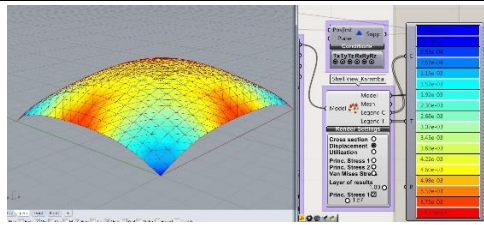
<p>Case 06: a 10-meter x 10-meter plate with nine holes that have a diameter of 1 m</p> <p>Compares: <u>Ansys</u> vs. <u>Karamba</u></p> <p>Boundary condition: <u>Fixed edge lines</u> a simple support is selected for the comparison since principal stress levels at edge are zero and other values can be compared.</p> <p>Modeling: A surface as an <i>stl</i> file type was imported to Ansys and then extruded. In Karamba, multiple points on the edge lines are chosen as supports as it does not provide other options.</p>		
	Ansys	Karamba
Case 06: Support		
Case 06: Load		
Case 06: Maximum deformation		
	0.091 [cm]	0.087 [cm]
Case 06: Stress at center	<p>-4.5 e5 [Pa], compression on top (min Princ. σ)</p> <p>+3.9 e5 [Pa], tension on bottom (max Princ. σ)</p>	<p>-4.36 e5 [Pa], compression on top (Princ. σ 2 at layer +1)</p> <p>+3.49 e5 [Pa], tension on bottom (Princ. σ 1 at layer -1)</p>
Case 06: Stress at edge	<p>0 [Pa], tension on top (max Princ. σ)</p> <p>0 [Pa], compression on bottom (min Princ. σ)</p>	<p>4.26 e-11 [Pa], tension on top (Princ. σ 1 at layer +1)</p> <p>-1.42 e-11 [Pa], compression on bottom (Princ. σ 2 at layer -1)</p>
Equivalent stress	<p>Min: 1.83 e4 [Pa]</p> <p>Max: 5.8 e5 [Pa]</p>	<p>Min: 4.1 e4 [Pa]</p> <p>Max: 6.05 e5 [Pa]</p>

*Conclusion: The deformation, principal stresses and von Mises stress levels correspond well.

A.4 Validation of a solid dome

This section explains the validation process for a simple dome in Ansys and Karamba.

Table A.14. Comparing Ansys with Karamba results for a solid dome

<p align="center">Case 07: a 10-meter x 10-meter shell Compares: Ansys vs. Karamba Boundary condition: Four corner points are selected as supports. Modeling: A curved surface as a <i>stl</i> file type was imported to Ansys and then extruded. In Karamba, multiple points on the edge lines are chosen as supports as it does not provide other options.</p>		
	Ansys	Karamba
Case 07: Support		
Case 07: Load		
Case 07: Maximum deformation	 <p align="center">0.0069 [cm]</p>	 <p align="center">0.0061 [cm]</p>
Case 07: Stress at center	<p>-1.16 e4 [Pa], compression on top (min Princ. σ)</p> <p>-1.4 e4 [Pa], compression on bottom (min Princ. σ)</p>	<p>-1.14 e4 [Pa], compression on top (Princ. σ 1 at layer +1)</p> <p>-1.14 e4 [Pa], tension on bottom (Princ. σ 1 at layer -1)</p>
Case 07: Stress at edge (perpendicular to edge cut lines)	<p>-3.8 e4 [Pa], compression on top (min Princ. σ)</p> <p>+2.7 e4 [Pa], tension on bottom (max Princ σ)</p>	<p>-1.14 e4 [Pa], compression on top (Princ. σ 1 at layer +1)</p> <p>+3.01 e3 [Pa], tension on bottom (Princ. σ 2 at layer -1)</p>
Equivalent stress	<p>Min: 6.9 e3 [Pa]</p> <p>Max: 2.1 e5 [Pa]</p>	<p>Min: 6.2 e3 [Pa]</p> <p>Max: 4.8 e5 [Pa]</p>

The results demonstrate that the shell is in compression on top and bottom layer at the center. Tension starts to appear underneath the shell in the middle of the edges. However, since the shell is supported on the corner points, tension develops on the top layer of the shell close to the corner points. For further investigation, the shell is cut orthogonally as well as diagonally to scrutinize the principle stress levels. In Ansys, the *cut plane* tool has been used to cut the geometry in the desired directions and then *probe* tool has been used to manually read the data (Figure A.3).

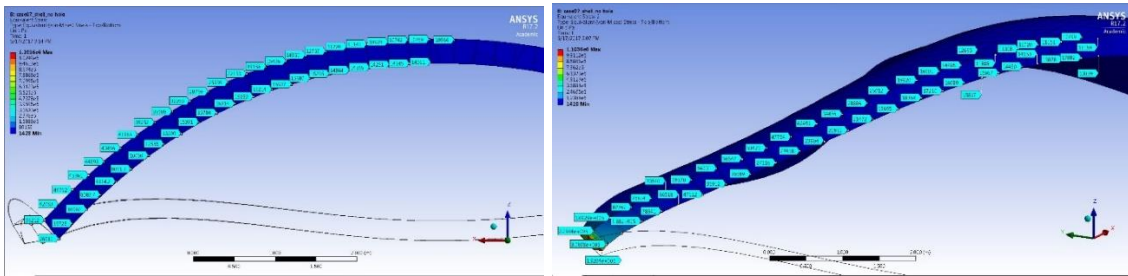


Figure A.3. Orthogonal cut of the shell (left), diagonal cut (right), and then reading the von Mises stress levels on top and bottom layer in Ansys

In Karamba, the node numbers of the shell are extracted in Grasshopper, along with a list of von Mises stress levels. Then the related index for the nodes lying on the cut line (either orthogonal or diagonal) are selected to read the corresponding von Mises stress levels (Figure A.4).

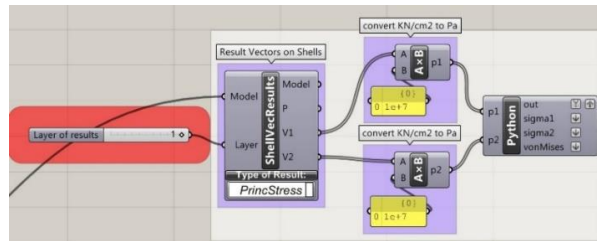


Figure A.4. step 01: principle stress of the desired layer are retrieved

```

File Help
# from karamba
print p1
# for i in p1:
#   print i

x = (p1[0])
y = (p1[1])
z = (p1[2])
sigma1 = ((x**2)+(y**2)+(z**2))**0.5
print sigma1

print p2
# for j in p2:
#   print j

u = (p2[0])
v = (p2[1])
w = (p2[2])
sigma2 = ((u**2)+(v**2)+(w**2))**0.5
print sigma2

vonMises = ((sigma1**2)+(sigma2**2) - (sigma1*sigma2))**0.5
print vonMises
  
```

Figure A.5. step 02: a python script calculates von Mises stress levels from the principal stress levels using $\sqrt{(\sigma_1^2) + (\sigma_2^2) - (\sigma_1 * \sigma_2)}$

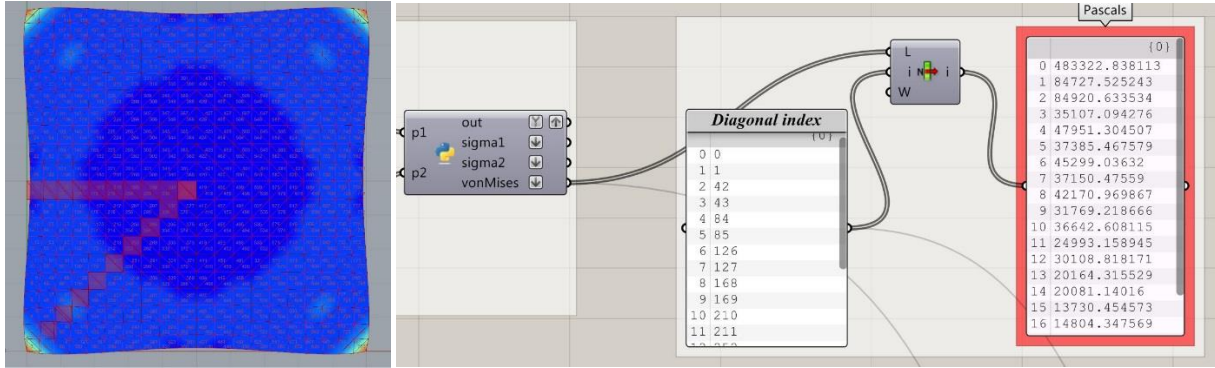


Figure A.6. step 03: The orthogonal and diagonal index numbers are identified based on the mesh numbers and then used as a list of indices to extract the related von Mises stress levels.

Plotting the read data, the results retrieved from Ansys and Karamba correspond very well. The data points of the orthogonal cut are plotted in Figure A.7 and A.8, whereas the data points of the diagonal cut are plotted in Figure A.9 and A.10.

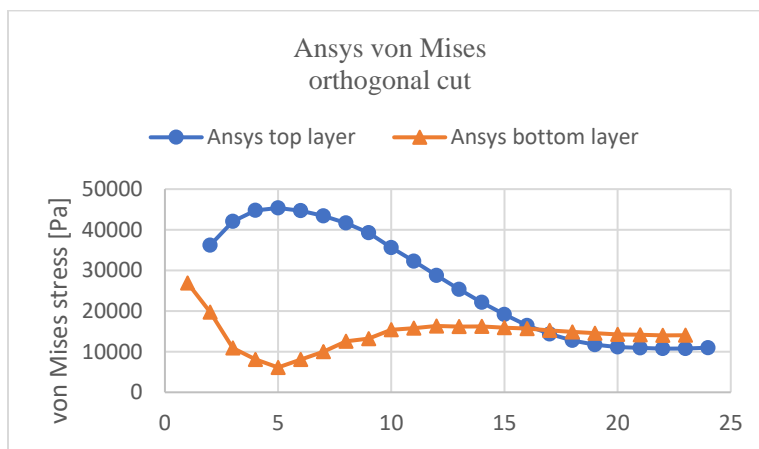


Figure A.7. von Mises stress on top and bottom layer of an orthogonally cut shell in Ansys

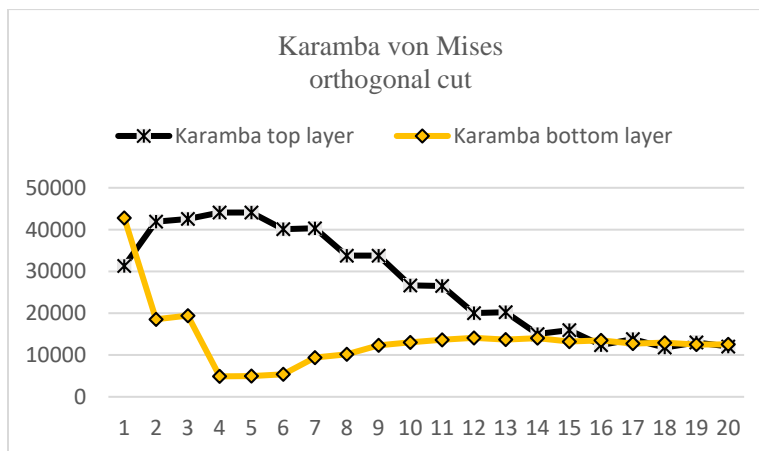


Figure A.8. von Mises stress on top and bottom layer of an orthogonally cut shell in Karamba

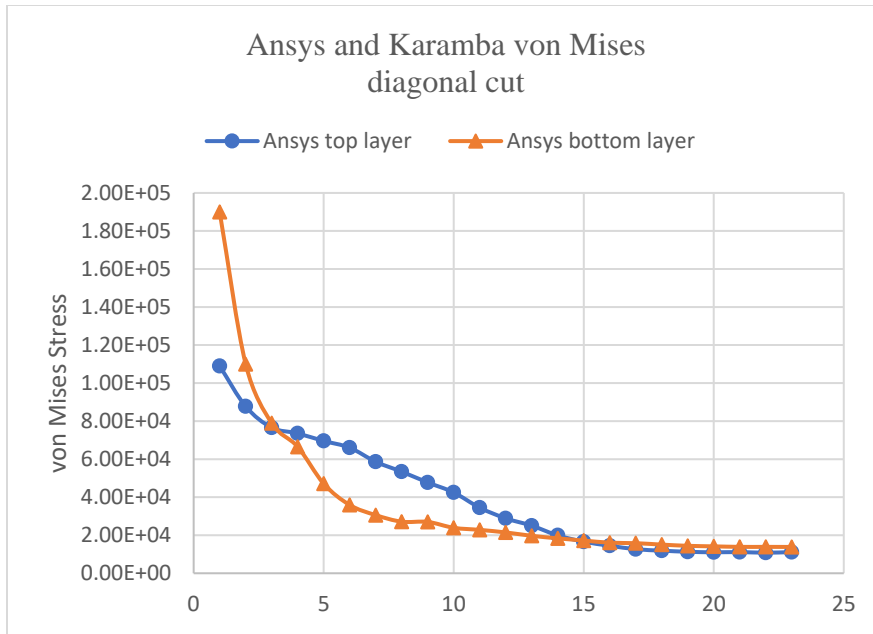


Figure A.9. von Mises stress on top and bottom layer of a diagonally cut shell in Ansys

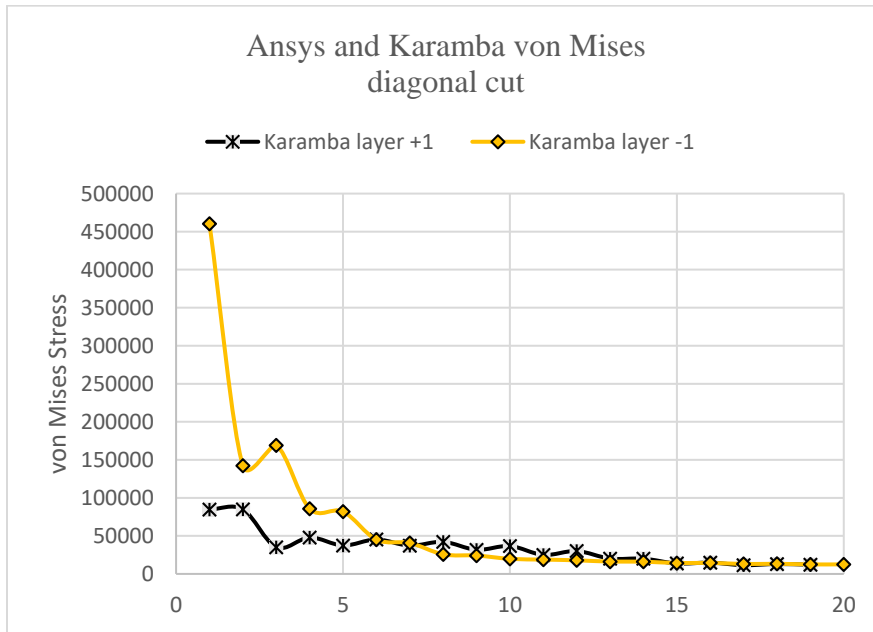


Figure A.10. von Mises stress on top and bottom layer of a diagonally cut shell in Karamba

After extensive validation processes, the results retrieved from Karamba corresponds well with ANSYS which is a well-known and reliable FEM simulation engines. Therefore, Karamba was chosen as the simulation engine for structural analysis

Appendix B:

Structural settings and analysis criteria in Karamba

Once the form is found through Rhino Membrane, it is analyzed for structural performance using Karamba plugin for Grasshopper. In general, structural analysis is consisted of three steps: pre-processing, processing and post-processing. Pre-processing changes the geometry to a representation that is appropriate for structural analysis engine to analyze. Processing occurs when the structural analysis is being operated on the prepared geometry. Post-processing is the stage when the user looks at different results available to him to make sense of them.

B.1 Pre-processing

In this phase, the geometric model is being prepared for structural analysis through adding supports, loads, and materials, as well as through defining the element for analysis and its cross section. Each setting is described below

B.1.1 support

The corners of the shell are chamfered before the supports are defined. This reduces formation of local stresses at the support and transfers load to the ground on a wider support (Figure B.1). The geometrical output of this phase is a BRep.

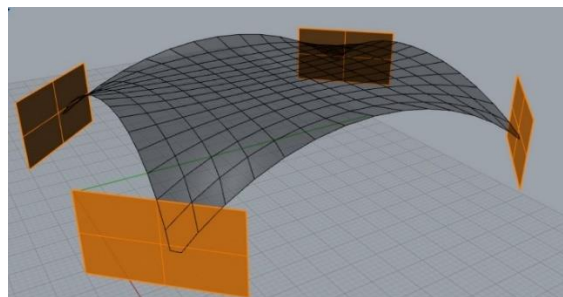


Figure B.1. Chamfering shell edges to avoid point supports

The next step is to extract edge curves in the support area. Karamba requires the support points to be directly extracted from the geometry. For this, the found form is changed from a BRep to a mesh, to extract the edge curves (Figure B.2).

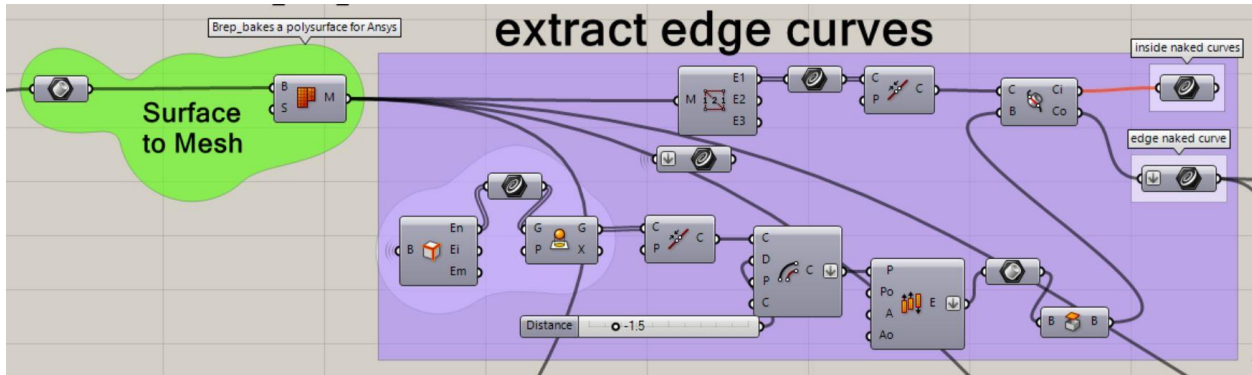


Figure B.2. Extracting edge lines to define supports

Once the edge curves for support are extracted, the points lying on the line are being extracted since Karamba only accepts points as supports at the time of writing this procedure (Figure B.3).

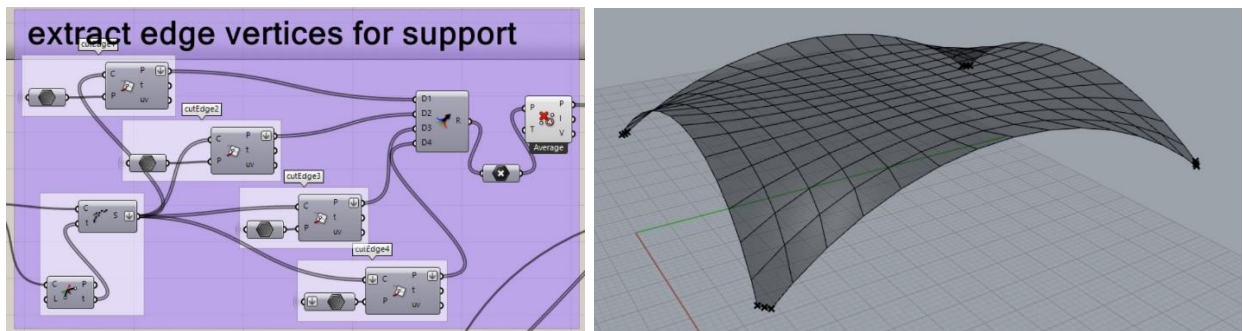


Figure B.3. Extracting edge vertices from edge lines to define supports

These points are then inserted to the *support* component by Karamba. The movement and rotation of the supports is restricted in x, y and z directions (Figure B.4).

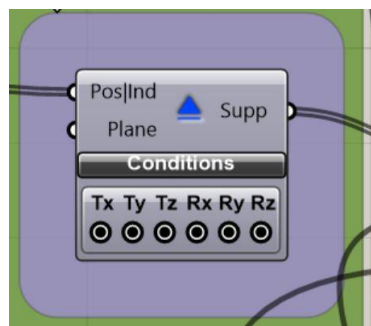


Figure B.4. Supports are restrained in x, y and z-direction for moving and rotation

B.1.2 Shell element

The mesh geometry which was chamfered will be used as the main geometry for structural analysis. This geometry should be passed through Karamba's *mesh to shell* element in order to be ready for structural analysis.

B.1.3 Load

A uniform load of 1 KN/m² is applied to the shell in the negative z direction (equation B.1).

$$Load = \frac{Area_{solidShell}}{Area_{perforatedShell}} \times 1[KN / m^2] \quad (B.1)$$

This load is adjusted once the shell is perforated. The equation for adjusting the load is described below. As an instance, a 1 KN/m² load is applied to a solid shell of any shape, but if the same shell is 50% perforated, then the load will be doubled (equation B.2).

$$Load \text{ For } 50\% \text{ Perforated Shell} = \frac{1}{0.5} * 1[KN / m^2] = 2[KN / m^2] \quad (B.2)$$

The load adjustment is necessary since the glazing are not loaded to the model, towards comparing different shells under the same loading conditions (Figure B.5).

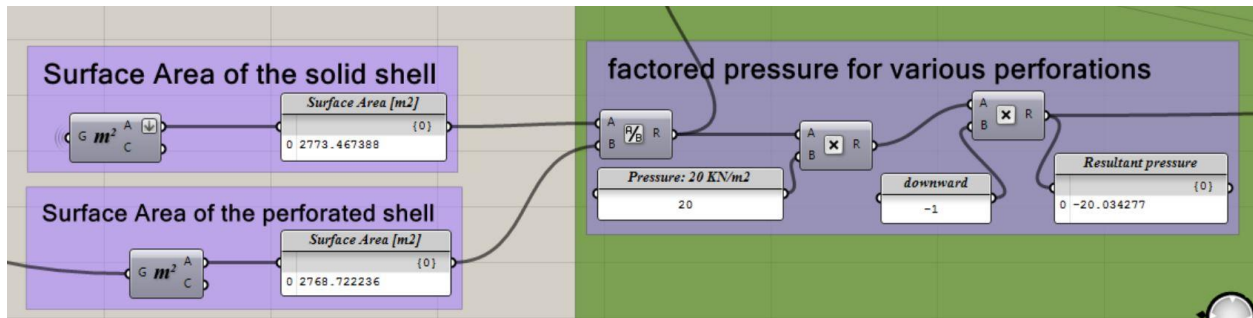


Figure B.5. factoring load based on the solid area of the shells

Dead load is also calculated and applied to the shell. The weight of the shell is calculated based on the solid parts only whereas holes are simply zero weight. In other words, the weight of the glazing on the shell is not included in the dead load, which gives an approximation of the self-weight of the shells (Figure B.6).

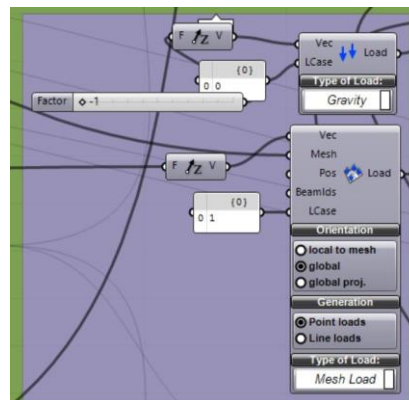


Figure B.6. Loading the shell, gravity load to consider dead load, as well as an applied load for live load

B.1.4 cross section

Thickness of the shell cross section is designed to vary from 10 cm to 40 cm in 5cm increments. This is fed as a list to the cross-section component of Karamba.

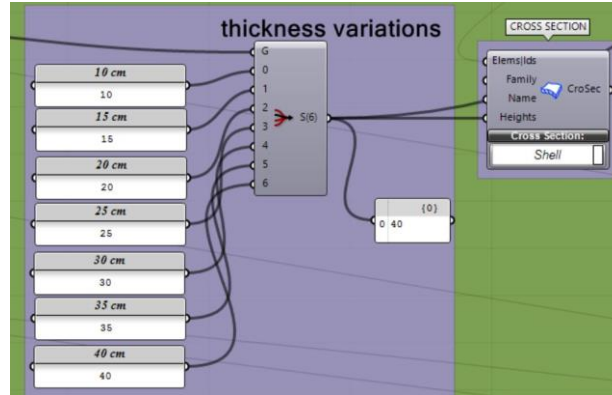


Figure B.7. defining multiple thicknesses to feed the cross-section element

B.1.5 Materials

Concrete is used as the shell material. The material is assumed to be homogenous with two layers of mesh used as reinforcement. The material properties are inserted in Table B.1 and are changed to the units that are appropriate for Karamba analysis (Table B.2).

Table B.1. Material properties

Elastic Modulus (E) [MPa]	Shear Modulus (G) [MPa]	Density [kg/m ³]	Coefficient of thermal expansion (alpha T) [1/C°]	Yield Strength (f _y) [MPa]
26000	10800	2400	0.00001	30

Table B.2. Material properties inserted in Karamba with related units

Elastic Modulus (E) [KN/cm ²]	Shear Modulus (G) [KN/cm ²]	Specific weight (Gamma) [KN/m ³]	Coefficient of thermal expansion (alpha T) [1/C°]	Yield Strength (f _y) [KN/cm ²]
2600	1080	23.52	0.00001	3

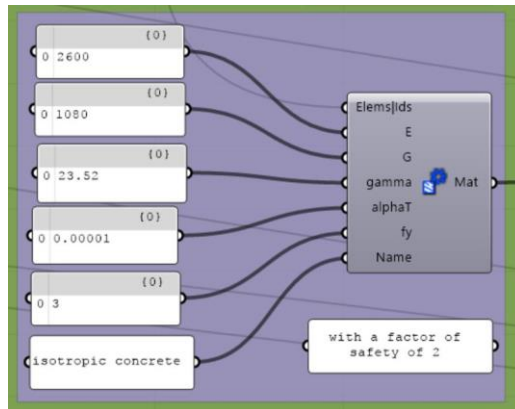


Figure B.8. Material properties to define concrete

B.2 Processing

Once the supports, shell element, load, cross section and materials are defined, they are fed into Karamba's *assemble model* component which assembles all of them together. Then, it can be fed into the *analyze* component for structural analysis.

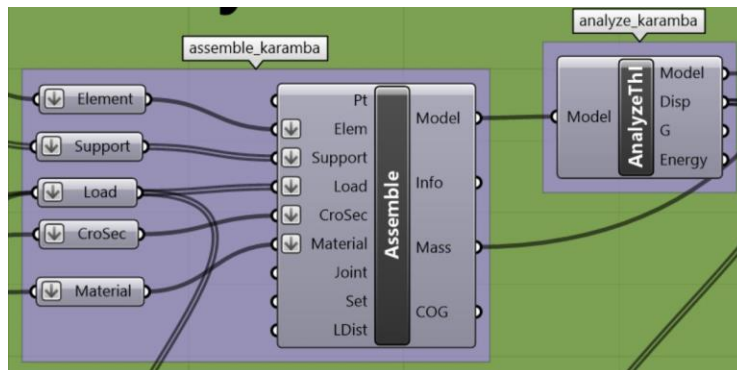


Figure B.9. Assembling the shell element, supports, load, cross section and material for analysis

B.3 Post-processing

Once the structural analysis is processed, the results can be fed into the *model view* for interpreting the results (Figure B.10), called post-processing. This can be done both graphically and numerically.

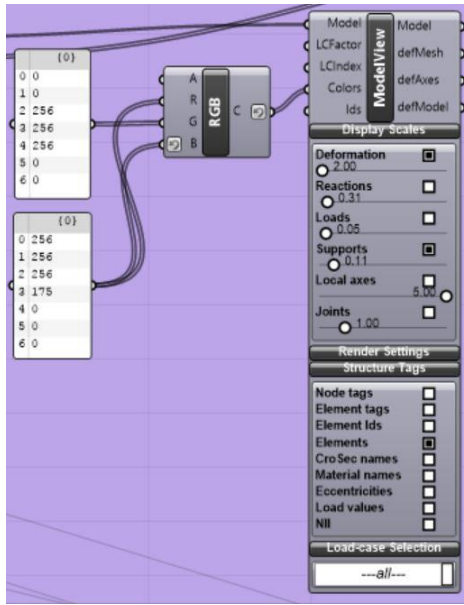


Figure B.10. Feeding the analysis results to model-view for post-processing

B.3.1 graphical post-processing

To scrutinize the results graphically, *shell view* is connected to *model view* to represent the results in the Rhino window. Different performance criteria can be selected in Grasshopper and then visualized in Rhino window, including deformation, von Mises stress levels, utilization ratio and the like.

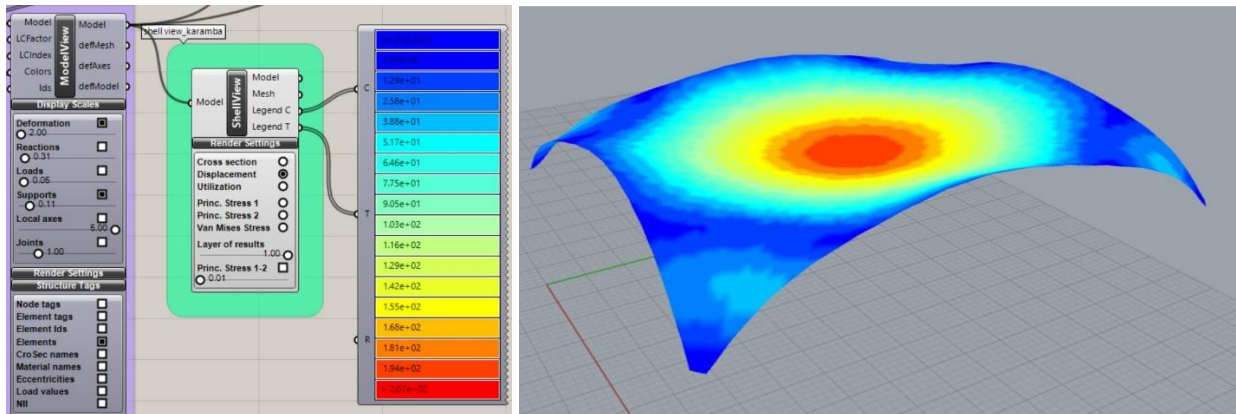


Figure B.11. Feeding the *model-view* to *shell-view* for graphical post-processing

B.3.2 numerical post-processing

Numerical results can also be extracted from the *model view* to be further processed. In this study, the goal was to extract von Mises stress values. Unlike maximum deformation, Karamba does not output maximum von Mises stress levels. Rather, it only outputs principal stress 1 and 2, by which

von Mises stress can be calculated. The rationale for calculating the von Mises is explained in the following.

Karamba outputs principal stress values as vectors with x, y and z component, representing the principal stress in x, y and z-direction. Therefore, these three vectors first need to be translated into one vector representing the principal stress.

σ_1 = First principal stress

σ_2 = Second principal stress

$$\sigma_1 = \sqrt{x^2 + y^2 + z^2}$$

$$\sigma_2 = \sqrt{x^2 + y^2 + z^2}$$

$$\text{von Mises stress} = \sqrt{\sigma_1^2 + \sigma_2^2 - (\sigma_1 \times \sigma_2)} \quad (3)$$

The results from *model view* were connected to *shell vector results* where the V_1 and V_2 at a specific layer of the shell are accessible. The unit is then converted from KN/cm²to Pa, and then a python code is developed to calculate the von Mises stress (Figure B.12).

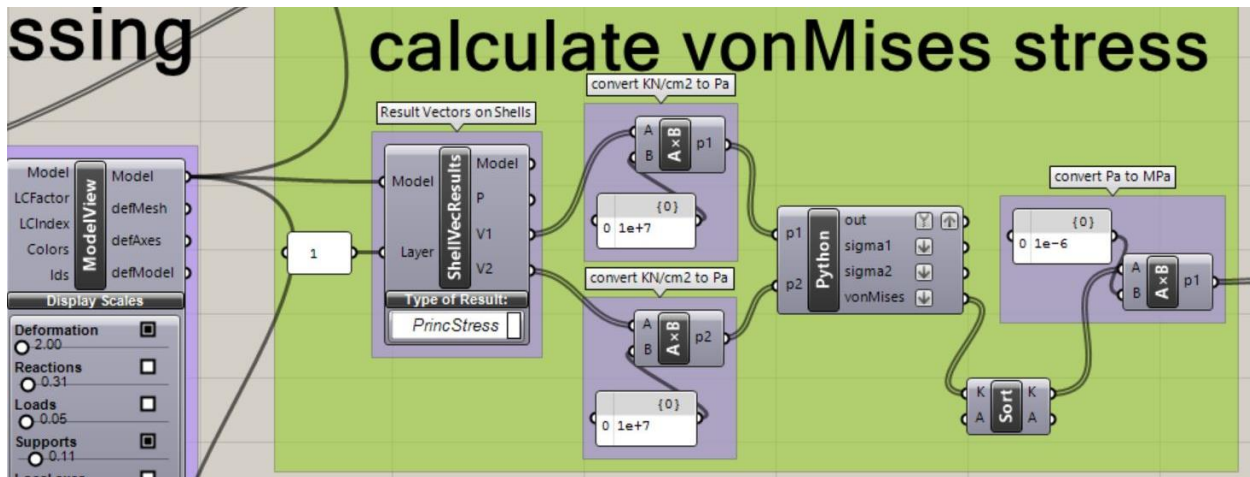


Figure B.12. Feeding the *model-view* to *shell vector results* for numerical post-processing

The python code that was used to implement the calculation is copied below.

```

print p1
x = (p1[0])
y = (p1[1])
z = (p1[2])
sigma1 = ((x**2) +(y**2) +(z**2)) **0.5
print sigma1
    
```



```

print p2
u = (p2[0])
v = (p2[1])
w = (p2[2])
sigma2 = ((u**2) +(v**2) +(w**2)) **0.5
print sigma2

vonMises = ( (sigma1**2)+(sigma2**2) - (sigma1*sigma2) )**0.5
print vonMises

```

It should be noted that although maximum displacement is calculated for serviceability conditions, maximum von Mises is not considered for the strength criteria. The analysis software tends to predict extremely high stresses at points of discontinuity, which is also dependent on the mesh configuration used by the analysis algorithm, this stress value cannot be the basis for assessing the performance of a whole shell. These highly localized extreme stresses are considered local effects that do not impact on the sizing criteria for the shell as a whole, and can be addressed locally.

Therefore, a proportional statistical distribution analysis is carried out using the von Mises stress levels of all the nodes, where only von Mises stress at the third quartile (Q₃) is considered. In statistics, the quartiles of a ranked set of data are described as three points that divide the data set into four equal groups. The third quartile is the middle value between the median and the highest value of the data, meaning that 75% of the data lie below it. This approach acknowledges the fact that the nodes that are subject to extreme stresses significantly higher compared to the majority of the remaining nodes are not the baseline for designing the shell. It averages out the maximum stresses, assuming that a degree of redistribution will take place in reality, and that high local stresses will be addressed locally.

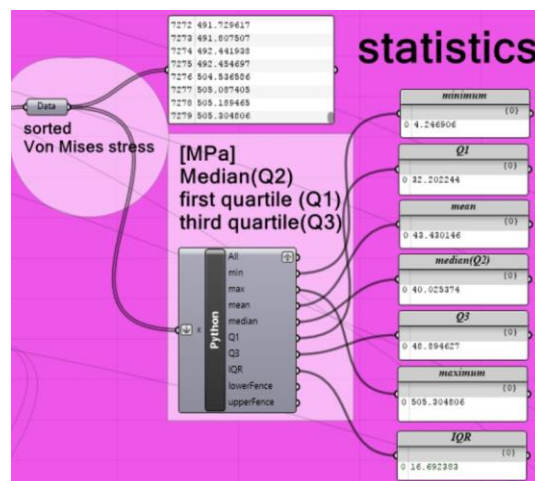


Figure B.13. The python code developed for statistical analysis outputs the Q₃ of von Mises stress levels

A python code that was developed to do statistical analysis, and extract minimum, maximum, and quartiles of data is copied below.

```

#*****calculate Min/Max
min = float(x[0])
indexMin = 0
print min
print 'min is', min, 'with index of', indexMin

max = float(x[-1])
indexMax = len(x)
print max
print 'max is', max, 'with inde of', indexMax
#*****calculate Mean
mean = sum(x)/len(x)
print 'mean is',mean
#*****calculate Median
median = 0
indexMedian = 0

if len(x)%2 == 0:
    #find the two middle values, located at index A & index B
    indexA = int((len(x)/2)-1)
    a= float(x[indexA])
    indexB = int(len(x)/2)
    b= float(x[indexB])
    median = (a+b)/2
    indexMedian = indexB #when median is calculated from two
values, the higher index is used for later processes
else:
    #find the middle value, located at index C
    indexC = int( (len(x)/2) )
    median = x[indexC]
    indexMedian= indexC

print 'median is', median, 'with index of', indexMedian

if len(x)%2 == 0:
    lowerQ2List = x[:indexMedian]
    upperQ2List = x[indexMedian:]
else:
    lowerQ2List = x[:indexMedian]
    upperQ2List = x[indexMedian+1:]
#*****Q1
Q1 = 0
print x
print lowerQ2List

if len(lowerQ2List)%2 == 0:
    #print 'even'
    indexD = int((len(lowerQ2List)/2)-1)
    valueD = float(lowerQ2List[indexD])
    indexE = int(len(lowerQ2List)/2)
    valueE = float(lowerQ2List[indexE])
    print valueD, 'and', valueE
    Q1 = (valueD + valueE)/2

```

```

else:
    #print 'odd'
    midIndex = int(len(lowerQ2List)/2)
    Q1 = lowerQ2List[midIndex]

print Q1
#*****calculateQ3
Q3 = 0
print x
print upperQ2List

if len(upperQ2List)%2 == 0:
    #print 'even'
    indexF = int((len(upperQ2List)/2))
    valueF = float(upperQ2List[indexF])
    indexG = int((len(upperQ2List)/2)+1)
    valueG = float(upperQ2List[indexG])
    print valueF , 'and' , valueG
    Q3 = (valueF + valueG)/2
else:
    #print 'odd'
    midIndex = int(len(upperQ2List)/2)
    Q3 = upperQ2List[midIndex]

print Q3
#*****calculate IQR
IQR = Q3 - Q1
#*****calculate lower & upper fence
lowerFence = Q1 - (1.5*IQR)
upperFence = Q3 + (1.5*IQR)

```

B.4 Concrete and formwork costs

There are three components that affect the cost:

- 1/concrete cost
- 2/reinforcement cost
- 3/Formwork cost (formwork material and labor)

The concrete and reinforcement costs are retrieved from the Grasshopper model and outputted as one number. The formwork cost is calculated as a ratio of concrete and reinforcement cost.

B.4.1 Concrete cost

The mass of the shell is calculated by Karamba's *assemble* component and is outputted in kilograms as the units. This is multiplied by a factor of 0.001, to calculate weight in tones (Figure B.14).

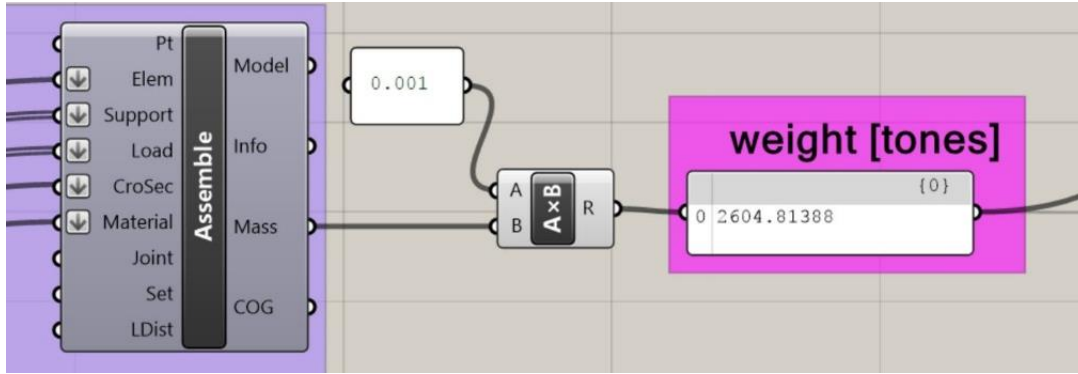


Figure B.14. *Assemble* module in Karamba outputs mass in kilograms, which is then converted to tones

On the other hand, the unit price for concrete is considered to be \$0.17 per kg, by looking at the CES Edu Pack material database. This unit cost is multiplied by the mass of the shell to retrieve the total material cost associated with each shell.

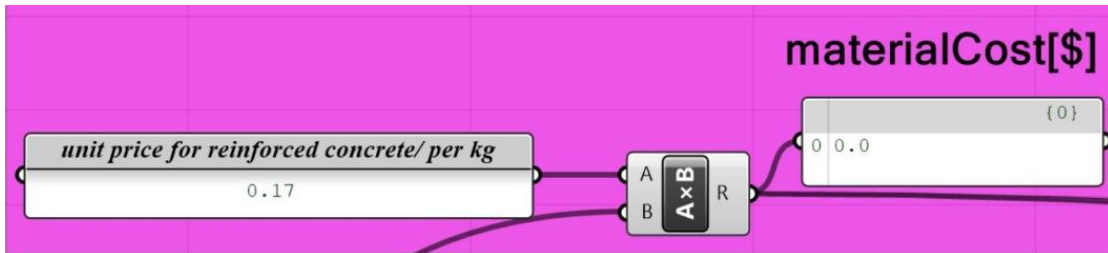


Figure B.15. Calculating material cost using the mass output of Karamba's *Assemble* module

B.4.2 Formwork cost

Formwork cost is a variable that is not calculated in the grasshopper script, rather it is calculated when all the generative runs are completed and by using output variables such as concrete weight and cost. Relative cost of construction in reinforced concrete splits between formwork, concrete and reinforcement cost. A typical range includes:

Formwork: 40 – 60% of total cost

Concrete: 30 - 40% of total cost

Reinforcement: 20 - 40% of total cost

These percentages are based on the assumption that the shells are lightly reinforced due to the compression efficiency of the shell. The ratio between formwork and concrete cost varies depending on the perforation ratio. In this regard, the two extremes, the continuous shell and the grid shell are assumed to have cost percentages as following:

Solid shell

Formwork = 40% of total cost

Concrete = 40% of total cost

Reinforcement = 20% of total cost

Grid shell

Formwork = 60% of total cost

Concrete = 20% of total cost

Reinforcement = 20% of total cost

Solid shell		Grid shell
Formwork: 40%	←————→	60%
Concrete: 40%	←————→	20%
Reinforcement: 20%	←————→	20%
$\frac{\text{Formwork ratio}}{\text{concrete ratio}} = 1$	←————→	$\frac{\text{Formwork ratio}}{\text{concrete ratio}} = 3$

Based on the calculations, the cost of formwork and concrete are assumed to be equal in solid shells, while the formwork cost is assumed to be 3 time more than the concrete costs in grid shells.

Therefore, it can be assumed that shells that lay in between have $\frac{\text{formwork cost}}{\text{concrete cost}}$ ratio that varies between 1 to 3.

The concrete cost is calculated from the Grasshopper model. The goal is to come up with a factor that can estimate the formwork cost using the concrete cost, knowing the perforation ratio of the shell (varying from 0 to 66%) which is also calculated from the Grasshopper model.

$$\text{Factor} = 1 + (\text{Perforation ratio} \times 3)$$

$$\text{When Perforation ratio is 0 (solid shell): factor} = 1 + (0 \times 3) = 1$$

$$\text{When Perforation ratio is 0.66 (grid shell): factor} = 1 + (0.66 \times 3) = 2.98$$

$$\text{When Perforation ratio is 0.9 (extreme grid shell): factor} = 1 + (0.9 \times 3) = 3.7$$

Using this formula, a factor is calculated based on the perforation ratio first. Then the concrete cost is multiplied by this factor to estimate the formwork cost. The goal is to maintain the concrete/formwork ratio in the two extreme as well as in all the cases in between.

B.5 Performance limits

This section reviews the performance criteria for assessing the performance of the shells.

As noted in table 1, the yield stress (f_y) is set to 30 MPa. Considering a safety factor of 2, this means that no shell should pass the stress limit of 15 MPa. Shells that are undergoing von Mises stress levels lower than 15 MPa, are considered *working and safe*. Shells that are undergoing Von Mises stress levels higher than 15 MPa but still under 30 MPa, are not considered *unsafe and working*. Shells that have a stress number higher than 30 MPa are considered *failed*. Note that the Von Mises stress that is based for this assessment is not the maximum stress level, rather the von Mises at the third quartile.

- Von Mises stress at Q3 < 15 MPa → working and safe
- 15 MPa < Von Mises stress at Q3 < 30 MPa → working and unsafe
- Von Mises stress at Q3 > 30 MPa → failed

Deformation limit is calculated relative to span. Deflection caused by dead load should be 1/360 of the span. The same ratio applies to the deflection limit caused by live load. Therefore, the

$$A = 1/360 \text{ span (deflection limit by Dead Load)}$$

$$B = 1/360 \text{ span (deflection limit under Live Load only)}$$

$$\text{Deflection criteria} = A + B = 1/360 \text{ span} + 1/360 \text{ span} = 1/180 \text{ span}$$

It should be noted that the 1/180 span deflection limits assumes that plaster is not used as finishing in the building. For the designed shell with a 50 meter by 60-meter span, first the span is averaged to 55, and then the deflection limit is calculated as:

$$55/180 = 0.3 \text{ meter}$$

Another deflection limit is retrieved by calculating the 1/120 span ratio which is a rule of thumb for industrial spaces. Using this criterion, the acceptable deflection is calculated as 0.45 meter.

$$55/120 = 0.45 \text{ meter}$$

These limits are used to break the performance values into subgroups for further analysis.

- Deflection < 0.3 meter \rightarrow acceptable
- $0.3 < \text{deflection} < 0.45$ \rightarrow acceptable
- $0.45 < \text{deflection} < 1$ \rightarrow unacceptable
- Deflection > 1 \rightarrow extreme and unacceptable

Appendix C:

Daylighting settings in DIVA

C.1 Surface properties

The materials assigned to surfaces in DIVA are outlined in the table. It should be noted that the program of the space is assumed to be a courtyard surrounded by buildings, thus having an adiabatic property. Therefore, the walls are modeled as one surface with one material assigned to it, in this case, the *outside façade* material. It should be noted that the surface properties of a material such as its color and reflectivity affect daylighting performance. The construction and thermal properties of the material is defined in the Archsim plug-in for Rhino, which ultimately affects the energy performance of the space.

Table C.1. Surface properties in DIVA

Roof	Generic Ceiling_80%
Wall	Outside façade_35%
Floor	Generic floor_20%
Ground	Outside ground_20%
Glazing	Generic Translucent panel_20%

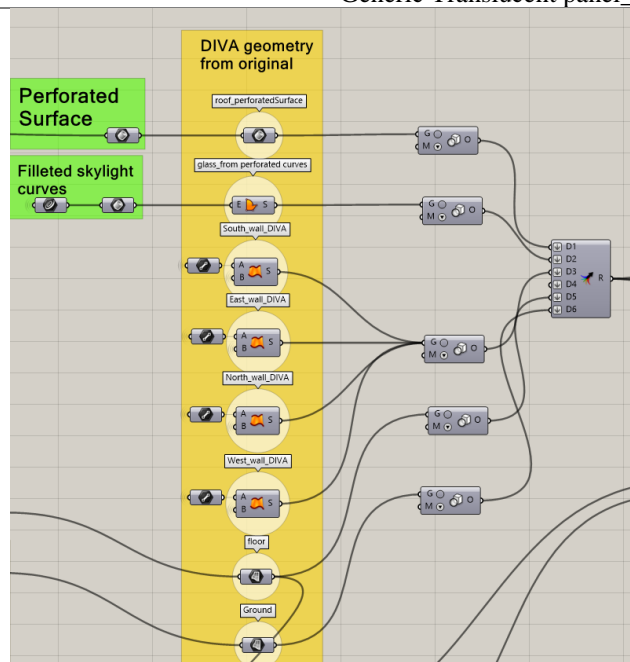


Figure C.1. DIVA setup

C.2 Daylighting Grid, occupancy schedule and daylighting settings

A horizontal plane was placed at 90 cm height from the ground with a grid division of 1 meter by 1 meter. This plane was used to measure the horizontal illuminance that falls upon it. It should be noted that hidden inputs need to be exposed in the *daylighting grid* icon, in order to change the grid settings.

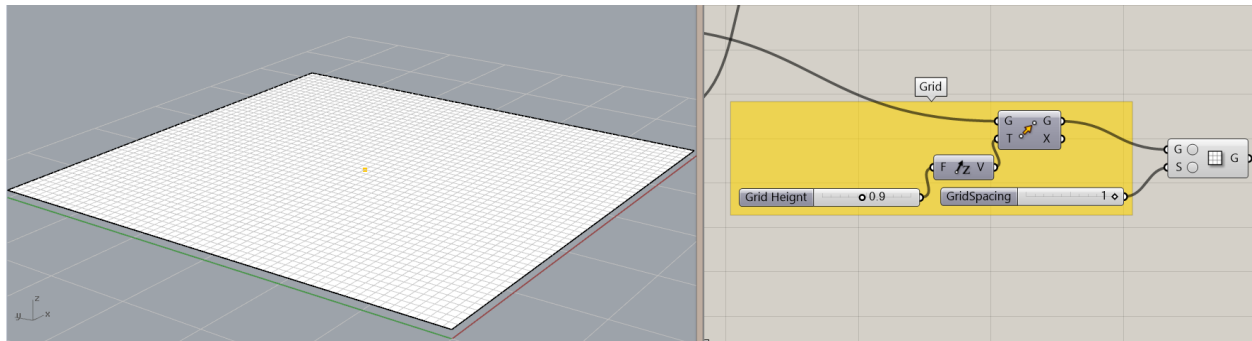


Figure C.2. Daylighting grid

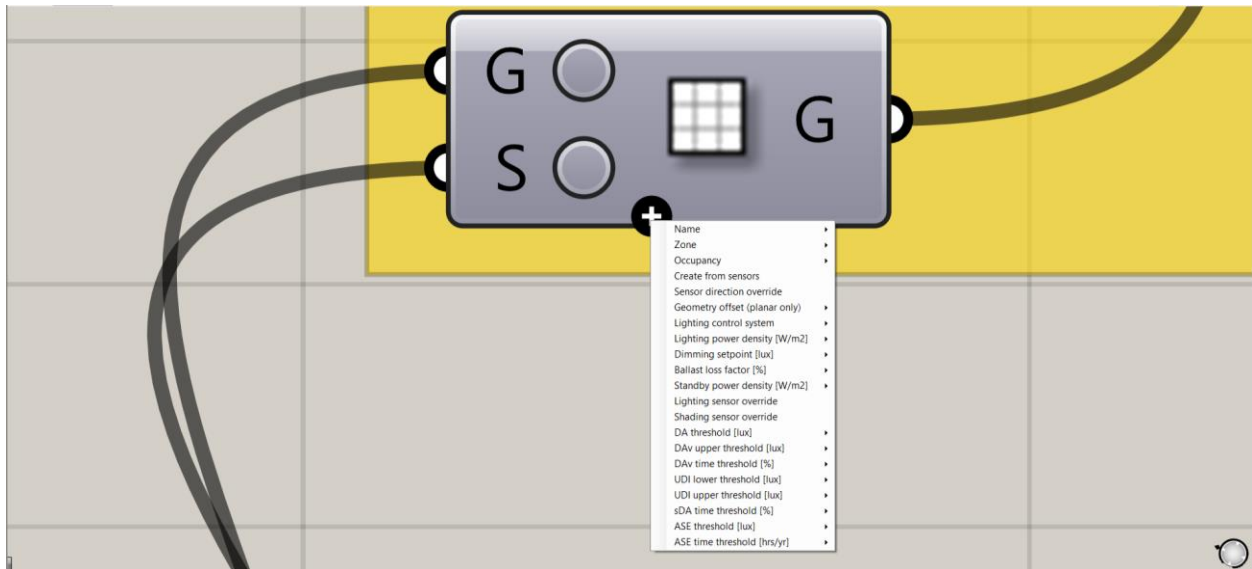


Figure C.3. Grid settings

Table C.2. Daylighting settings

Occupancy	8 to 6 with DST (Daylight Saving Time)
Lighting Control System	Manual on/off switch
Lighting power density	10.76 [W/m ²]
DA threshold	300 [lux]
UDI lower threshold	100 [lux]
UDI upper threshold	2000 [lux]
sDA (spatial Daylight Availability) time threshold	50 [%]

C.3 Assemble of components

The geometry and the horizontal grid are fed into DIVA's annual daylighting component. In addition, a name tag and a button to run the analysis.

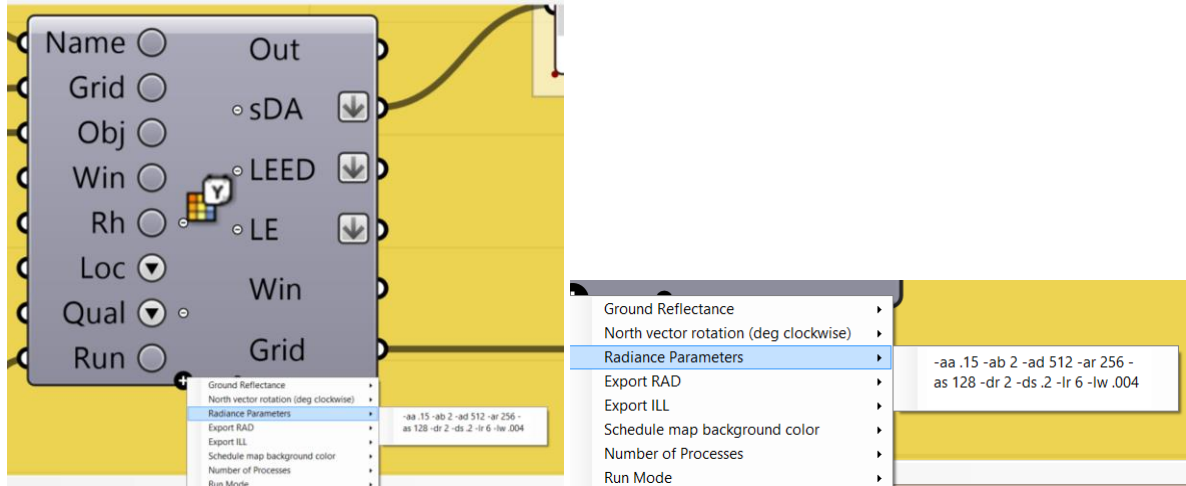


Figure C.4. Radiance settings

Table C.3. Radiance parameters

aa	ab	ad	ar	as	dr	ds	Ir	Iw
0.15	2	512	256	128	2	0.2	6	0.004

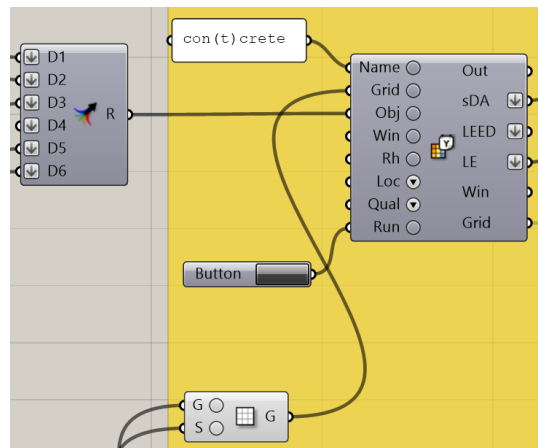


Figure C.5. Merging components for analysis

C.4 Location

The location is set to Boston-Logan International Airport.

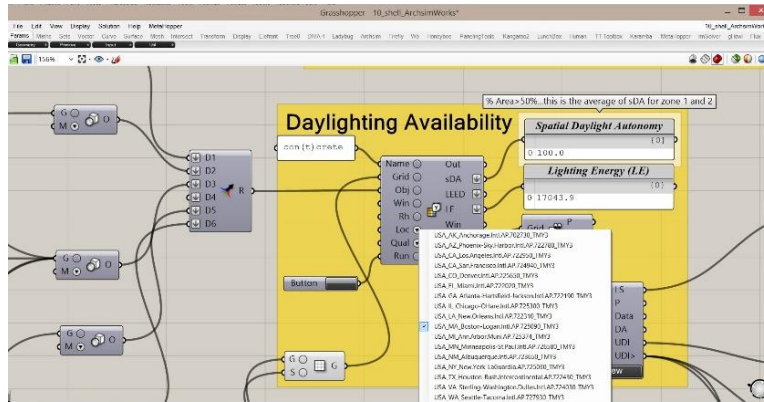


Figure C.6. Location settings

C.5 Outputs from the Grid viewer

The climate-based metrics such as the spatial daylight autonomy (sDA), Daylight Availability (DA_v), and useful daylight illuminance (UDI) can be retrieved from the *grid viewer* component. In addition, a lighting schedule (LS), as well as the occupancy schedule (OS) can be extracted based on daylight availability. These schedules can be fed into energy analysis settings to control electric lighting switches later on.

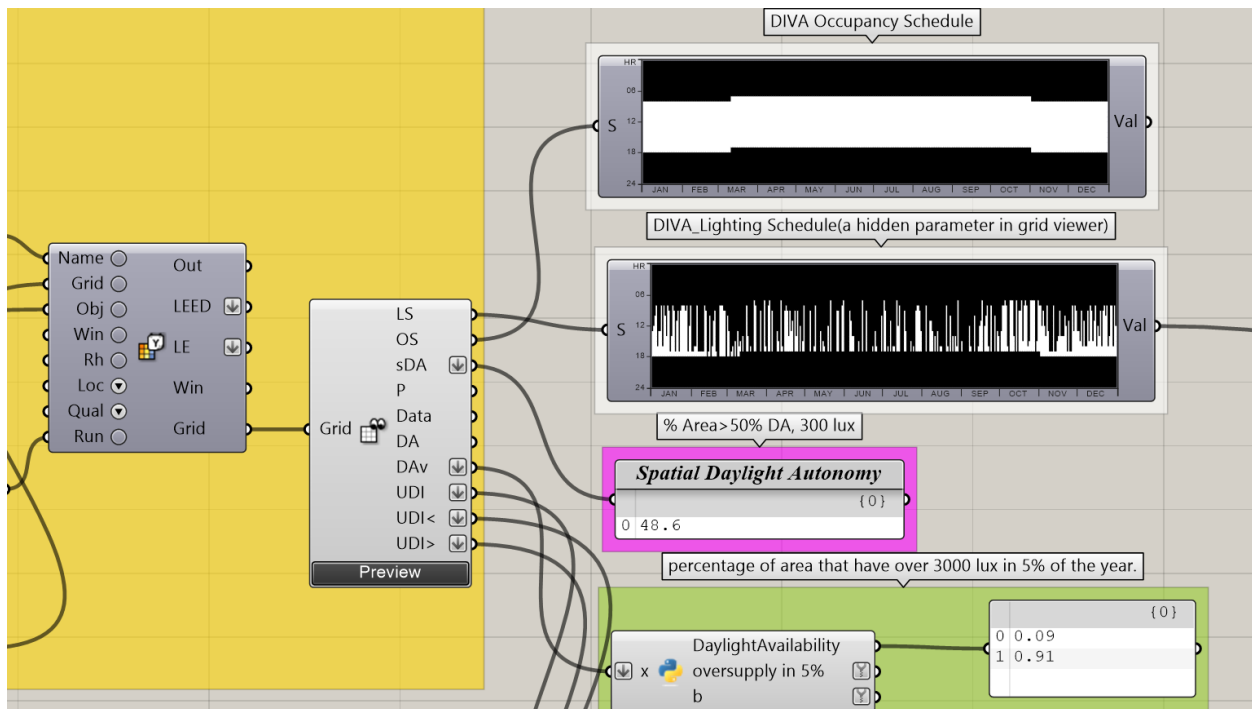


Figure C.7. Daylighting results

SDA (spatial daylight autonomy): this is defined as the percentage of area that receives the daylight threshold (300 lux) in 50% or more of the times of the year. Daylight availability outputs

a list of performance values for all the nodes, where a positive value indicates being within the threshold, and a negative number indicates having an oversupply of daylight throughout the year. As noted in the daylighting chapter, an oversupply up to 5% can be tolerated by the occupants. Therefore, further processing has been done on the list of values, to split them into two lists, one list for the positive values to recognize what percent of the year the received daylight is useful; and the other list for the negative values to highlight the percentage of the working year with oversupply more than 5%.

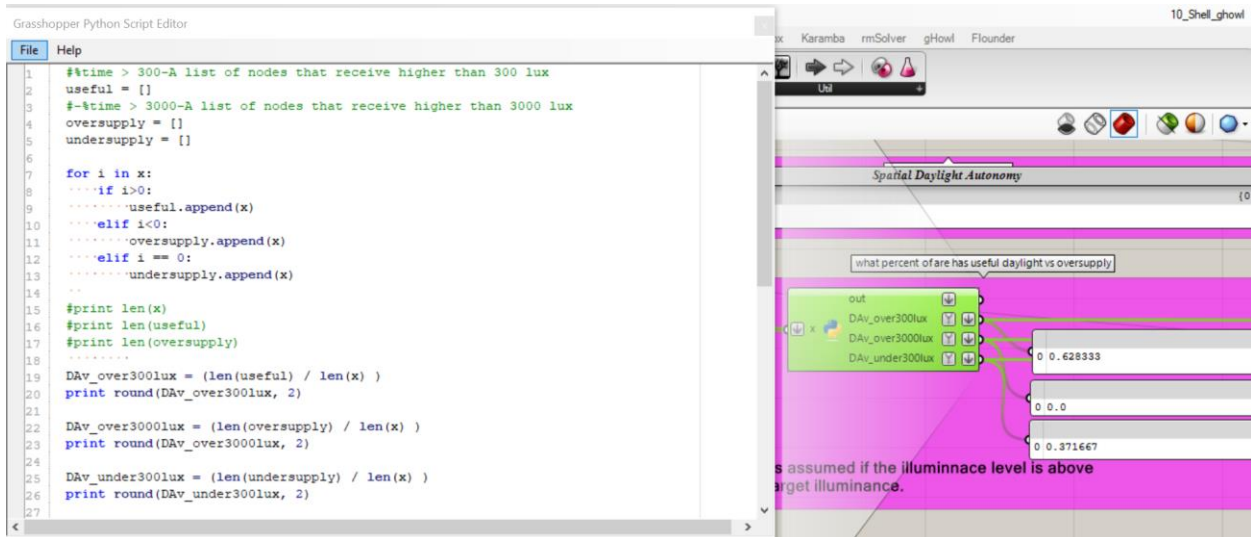


Figure C.8. Python script editor in grasshopper

C.6 Code block for calculating UDI 50%

```

#%time > 300-A list of nodes that receive higher than 300 lux
useful = []
#-%time > 3000-A list of nodes that receive higher than 3000 lux
oversupply = []
undersupply = []

for i in x:
    if i>0:
        useful.append(x)
    elif i<0:
        oversupply.append(x)
    elif i == 0:
        undersupply.append(x)

#print len(x)
#print len(useful)
#print len(oversupply)

DAV_over300lux = (len(useful) / len(x) )
print round(DAV_over300lux, 2)

DAV_over3000lux = (len(oversupply) / len(x) )
print round(DAV_over3000lux, 2)

DAV_under300lux = (len(undersupply) / len(x) )
print round(DAV_under300lux, 2)

```

```

DAv_over3000lux = (len(oversupply) / len(x) )
print round(DAv_over3000lux, 2)

DAv_under300lux = (len(undersupply) / len(x) )
print round(DAv_under300lux, 2)

DAv_oversupplyDes = ""
if DAv_over3000lux > 0.05:
    DAv_oversupplyDes = "daylight oversupply exceeded 5% of the occupied
times"
    print DAv_oversupplyDes
else:
    DAv_oversupplyDes = "daylight oversupply is within limits"
    print DAv_oversupplyDes

```

C.7 Grid viewer-Lighting Schedule

The lighting schedule provides an array of 0 and 1s, where 0 represents presence of adequate daylight thus no need for electric lighting; and 1 represents being underlit thus the necessity of electric lights to be turn on. The schedule is calculated from all the days of a year, for the 24 hours of a day (365 days x 24 hours = 8760).

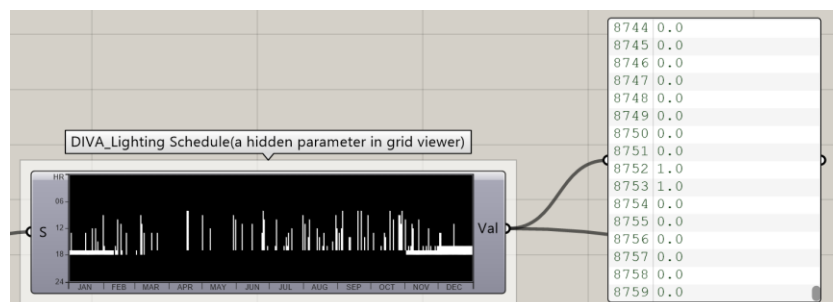


Figure C.9. Exporting a daylighting schedule

Appendix D:

Energy settings in ARCHSIM

D.1 Custom geometry for Archsim energy analysis

An instance of the approximation of the NURBS geometry-to-a-mesh which is appropriate for energy analysis is created. This model is used for all the energy analysis.

D.2 Custom materials and construction assemblies in Archsim

The *layer* component in Archsim is used to create a custom material. Here, *concrete reinforced 30-50 MPa* from the Archsim library is used and a custom thickness is assigned to it. In the next step, one or multiple layers of material with different thicknesses can be fed into the *opaque construction* component. Here, only one layer of concrete was used to make different concrete constructions with different thicknesses. The construction needs to then be added to the *library* to be accessible in analysis components.

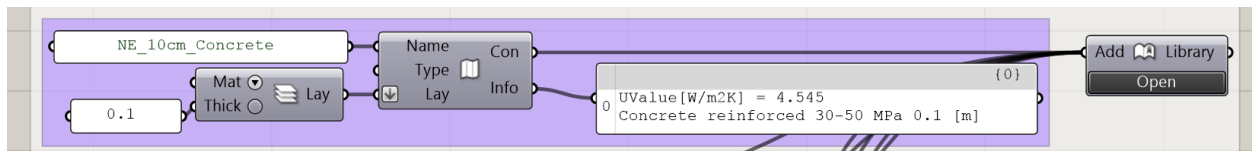


Figure D.1. Creating new materials and adding them to the library

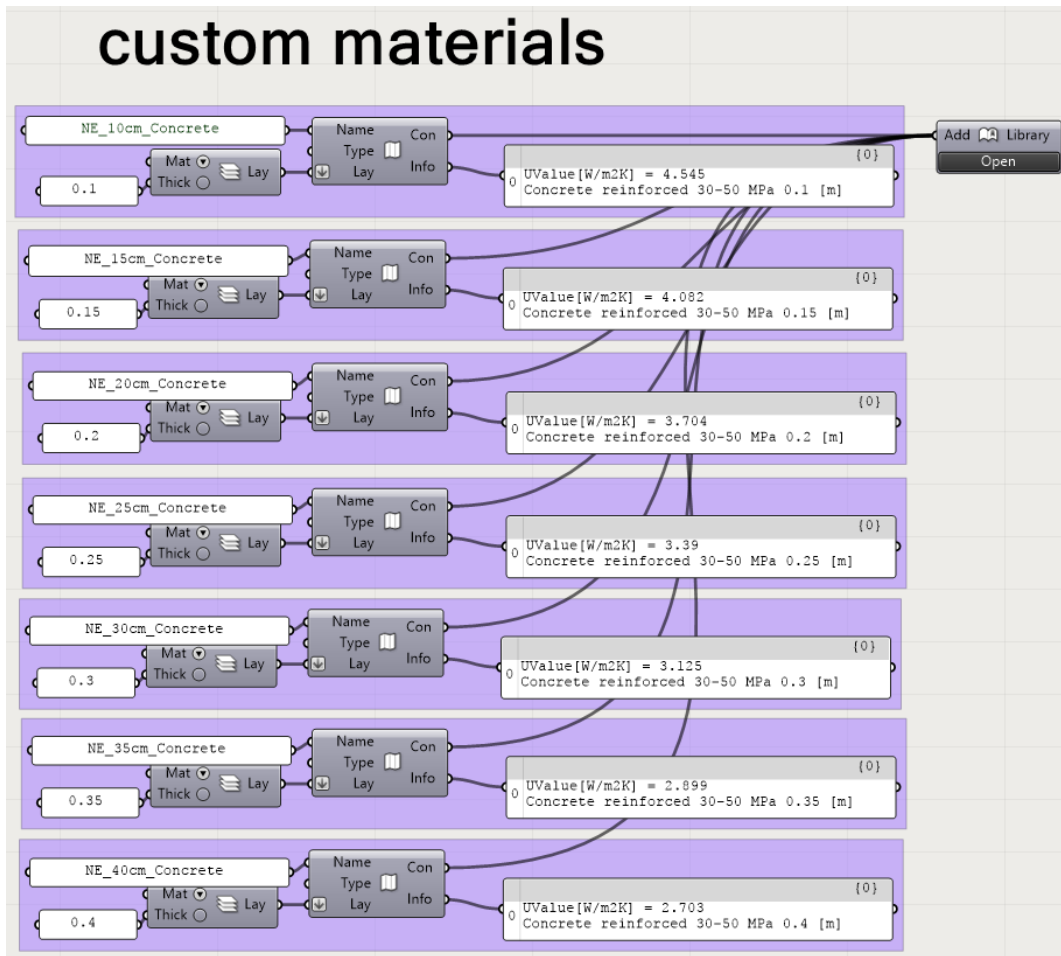


Figure D.2. Concrete with different thicknesses is created

D.3 Custom schedules in Archsim

The lighting schedule extracted from DIVA earlier in the process is inserted into Archsim's *array schedule* component, and then inserted to the *library* component. This will make this particular schedule available in the energy analysis in the drop-down menus.

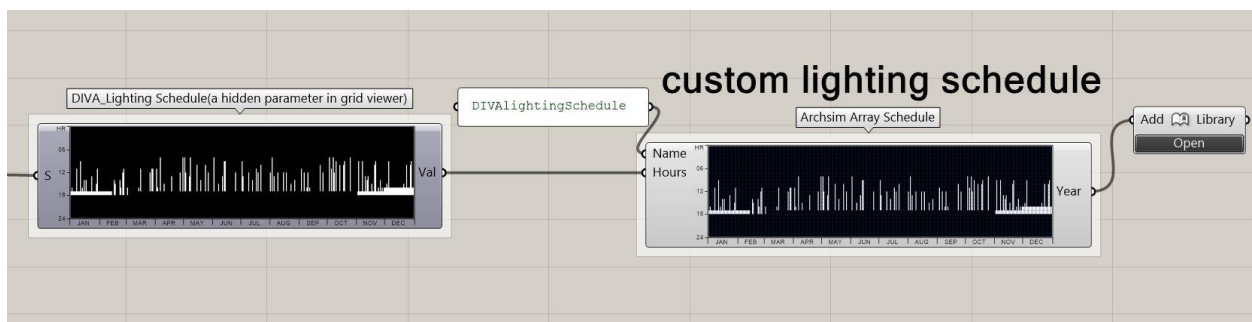


Figure D.3. Using daylighting schedule in the energy runs

D.4 Thermal zone

Once the geometry is converted into a closed mesh geometry and appropriate for the Energy plus simulation engine, the BREP geometry is inserted into the Archsim *thermal zone* component. This analysis assumes the whole volume being one single zone. The glazing geometry is also inserted into the Archsim *window* component. The two are then fed into the Archsim *zone connectivity network*. It should be noted that the walls and ground of the zone are assumed to be adiabatic, thus are separately inserted as a special boundary condition into the *Bco* section of the *zone connectivity network*. These are mesh surfaces with their normal directions pointing inward.

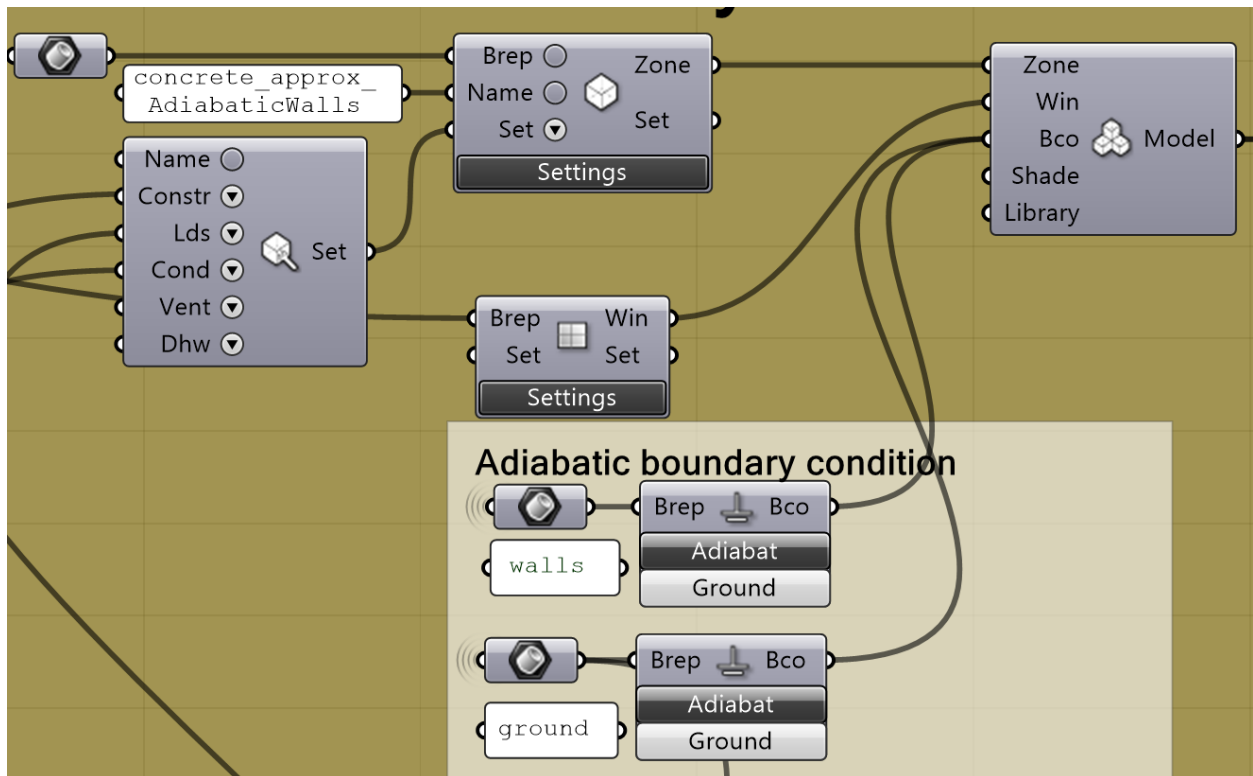


Figure D.4. Thermal zones

Once all the necessary components are linked to the zone connectivity network, they can be checked with *surface analysis* to visualize how the energy plus is seeing our model.

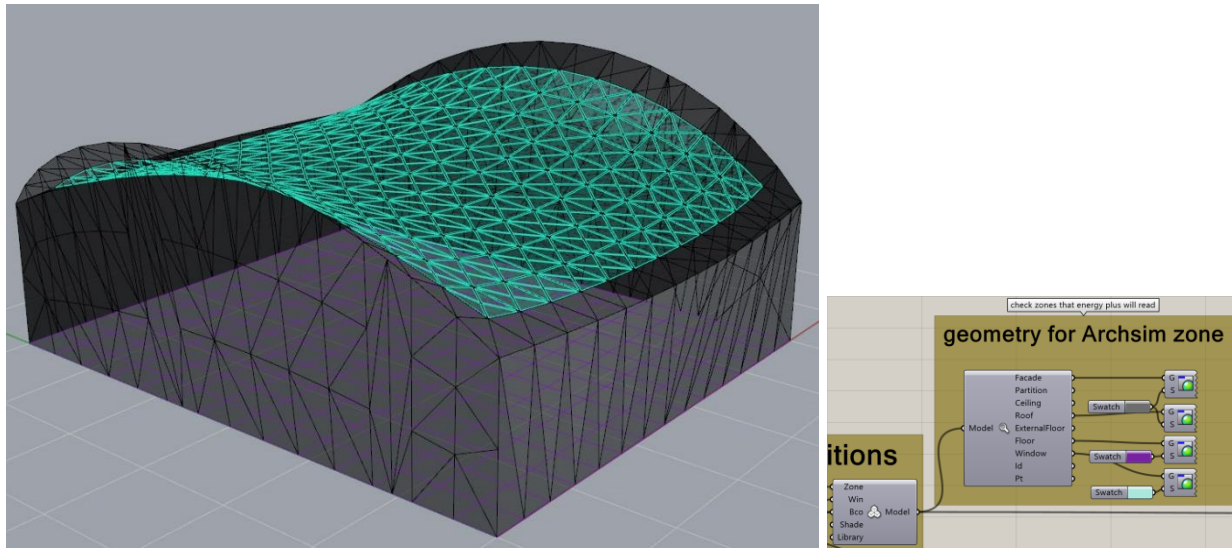


Figure D.5. Energy model visualization

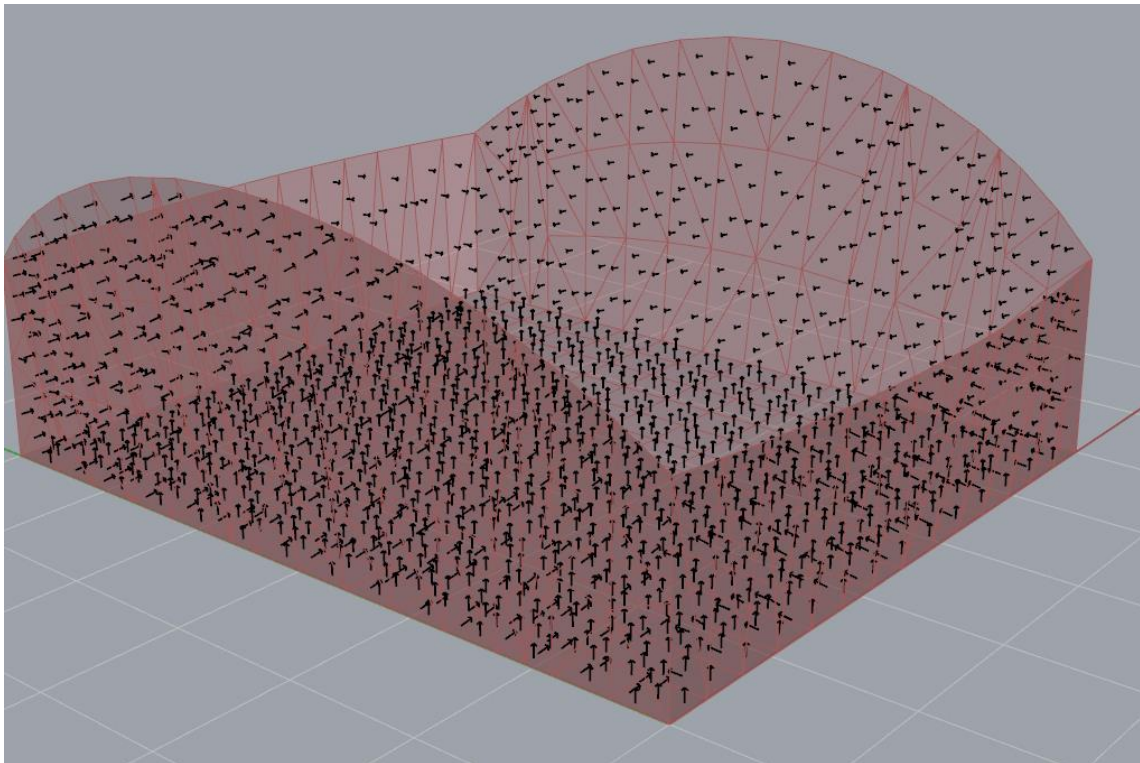


Figure D.6. Adiabatic surfaces with Normals pointing inside

D.5 Zone settings

The thermal zone settings are described more in depth here. The *zone settings* component has several inputs, including *zone construction*, *zone loads*, *zone conditioning*, *zone ventilation* and *zone hot water*. Each component is described below.

D.5.1 Zone settings- zone constructions

As noted before, different concrete constructions with different thicknesses were created and added to the library. These are used to create a predefined constructions for the zone, including roof, façade, slab, partition and ground construction. It should be noted that:

a/ all the elements need to have a construction material assigned to them, even though they are later considered to be adiabatic.

b/ in this research study, the roof construction varies while the remaining construction materials remain consistent for future comparison studies.

Table D.1. material settings for the energy analysis

roof	facade	slab	partition	ground
Variable	10 cm concrete in all cases	10 cm concrete in all cases	10 cm concrete in all cases	Default construction

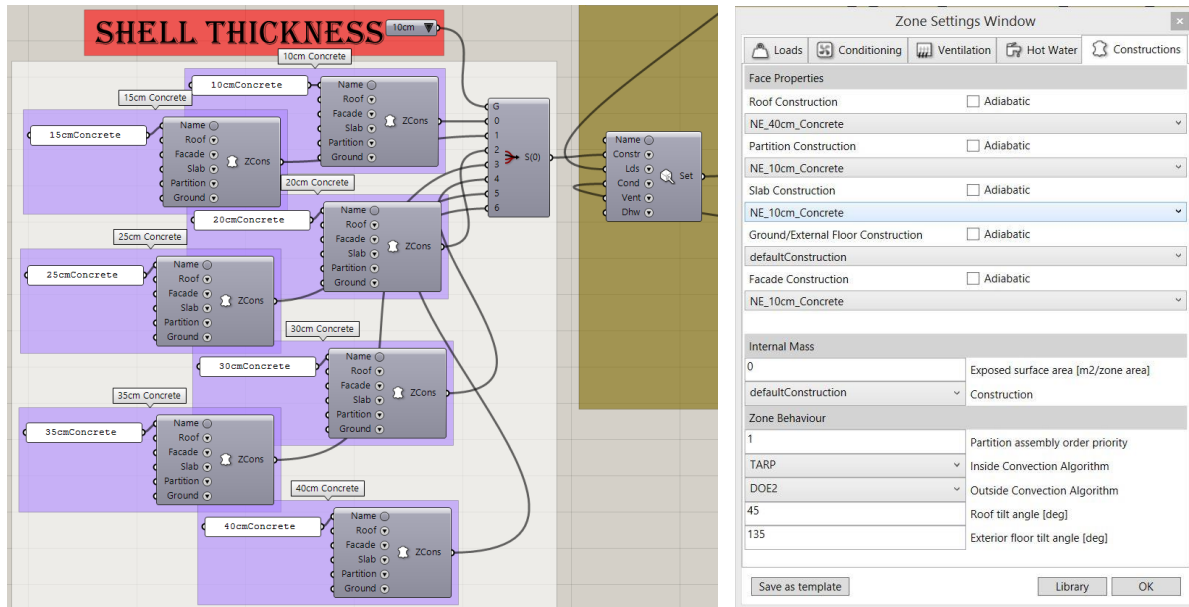


Figure D.7. Zone setting construction

D.5.2 Zone settings- zone loads

The target illuminance level is set to 300 lux, and the occupancy schedule is set to 8 to 6 with DST (daylight saving time). Note that these two settings are consistent with DIVA settings. The lighting schedule is set as the *DIVA lighting schedule* which will be extracted from the daylighting analysis in each run.

D.5.3 Zone settings- zone conditioning

The heating and cooling set points are set to 20 and 26 Celsius respectively. The equipment is always on, once they meet the set point will turn off. When the temperature drops or increase, they kick back to the system and so on.

D.5.4 Zone settings- zone ventilation and zone hot water

These are left unchanged and as default.

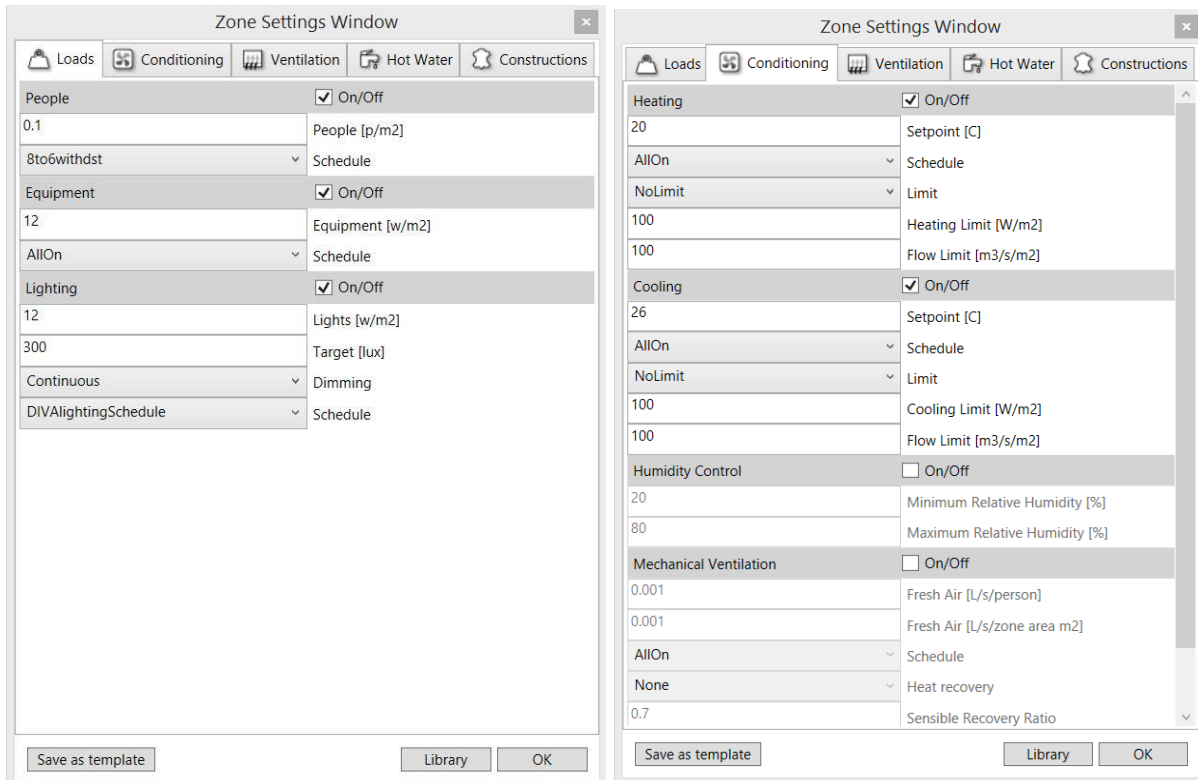


Figure D.8. Zone load and conditioning settings

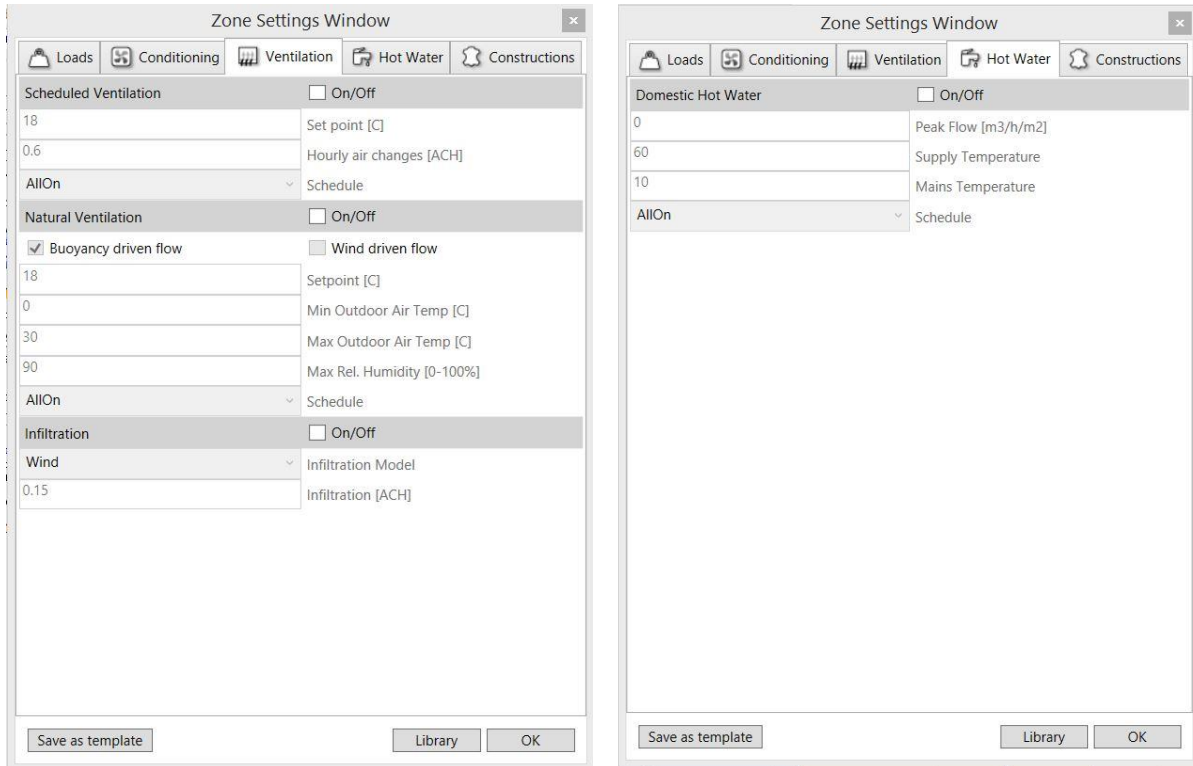


Figure D.9. Zone ventilation and hot water settings

D.6 Window settings

The window has been set as an external window with a double pane clear glazing. Again, this is consistent with DIVA settings.

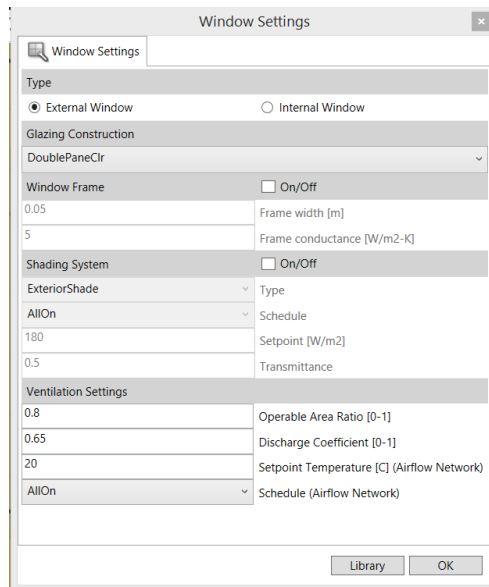


Figure D.10. Window settings

D.7 Energy plus run

Once all the settings are well-defined and inserted into the *zone connectivity network*, the energy plus run is ready. A name is picked for the project, as well as a directory for saving the results. In addition, the EPW is set to Boston Logan International airport. Again, this is consistent with DIVA daylighting settings.

By clicking on the settings, the desired outputs and run period can be set. Here, an annual analysis from January 1st to December 31st with a monthly resolution will be simulated. The output variables selected are *zone lights electric energy*, *zone ideal loads zone total heating energy*, *zone ideal loads zone total cooling energy*.

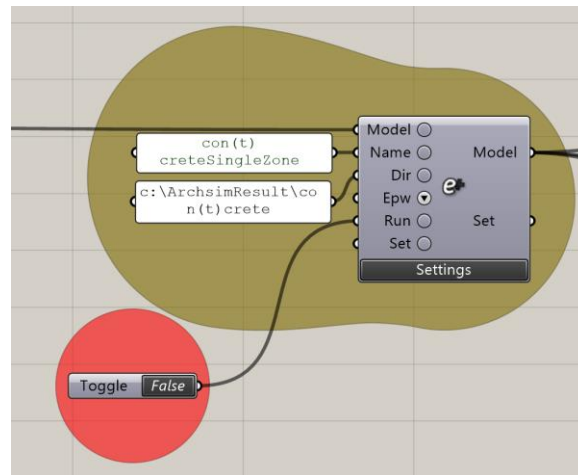


Figure D.11. Energy plus component

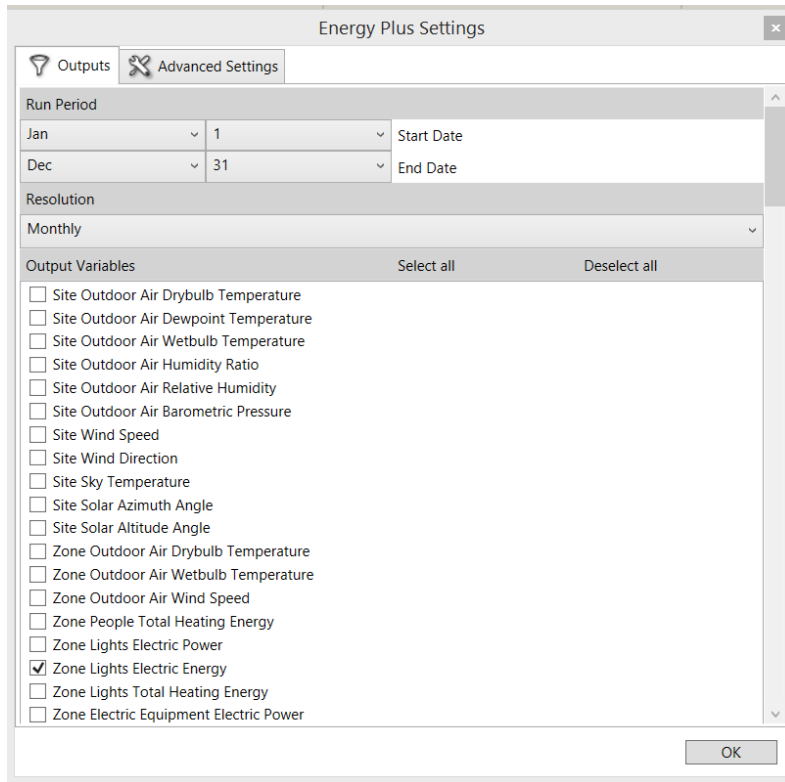


Figure D.12. Energy plus output

D.8 Cooling, heating & lighting results

After the energy analysis is completed, the *model* output of the energy plus is connected to the *model* input of the *load zones result*. The boolean toggle is set to True to read the data.

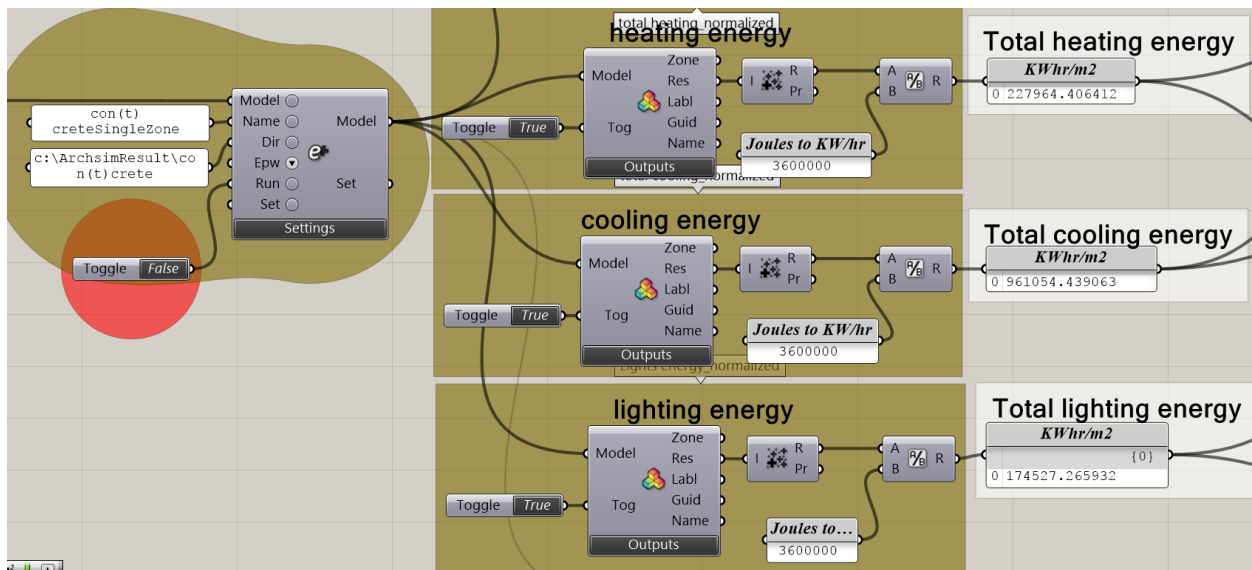


Figure D.13. Model output from Energy Plus run

It should be noted that by clicking on *outputs* on *load zones results*, a list of calculated output variables is available. The desired output variable can be checked for further processing. Heating, cooling and lighting energy are extracted separately, and then summed up to calculate the total energy use. Twelve values representing twelve months are calculated for each output variable, and then summed up with native grasshopper component, *mass addition*, to calculate the annual energy use. Note that the results are in joules and need to be converted to KW/hr.

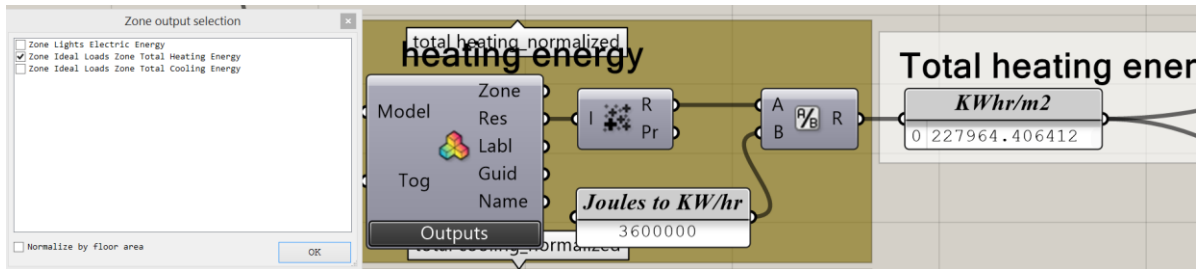


Figure D.14. Jules to KW.hr conversion

D.9 Energy costs

US Energy Information Administration for Boston website has been used to extract electricity and gas prices^{1 & 2}.

Electricity price for Commercial buildings in Massachusetts in 2016:

15.7 cents/kWh

Natural Gas price (city gate): \$6.95 for thousand cubic feet:

1000 cubic feet = 293.07 kWh

695 cents for 293.07 kWh

2.3 cents/kWh

CO2 equivalent emission factors

Electricity: 0.758 kgCO2/kWh

Natural gas: 0.232 kgCO2/kWh

Material costs for building operations

¹ <http://www.eia.gov/>

² <http://www.eia.gov/state/print.cfm?sid=MA>

No transportation is assumed, and it's assumed that all raw materials will be provided locally.
This information is retrieved from CES Edupack

Table D.2. Electricity and natural gas costs

	<i>Cost [cents]</i>	<i>CO2 emission [kgCO2/kWH]</i>
<i>Electricity</i>	<i>15.7 cents/kWH</i>	<i>0.758</i>
<i>Natural Gas</i>	<i>2.3 cents/kWH</i>	<i>0.232</i>

Appendix E:

Statistical analysis

E.1 Exploring nested variables

As discussed in chapter seven and previous appendices, the parametric model of the shell is created in Rhino and Grasshopper, and independent and dependent variables are retrieved from the model. Some of these variables are derived from one or a combination of two other variables through mathematical calculations, which are referred as “nested” variables. The nested variables need to be recognized so that the statistical analysis is restricted to only one of the variables to eliminate redundancy. Simple explorative plots have been generated to validate the expected linear relationship between these nested variables, which are summarized in Table E.1.

Table E.1. Process of deriving independent variables (control variables)

Variable	Role of the variable	The range of the variables or the range of its effect	Nested Independent Variable-a	Nested Independent Variable-b	Retrieved Variable
Rise of curve in width	The combination of these two variables affects the global geometry of the shells	<i>Roof Geometry</i>	–	–	IV-1: Roof geometry [type: categorical]
Rise of curve in length		0 – Dome 1 – Vault 2 – Flat 3 – Saddle 4 – Inverted vault			
Elevation of corner points	Either of these variables creates a geometric variation within the same global geometry	–	–	–	Not considered
Tilt of edge curve in width					
Tilt of edge curve in length					
Zone combination index	Each of these variables affects the perforation ratio of the shells	Number of selected zones varies from 1 to 9	Skylight Area (Multiplication of the two variables)	<i>Perforation ratio</i> (dividing skylight area by total surface area)	IV-2: Perforation ratio [type: scale]
Subtraction pattern index		Subtraction pattern is either 0.25, 0.5, 0.75, 1			
<i>Thickness</i>	The index of this variable varies from 0 to 6, defining different thicknesses for the shells.	0 = 10 cm, 1 = 15 cm 2 = 20 cm 3 = 25 cm 4 = 30 cm 5 = 35 cm 6 = 40 cm	–	–	IV-3: Thickness [type: scale]

The independent variables are summarized in Table E.2. while the dependent variables in the structural and daylighting disciplines are summarized in Tables E.3. and E.4. respectively, along with the pass/fail criteria.

Table E.2. Summary of independent variables (IV) or control variables

variable number	variable name	variable type
IV-1	Roof Geometry	Categorical (dome/ vault/ saddle)
IV-2	Perforation Ratio	Scale
IV-3	Thickness	Scale

Table E.3. Summary of Dependent Variables (DV) or response variables in structural discipline

variable number	variable name	variable evaluation	criteria
DV-1	Weight	Minimize Weight	-
DV-2	Maximum displacement	Pass/Fail	Deflection (D.L+L.L)<0.45m
DV-3	Von Mises stress at Q3	Pass/Fail	von Mises < 30MPa
DV-4	Material and formwork cost	Minimize Cost	-

Table E.4. Summary of dependent variables (DV) or response variables in daylighting discipline

variable number	variable name	Variable evaluation	Criteria
DV-5	Spatial daylight autonomy	Pass/Fail	sDA > 55%
DV-6	Daylight oversupply	Pass/Fail	DAv oversupply < 0.05
DV-7	Total energy	Minimize	-
DV-8	Total operational costs	Minimize	-

E.2 Trimming data and deriving three subsets

The input data generated by ParaGen had employed various algorithms to generate the cases. The initial population, cases 1 to 500, were generated mainly randomly and partially systematically. The order of algorithms for generating the input values is outlined below:

- Cases 1 -17: random generation
- Cases 18 - 102: systematic generation
- Cases 103 - 502: random generation
- Cases 503 - 604: breed from two parents, based on certain fitness function
- Cases 633 - 699: breed from two parents, based on certain fitness functions
- Cases 700 - 821: mutated from a single parent, Pareto Material Cost vs. Operational Cost
- Cases 822 – 900: mutated from a single parent, Pareto sDA vs. DAv
- Cases 901 - 1001: mutated from a single parent, Pareto Weight vs. von Mises
- Cases 1002 - 1061: mutated from a single parent, Pareto Weight vs. Displacement
- Cases 1062 - 1125: mutated from a single parent, Pareto Material Cost vs. Operational Cost
- Cases 1126 - 1176: mutated from a single parent, Pareto Weight vs. Displacement vs von Mises

All the cases that were generated after case 502 employed a fitness function to meet a particular performance criterion. This has created a biased population with a majority of the shells being Saddles (Figure E.1).

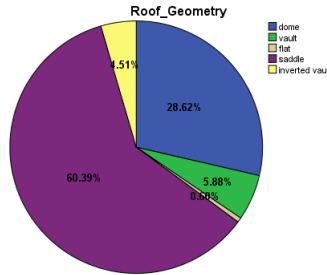


Figure E.1. Distribution of shell typologies in the whole population showing that it is skewed towards one typology upon using fitness functions

To eliminate the bias, the data is trimmed, and only the randomly or systematically generated cases with ids ranging from 1 to 502 are included in the statistical analysis. The distribution of typologies after trimming the data is illustrated in Figure E.2 and Table E.5.

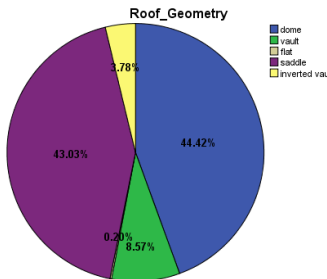


Figure E.2. Distribution of shell typologies in the trimmed population

Table E.5. distribution of shell typologies in the trimmed population

	Frequency	Percent	Valid Percent	Cumulative Percent
Dome	223	44.4	44.4	44.4
Vault	43	8.6	8.6	53.0
Flat	1	.2	.2	53.2
Saddle	216	43.0	43.0	96.2
Inverted vault	19	3.8	3.8	100.0
Total	502	100.0	100.0	

After trimming the data and by looking at the distribution of the randomly and systematically generated cases, domes and saddles have the same distribution, whereas vaults and inverted vaults constitute about 11 percent of the population. This may look biased at first, but it is a function of the parametric model setup and can be explained based on the parameter ranges. As explained in the parametric model setup, the midpoint of curve-a is changing within the range of +1 to +10,

thus is having a positive curvature at all time. On the other hand, the midpoint of the curve-b is changing within the range of +10 to +10, thus can create a curve with a positive, zero, or a negative curvature. Knowing that the curvature of the final geometry is a product of curve-a's and curve-b's curvature, the shape can be:

(curve-a's positive curvature) × (curve-b's positive curvature) = positive surface curvature or dome

(curve-a's positive curvature) × (curve-b' zero curvature) = zero surface curvature or vault

(curve-a's positive curvature) × (curve-b's negative curvature) = negative surface curvature

- There are 10 possibilities for curve-b to have a positive curvature value, {1, 2, 3, 4, 5, 6, 7, 8, 9, 10}, thus creating a dome.
- There are 10 possibilities for curve-b to have a negative curvature value, {-10, -9, -8, -7, -6, -5, -4, -3, -2, -1}, thus creating a saddle.
- There is only 1 possibility for curve-b to have a zero value, {0}, thus creating a vault.

The chances of having a value for curve-b that generates a dome or a saddle, are the same, and 10 times more than the chances of generating a vault. This can explain the unequal distribution of the shell typologies in the dataset.

This study is focused on domes, vaults, and saddles, therefore the flat roof (1 incident) and the inverted vaults (19 incidents) are carved out of the dataset, arriving at a total of 482 cases. The finalized distribution of the typologies is presented in Figure E.3, and the frequencies are summarized in Table E.6.

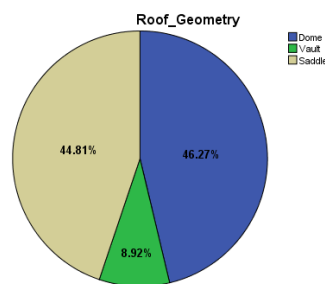


Figure E.3. Final distribution of shell typologies subject to statistical analysis

Table E.6. Final distribution of shell typologies in the trimmed population

	Frequency	Percent	Valid Percent	Cumulative Percent
Dome	223	46.3	46.3	46.3
Vault	43	8.9	8.9	55.2
Saddle	216	44.8	44.8	100.0
Total	482	100.0	100.0	

For further analysis, the data is broken into three subsets including domes, vaults, and saddles; thus, the difference in the typologies' distribution does not affect the statistical results. In other words, IV-1 or the roof geometry is broken into geometric typologies. Roof geometry 0 is the domes, roof geometry 1 is the vaults, and roof geometry 3 is the saddles

E.3 Statistical analysis to uncover the relationship between parameter and performance

IBM SPSS software is used for statistical analysis. First, a histogram plot is computed to visually inspect the distribution of the response variables. After computing tests of normality, if the distribution is normal, a *general linear regression model* (GLM) is suited for the analysis. If the distribution is skewed, the variables are re-coded into categories, and then an *ordinal regression model* is computed. In this case, the test of parallel lines is conducted. Parallel lines are defined as the thresholds that are used to break the continuous data into categories. Test of parallel lines demonstrates if these lines maintain their distance from each other when their values are shifted in different scenarios. If the test of parallel lines shows a significance higher than 0.05, it means that we fail to reject the null hypothesis (which is the lines maintaining their distance with each other while they are being shifted). In this case, the ordinal regression model is fitted. If the test of parallel lines shows a significance smaller than 0.05, it means that we reject the null hypothesis that the lines maintain their distance with each other while they are being shifted. In this case, the significance of parallel line analysis is violated, thus *multinomial regression model* is computed. The flowchart is showed in Figure E.4.

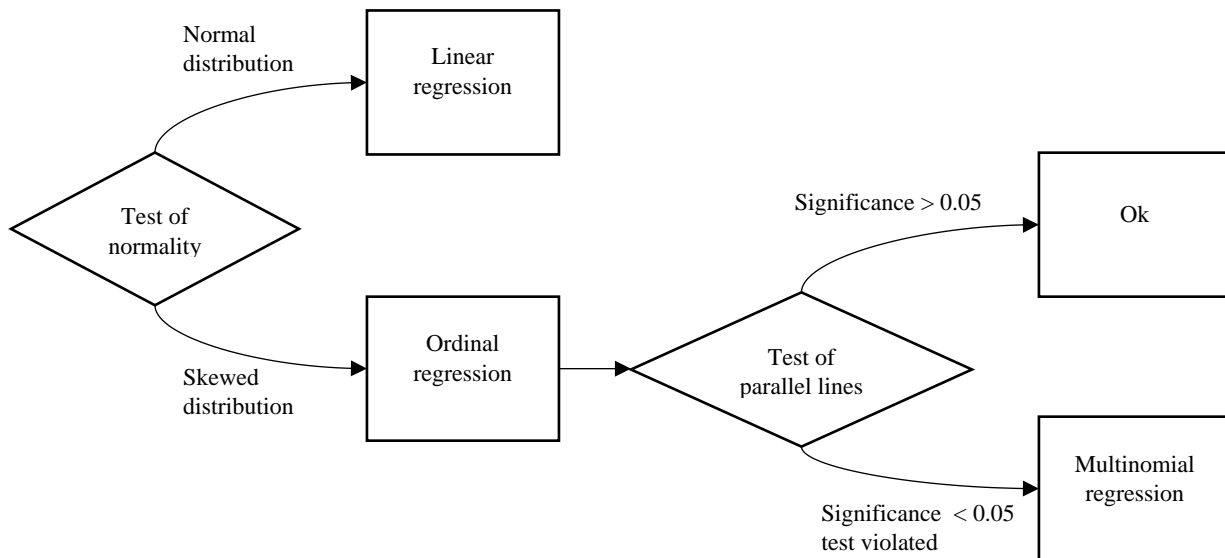


Figure E.4. Flowchart of statistical analysis

There are two ways of interpreting the results. Either, one could use them to predict the probabilities of getting a response value based on the current response values. Or one could explain the relationship between the predictor values and the means of response variables, and how much the mean of response variables may vary, when a predictor value changes. The scope of this analysis is the latter. The null hypothesis tests *if variable x is not an important predictor*, and we are in favor of rejecting that hypothesis with a significance value less than 0.05 ($\text{sig} < 0.05$), concluding that *variable x is an important predictor*.

A general linear regression model was found to produce the best fit for the following three variables: DV-1 (weight), DV-3 (von Mises stress), and DV-4 (structural costs). For these variables, diagnostic plots indicated that assumptions of normality and constant variance for the residuals in the model were satisfied, and there was no evidence of any extreme outliers. Related tables present the estimated regression coefficients for each of these models, along with tests of significance for the regression parameters.

For variables with unusual distributions, where assumptions about residuals were not satisfied, these variables were re-coded into a smaller number of ordered categories and were analyzed using ordinal logistic regression. An ordinal regression model provided the best fit for these two variables: DV-5 (spatial daylight autonomy) and DV-8 (total operating costs). For each of these variables, the assumption of proportional odds was justified via the parallel lines test in SPSS. Related Tables present the estimated coefficients in the ordinal models for these variables. In these models, a positive estimated regression coefficient suggests that the odds of a *higher* valued category become larger as a predictor increase.

Finally, there were dependent variables that did not satisfy assumptions for linear regression or ordinal regression, and these re-coded variables were modeled using multinomial logistic regression. These dependent variables include DV-2 (deflections), DV-6 (light oversupply), and DV-7 (total operating energy). The relevant Tables report the estimates in these models.

E.3.1 General Linear Regression Model for DV-1 (weight)

The range of weight in the shells has a minimum value of 319 tonnes, and a maximum value of 3218 tonnes. The histogram that shows the distribution of weight is presented in Figure E.5, and the scatterplots of weight against perforation ratio and weight against thickness which is color-coded by roof geometry is presented in Figure E.6.

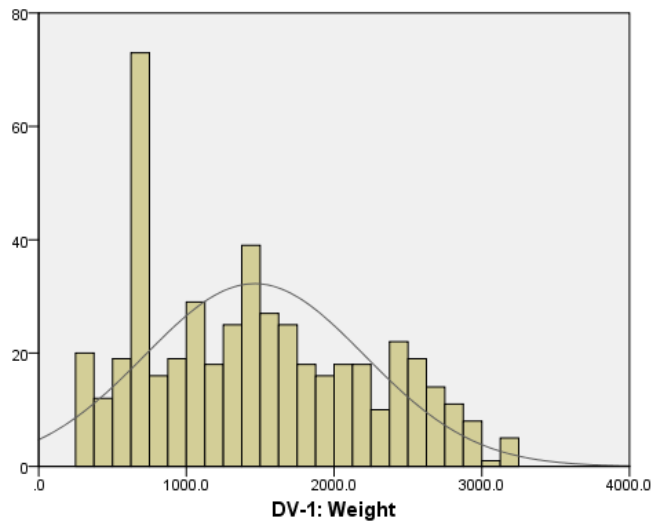


Figure E.5. Distribution of Weight

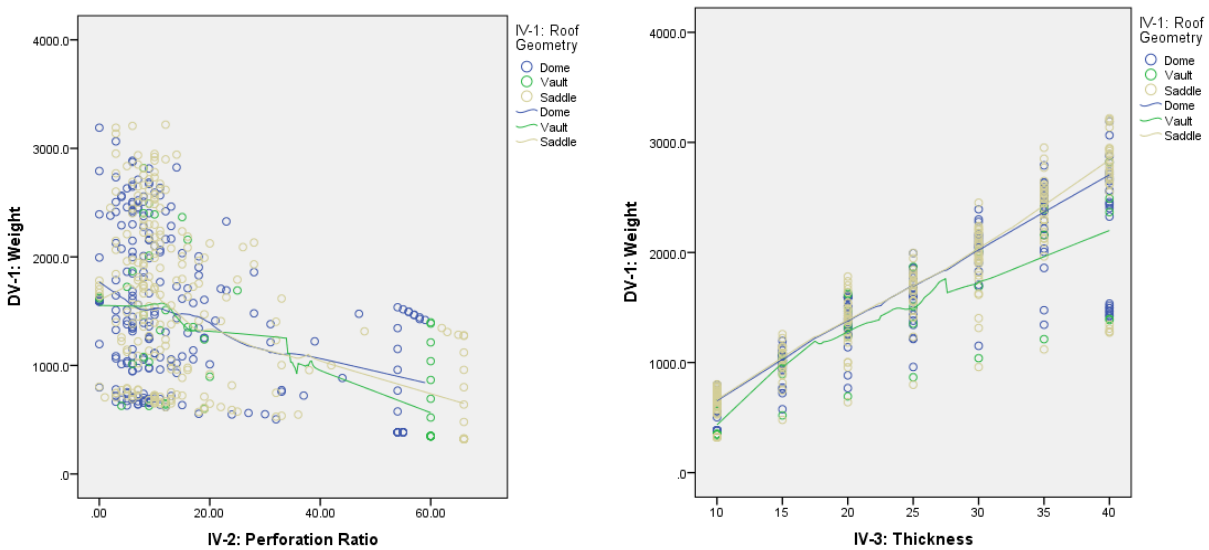


Figure E.6. Scatter plots of Weight versus Perforation Ratio (a) and Weight versus Thickness (b)

The model for weight explained 94.4% of the variance in the values on weight. Examining the estimated coefficients (Table E.7), we find that the most important predictors were perforation ratio, and thickness. Interpreting the coefficients for these predictors for saddles, we find that:

- a one-unit increase in perforation ratio results in a 14.76 unit expected decrease in weight, holding the other predictors fixed.
- a one-unit increase in thickness results in a 63.89 unit expected increase in weight, holding the other predictors fixed.

We also found evidence of a significant interaction, where for vaults, the estimated relationship of thickness with weight becomes $63.89 - 12.97 = 50$. In other words, the relationship of thickness with weight is significantly weaker with vaults compared to saddles which are the reference category. Figure E.7 below illustrates this interaction between roof geometry and perforation ratio, as well as roof geometry and thickness.

Table E.7. Dependent variable (DV-1) - weight

Predictor	B	Std. Error	Sig. (P-value)
[Dome]	-55	23.4	0.018*
[Vault]	-120	45.7	0.009**
Perforation ratio	-14.76	0.68	0.00***
Thickness	63.892	1.131	0.00***
[Dome] * Perforation Ratio	-1.063	1.002	0.29
[Vault] * Perforation Ratio	1.494	1.329	0.26
[Dome] * Thickness	-2.96	1.601	0.065
[Vault] * Thickness	-12.969	2.846	0.00***

R Squared = 0.94 – sample size = 482 – *p-value<0.05 **p-value<0.01 ***p-value<0.001

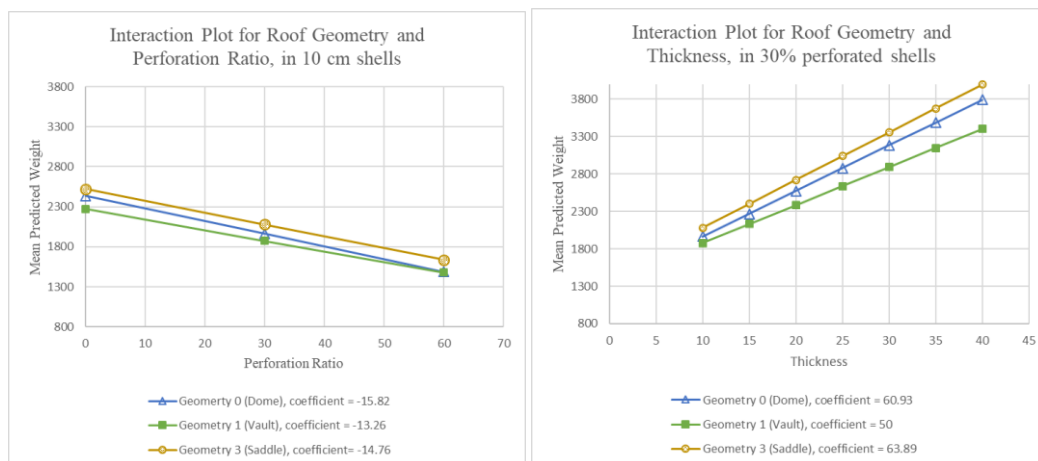


Figure E.7. Saddles have the largest negative relationship with perforation ratio (a); saddles have the largest positive relationship with thickness (b)

E.3.2 General linear regression model for DV-3 (von Mises stress)

The range of von Mises stress levels in the shells has a minimum value of 4.2 MPa, and a maximum value of 97.5 MPa. The histogram that shows the distribution of von Mises stress level is presented in Figure E.8, and the scatterplots of von Mises stress against perforation ratio and von Mises stress against thickness which is color-coded by roof geometry is presented in Figure E.9.

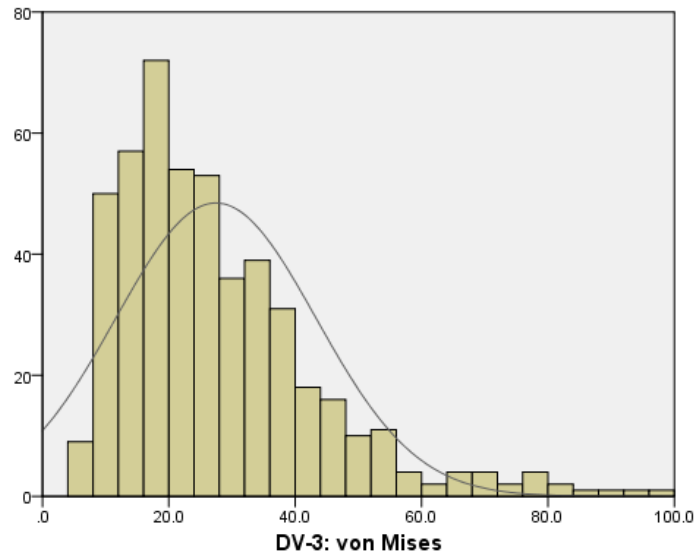


Figure E.8. Distribution of von Mises Stress levels

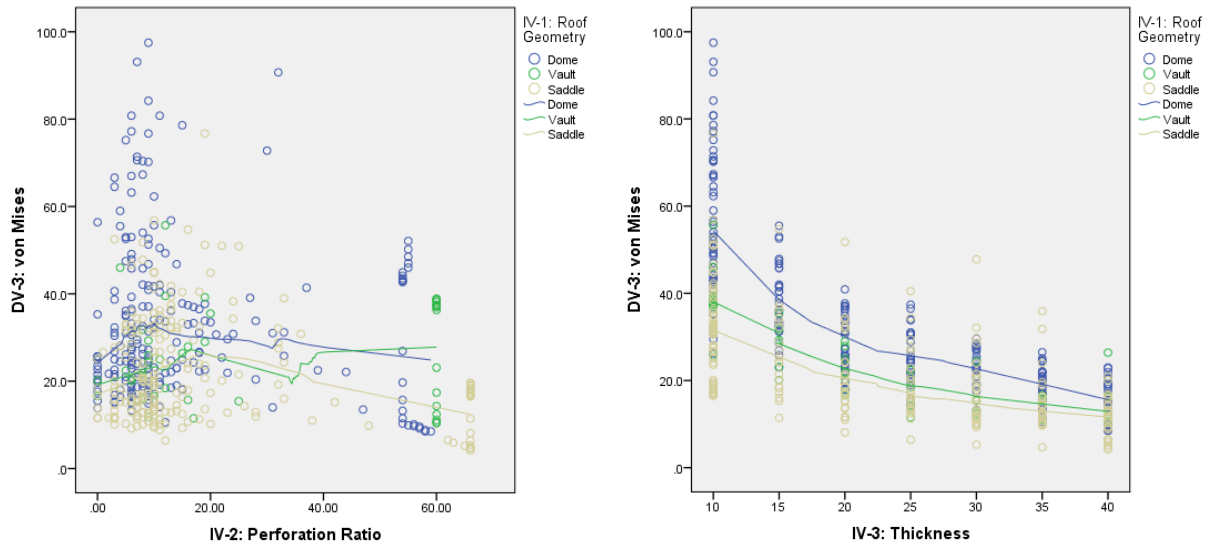


Figure E.9. Scatter plots of von Mises versus Perforation Ratio (a); and von Mises versus Thickness (b)

Von Mises stress values were transformed to square root of von Mises stress values and then were used for the statistical analysis. Although a general linear model was fitted to the data, there were some outliers with values higher than 80 MPa which are scrutinized. The unusual high von Mises stress level is scrutinized in two example shells with both small and large perforation ratio (case 389 and case 471 respectively) presented in Figure E.10. The common feature in the outliers is that they are 10 cm thick shells, with an asymmetric perforation pattern. This can explain the extremely high von Mises stress levels that is observed in these shells.

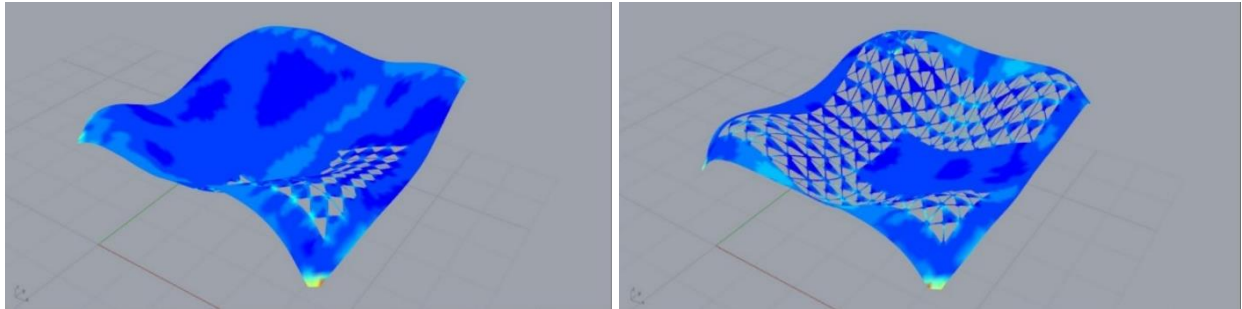


Figure E.10. Von Mises stress in case 389 (a) and 471 (b) which have unusually high values presented as outliers

The model for von Mises stress explained 67% of the variance in the values on von Mises stress. Examining the estimated coefficients (Table E.8), we find that the most important predictors were perforation ratio, and thickness. Interpreting the coefficients for these predictors for roof geometry 3 (saddles), we find that:

- a one-unit increase in perforation ratio results in a 0.021 unit expected decrease in von Mises stress levels, holding the other predictors fixed.
- a one-unit increase in thickness results in a 0.078 unit expected decrease in von Mises stress levels, holding the other predictors fixed.

We also found evidence of a significant interaction, where for domes and vaults, the estimated relationship of perforation ratio with von Mises stress becomes $-0.021+0.01=-0.02$, and $-0.021 + 0.017 = -0.004$ respectively. In other words, the relationship of perforation ratio with von Mises stress is weaker in vaults compared to saddles which are the reference category.

There is also evidence of a significant interaction, where for domes, the estimated relationship of thickness with von Mises stress is $-0.078 -0.035 = -0.113$. This means that the relationship of thickness with von Mises stress becomes stronger in domes compared to saddles which are the

reference category. Figure E.11 below illustrates this interaction between roof geometry and perforation ratio, as well as roof geometry and thickness.

Table E.8. Dependent Variable (DV-3) – von Mises Stress

Predictor	B	Std. Error	Sig. (P-value)
[Dome]	0.72	0.108	0.00***
[Vault]	-0.004	0.211	0.985
Perforation ratio	-0.021	0.003	0.00***
Thickness	-0.078	0.005	0.00***
[Dome] × Perforation ratio	0.01	0.005	0.026*
[Vault] × Perforation ratio	0.017	0.006	0.005*
[Dome] × Thickness	-0.035	0.007	0.00***
[Vault] × Thickness	-0.009	0.013	0.479

R Squared = 0.67 – sample size = 482 – *p-value < 0.05 **p-value < 0.01 ***p-value < 0.001

The interaction plot for 10 cm shells is picked arbitrary to demonstrate the interaction between von Mises Stress and Perforation Ratio. The interaction plot of 30% perforated shells is also arbitrary chosen to demonstrate the interaction between von Mises Stress and Thickness. Saddles have the largest negative relationship with von Mises stress in 10 cm shells. Domes have the largest negative relationship with von Mises Stress in 30% perforated shells (Figure E.11).

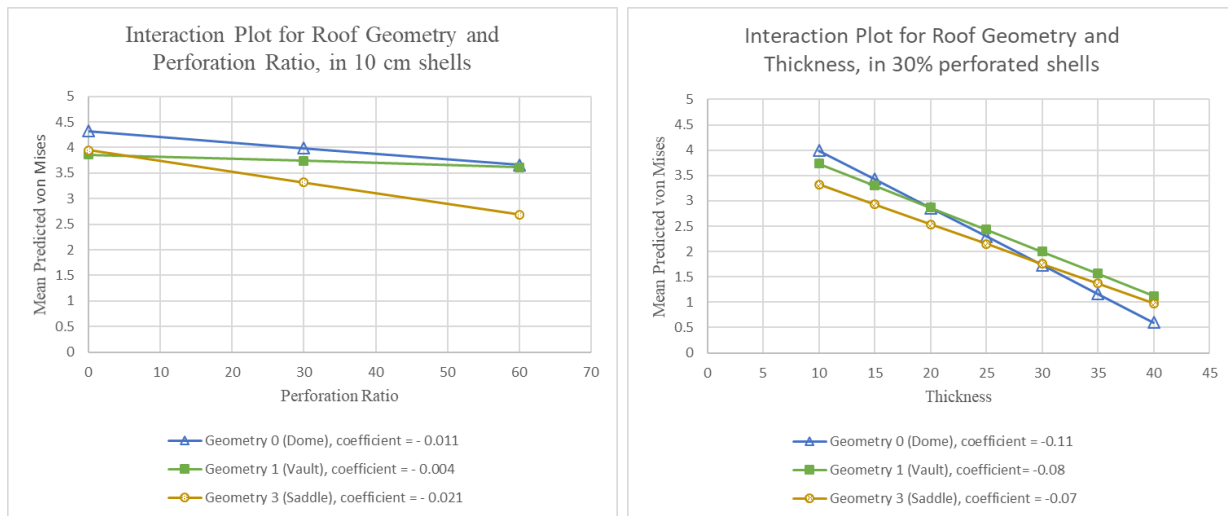


Figure E.11. Saddles have the largest negative relationship with perforation ratio (a); domes have the strongest negative relationship with thickness (b)

E.3.3 General linear regression model for DV-4 (total structural costs)

The Total structural costs were transformed by dividing by 1000. The range of total structural costs in the shells has a minimum value of \$216 in thousand and a maximum value of \$1,291 in thousands. The histogram that shows the distribution of total structural costs is presented in Figure E.12, and the scatterplots of total structural costs against perforation ratio and total structural costs against thickness which is color-coded by roof geometry is presented in Figure E.13.

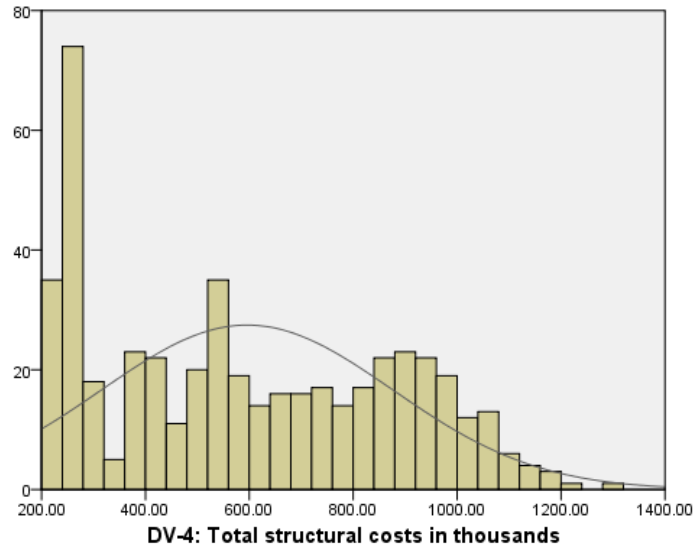


Figure E.12. Distribution of structural costs

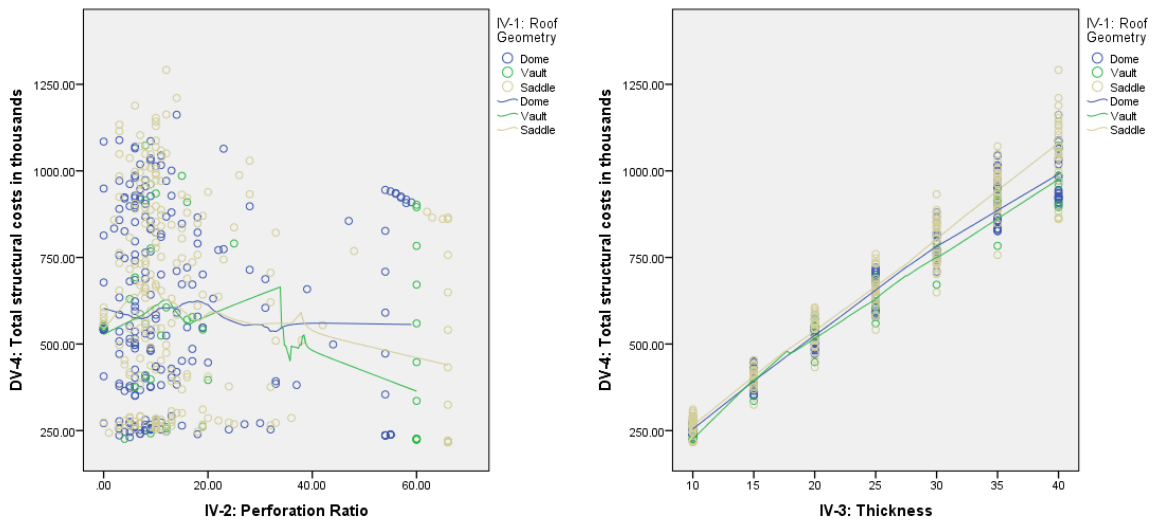


Figure E.13. Scatter plots of total structural costs versus perforation ratio (a); and total structural costs versus thickness (b)

Although a general linear model was fitted to the data, there were two outliers with values higher than \$1,188 in thousands which are scrutinized. The unusual high total structural costs are observed in case 13 (\$1,210,595) and case 16 (\$1,291,363). Both of these shells shown in Figure E.14 have a thickness of 40 cm and have a perforation ratio of 0.14 or 0.12. In other words, they have the disadvantage of using more material by having a high thickness, while they are having the added cost of formwork for constructing the perforations. This explains the outliers for structural costs.



Figure E.14. Structural cost the cases that have unusually high Total structural costs

The model for total structural costs explained 97% of the variance in the values on structural costs. Examining the estimated coefficients (Table E.9), we find that the most important predictors were perforation ratio, and thickness. Interpreting the coefficients for these predictors for roof geometry 3 (saddles), we find that:

- a one-unit increase in perforation ratio results in a 1.75 unit in one thousand expected decrease in structural costs, holding the other predictors fixed.
- a one-unit increase in thickness results in a 26 unit in one thousand expected increase in structural costs, holding the other predictors fixed.

We also found evidence of a significant interaction, where for roof geometry is a dome, the estimated relationship of perforation ratio with structural costs becomes $-1.75 + 0.74 = -1.01$. In other words, the relationship of perforation ratio with structural costs is weaker in domes compared to saddles which are the reference category.

There is also evidence of a significant interaction, where for domes and vaults, the estimated relationship of thickness with structural costs becomes $26.3 - 1.3 = 25$, and $26.3 - 2.2 = 24.1$. This means that the relationship of thickness with structural costs is weaker in domes and vaults

compared to saddles which are the reference category. Figure E.15 below illustrates this interaction between roof geometry against perforation ratio, as well as roof geometry against thickness.

Table E.9. Dependent variable (DV-4) – structural costs

Predictor	B	Std. Error	Sig. (P-value)
[Dome]	-37.5	6.17	0.00***
[Vault]	-34.3	12.06	0.005*
Perforation ratio	-1.75	0.18	0.00***
Thickness	26.36	0.29	0.00***
[Dome] × Perforation ratio	0.741	0.264	0.005***
[Vault] × Perforation ratio	0.302	0.35	0.38
[Dome] × Thickness	-1.31	0.42	0.002***
[Vault] × Thickness	-2.26	0.75	0.003***

R Squared = 0.972 – sample size = 482 – *p-value < 0.05 **p-value < 0.01 ***p-value < 0.001

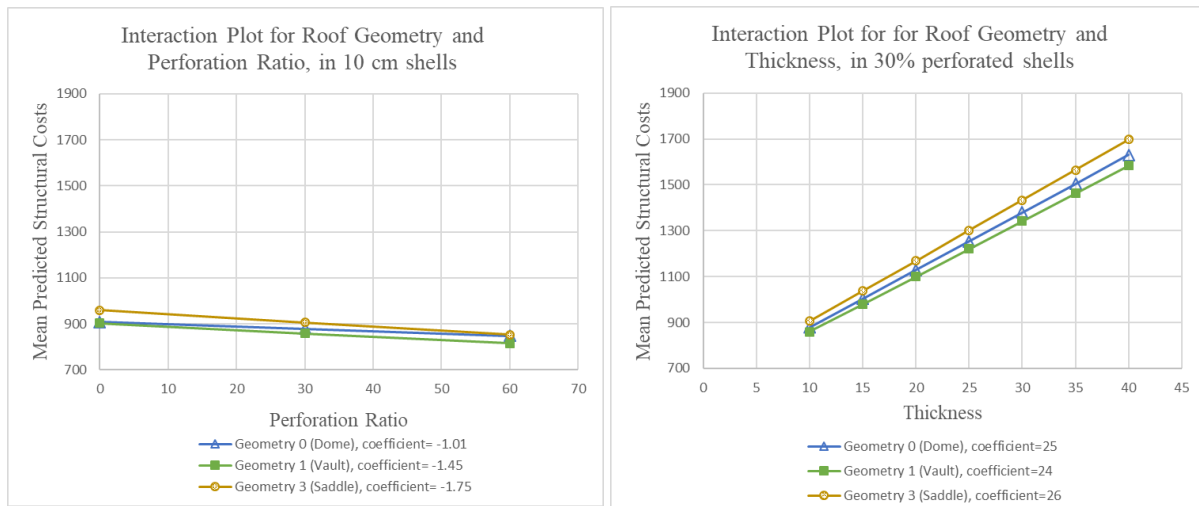


Figure E.15. Saddles have the largest negative relationship with perforation ratio (a); Saddles have the strongest positive relationship with thickness (b)

Looking at the interaction plots, although there is statistical significance, but the cost-difference among different roof geometries is not practically significant.

E.3.4 Ordinal logistic regression for DV-5 (spatial daylight autonomy)

The range of sDA in the shells has a minimum value of 0 and maximum value of 100 percentage. The histogram that shows the distribution of sDA is presented in Figure E.16, and the scatterplots of sDA against perforation ratio and sDA against thickness which is color-coded by roof geometry is presented in Figure E.17.

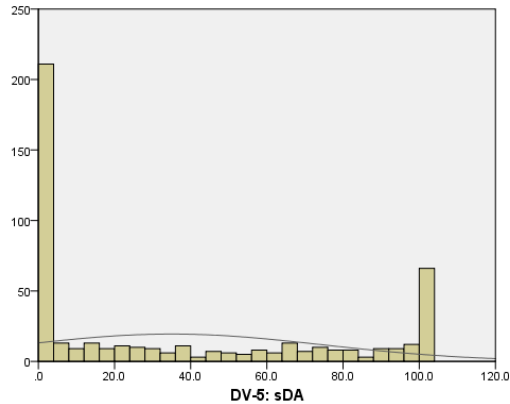


Figure E.16. Distribution of spatial daylight autonomy

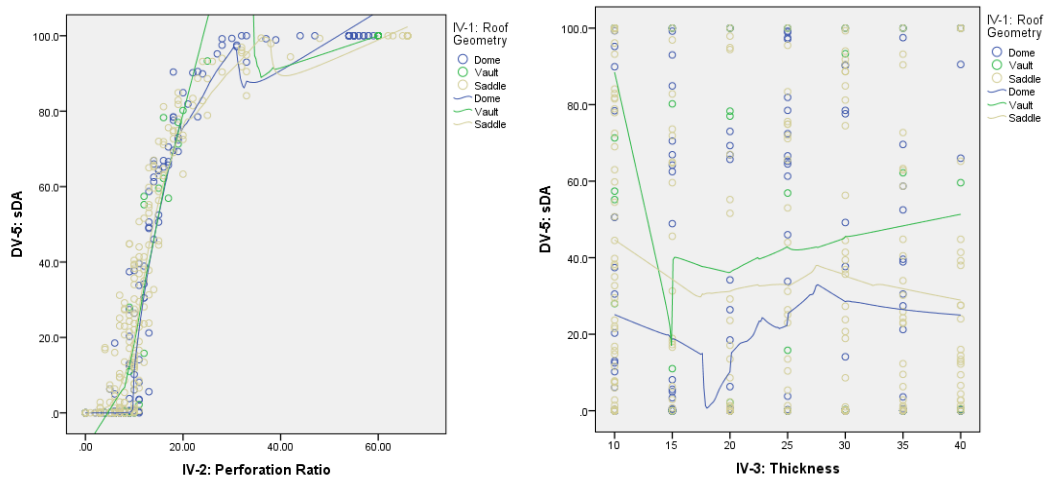


Figure E.17. Scatter plots of sDA versus perforation ratio (a); and sDA versus thickness (b)

Figure E.17 on the left suggests that once perforation ratio is about 30%, the sDA hits 100%. This means that the increase of perforation ratio beyond 30% no longer changes the daylighting performance.

To conduct the ordinal regression analysis, DV-5, the spatial daylight autonomy, is re-coded into four categories as:

- Category 1 = sDA lower than 25%. _unacceptable.
- Category 2 = sDA between 25% and 55% _unacceptable.
- Category 3 = sDA between 55% and 75% _acceptable.
- Category 4 = sDA higher than 75% _acceptable.

The rationale for recoding DV-5 is twofold: first, the distribution of values presented in the histogram suggests that the cases lying at the two extremes ($sDA = 0$ or $sDA = 100$) may be grouped. Second, knowing that sDA higher than 55% is the acceptance threshold for sDA , the cases below and above the threshold are grouped together.

The ordinal logistic regression model was computed, and its Pearson goodness-of-fit has a significance of 1. Predictor perforation ratio was found to significantly increase the probability of a higher-valued category (category 4: sDA higher than 75%) in saddles which are the reference category. In other words, the probability of *better* outcomes increase as this predictor increase by one unit. Thickness has no significance in the odds of having a better sDA . There is evidence of significant interaction, where for domes, the estimated relationship of perforation ratio with sDA becomes $0.9 + 0.208 = 1.1$. The coefficients are summarized in Table E.10, and the interaction plots are presented in Figure E.18.

Table E.10. Dependent Variable (DV-5) – Spatial Daylight Autonomy

Predictor	B	Std. Error	Sig. (P-value)
[sDA lower than 25%]	9.59	1.008	0.00***
[sDA between 25% and 55%]	12.5	1.21	0.00***
[sDA between 55% and 75%]	17.4	1.65	0.00***
[Dome]	-3.12	1.38	0.024*
[Vault]	-2.65	2.66	0.32
Perforation ratio	0.90	0.093	0.00***
Thickness	0.019	0.019	0.32
[Dome] × Perforation Ratio	0.208	0.105	0.048*
[Vault] × Perforation Ratio	0.21	0.199	0.29
[Dome] × Thickness	0.009	0.035	0.78
[Vault] × Thickness	-0.13	0.066	0.045*

The reference category is roof geometry = 3 (saddle). Pearson goodness-of-fit has a significance of 1.

Nagelkerke Pseudo R Squared = 0.907 – sample size = 482 – *p-value < 0.05 **p-value < 0.01 ***p-value < 0.001

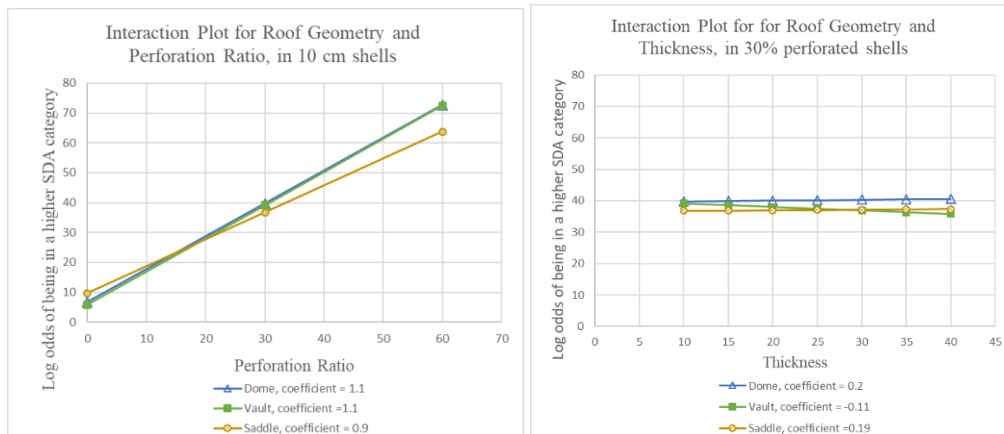


Figure E.18. As perforation ratio increases, the log odds of having a higher sDA increases (a); as thickness increases, the log odds of having higher sDA does not change significantly (b)

E.3.5 Ordinal logistic regression for DV-8 (total operating costs)

DV-8 or total operating costs was transformed by dividing by 1000. The range of total operating costs in the shells has a minimum value of \$33 in-thousand and a maximum value of \$164 in thousands. The histogram that shows the distribution of total operating costs is presented in Figure E.19, and the scatterplots of total operating costs against perforation ratio and total operating costs against thickness which is color-coded by roof geometry is presented in Figure E.20.

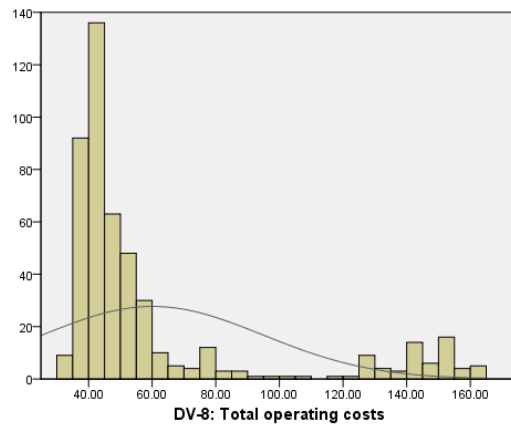


Figure E.19. Distribution of total operating cost in thousands

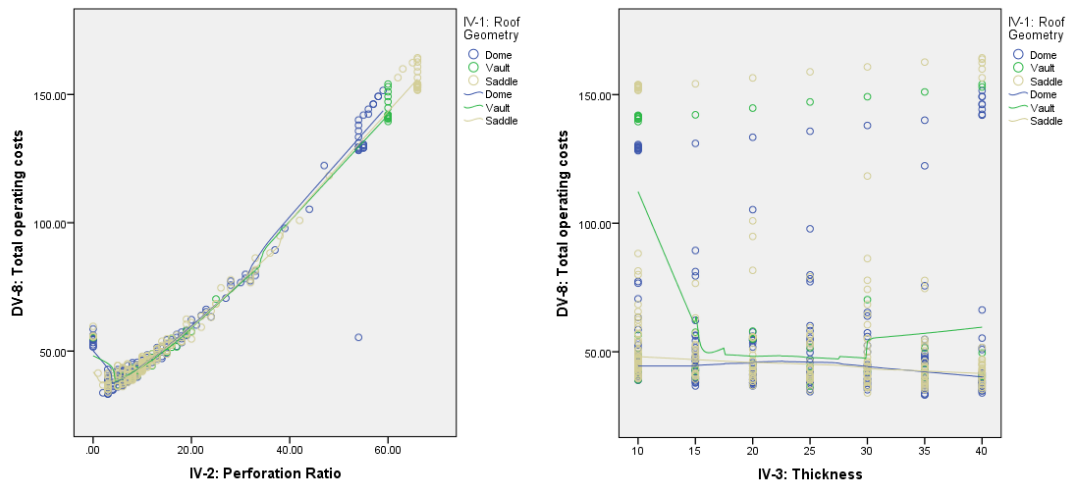


Figure E.20. Scatter plots of total operating costs versus perforation ratio (a); and total operating costs versus thickness (b)

To conduct the ordinal regression analysis, DV-8, total operating costs, is re-coded as follow:

Category 1= Total operational costs < \$45 in thousands

Category 2= Total operational costs > \$45 in thousands

The rationale for this re-coding is the distribution of the cases regarding their energy costs, where a group having low energy costs is formed at the left tail of the histogram, a group with high

energy costs is formed at the right tail of the histogram, and then there are some cases in between. The ordinal logistic regression model is computed, and its Pearson goodness-of-fit has a significance of 0.0, indicating that it is not a good fit and fit is questionable (Table E.11). The interaction plots are illustrated in Figure E.21.

Predictor perforation ratio was found to increase the probability of a higher-valued category (category 3: total operational costs >\$45 in thousands) significantly. In other words, the probability of higher energy costs or *worst* outcomes increase as this predictor, perforation ratio, increase by one unit.

Predictor thickness was found to decrease the probability of a higher-valued category (category 3: total operational costs > \$45 in thousands) significantly. In other words, the probability of higher energy costs, or *worst* outcome decrease as this predictor, thickness, increase by one unit. There is also no evidence of significant interaction.

Table E.11. Dependent Variable (DV-8) – total operating costs

Predictor	B	Std. Error	Sig. (P-value)
[Total operating costs < \$45 in thousands]	4.75	0.71	0.00***
[Dome]	2.27	0.81	0.005
[Vault]	1.92	1.41	0.174
Perforation ratio	0.435	0.07	0.00***
Thickness	-0.083	0.021	0.00***
[Dome] × Perforation ratio	-0.22	0.079	0.005*
[Vault] × Perforation ratio	-0.187	0.127	0.14
[Dome] × Thickness	0.064	0.027	0.017
[Vault] × Thickness	0.034	0.051	0.51

The reference category is roof geometry = 3 (saddle). Pearson goodness-of-fit has a significance of 0.0 Nagelkerke Pseudo R Squared =0.607– sample size = 482 – *p-value < 0.05 **p-value < 0.01 ***p-value < 0.001

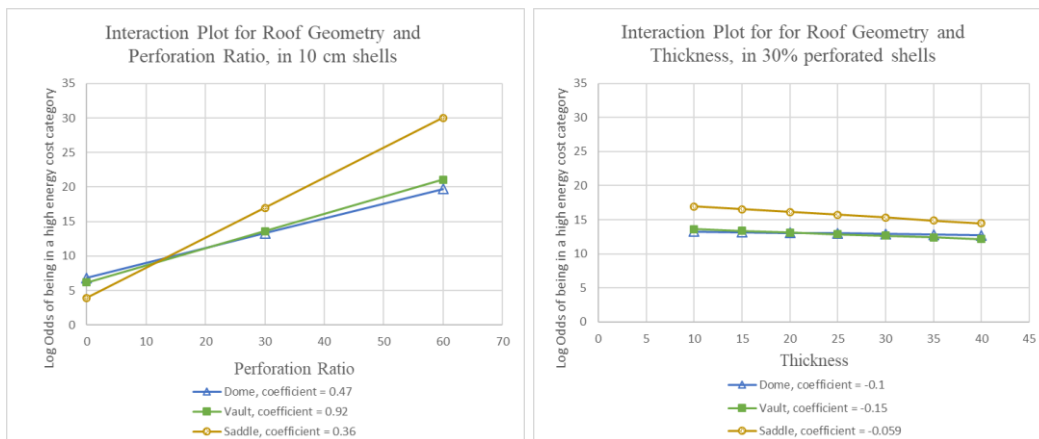


Figure E.21. As perforation ratio increases, the log odds of having an operational costs higher than \$45 in thousands increases (a); as thickness increases, the odds of having a higher operational costs slightly decreases (b).

E.3.6 Multinomial Logistic Regression for DV-2 (deflection)

The range of maximum deflection in the shells has a minimum value of 0.12 meter and maximum value of 10.85 meter. The histogram that shows the distribution of maximum deflection is presented in Figure E.22, and the scatterplots of deflection against perforation ratio and deflection against thickness which is color-coded by roof geometry is presented in Figure E.23.

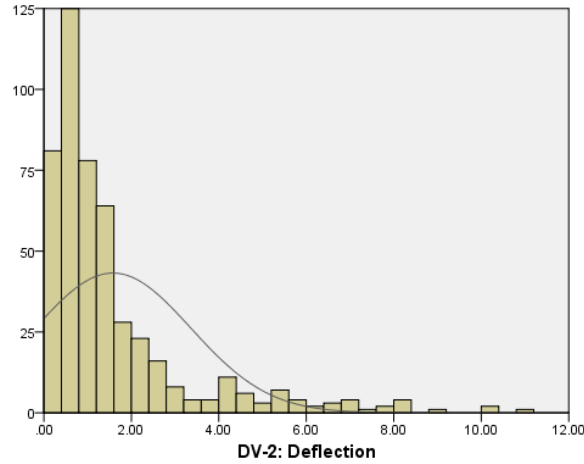


Figure E.22. Distribution of total operating cost in thousands

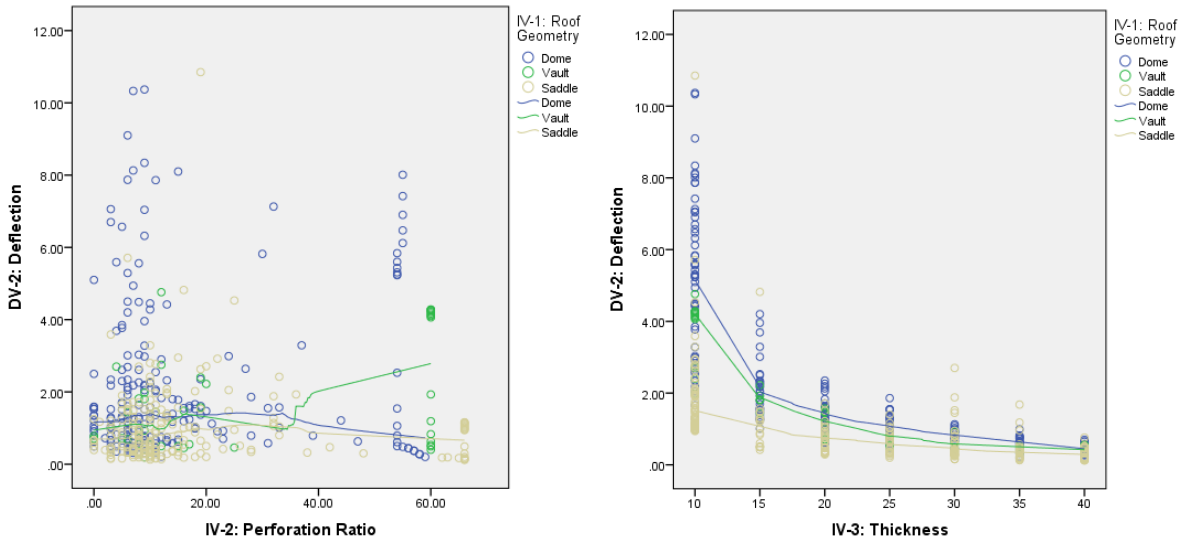


Figure E.23. Scatter plots of deflection versus perforation ratio (a); and deflection versus thickness (b)

To conduct the multinomial regression analysis, DV-2, maximum deflection, is recoded as follow:

- Category 1 = deflection < 0.3 meter _ acceptable.
- Category 2 = 0.3 < deflection < 0.45 _ acceptable.
- Category 3 = 0.45 < deflection < 1 _ unacceptable.
- Category 4 = deflection > 1 _ unacceptable.

The reason behind this re-coding is deflection acceptance limit, which is explained in Appendix C. On the other hand, the outliers and cases with high values of deflection (higher than 1 meter) are inspected. Looking at the elevation of the shells presented in Figure E.24, a lot of the cases showing high deflection have low curvature and, in some cases, a relatively flat area in great parts of the shell.

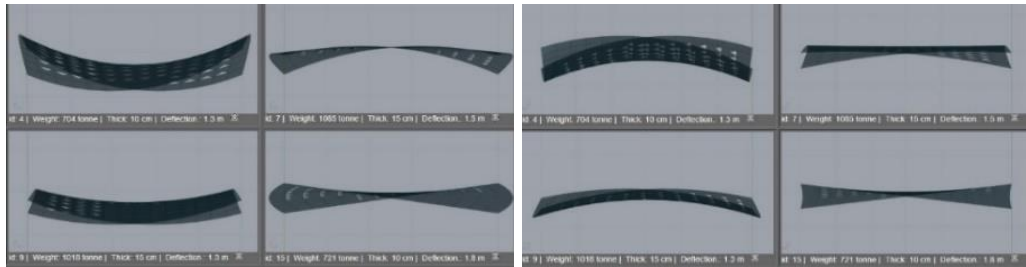


Figure E.24. Front and left elevation of four arbitrary cases that have high deflection

The forms that do not have adequate curvature are a result of the input values used in shell form finding and is not limited to independent variables such as perforation ratio or thickness. To explore this more, the dataset was filtered to show the cases with high deflection first (deflection > 1), and then a scatter plot was computed, to show the thickness and perforation ratio spread for the cases with high deflection (Figure E.25). As seen in Figure E.25, cases with high deflection is seen among all thicknesses (10 to 40 cm), and all perforation ratios (0 to 60%).

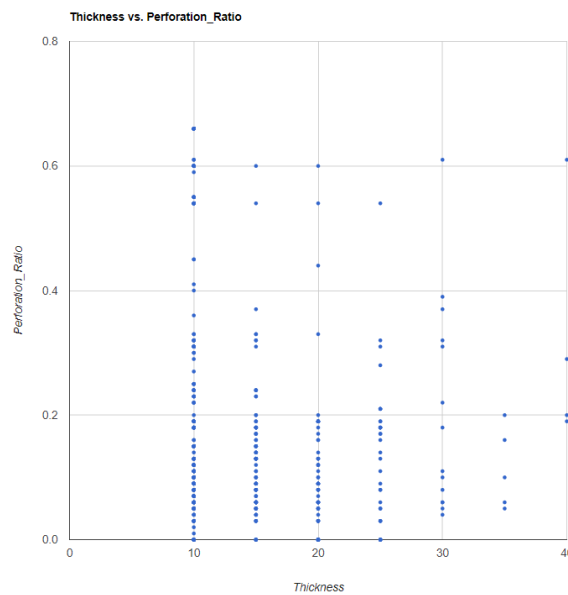


Figure E.25. The cases with high deflections exist among shells with a range of thickness and perforation ratios

The multinomial regression model is computed, and its Pearson goodness-of-fit has a significance value of 1. Vaults are carved out of the dataset for this analysis as the small sample size for vaults led to unreasonable numbers for parameters estimates and standard errors. Table E.12 summarizes the results for domes and saddles.

Table E.12. Dependent Variable (DV-2) – deflections

Outcome category	Predictor	B	Std. Error	Sig. (P-value)
Deflection > 1	[Dome]	4.83	2.64	0.067
	Perforation ratio	-0.056	0.019	0.003**
	Thickness	-0.36	0.048	0.00***
	[Dome] × Perforation ratio	0.027	0.043	0.53
	[Dome] × Thickness	-0.25	0.21	0.22
0.45<deflection<1	[Dome]	4.66	2.5	0.072
	Perforation ratio	-0.05	0.018	0.005*
	Thickness	-0.18	0.04	0.00***
	[Dome] × Perforation ratio	-0.019	0.036	0.59
	[Dome] × Thickness	-0.005	0.20	0.98
0.31<deflection<0.45	[Dome]	1.45	2.67	0.58
	Perforation ratio	-0.079	0.026	0.002**
	Thickness	-0.112	0.04	0.005*
	[Dome] × Perforation ratio	0.026	0.041	0.52
	[Dome] × Thickness	0.08	0.207	0.7

The reference category is deflection < 0.3 and roof geometry = 3 (saddle)

Pearson goodness-of-fit has a significance of 1

Nagelkerke Pseudo R Squared =0.744 – sample size = 482 – *p-value < 0.05 **p-value < 0.01 ***p-value < 0.001

Considering the coefficients in different deflection categories, perforation ratio is having the same effect in various deflection categories for domes and saddles. In saddles, which is the reference category, with one unit increase in perforation ratio, the log odds of having a deflection higher than 1, between 0.45 and 1, and between 0.3 and 0.45 relative to less than 0.3 is expected to *decrease* by -0.056, -0.05, and -0.079 units respectively. In domes, with one unit increase in perforation ratio, the log odds of having a deflection higher than 1, between 0.45 and 1, and between 0.3 and 0.45 relative to deflection less than 0.3, is expected to *decrease* by -0.029 (-0.056+0.027), -0.069 (-0.05-0.019), and -0.053 (-0.079+0.026) units relative to saddles.

On the other hand, as thickness increases, the log odds of having a deformation higher than 1, between 0.45 and 1, and between 0.3 and 0.45 in domes, vaults, and saddles decreases. In saddles, which is the reference category, with one unit increase in thickness, the log odds of having a deflection higher than 1, between 0.45 and 1, and between 0.3 and .45 is expected to *decrease* by 0.36, 0.18, and 0.112 units respectively. In domes, with one unit increase in thickness, the log odds of having a deflection higher than 1, between 0.45 and 1, and between 0.3 and 0.45 is

expected to *decrease* by 0.61 (-0.36-0.25) , 0.185 (-0.18-0.005), and 0.032 (-0.112+0.08) units respectively. There is also no evidence of significant interaction.

Figure E.26, E.27, and E.28 below illustrates this interaction between roof geometry and perforation ratio, as well as roof geometry and thickness.

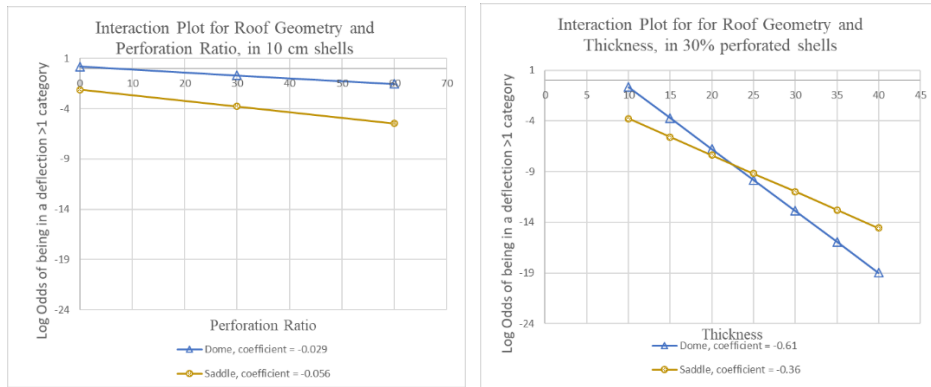


Figure E.26. As perforation ratio increases, the log odds of having deformation higher than 1-meter decreases (a); as thickness increases, the log odds of having deformation higher than 1-meter decreases (b)

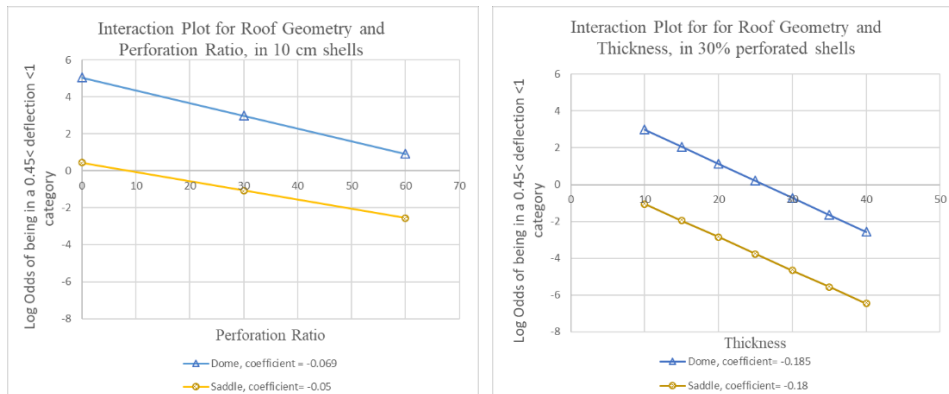


Figure E.27. As perforation ratio increases, the log odds of having deformation between 0.45 and 1 m decreases (a); as thickness increases, the log odds of having deformation between 0.45 and 1 m decreases (b)

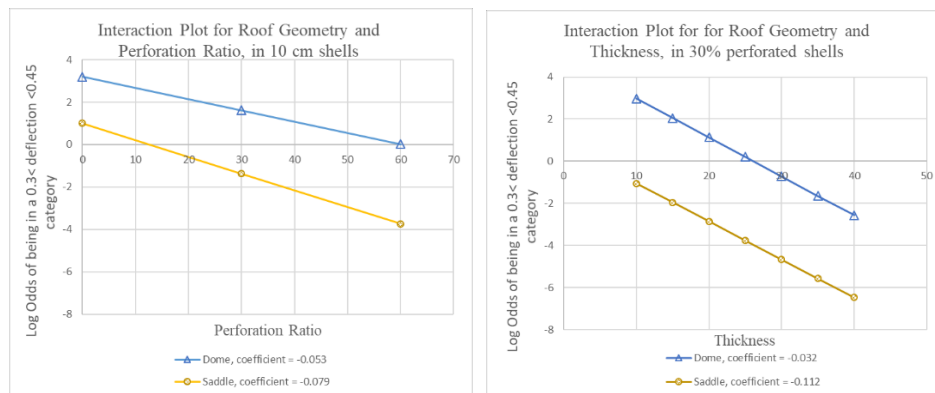


Figure E.28. As perforation ratio increases, the log odds of having deformation between 0.3 and 0.45-meter decreases (a); as thickness increases, the log odds of having deformation between 0.3 and 0.45-meter decreases (b)

E.3.7 Multinomial logistic regression for DV-6 (light oversupply)

The range of DV-6, light oversupply in the shells has a minimum value of 0 and maximum value of 0.99. The histogram that shows the distribution of light oversupply is presented in Figure E.29, and the scatterplots of light oversupply against perforation ratio and light oversupply against thickness which is color-coded by roof geometry is presented in Figure E.30.

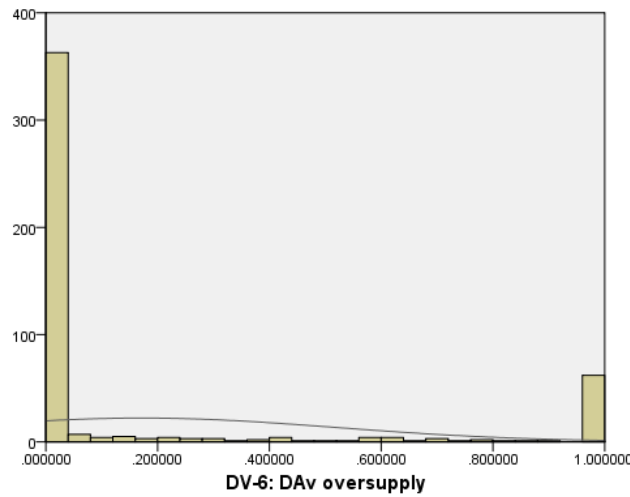


Figure E.29. Distribution of total operating cost in thousands

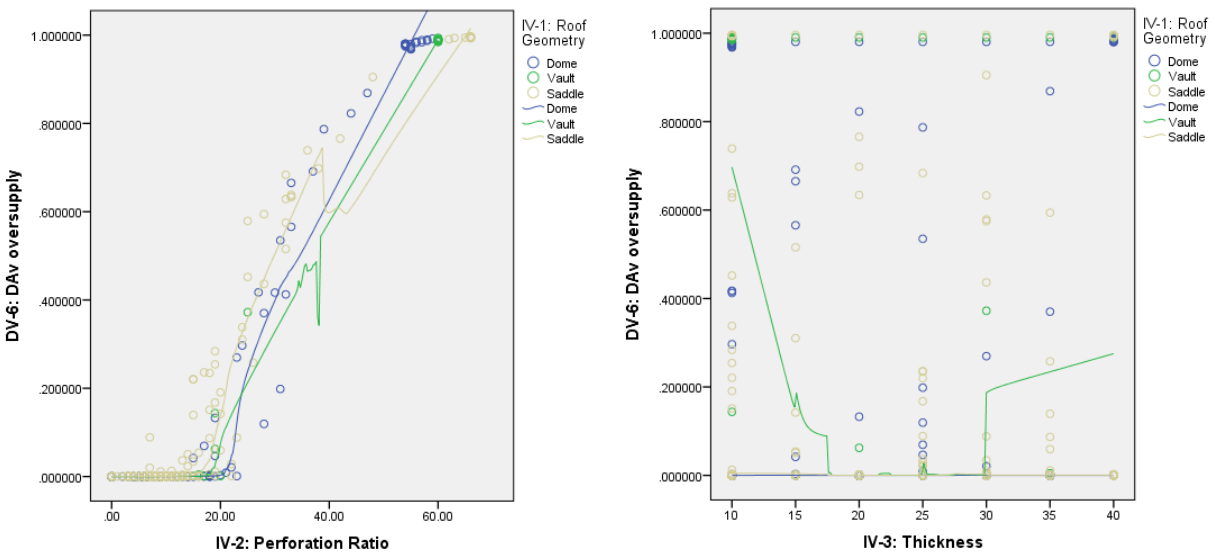


Figure E.30. Scatter plots of light oversupply versus Perforation ratio (a), and light oversupply versus thickness (b). Looking at the perforation ratio versus DAv oversupply plot, it's noticeable that cases with 20% or less perforation ratio are having a low light oversupply (which is desirable). But once the perforation ratio is passed this limit, the light oversupply spikes up (which is not desirable).

To conduct the multinomial regression analysis, DV-6, light oversupply, is recoded as follow:

- Category 1= oversupply less than 0.05_acceptable.
- Category 2= 0.05 < oversupply < 0.1 _unacceptable.
- Category 3 = 0.1 < oversupply < 0.5_unacceptable.
- Category 4 = oversupply > 0.5_unacceptable.

The rationale behind this re-coding is twofold: first to group the cases that pass the performance criteria, and second, to group the extreme cases at the right tail of the distribution.

The multinomial regression model is computed, and its Pearson goodness-of-fit has a significance of 1. Considering Table E.13 for DV-6 (light oversupply), we find that increases in perforation ratio significantly increase the odds of having light oversupply higher than 0.5, between 0.1 and 0.5, and between 0.05 and 0.1, relative to less than 0.05, relative to saddles. There is also no evidence of significant interaction.

Table E.13. Dependent Variable (DV-6) – light oversupply

Outcome category	Predictor	B	Std. Error	Sig. (P-value)
oversupply > 0.5	[Dome]	-555	6.4	0.00***
	[Vault]	-2353	0.00	-----
	Perforation ratio	1.31	0.35	0.00***
	Thickness	0.007	0.11	0.94
	[Dome] × Perforation ratio	17.92	0.00	-----
	[Vault] × Perforation ratio	102.9	1067	0.92
	[Dome] × Thickness	2	68.12	0.97
	[Vault] × Thickness	-26.27	1791	0.98
0.1 < oversupply < 0.5	[Dome]	-12.9	12.37	0.29
	[Vault]	-2324	41009	0.95
	Perforation ratio	0.54	0.109	0.00***
	Thickness	-0.05	0.043	0.246
	[Dome] × Perforation ratio	0.511	0.592	0.388
	[Vault] × Perforation ratio	102.45	1799	0.95
	[Dome] × Thickness	-0.112	0.149	0.45
	[Vault] × Thickness	-26.17	524	0.96
0.05 < oversupply < 0.1	[Dome]	-1.1	4.11	0.78
	[Vault]	-204	9778	0.98
	Perforation ratio	0.37	0.102	0.00***
	Thickness	0.028	0.046	0.54
	[Dome] × Perforation ratio	-0.066	0.24	0.78
	[Vault] × Perforation ratio	11.36	543	0.98
	[Dome] × Thickness	-0.035	0.13	0.78
	[Vault] × Thickness	2.2	108	0.98

The reference category is light oversupply <0.05 and roof geometry = 3 (Saddle)

Pearson goodness-of-fit has a significance of 1

Nagelkerke Pseudo R Squared =0.92 – sample size = 482 – *p-value < 0.05 **p-value < 0.01 ***p-value < 0.001

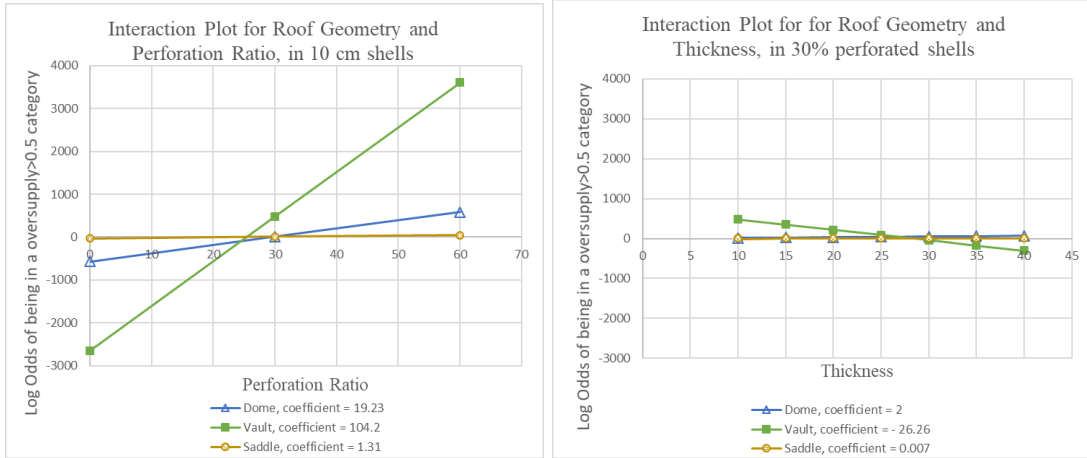


Figure E.31. As perforation ratio increases, the log odds of having light-oversupply higher than 0.5 increases (a); as thickness increases, the log odds of having light oversupply does not change significantly (b)

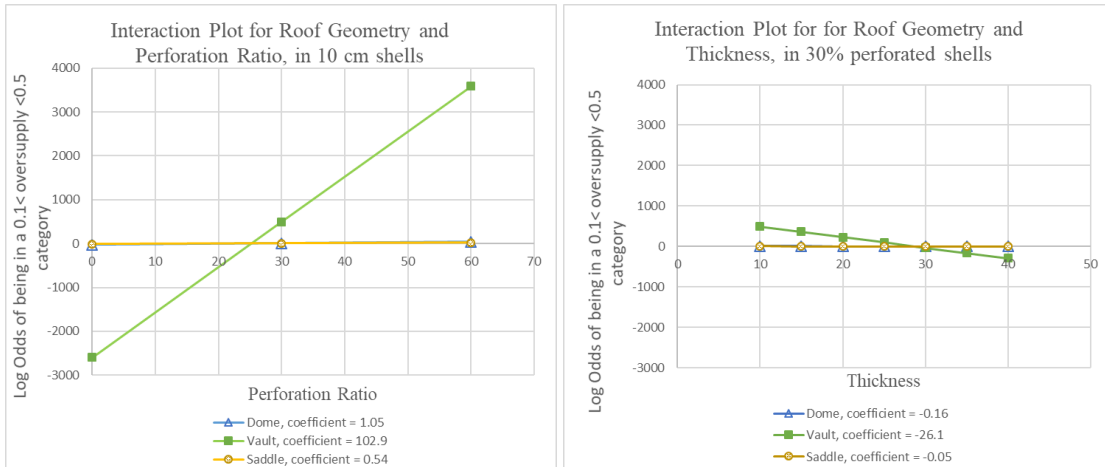


Figure E.32. As perforation ratio increases, the log odds of having light-oversupply higher than 0.5 increases (a); as thickness increases, the log odds of having light oversupply does not change significantly (b)

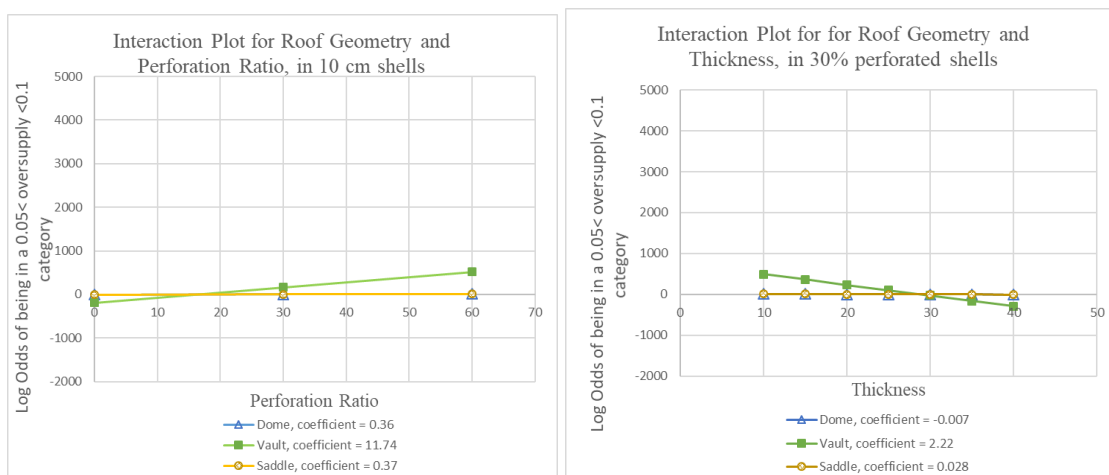


Figure E.33. As perforation ratio increases, the log odds of having light oversupply higher than 0.5 increases (a); as thickness increases, the log odds of having light-oversupply does not change significantly (b)

E.3.8 Multinomial logistic regression for DV-7 (total energy)

The range of total operational energy in the shells has a minimum value of 400 MWh/m³ and maximum value of 1,200 MWh/m³. The histogram that shows the distribution of total operational energy is presented in Figure E.34, and the scatterplots of total operational energy against perforation ratio and total operational energy against thickness are both color-coded by roof geometry are presented in Figure E.35.

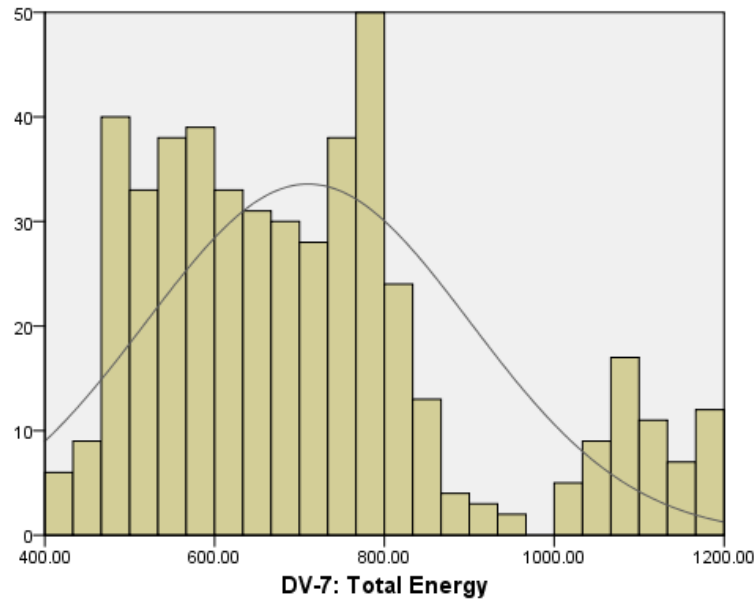


Figure E.34. Distribution of total energy costs per volume

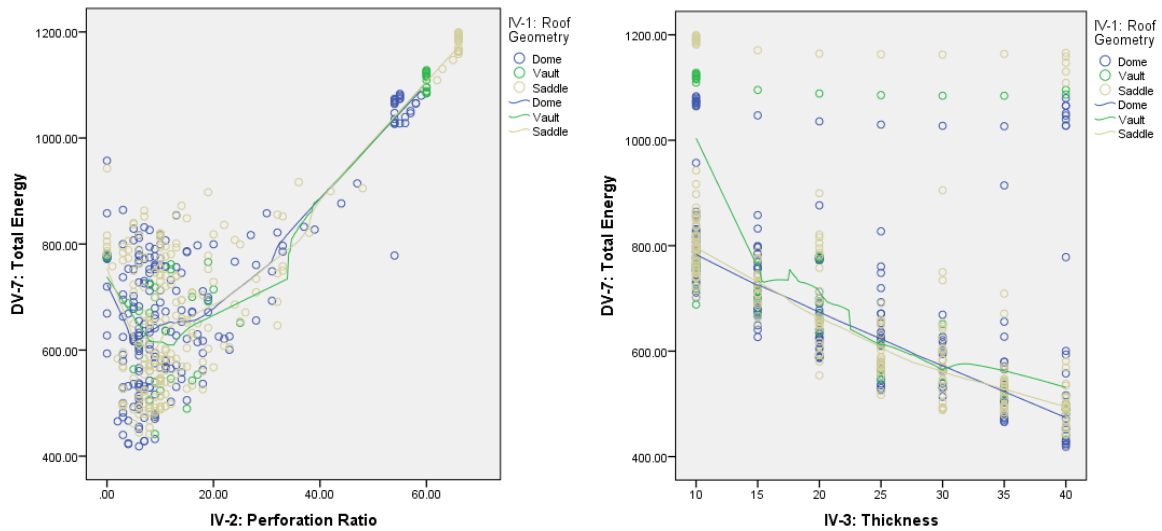


Figure E.35. Scatter plots of total operational energy versus perforation ratio (a); and total operational energy versus thickness (b)

To conduct the multinomial regression analysis, DV-7, total operational energy, is recoded as follow:

- Category 1= total energy less than 600 MWh/m³
- Category 2= 600 < total energy < 800 MWh/m³
- Category 3 = total energy higher than 800 MWh/m³

The rationale behind this re-coding is to group the extreme cases at the right tail, as well as to break the cases with a total energy less than 800 MWh/m³ into two categories.

The multinomial regression model is computed, and its Pearson goodness-of-fit has a significance of 1. Considering Table E.14 for DV-7 (total operational energy), we find that increases in perforation ratio significantly increase the odds of having total energy higher than 800, and between 600 and 800, relative to total energy less than 600, relative to saddles. In other words, the odds of getting a *worst* total energy increase as the perforation ratio increases.

We also found that increases in thickness significantly decrease the odds of having total energy higher than 800 MWh/m³, and between 600 and 800 MWh/m³, relative to higher than 1200 MWh/m³, relative to saddles. In other words, the odds of getting a *better* total energy increases as the thickness increases. There is also no evidence of significant interaction.

Table E.14. Dependent variable (DV-7) – total energy

Outcome category	Predictor	B	Std. Error	Sig. (P-value)
Total energy > 800	[Dome]	1.29	1.42	0.36
	[Vault]	-42	0.00	-----
	Perforation ratio	0.365	0.061	0.00***
	Thickness	-0.57	0.086	0.00***
	[Dome] × Perforation ratio	-0.08	0.075	0.28
	[Vault] × Perforation ratio	0.96	457	0.99
	[Dome] × Thickness	0.104	0.109	0.34
	[Vault] × Thickness	0.014	2016	1.00
600 < Total energy < 800	[Dome]	1.99	0.75	0.008*
	[Vault]	1.48	1.7	0.38
	Perforation ratio	0.24	0.056	0.00***
	Thickness	-0.41	0.073	0.00***
	[Dome] × Perforation ratio	-0.109	0.065	0.095
	[Vault] × Perforation ratio	-0.12	0.14	0.386
	[Dome] × Thickness	0.098	0.087	0.263
	[Vault] × Thickness	-0.116	0.28	0.684

The reference category is total energy <600, and saddles. Pearson goodness-of-fit has a Significance of 1
Nagelkerke Pseudo R Squared =0.822 – sample size = 482 – *p-value < 0.05 **p-value < 0.01 ***p-value < 0.001

The interaction between variables is insignificant. The interaction plots are presented in Figure E.36 and E.37.

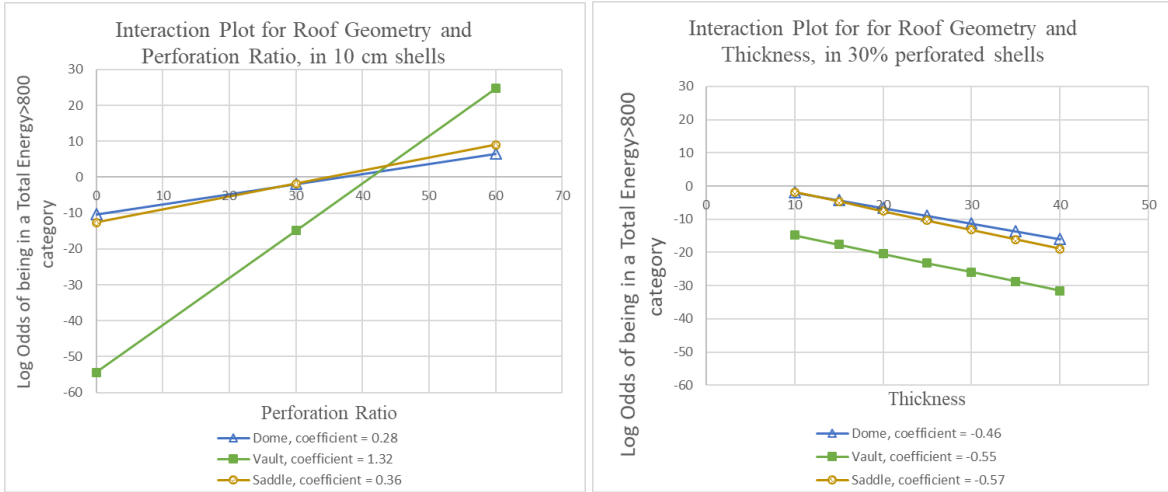


Figure E.36. As perforation ratio increases, the log odds of having total energy higher than 800 MWh/m³ increase (a); as thickness increases, the log odds of having total energy higher than 800 MWh/m³ decreases (b)

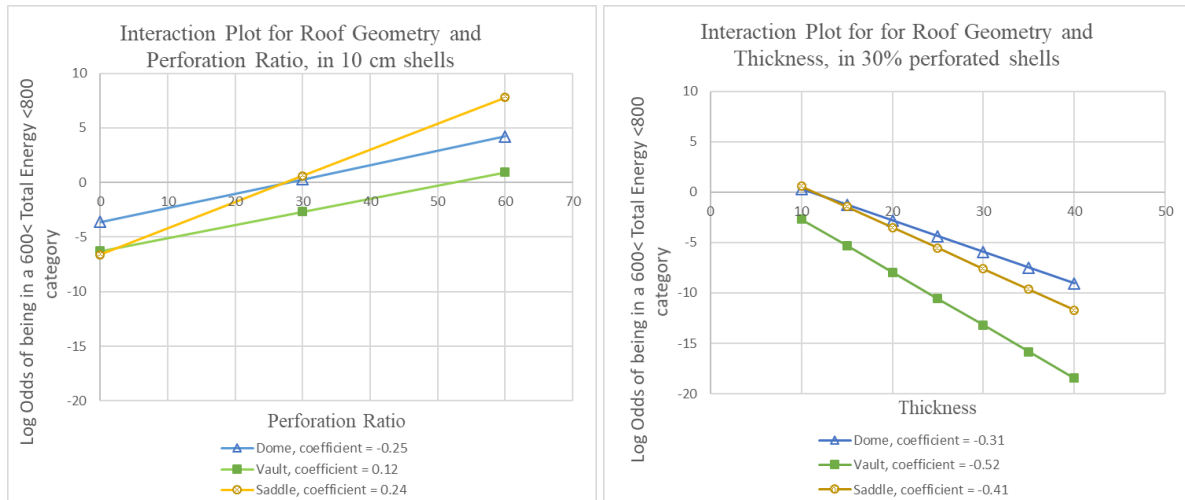


Figure E.37. As perforation ratio increases, the log odds of having total energy between 600 and 800 MWh/m³ increase (a); as thickness increases, the log odds of having total energy between 600 and 800 MWh/m³ decreases (b)

E.4 Heat map and surface plots

A heat map summarizes the correlation between parameters and performance criteria. Green indicates a positive correlation, whereas orange indicates a negative correlation. The intensity of the color represents the significance, as darker intensities represent significance p-values (Table E.15).

Table E.15. Heat map summarizing the correlation between parameters and performance

	Dome		Vault		Saddle	
	Perforation ratio	Thickness	Perforation ratio	Thickness	Perforation ratio	Thickness
DV-1 :Weight						
DV-2: Deflection						
DV-3: von Mises stress						
DV-4: Structural cost						
DV-5: Spatial daylight autonomy						
DV-6: Light oversupply						
DV-7: Total energy						
DV-8: Total energy costs						

legend		
positive correlation	negative correlation	
lowest	lowest	p < 0.05
		p < 0.01
highest	highest	p < 0.001

IV-2 (thickness) and IV-3 (perforation Ratio) are plotted on the x and y-axis, while every dependent variable is plotted on the z-axis for each roof geometry, presented in Figure E.38.

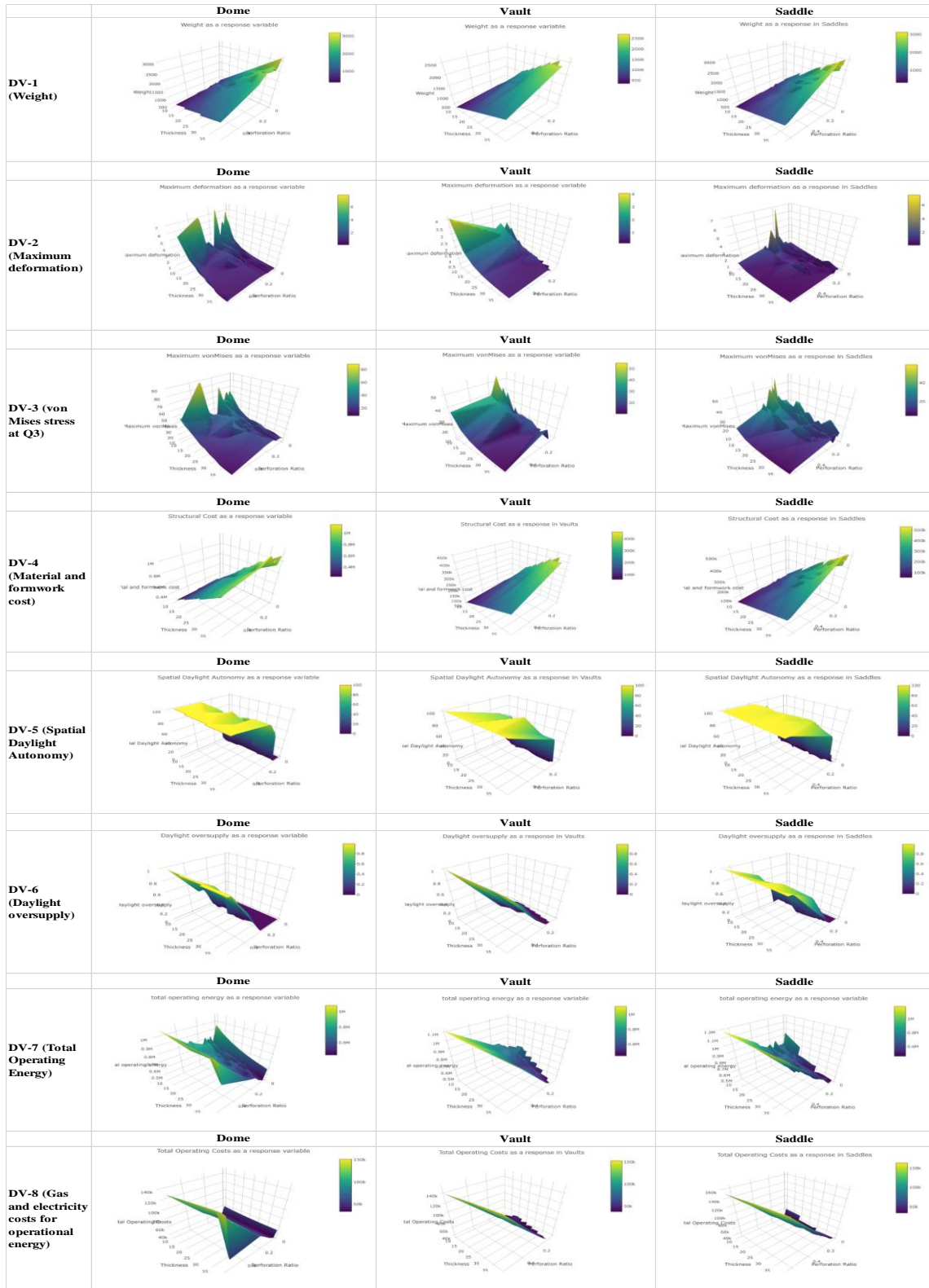


Figure E.38. Plotting dependent variables against two dependent variables for each roof geometry

Appendix F :

Case study validation and results

F.1 Verify the effect of zone combination on the daylighting performance

As explained in chapter 7, nine zones are created on the shell surface which work as an underlying pattern for subtracting holes (Figure F.1). Considering lighting and that some zones may be shadowed more than the others due to different curvatures of the roof in each zone, it is assumed that daylighting will be affected. In order to understand this effect, an exploration analysis has been conducted. In the analysis, while only one zone is being fully subtracted in each simulation, the daylighting performance is assessed when the zone is being changed. This is repeated for a dome with low curvature and a dome with high curvature.

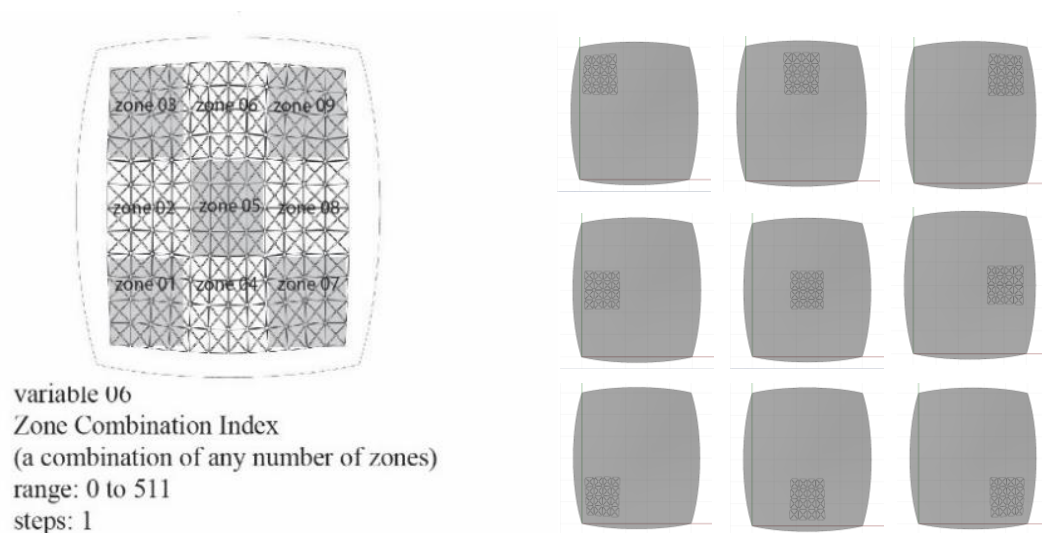


Figure F.1. The surface of the shell is subdivided into 9 zones, where each zone can be used for subtracting holes

Table F.1 illustrates the false color rendering of sDA (spatial daylight autonomy) as an indicator for daylighting performance. Translucent glazing is used for glazing, which matches the glazing that is used at the time of in generating the shells in the solution space. Figure F.2 illustrates a graph that compares sDA in a dome with low curvature with a dome with high curvature.

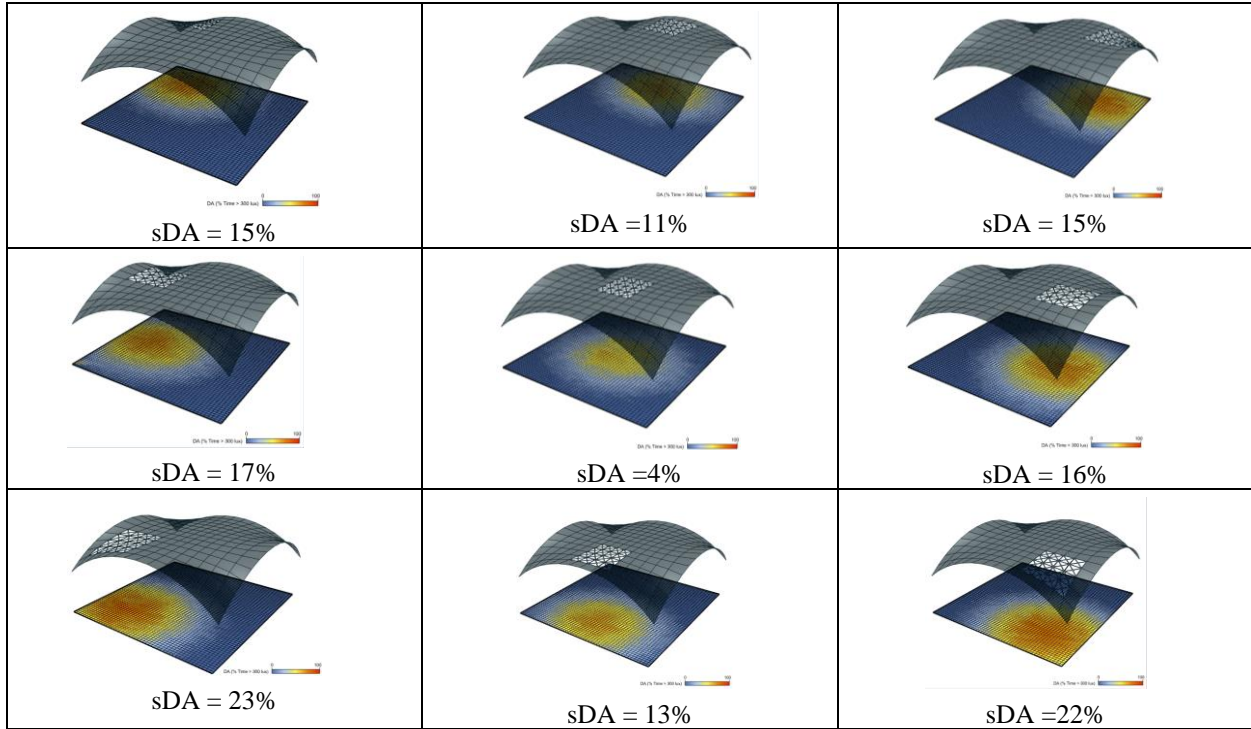


Figure F.2. False color rendering of sDA for a dome with low curvature when different zones are subtracted

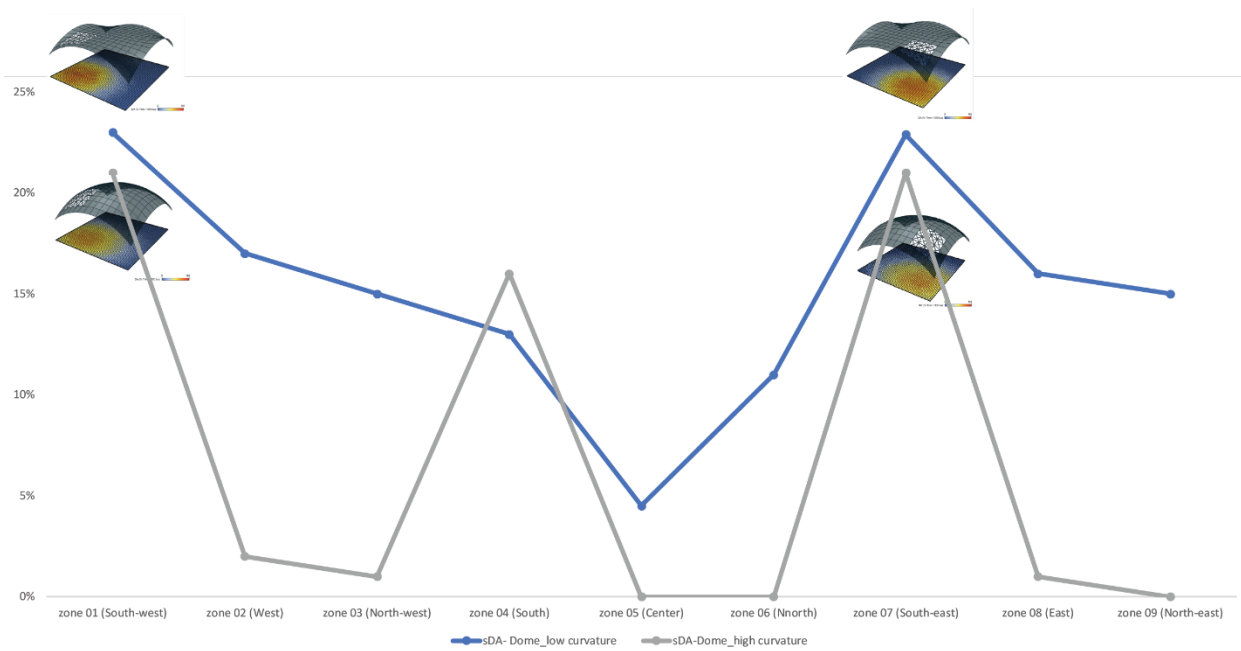


Figure F.3. Comparing sDA between a dome with a low curvature and high curvature

Looking at Figure F.3, it is noticed that the location of the zone affects the daylighting in the shell. Zone 01, 04, and 07, located on South-west, South, and South-east respectively, provide the

highest sDA. On the other hand, zone 3, 5, 6, and 9 located on north-east, center, north, and north-west provide the least sDA. It is also noticed that as the curvature of the dome increases, the zones with low sDA have even lower daylight.

F.2 Verify deflection under Live Load in the Solution space

Total deflection consists of deflection under dead load (D.L.) and live load (L.L.). It is assumed that deflection under D.L. can be eliminated during construction by adjusting the formwork and using pre-camber. Knowing this, the deflection under L.L. should ideally be less than the absolute value of 2.5 cm (1 inches) and never exceed 5 cm (2 inches). However, at the time of generating shells using ParaGen, only Total deflection was recorded in the database. Then, an acceptance limit of total deflection less than 0.3 meters (1 foot) was applied. In order to verify that the shells with a total deflection < 0.3 meters (30 cm) are not violating deflection under L.L. criterion of less than 25 mm, the shells in the database are sampled to check the breakdown of deflection under D.L. and L.L. For this, all shells are filtered using total deflection < 0.3 m. 378 cases match pass this filter. The next step is to sample cases based on their thicknesses, namely a 20 cm shell and a 40 cm thick shell. Perforation ratio is the other criterion coupled with thickness, where two extreme perforation ratios, 0% and 65%, are tested. It should be noted that if a combination with the exact perforation ratio does not exist in the database, the closest value is picked. Therefore, 4 cases are sampled. Table F.1 summarizes the id of the sampled shells, and the breakdown of deflection under D.L. and L.L. along with the properties of the shell.

Table F.1. Comparing performance of four samples from the Solution space

	Sample 01	Sample 02	Sample 03	Sample 04
id	534	59	440	38
Thickness [cm]	20	20	40	40
Perforation ratio	0%	65%	0.03	58%
Rise in width	-1	-10	-9	2
Rise in length	1.5	10.5	10	10.5
D.L. deflection[m]	0.205	0.18	0.153	0.227
L.L. deflection[m]	0.043 (4.3 mm)	0.106 (10.6 mm)	0.016 m (16 mm)	0.054 (5.4 mm)
Total deflection [m]	0.25	0.29	0.17	0.28

Looking at the breakdown of deflection under D.L. and L.L. in the cases that have a total deflection less than 30 cm, the deflection under L.L. for Sample 01, 02, 03, and 04 is 4.3, 10.6, 16, and 5.4 mm respectively, which is all less than the 25 mm limit. This verifies that the general filter of total deflection < 0.3 works fine without violating the requirement for deflection under L.L.

F.3 High Life Textile Factory

As discussed in chapter seven, an abstract hypar that spans a 50 by 60-meter span is used for structural simulation of Candela’s perforated umbrella structure. The first abstract morphology with a rise/area ratio of 0.015 thus a rise of 45 meters, has the highest surface curvature and surface area. Abstract morphology-A is simulated using different thicknesses starting from 5 cm to 35 cm. Figure F.4 demonstrates deflection shape of the first six hypars. Deflection is observed at the legs of the hypars, where the surfaces are relatively flat compared to the curved surface of the upper portions.

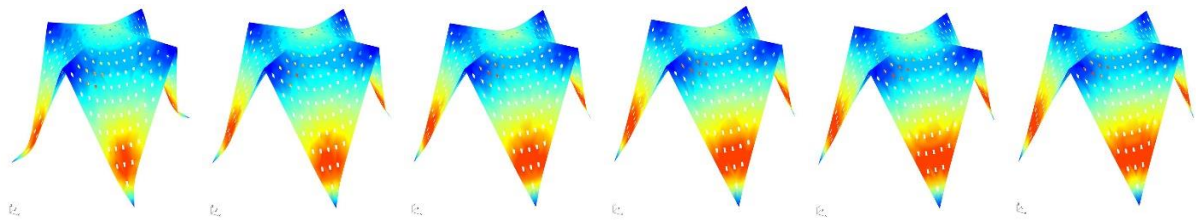


Figure F.4. Maximum total deflection in shells starting from 5 cm to 30 cm thickness in 5 cm increments

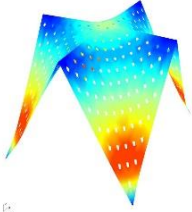

Table F.2 summarizes performance values of different variations of abstract morphology-A. The hypars that are 25, 30, and 35 cm thick have a deflection under L.L. of 40, 27, and 19 mm, all less than 50 mm which is still acceptable. It should be noted that the total deflection in these hypars is 27, 21, and 17 cm, all within the general limit of deflection < 30 cm that was used for exploring shells generated using ParaGen.

Table F.2. Abstract Morphology A simulated with different thicknesses

		A-5	A-10	A-15	A-20	A-25	A-30	A-35
D.L.	deflection	123	63	41	29	22	18	15
	[cm]							
L.L.	deflection	111	28	12	6.7	4	2.7	1.9
	[cm]							
Total	deflection	235	92	54	36	27	21	17
	[cm]							
Von Mises stress		7.16	5.19	4.45	3.92	3.61	3.35	3.08
	at Q3 [MPa]							

From another perspective, a general trend is observed, which is as thickness decreases, deflection under both D.L. and L.L. increase. It may be intuitive to assume that thinner shells deflect less under self-weight (D.L.) simply because there is less material in thinner shells. This is partly true since as thickness decreases, self-weight decreases linearly. However, moment of inertia (I) calculated by $I = \frac{ba^3}{12}$ in rectangular cross sections is also negatively affected by the reduction in the thickness, which ultimately reduces the bending stiffness. In other words, when depth is decreased by one unit, moment of inertia is decreased by a cubic factor of one unit, reducing the shell's bending stiffness which ultimately creates larger deflections. Structural performance of Candela's abstracted hyper shells with a rise of 45 meter, named Abstract Morphology-A, is simulated using two thicknesses: 15 and 25 cm. The geometric properties and the results are employed to validate this relationship (Table F.3).

Table F.3. Hypar shells with 45-meter rise, simulated using two thicknesses

	Case A-15 Morphology A 15 cm thick	Case A-25 Morphology A 25 cm thick
		
Deflection under D.L. [cm]	41	22
Deflection under L.L. [cm]	12	04
Total deflection [cm]	54	27

Thickness and moment of inertia of case A-15 is denoted as Th_i and I_i . The same convention is used for Case A-25.

$$\text{Case A-15: } Th_i = 15, I_i = b \frac{15^3}{12}$$

$$\text{Case A-25: } Th_{ii} = 25, I_{ii} = b \frac{25^3}{12}$$

Anticipated ratio of change in deflection under D.L. and L.L. when thickness increases from 15 to 25 cm is 1.6. In other words, it is anticipated that a 25 cm shell deflects 1.6 times more than a 15 cm shell.

$$\frac{Th_{ii}}{Th_i} = \frac{25}{15} = 1.6$$

Anticipated ratio of change in deflection under D.L. and L.L. when thickness (cross section depth) increases from 15 to 25 cm affects moment of inertia by a factor of 4.62. In other words, bending stiffness of a 25 cm shell is 4.62 times more than that of a 15 cm shell.

$$\frac{I_{ii}}{I_i} = \frac{\frac{b \times 25^3}{12}}{\frac{b \times 15^3}{12}} = 4.62$$

Considering the calculations, making the shells thicker (25 cm relative to 15 cm) will increase deflection caused by self-weight by a factor of 1.6, while will decrease deflection by a factor of 4.62 due to having a greater moment of inertia. Anticipated net ratio of increase in deflection when thickness is reduced from 25 to 15 cm is 3.

$$4.62 / 1.6 = 2.88$$

In other words, thinning the shell from 25 to 15 cm should roughly increase deflection by a factor of 3. Looking at the results of simulation in Table F.3, total deflection of a 25 cm shell is 27 cm, whereas total deflection of the 15 cm shell is 54 cm, which is 2 times more ($54/27 = 2$). This ratio roughly corresponds with the anticipated ratio and validates the observed trend.